Resonant Excitation of White Dwarf Oscillations in Compact Object Binaries

Thesis by

Yasser Rathore

In Partial Fulfillment of the Requirements

for the Degree of

Doctor of Philosophy

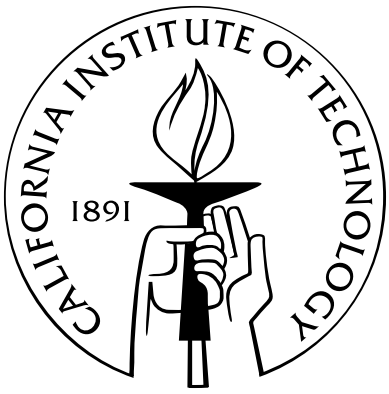

California Institute of Technology

Pasadena, California

2005

(Defended May 18, 2005)

"These, Gentlemen, are the opinions upon which I base my facts."

—Winston Churchill

Acknowledgements

I am grateful to the following persons who have, either directly or indirectly, enriched my life during the last seven years.

Roger Blandford, my thesis advisor, for his patience and generosity, and for giving me the opportunity to work with him. Also, special thanks to both Roger and Liz (Blandford) for the warmth of their hospitality on many occasions.

Avery Broderick, friend and colleague, from whom I've learned many things over the course of our collaboration. This thesis would be much the lesser without his assistance and contributions.

Dane Boysen, whose friendship and support over the years have meant a lot to me.

The Tapir group, my home for most of my time at Caltech.

The people at the Kavli Institute for Particle Astrophysics and Cosmology, who treated me as one of their own during my one-year sojourn at SLAC.

And, finally, my parents, without whose unwavering support I would not have had many of the opportunities that I have been fortunate enough to have.

Abstract

White dwarfs are ubiquitous in the known Universe. They are frequently found in binary systems with ordinary stars, giants, or compact objects as companions. Depending upon their histories, such systems may have significantly eccentric orbits. Because of gravitational radiation, a white dwarf-compact object binary will shrink and circularize with time. If the system is initially close enough, then the inspiral will occur on a time-scale shorter than a Hubble time. As an eccentric system inspirals, it will pass through resonances when harmonics of the orbital period match one of the white dwarf's normal mode eigenfrequencies. At these tidal resonances, energy can be transferred from the orbit to the white dwarf normal modes, and the system will pass through a sequence of such resonances for each mode. If the amplitude of a mode is driven high enough, the modes may damp due to non-linear processes and heat the white dwarf. If the temperature of the white dwarf can be raised in this way to a critical value, then the star may undergo a thermonuclear detonation that results in a Type Ia supernova. In order to determine whether such a scenario is possible, and what other observable consequences of tidal resonances may be, it is necessary to understand the resonant energy transfer and the non-linear evolution of modes on a white dwarf in some detail.

A variational approach to the excitation of dynamical tides is presented. This is then used to study the energy transfer in the resonant excitation of tides. The energy transfer problem is complicated by the fact that a mode perturbs the orbit as it is resonantly excited, effectively creating a non-linear feedback loop. We call this effect 'back reaction.' In the present work, the problem is considered both in the approximation when back reaction is neglected, and when it is included. It is

found that back reaction changes the resonant energy transfer both qualitatively and quantitatively. In particular, unlike the no back reaction case, the energy transfer with back reaction is shown to be always positive to lowest order in the rate of dissipation by gravitational radiation, and any initial energy in the mode before resonance is shown to increase the energy transfer.

Numerical simulations of resonant mode excitation and non-linear evolution of white dwarf oscillations are also considered. An adiabatic, parallel hydrodynamic code is described for this. Results from several test problems and preliminary simulations of resonant tidal excitation are presented.

The formalism developed for resonant tidal excitation is applied to studying the feasibility of a tidally triggered supernova via resonant excitation of quadrupolar f-modes. It is found that a 1.4 $M_\odot$ companion to the white dwarf is not viable, which rules out double degenerates and white dwarf-neutron star binaries as potential progenitors. However, it is found that with companion masses of $\sim$ 10–10^5 $M_\odot$, there exist regions in the parameter space where the white dwarf can be detonated before tidal disruption. It is calculated that the ejecta from such a detonation would remain trapped in orbit around the companion for the majority of cases, and would presumably be accreted eventually.

A preliminary calculation of the importance of tidal effects for gravitational wave observations of capture sources with central masses of $\sim 10^6$ $M_\odot$ is also presented. The resonant excitation of f-modes is found to be unimportant because of the long orbital periods at the last stable orbits. It is, however, found that the excitation of g-modes could introduce significant errors in the parameter estimation for such systems, though it would probably not affect detection capability. The exact magnitude of the errors depends upon the density of resonances during the period of observation, and therefore depends upon details of the white dwarf model.

Contents

List of Figures

List of Tables

Part I

Introduction

Chapter 1

Motivation

White dwarfs, the normal evolutionary endpoint for stars less massive than ~ 8 $M_\odot$, are extremely common; the halo of our Galaxy contains several billion of them. They are observed frequently in binary systems, with normal stellar companions, as cataclysmic variable stars and, less often, with compact object companions, as white dwarf-compact object (WDCO) systems. Many of these systems are produced naturally in binary star evolution and, as a consequence, mostly have circular orbits. However, it is also possible to form eccentric, WDCO binaries following stellar capture or exchange in a dense stellar environment.

Whatever their detailed nature and origin, WDCO binaries evolve dynamically under the action of gravitational radiation (e.g., Peters & Mathews, 1963; Peters, 1964; Iyer & Will, 1995). The orbital period and eccentricity of such a binary will decrease until the former reaches the Roche period, $\sim 10-100$ s depending upon mass, when the white dwarf will be torn apart by tidal forces. During inspiral, the system will pass through a series of resonances between harmonics of the orbital frequency and the white dwarf normal mode eigenfrequencies. Typically, the system will spend many orbits near each resonance, and consecutive resonances for a given mode will be separated by a much larger number of orbits associated with the gravitational inspiral time-scale. Passage through a sequence of such resonances will result in transfer of energy from the orbit to the oscillations and may drive the amplitudes of the oscillations non-linear, with possibly observable consequences. For example, if it is possible to thermalize the energy in the modes on a short enough time-scale through

some dissipative process such as non-linear damping or, perhaps, wave breaking, then the white dwarf can be heated in this way. If the temperature can be raised to $\sim 10^8$ K, then it may even be possible to detonate the white dwarf tidally, leading to a Type Ia supernova. A different (and less spectacular) consequence of significant energy transfer during tidal resonances would be modulation of the WDCO binary's orbital parameters, which would impact the gravitational wave signal from the system.

1.1 WDCO Binary Formation Mechanisms

An important factor in determining whether resonant tidal effects during the evolution of WDCO binaries are of practical interest is determining whether there exist mechanisms through which sufficiently eccentric, close WDCO binaries may be formed. The requirement that the binaries be close is an obvious one for finite-size effects to be significant. The eccentricity requirement is more flexible. It is possible, in principle, that resonant tidal effects may be important in binaries with circular orbits—especially when g-modes are considered. However, the normal modes with the largest tidal overlap are the quadrupolar f-modes, which typically have frequencies higher than the Roche frequency. Hence, a resonance between an f-mode and the fundamental Fourier component of the companion compact object's tidal force (which is the only component for a circular orbit) is not accessible before the white dwarf is tidally disrupted. Higher eccentricities greatly increase the number of harmonics of the tidal force available for resonant interactions, as the amplitude of the k-th harmonic goes as $\sim e^{|k-|m||}$, where e is the orbital eccentricity and m is the azimuthal order of the Fourier component. Thus, the most interesting systems are likely to be those with significant eccentricities. Several possible mechanisms for generating close, eccentric WDCO binaries are briefly discussed below.

1.1.1 Primordial Binary Evolution

The most common mechanism for the formation of WDCO binaries is likely to be primordial binary evolution. As the two components of a binary evolve to the end

of their lifetimes, various mechanisms operate which determine the outcome. If the binary is too wide, then the two components will evolve more or less independently, with each one following its own evolutionary track. However, if the binary is close enough that at least one of the stars fills its Roche lobe at some point, then that star will transfer mass to its companion. If the rate of mass transfer is too high, then the companion will be unable to accrete the transferred mass rapidly enough, which will result in the formation of an envelope of hot material around it. At some point, the companion's envelope will overflow its Roche lobe as well, resulting in the formation of a common envelope (Paczyński, 1976; Iben & Livio, 1993). When the common envelope is not corotating with the orbit, it will exert a drag upon the stars, which will tend to shrink and circularize the orbit. It is believed that such a period of common envelope evolution may have occurred in the history of any binary with at least one compact object which has an orbital period of less than a few days (Iben & Livio, 1993).

In addition to common envelope evolution, binaries may also circularize due to tidal dissipation in one or both of the components. Obviously, for this to affect the orbit significantly within a Hubble time, the binary must not be too wide initially. In practice, for significant changes to occur, at least one of the stars must have a radius of the order of its Roche lobe, because the circularization time-scale is thought to be proportional to $(a/R_0)^8$, where a is the semimajor axis and R_0 is the radius of the star exerting the tidal force (Zahn, 1977; Hut et al., 1992).

Because of the above considerations, most close WDCO binaries formed via evolution of primordial binaries are expected to be circular, with possibly a few exceptions. One circumstance in which this need not be the case is when the companion compact object is formed in a supernova explosion. This would occur when the companion is either a neutron star or black hole progenitor (in which case the white dwarf will not have formed yet, presumably), or perhaps another white dwarf which accretes material from its companion and exceeds the Chandrasekhar limit. In either case, if the binary is not unbound by the supernova, it may be left with a significantly eccentric orbit (Hills, 1983).

1.1.2 Tidal Capture

If two unbound stars have a close encounter, then it is possible for them to become bound by transferring energy from the orbit to non-radial oscillation modes of the stars via tidal interaction. This mechanism for binary formation was first suggested by Fabian et al. (1975), calculated in detail by Press & Teukolsky (1977), and further elaborated by Lee & Ostriker (1986), McMillan et al. (1987), Ray et al. (1987), and Kochanek (1992b). Fabian et al. proposed the mechanism as a way of producing sufficient compact object-ordinary star binaries to account for variable X-ray sources observed to coincide with globular clusters (e.g., Clark et al., 1975). While the mechanism is no longer believed to be important in that context, it has more general applicability, and a binary formed via tidal capture will necessarily be close, with a highly eccentric initial orbit. If there is significant tidal dissipation, then the orbit will gradually circularize with subsequent periastron passages.

The analysis of Fabian et al. and Press & Teukolsky relies upon the important assumption that the tides excited during the initial passage are dissipated on an orbital time-scale. This process is presumed to repeat during subsequent orbits. This assumption, which is necessary to ensure stability of the newly-formed bound system, exposes several problems with the tidal capture mechanism. If the tides are not dissipated rapidly enough, the orbit can become unbound during subsequent periastron passages, because energy may be transferred back to the orbit from the tides (e.g., Kochanek, 1992b). If the tides are dissipated rapidly enough, the typical amount of energy that has to be dissipated is a significant fraction of the star's gravitational binding energy, which makes it unlikely that the star will manage to retain its original structure (McMillan et al., 1987). Furthermore, even if the system manages to remain bound, once the perturbation of the orbit by the excited tides is taken into account, the subsequent evolution can be chaotic rather than simply dissipative (Mardling, 1995a,b).

In the context of WDCO binaries, the tidal capture mechanism is likely to be only viable in dense environments such as the cores of globular clusters. The compactness

of both components of the binary decreases the tidal capture cross-sections significantly, since the tidal force scales as $\sim R_*/R^3$, where R_* is the stellar radius, and R is the separation of the two objects. It is also unlikely that tidal dissipation in a white dwarf will be effective on the time-scale of a single orbit (Osaki & Hansen, 1973; Kumar & Goodman, 1996). Nevertheless, the possibility of WDCO binary formation via tidal capture exists in principle; and the energy transfer need be no more than $\sim$(10–100 km s^{-1})$^2 \equiv 10^{12-14}$ erg g^{-1} for capture to ensue. In addition, the tidal capture mechanism has the merit that the resulting binaries are close and highly eccentric, which is important for the WDCO problem.

1.1.3 Three-Body Processes

The basic requirement for any capture process for the formation of a binary system to operate is the presence of degrees of freedom, in addition to the orbit, to which energy and angular momentum may be transferred, and, subsequently, dissipated. The tidal capture mechanism fulfills this requirement by relying upon the internal structure of one or both of the bodies to provide the additional degrees of freedom. Alternatively, the additional degrees of freedom can be supplied by a third body. Of three-body encounters, the most likely are those between an existing binary and an unbound object. Encounters between three unbound bodies are much less likely, as the probability of such an encounter scales as the cube of the number density of unbound bodies. Furthermore, studies of globular cluster dynamics suggest that binary-single body encounters play an important role (for example, as a cluster heating mechanism) in determining the evolution of such systems (e.g., Heggie, 1975; Hills, 1975b,a; Hut, 1983a; Elson et al., 1987; Goodman & Hut, 1989; Sigurdsson & Phinney, 1995).

Encounters between a binary and a single object may be broadly categorized into four types: scattering, exchange, collision, and ionization (Sigurdsson & Phinney, 1993, 1995). In the scattering case, an unbound body encounters a binary system, scatters off it gravitationally, and then leaves, with the binary remaining intact. The outcome of the encounter upon the binary is a modification of its orbital parameters,

such as the semimajor axis and eccentricity. Alternatively, it may happen that one of the components of the binary becomes unbound and escapes, while the other component becomes bound to the intruder and forms a new binary. In this case, the encounter is an exchange. It is also possible that the intruder collides with one of the binary components, or, perhaps, induces chaotic trajectories that cause the two binary components to collide. In either case, the encounter is appropriately referred to as a collision. Finally, the remaining case is when all three participating bodies become unbound—hence the term 'ionization.' In the point-mass approximation, three-body encounters never result in the formation of a stable trinary (Hut, 1983b).

In general, binary-single body encounters of the scattering type tend to both harden the binary (i.e., decrease its semimajor axis) and increase its eccentricity (Hills, 1975b; Sigurdsson & Phinney, 1993). In exchanges, the lightest body is usually ejected, and the average eccentricity of the new binary, which is insensitive to the eccentricity of the original binary, is approximately given by $\langle e \rangle \approx 1 - M_{\rm e}/M_{\rm f}$, where $M_{\rm e}$ is the mass of the ejected body, and $M_{\rm f}$ is the mass of the intruder (Sigurdsson & Phinney, 1993). For collisions, in cases when there is a surviving binary, the orbital eccentricity appears to increase most of the time, but the orbit also tends to be wider (Sigurdsson & Phinney, 1993).

For the formation of close, eccentric WDCO binaries, binary-single body encounters are probably the most interesting mechanism, as they are not only capable of generating close orbits with high eccentricities, but also have significantly larger cross-sections than tidal capture.

1.1.4 Gravitational Bremsstrahlung

As two unbound stars scatter off each other gravitationally, energy and angular momentum will be emitted from the system in the form of gravitational radiation, which, by analogy with its electromagnetic counterpart, is called gravitational bremsstrahlung (Thorne & Kovacs, 1975; Crowley & Thorne, 1977; Kovacs & Thorne, 1977; Turner & Will, 1978). Gravitational bremsstrahlung offers the additional de-

grees of freedom required for a binary capture mechanism to operate, so it is possible to form binaries in this way. Clearly, for the mechanism to operate, the stars have to be massive enough to radiate a sufficient amount of energy and angular momentum. This requirement makes the cross-section for capture by gravitational bremsstrahlung negligible for most encounters involving a white dwarf and another object. Only when the companion mass exceeds a few times $10^5\ M_\odot$ does gravitational bremsstrahlung contribute a larger cross-section than tidal capture. As objects with masses higher than this are unlikely to be found anywhere other than in galactic centers, this mechanism is unlikely to be of any importance for WDCO binary formation, except, perhaps, in a few exotic cases.

1.2 Intermediate Mass Black Holes

The strength of the tidal force exerted by the companion in a WDCO binary scales as $\propto M_0/R^3$, where M_0 is the companion mass, and the Roche separation is approximately given by $R_{\rm Roche} \sim (M_0/M_*)^{1/3} R_*$, where M_* and R_* are the white dwarf mass and radius, respectively. This simple scaling implies the physically obvious fact that the excitation of tides on the white dwarf is most interesting for small separations and large companion masses. For the case when the companion compact object is a black hole, however, if the mass is too large, then the event horizon extends beyond the Roche separation, which implies that the white dwarf will be swallowed whole rather than tidally disrupted. For interesting tidal effects with black holes, we therefore require that the Roche limit lies not too far inside the horizon. This requirement gives an upper limit for interesting black hole masses of $\sim 10^6\ M_\odot$. Thus, the problem is still of interest for black holes such as the one thought to exist in the Galactic center ($\sim 3.5 \times 10^6\ M_\odot$; Schödel et al., 2003; Ghez et al., 2005), but for black hole masses which are relevant for more massive galaxies and active galactic nuclei (AGN) ($\gtrsim 10^7\ M_\odot$; Onken et al., 2004), tidal effects are unlikely to be important with white dwarf companions.

Until recently, the population of black holes was thought to be divided into two

groups: those with masses in the stellar range, which are observed indirectly in X-ray binaries (e.g., Blumenthal & Tucker, 1974; Bahcall, 1978; Bradt & McClintock, 1983; Liu et al., 2000; Orosz, 2003), and supermassive black holes ($\gtrsim 10^6\ M_\odot$), which are observed indirectly in AGN (e.g., Kormendy & Richstone, 1995; Nelson et al., 2004) as well as in the Galactic center (e.g., Ghez et al., 2003; Schödel et al., 2003; Ghez et al., 2005). Recently, however, there has been a growing body of theoretical evidence for, and observational evidence consistent with, the existence of intermediate mass black holes (IMBHs). In addition to having masses that lie in the 'interesting' range for companions in WDCO systems, WDCO systems with IMBH companions will have significantly shorter gravitational inspiral times than less massive systems (Peters, 1964), and the required orbital separations to access low order harmonics of the tidal force will be larger—i.e., the systems need not be as compact as those with lower masses have to be. This makes the existence of IMBHs of considerable interest to the present work.

In 1999, Colbert & Mushotzky reported observations of compact X-ray sources near the centers of 21 nearby galaxies. These sources which are, on average, ~ 390 pc off the host galaxy's optical center, have inferred isotropic X-ray luminosities in the range $\sim 10^{37-40}$ erg s^{-1}, which, if the sources are indeed isotropic, makes them too luminous to be X-ray binaries with stellar mass black holes. Colbert & Mushotzky found that the spectral data were fit well by a multicolor disk blackbody model, which lends credence to the hypothesis that these sources are at least qualitatively similar to X-ray binaries. Assuming source isotropy, they inferred black hole masses of $\sim 10^{2-4}\ M_\odot$. Subsequently, these sources have attracted a great deal of attention (e.g., King et al., 2001; Mizuno et al., 2001; Strickland et al., 2001; Colbert & Ptak, 2002; Körding et al., 2002; Miller et al., 2003, 2004; Portegies Zwart et al., 2004; Hopman et al., 2004; Abramowicz et al., 2004), and these objects, dubbed ultraluminous X-ray sources (ULXs) or intermediate-luminosity X-ray objects (IXOs), have become prime candidates for IMBHs. However, it should be noted that there are other interpretations of ULXs which do not require IMBHs. In particular, it has been suggested that the sources may be relativistically beamed rather than isotropic, which could

reduce the mass requirement to ordinary stellar mass black holes (King et al., 2001; Körding et al., 2002). It has also been suggested that some fraction of ULXs may in fact be background AGN. Thus far, the case is undecided. But, despite the fact that the interpretation of ULX observations is a subject of considerable debate, it seems fair to claim that the existence of IMBHs appears a lot more plausible now than it did in the past.

On the theoretical end, recent simulations of globular cluster dynamics have shown that runaway growth via collisions in the core can lead rapidly to the formation of black holes with masses in the range $\sim 10^{2-3}\ M_{\odot}$ (Portegies Zwart & McMillan, 2002; Portegies Zwart et al., 2004). Currently, there are no observations to support these results, but it has been suggested by Maccarone (2004) that IMBHs at the centers of globular clusters could be identified by deep radio observations.

1.3 WDCO Binary Populations

A thesis about tidal interactions between white dwarfs and other compact objects in binary systems would be somewhat incomplete without any mention of the Galatic population of such binaries. There are three possible companions to a white dwarf in a WDCO system: another white dwarf, a neutron star, or a black hole. Unfortunately, our current understanding of these populations leaves a lot to be desired—due, in large part, to the selection effects inherent in the observations of such systems. Nevertheless, there are some known examples.

The most common WDCO systems are probably double degenerates. The reason for this is simple: white dwarfs appear to be by far the most common compact objects. For example, Monelli et al. (2005) have recently reported the discovery of more than 2000 white dwarfs in the globular cluster ω Centauri. However, relatively few examples of double degenerates are known (e.g, Saffer et al., 1988; Marsh et al., 1995; Marsh, 1995; Saffer et al., 1998; Ramsay et al., 2002), as they are difficult to detect. Double degenerates have been observed to have periods as short as ~ 5 min (Ramsay et al., 2002). Systems in which the total mass exceeds the Chandrasekhar

limit have been proposed as progenitors of Type Ia supernovae, and it has been estimated that the number of such systems exceeds the observable number by about 20 (Iben et al., 1997). Iben et al. predict a Galactic birth rate of 0.17 yr^{-1} for systems where one star is a helium or carbon-oxygen white dwarf, and the other star is either a similar white dwarf or a low-mass main-sequence star. They also estimate that $\sim 10\%$ of observed white dwarfs are close white dwarf binaries, and that, of those, $\sim 40\%$ will merge in a Hubble time under the influence of gravitational radiation. They predict a Galactic merger rate of 0.02 yr^{-1}.

There are a total of ~ 50 known white dwarf-neutron star binaries, with orbital periods as short as 3 h (e.g., van Kerkwijk & Kulkarni, 1999; Kaspi et al., 2000; Edwards & Bailes, 2001; Camilo et al., 2001). Most of them are in nearly circular orbits with low inferred white dwarf masses (~ 0.15–$0.4\ M_{\odot}$), which presumably correspond to helium white dwarfs (Camilo et al., 2001). The high incidence of circular orbits is to be expected based upon the common envelope evolutionary path these systems are expected to have followed (e.g., van den Heuvel, 1994; Phinney & Kulkarni, 1994). However, there is a small but growing group of systems with heavier white dwarfs ($\gtrsim 0.5\ M_{\odot}$; likely carbon-oxygen), for which the orbital eccentricities are higher (Brown et al., 2001; Camilo et al., 2001). These systems probably follow a different evolutionary path (Tutukov & Yungelson, 1993; Portegies Zwart & Yungelson, 1999; Tauris & Sennels, 2000; Brown et al., 2001; Davies et al., 2002). Therefore, it appears plausible that there is a significant Galactic population of eccentric white dwarf-neutron star binaries. Kalogera et al. (2004) estimate that the Galactic birth rate of such systems is ~ 7 Myr^{-1}. The estimated Galactic merger rate for all white dwarf-neutron star binaries is estimated to be 0.2–10 Myr^{-1} (Kim et al., 2004).

For white dwarf-black hole binaries, there are currently no known examples—they would be extremely hard to detect. Nevertheless, given the large known population of white dwarfs in the Galaxy, and a large predicted population of black holes ($\sim 10^{8-9}$; van den Heuvel, 1992; Brown & Bethe, 1994; Timmes et al., 1996), and several possible binary formation mechanisms, it would be remarkable if no white dwarf-black hole binaries exist. It is difficult to predict the distribution of their orbital parameters, but,

based on the likelihood of three-body processes being the dominant formation mechanism in globular clusters, it seems reasonable to expect that a significant fraction will be both close and eccentric. It is also perhaps not too far fetched to speculate that the white dwarfs in white dwarf-black hole binaries in globular clusters will tend to be heavier than average ($\gtrsim 0.6\ M_{\odot}$) as a result of both mass segregation and the issue of long-term binary survival (e.g., Sigurdsson & Phinney, 1995). Sigurdsson & Rees (1997) have calculated the capture rate of compact stellar remnants by supermassive black holes in galactic cusps to be $\sim 10^{-8}$ yr^{-1} per galaxy for nucleated spirals such as the Milky Way. Presumably, a substantial fraction of the captured remnants are white dwarfs. Fryer et al. (1999) estimate that the merger rate of white dwarf-black holes binaries may be as high as $\sim 10^{-6}$ yr^{-1} per galaxy.

It is worth noting that all of the estimates quoted above should be treated with caution, as calculations of birth and merger rates for compact object binaries tend to be exercises in small number statistics. Furthermore, there are clearly significant gaps remaining in the current understanding of Galactic stellar dynamics, evidenced recently by the puzzling observations of young stars on close, highly eccentric orbits around Sgr A* (Ghez et al., 2005).

Chapter 2

Previous Work

2.1 General Comments

Research on the excitation of tides has spanned at least four centuries, with a host of illustrious names such as Galileo, Descartes, Newton, Bernoulli, Euler, Laplace, (George) Darwin, Kelvin, Lamb, and Chandrasekhar making contributions to the theory. It is neither possible, nor desirable, to provide here even a modest outline of this long history. A recent such survey may be found in the book by Cartwright (1999). The focus here is on tidal excitation in the modern astrophysical context, and, specifically, the excitation of dynamic tides in stellar objects.[1]

Most modern analyses of the excitation of dynamic tides deal with harmonic decompositions. The underlying idea is simple, and more general than the particular case of tides: for the system at hand, a set of linearized normal modes is calculated, as well as the coupling of the modes to the tidal force. If, as is often the case, the modes form a complete, orthogonal set, then the problem is reduced to the excitation of a (usually infinite) number of harmonic oscillators, which may be coupled via the tidal force. Thus far, the analysis is typically straightforward. The difficult part of the problem is solving the forced harmonic oscillator equations, which is rarely possible *in toto*, and, therefore, various simplifying approximations, specific to the problem

[1] A distinction is made between 'static' and 'dynamic' tides. Static tides are assumed to be in hydrostatic equilibrium; for example, a corotating binary system will raise static tides on both objects in the co-rotating frame. A dynamic tide is a perturbation away from, and, typically, an oscillation around, an underlying equilibrium configuration.

at hand, are usually made in the solution. An example of such a simplification may be to consider only the subset of modes which are the dominantly excited ones. The equations of motion can then be solved numerically for specific choices of parameters. It is, of course, always desirable to find good analytic approximations whenever possible, even for a subset of the parameter space, as they make the dependence on parameters, and hence the scalings, explicit.

The preceding paragraph is the theory of tidal excitation, in a nutshell, as it is used and described in guises as varied as the number of authors. Two important advantages of the normal mode analysis are the reduction from an uncountable infinity of degrees of freedom to a countable infinity, and the encapsulation of the internal physical details of the system into normal mode frequencies and tidal coupling constants. A disadvantage is that, because of the neglected non-linear terms, the orthogonality of the normal modes is often violated for large amplitudes. Such effects can be taken into account either by explicitly including the non-linear coupling terms to some order in the mode amplitudes, or by using a different approach. For example, tidal excitation in stars can be considered in terms of the so-called affine model, which assumes that the structure of the star can be represented by a global distortion such that surfaces of constant density are distorted into self-similar ellipsoids (Carter & Luminet, 1985; Luminet & Carter, 1986; Kochanek, 1992b). This approach has the advantage that arbitrary amplitudes can be considered, but has the disadvantage that the affine model has only a limited number of normal modes. However, these modes include those which tend to be the dominant tidally excited ones, such as the quadrupolar f-modes (Kochanek, 1992b).

2.2 Non-Variational Formulations

An early account of the excitation of dynamic tides in stars was given by Cowling (1941), who considered the non-radial, adiabatic oscillations of non-rotating polytropes, and coined the terminology of f-, p-, and g-modes, that is now in common usage. Cowling considered the possibility of both resonant and non-resonant exci-

tation of g-modes in binary systems, but did not actually calculate the resulting amplitudes or energy transfers. He considered a harmonic external tidal potential, and concluded that g-mode resonances would not significantly contribute to the tides in binary systems for two reasons: (i) g-modes have relatively small overlap with the tidal potential compared to the f-modes, and (ii) non-linear effects such as shifts in the eigenfrequencies will quench the excitation of the modes before large amplitudes can be excited resonantly. While (i) is generally true, it is difficult to see how that matters if the system spends enough time near a resonance for a g-mode. The overlap coefficients only determine the rate at which the mode can be excited, and not the maximum attainable amplitude. Therefore, the validity of Cowling's argument really rests on (ii). This issue, in the context of cold, carbon-oxygen-helium white dwarfs, is addressed in this thesis. For the case of main-sequence stars, Cowling's work was extended and improved on by Zahn (1970, 1975), who argued that non-adiabatic effects from radiative dissipation in the outer layer of stars are likely to be the dominant damping mechanism for g-modes. Zahn's work has relatively little relevance for dynamical tides in cold, carbon-oxygen-helium white dwarfs, where adiabaticity is probably an excellent approximation.

Possibly the first actual calculation of the excitation of dynamic tides in stars was done in a little-known paper by Burke (1967), where only quadrupolar modes were considered in a rather unwieldy manner. It is therefore, perhaps, not surprising that the real forerunner to most current calculations is the elegant analysis by Press & Teukolsky (1977) of the tidal capture mechanism of Fabian et al. (1975). Press & Teukolsky calculated the energy transferred to the normal modes of a star as it and a point-mass pass each other on a relative parabolic orbit, which is a good approximation to a periastron passage at high eccentricities. The result is summarized in the well-known formula:

$$\Delta E = \left(\frac{GM_*^2}{R_*}\right)\left(\frac{M_0}{M_*}\right)^2 \sum_{\ell=2}^{\infty}\left(\frac{R_*}{R_{\rm p}}\right)^{2\ell+2} T_\ell(\eta)\ , \tag{2.1}$$

where $R_{\rm p}$ is the periastron separation, $T_\ell(\eta)$ is a dimensionless, positive definite func-

tion, and η is a quantity which measures the duration of periastron passage (Press & Teukolsky, 1977). Press & Teukolsky assumed that mode damping times are long compared to the periastron fly-by time, but short compared to an orbital period. This effectively reduces the total energy transfer over a number of orbits to the sum of energy transfers over each individual periastron passage (it is assumed that the orbit is eccentric enough for tidal effects to be ignored away from periastron). In this case, an energy-based formalism, such as the one used by Press & Teukolsky, suffices, because the initial amplitudes of the modes before each periastron passage are negligible. However, if the mode damping times are longer than the orbital period, then the formalism is clearly inadequate, as it does not account for the relative phasing of the modes and the orbit. Depending upon the phasing, energy can be transferred from the modes to the orbit as well as vice versa. Another way of saying this is that the energy transfer to the modes can be positive as well as negative, which the Press & Teukolsky formula obviously does not allow.

Subsequent to Press & Teukolsky (1977), there were a number of authors who considered the excitation of modes on main-sequence stars, mostly for applications to X-ray binaries (e.g., Papaloizou & Pringle, 1980, 1981b,a; Savonije & Papaloizou, 1983, 1984). Papaloizou & Pringle (1980) used a perturbative approach to consider the effect of tidal resonances on the motion of the apsidal line in close, nearly circular systems, and found that the resonances could alter the motion to the point of changing the direction of precession. Their work was extended and elaborated by Quataert et al. (1996), Smeyers et al. (1998), and Willems et al. (2003). Savonije & Papaloizou (1983, 1984) considered the passage of close binary systems with massive stars through resonances due to tidal and stellar evolution, and concluded that resonance passages could increase the efficiency of circularization, especially for low-eccentricity systems. They also identified a possible phenomenon which they termed 'resonance locking.' Essentially, the idea is that a star with a resonant mode in a binary evolves in such a way so as to counteract the effect of spin-up due to tidal torques, and so 'locks' into a resonance. While an interesting possibility, resonance locking in this way seems to require a rather delicately fine-tuned system. Further work on resonance locking has

been done by Witte & Savonije (1999, 2001). Rocca (1982, 1987) also considered the tidal excitation of toroidal and low-frequency g-modes in similar systems. Terquem et al. (1998) considered the excitation of g-modes on a non-rotating, solar-type star with a close companion that could either be another star, or a planet. They applied their results to the particular case of 51 Pegasi (Mayor & Queloz, 1995), and showed that the observed variations could not be due to a tidally excited g-mode.

The theory of tidal interactions in binaries found a new set of applications following the discovery of millisecond pulsars in globular clusters (e.g., Manchester et al., 1991). Kochanek (1992b), in extending the the work of Press & Teukolsky (1977), recognized the weakness of the assumption that mode damping time-scales are shorter than the orbital period following tidal capture. He generalized the Press & Teukolsky formalism to the case when the initial mode amplitudes are non-zero, and recognized correctly that, with non-zero inital amplitudes, it is necessary to have an amplitude-based formalism rather than an energy-based formalism, because the phasing of the modes relative to the orbit matters.[2] Successive periastron passages were modeled as a discrete random walk in the mode amplitude, with an exponential dissipation factor representing the damping of modes over some characteristic time-scale:

$$E_m^{n+1} = E_m^n \, \mathrm{e}^{-t_{\mathrm{orb}}^n/QT} + \Delta E^{n+1} + 2\sqrt{E_m^n \Delta E^{n+1}} \, \mathrm{e}^{-t_{\mathrm{orb}}^n/QT} \cos\phi \ , \qquad (2.2)$$

where E_m^n is the energy in the modes after the nth periastron passage, t_{orb}^n is the orbital period after the nth passage, ΔE^{n+1} is the mean energy transfer at the $n+1$ passage, QT is a damping time constant, and ϕ is an effectively random phase. The corresponding evolution of the orbit is also stochastic. Note that the assumption that ϕ is random makes it explicit that the process is assumed to be non-resonant. For very close encounters, Kochanek used the affine model to determine the energy transfer. He determined that the star would become dynamically unstable if the

[2]The label 'amplitude formalism,' or, more generally, the common usage of the word 'amplitude' in this context, is rather unfortunate. Strictly speaking, one would consider an amplitude formalism to be identical to an energy formalism, because the amplitude is simply a scaled square root of the energy. What is actually meant is a *displacement* formalism, which is one where the phase of the oscillation is included.

energy transfer exceeded $\approx 0.15\,GM_*^2/R_*$. This is for an encounter between a main sequence star and a compact object (modeled as a point-mass), which is the scenario to which the study was confined.

Kumar et al. (1995) considered the tidal excitation of modes in binary systems with arbitrary eccentricity. Their approach was rather heuristic, perhaps because it was tailored for an application to the pulsar PSR J0045–7319, which is believed to be in a close, highly eccentric orbit with a 10 $M_\odot$ B star companion. The emphasis was on observational properties which could be used to probe stellar or orbital parameters.

In anticipation of gravitational wave detectors, there have been studies of how the gravitational wave signals from sources such as coalescing neutron star-neutron star binaries would be affected by finite-size effects. Generally, the consensus has been that tidal effects will be small except for the final few orbits before coalescence (e.g., Kochanek, 1992a; Bildsten & Cutler, 1992). However, Lai (1994) noted that these studies assumed static or quasi-static tides. Lai considered the effects of the resonant excitation of g-modes in coalescing neutron stars. His results were that a dynamical tidal lag develops even in the absence of fluid viscosity, but that the excitation of g-modes would not be important for gravitational wave detections, though it may contribute to tidal heating of the neutron stars up to a temperature of $\sim 10^8$ K before merger. Similar considerations for the more general case of rotating stars were discussed by Ho & Lai (1999), based on a study on the effects of rotation on excitation of dynamical tides in stars by Lai (1997). Reisenegger & Goldreich (1994) also considered the resonant excitation of g-modes during a neutron star binary inspiral slightly before Lai (1994), and reached a similar conclusion regarding the importance for gravitational wave detections.

Polfliet & Smeyers (1990) presented yet another formulation of the theory of forced, adiabatic, stellar oscillations in a language that is, perhaps, rather more complicated than necessary. The stars were assumed to be non-rotating, and perturbations of the orbit due to the excitation of tides were ignored. Ruymaekers & Smeyers (1994) presented a similar formalism to investigate the resonant excitation of modes in a rapidly evolving star, and used a multiple-variable expansion procedure

to describe the passage through resonance. They found the existence of a phase lag of $\pi/2$ between the dynamic tide and the tidal force, analogous to the lag found by Lai (1994), near resonance. Their description did not include the perturbation of the orbit by the excited modes.

Ivanov & Papaloizou (2004) considered the tidal interaction of massive planets on highly eccentric orbits in the context of the evolution of the planet's orbital parameters. They used the so-called impulse approximation, which treats each periastron passage as a statistically independent, fly-by excitation event, with the tidal interaction being ignored away from periastron. This is essentially the same formalism as was given by Kochanek (1992b) for the evolution of tidal capture binaries.

2.3 Variational Formulations

A common feature, present in virtually all the descriptions of tidal excitation in binary systems mentioned in the previous section, is that, outside of some numerical integrations, the perturbation of the orbits by the excited tides is neglected. For all analytical and semi-analytical calculations, the assumption is made that the system is on a prescribed Keplerian orbit, and any evolution of the orbit is added as a consequence of tides previously excited. Assuming that the mode damping times are long compared to the orbital period, this approach is clearly inconsistent, as it violates conservation of energy and angular momentum during the excitation of the tides (if energy is being transferred to modes, it has to come out of the orbit, and hence the orbit must necessarily be evolving as the modes are being excited). Indeed, with such approaches, it may not even be obvious what the correct expressions for the conserved quantities are. For example, one might naïvely think that the conserved energy in the system (once again, assuming negligible dissipation in an orbital period) is the sum of the orbital and mode energies. This is, in fact, incorrect. The correct conserved energy includes a contribution from the perturbation of the gravitational field by the excited tides. Lest one think that such a contribution is negligible, for close systems, the contribution can be comparable to the energy in the modes.

One of the advantages to a variational formulation[3] of a mechanical problem is that conserved quantities are easier to identify, and self-consistency is explicitly maintained in the equations of motion. The first person to identify and use variational formulations in the context of stellar oscillations was Chandrasekhar (1963, 1964). However, the first variational formulation of tidal excitation was probably given by Gingold & Monaghan (1980) in a study of the Roche problem for polytropic stars. They wrote down a Lagrangian for a point mass-polytropic star system, assuming an inviscid, homentropic, irrotational flow within the star, and used that Lagrangian to derive the linearized (in fluid perturbations) equations of motion for the system. These equations were self-consistent in that they conserved both energy and angular momentum, explicit expressions for which were identified by Gingold & Monaghan. The equations of motion were not amenable to analytic solution (an all-too-common price of self-consistency), and so were integrated numerically for a variety of initial conditions. The Lagrangian of Gingold & Monaghan was later used by Mardling (1995a,b) in a study of chaos in the evolution of tidal capture binaries.

In contrast to Gingold & Monaghan, who started with a fluid Lagrangian and developed a description in terms of normal mode displacements (amplitudes, in common terminology), Alexander (1987) started with a Hamiltonian in terms of the normal mode displacements, derived from the Lagrangian, $L = T - V$, of classical mechanics.[4] He used this Hamiltonian, with an averaging technique, to study the dynamics near a resonance with a given set of modes, and was able to derive expressions for two constants of the near-resonant motion (one of them was an approximate constant, valid for low to moderate eccentricities) relating mode variables to orbital variables. Note that this analysis was fully self-consistent because of the Hamiltonian approach, and therefore these constants are integrals of the actual motion, and are not easily derivable via other means. The original analysis was valid for a non-rotating star, and was later extended to a slowly, rigidly rotating star (Alexander, 1988).

Kokkotas & Schäfer (1995) used the formulation of Alexander (1987) to study the

[3]Here, by a 'variational formulation,' is meant a formulation in terms of a Lagrangian or a Hamiltonian—i.e., a variational principle.

[4]Ultimately, though it may not be obvious, the two approaches are demonstrably equivalent.

resonant and non-resonant excitation of g-modes during the gravitational inspiral of circular neutron star binaries. An interesting aspect of their approach was to incorporate orbital evolution due to gravitational radiation to 5/2 post-Newtonian order by means of the following explicitly time-dependent reaction Hamiltonian derived by Schäfer (1990):

$$H_{\rm reac} = \frac{2G}{5c^5}\frac{d^3Q_{ij}(t)}{dt^3}\left(\frac{P_iP_j}{\mu} - GM\mu\frac{R_iR_j}{R^3}\right) \ , \tag{2.3}$$

where μ is the reduced mass, M is the total mass, R_i is the orbital separation vector, $P_i = \mu\dot{R}_i$ is the linear momentum, and $Q_{ij} = \mu(R_iR_j - \delta_{ij}R^2/3)$ is the mass quadrupole tensor of the two-body system. They integrated the equations of motion numerically, and reported a tidally induced phase difference from the Newtonian and first-order post-Newtonian gravitational waveform, which becomes significant at the final stage of coalescence. They also noted the existence of a orbital instability due to tidal interactions, which causes coalescence to proceed more rapidly inside a critical orbital separation. This instability was previously discovered by Lai et al. (1993b, 1994), who used an approach based on ellipsoidal figures of equilibrium (Chandrasekhar, 1969; Lai et al., 1993a) to study the tidal interactions.

The work of the following authors is not of direct relevance to the study of tidal interactions, but is tangentially related by their usage of variational formalisms. Kumar & Goldreich (1989) studied non-linear effects for solar non-radial oscillations in terms of a Hamiltonian describing oscillations of a stratified, plane-parallel, perfect gas atmosphere. They found that three-mode couplings were insufficient to limit the growth of overstable p-modes. Van Hoolst (1994) described a Hamiltonian formalism for the study of free, non-linear, adiabatic oscillations of stars. His approach was based on considering Lagrangian perturbations of a star's total energy (the sum of kinetic, internal, and gravitational potential energies) around a static equilibrium state, and he derived equations describing mode couplings up to third-order in the mode amplitudes. Forced oscillations were not considered.

Chapter 3

Summary of This Work

This dissertation is mostly concerned with developing techniques to answer two related sets of questions regarding tidal effects in WDCO binaries:

1. How much energy can be transferred resonantly to the white dwarf normal modes (mostly, the $\ell = m = 2$ f-mode) during gravitational inspiral? Is it possible to drive the mode amplitudes into potentially non-linear regimes before tidal disruption?

2. What is the full, non-linear evolution of a large amplitude f-mode excited resonantly? Does the mode damp via coupling to other modes, perhaps in a Kolmogorov-type cascade of energy to smaller scales? Or, does the mode 'break' like a surface wave on an ocean?

The answers to these questions will allow us to address issues, such as whether it is possible to heat a white dwarf tidally before disruption so that it may detonate, or whether finite-size effects are likely to be important in gravitational wave detections of WDCO systems.

There are a number of simplifying assumptions made throughout. We restrict ourselves to non-rotating stars because white dwarfs are observed generally to be slowly rotating, and they are not expected to maintain corotation during inspiral (cf. Bildsten & Cutler, 1992). However, this may need further investigation. In addition, we mostly confine our attention to the $\ell = m = 2$ f-mode, because it is expected to be the dominantly excited one. Nonetheless, our formalism may be applied to

other modes as well. Of particular interest may be g-modes, as these have lower frequencies than f-modes, and can therefore be excited at fundamental resonance in circular orbits before tidal disruption.

In Chapter 4, a variational approach to tidal excitation is developed. The starting point is the ordinary Lagrangian from classical mechanics generalized to a continuous system. The theory is then developed until a Lagrangian valid for any perfect fluid flow in an arbitrary non-inertial frame is obtained. This Lagrangian is then coupled to a point mass, and the description is specialized to a homentropic, irrotational flow, which is appropriate for a non-rotating, cold, carbon-oxygen-helium white dwarf. The next step is the expansion of fluid quantities into equilibrium and perturbation pieces. Retaining terms to quadratic order in the perturbations, a Lagrangian is obtained which consists of a zeroth-order piece that describes the equilibrium configuration, a first-order piece which describes the gravitational coupling of the perturbations to the point mass, and a quadratic piece which describes the structure of the perturbations. This Lagrangian is then used to solve for the normal mode structure and to obtain the equations of motion. Expressions for the conserved energy and angular momentum are identified. The equations of motion and the conserved quantities are expressed in terms of the mode displacements (which are the normal coordinates for the system), and a Hamiltonian is obtained in terms of the mode displacements and their conjugate momenta which completely encapsulates the excitation of tides, to linear order.

In Chapter 5, the equations of motion are considered in the approximation that the perturbation of the orbit by the excited modes can be neglected for the purpose of mode excitation. We refer to this as the no back reaction approximation. Using the Peters (1964) prescription for the secular evolution of orbital elements due to lowest-order gravitational radiation, the energy transfer is calculated semi-analytically by direct comparison with a harmonic oscillator problem solved previously in the chapter. A number of physical considerations such as the tidal limit, mode damping, thermal evolution of the white dwarf are discussed as well. A long-term picture of passage through many resonances for a given mode is developed, which bears a strong similarity to the description of tidal capture binaries given by Kochanek (1992b). It

is shown that back reaction will significantly modulate the energy transfer in some regimes, and those regimes are delineated in parameter space. It is also speculated that back reaction may determine the sign of energy transfer even when it does not modulate the magnitude significantly. In addition, it is shown that large, and potentially non-linear, amplitudes for the $\ell = m = 2$ f-mode can be excited for a variety of initial conditions.

In Chapter 6, the resonant energy transfer including back reaction (i.e., including the feedback effect of tidal pertubations to the orbit on mode excitation) is considered using a Hamiltonian formalism similar to that used by Alexander (1987). The first part of the analysis is inspired directly by his development. The problem is formulated in terms of action-angle variables of the uncoupled mode-orbit system. It is shown that, near a particular resonance, modes with $\ell = m$ are excited the most, and, as a simplification, are the only ones considered. A series of canonical transformations are carried out which allow the two constants of motion previously found by Alexander (1987) to be obtained. The problem is reduced in this way from four to two degrees of freedom. It is then shown that the problem may be further reduced to a single degree of freedom. Tidal resonances in this context are demonstrated as corresponding to separatrix crossings by the system in phase space. The one degree of freedom problem is shown to be similar to the Hamiltonian analysis of first-order eccentricity resonances in the restricted three-body problem. While, usually, reduction to the three-body problem is not the most promising step in solving a given problem, this case is an exception, and an estimate of the resonant energy transfer is obtained by leveraging results obtained for the eccentricity resonances in the literature.

In Chapter 7, a code for studying the fully non-linear evolution of large amplitude modes is described. The results from number of test problems such as advection of pulses, pressure-free collapse, and the Sod shock tube are presented. Issues with setting up satisfactory equilibrium configurations for barotropic stars such as cold white dwarfs are discussed. Results from simulations of white dwarfs both in hydrostatic equilibrium and pulsating are shown. It is found that the dominant quadrupolar pulsation frequency is in excellent agreement with the predicted quadrupolar f-mode

eigenfrequency from the linear theory. The numerical quality factor for the quadrupolar f-mode is estimated to be ~ 6000.

In Chapter 8, results from simulations of resonant excitation of the $\ell = m = 2$ quadrupolar f-modes are presented. Issues with estimating the mode amplitudes are discussed, as well as interpretations of the simulations. Evidence for non-linear coupling between the $\ell = m = 2$ f-mode and other modesis found. Limitations of the presented simulations and directions for future work are discussed.

In Chapter 9, the results obtained in the preceding chapters are applied to evaluate the plausability of tidally detonated supernovae, and impacts on gravitational wave signals from WDCO systems due to resonant tidal effects.

In Part IV, a summary of the main conclusions is presented.

Part II

Resonant Excitation of Modes

Chapter 4

Basic Formalism

The preferred approach to tidal excitation in this dissertation is a harmonic analysis based on a variational formulation of fluid mechanics. For the case of a perfect fluid, such a formulation is especially convenient in that it maintains self-consistency in the equations of motion, and allows for easy identification of conserved quantities.

We prefer to begin from first principles and derive most of our results *ab initio*. There is an important reason for this. One goal of this dissertation is to develop a fairly complete account of a variational approach to the excitation of dynamical tides (ignoring non-adiabatic effects and stellar rotation). The literature on the subject is varied, and fragmented. Heuristic approaches, which often suffice for individual problems, tend to obfuscate the common elements shared by many of those problems. There appears to be no single account that presents the material in an unified manner which both exposes the elegant, underlying simplicity of the theory, and maintains a level of flexibility that makes it applicable to a broad range of problems. More than just an aesthetic goal, there are real advantages to having an unified description which begins with first principles and elucidates the steps and, most importantly, the assumptions made in solving a given problem. Such a development makes explicit the limitations to the applicability of a result, and allows for clear paths to generalizations of existing results. For example, the Lagrangian of Gingold & Monaghan (1980) is only valid for irrotational, barotropic flows. Without knowing how one arrives at that Lagrangian, there is no obvious way to adapt their approach to a more general equation of state, or to a star with non-zero vorticity. While, for a non-rotating,

cold, carbon-oxygen-helium white dwarf, the Gingold & Monaghan Lagrangian is adequate, the generalization to a more realistic warm white dwarf model which can support g-modes is not obvious. Although this thesis does not need the generalization, the development of the Lagrangian in Section 4.1 maintains generality as long as possible, and then makes it clear where the assumption of a homentropic, irrotational flow enters. Hence, in principle, there is a path to generalization there that may be followed.

The development of the formalism is most elegantly done using complex functions and variables. However, for actual applications, real functions and variables are considerably simpler to deal with. As a compromise, we develop the formalism in terms of complex variables through most of the chapter. At the end, a summary is provided that serves the dual purposes of collecting important results which are used in later chapters, and writing these results in terms of real functions and variables.

4.1 The Lagrangian

4.1.1 Overview of Variational Fluid Mechanics

In this section, we outline some of the important results from a variational formulation of fluid mechanics. Our discussion follows the review by Salmon (1988), where a more detailed exposition may be found. An important difference is that we have extended the formalism to accommodate a self-gravitating fluid in a non-inertial reference frame. A more recent review, which describes the variational formulation of Newtonian fluid mechanics from a somewhat different perspective that is inspired by general relativistic analogues, has been given by Prix (2004).

The simplest variational formulation of fluid mechanics is to use a continuum version of the Lagrangian from classical particle mechanics. In this approach, the Lagrangian for the fluid is just the classical Lagrangian for a system of particles distributed continuously in space. Let $\boldsymbol{x}(\boldsymbol{a}, \tau)$ be the position, relative to the center-of-mass, of the fluid particle identified by the labeling coordinates $\boldsymbol{a}$ at time τ. We

shall distinguish between the time coordinates τ and t. These are equal in value, but partial derivatives with respect to τ are at constant $\boldsymbol{a}$, whereas those with respect to t are at constant $\boldsymbol{x}$—in other words, $\partial/\partial\tau$ corresponds to a convective derivative. There is considerable freedom in the choice of labeling coordinates, but it is convenient to choose them so that they are related to the mass density of the fluid by

$$\rho = \frac{\partial(\boldsymbol{a})}{\partial(\boldsymbol{x})} \ . \tag{4.1}$$

It should be noted that this just corresponds to the choice of a constant mass for the fluid particles (i.e., the mass density of the fluid is directly proportional to the number density of particles). This has the advantage that mass conservation is implicit in our choice of $\boldsymbol{a}$, as can be verified by a direct application of $\partial/\partial\tau$ to (4.1):

$$\frac{\partial\rho}{\partial\tau} + \rho\nabla\cdot\boldsymbol{u} = 0 \ , \tag{4.2}$$

where $\boldsymbol{u} \equiv \partial\boldsymbol{x}/\partial\tau$, ∇ is the gradient operator in $\boldsymbol{x}$-space, and we have used the fact that the inverse of a matrix $\mathbf{A}$ may be written as

$$A^{-1}_{ji} = \frac{\partial \ln\|\mathbf{A}\|}{\partial A_{ij}} \ , \tag{4.3}$$

where $\|\mathbf{A}\| \equiv \det(\mathbf{A})$. We can now write down the Lagrangian for the fluid as

$$L_* = \int d\boldsymbol{a} \ \left[\frac{1}{2}\left(\frac{\partial\boldsymbol{R}_*}{\partial\tau} + \frac{\partial\boldsymbol{x}}{\partial\tau}\right)^2 - \mathcal{E}\left(\frac{\partial(\boldsymbol{x})}{\partial(\boldsymbol{a})}, S(\boldsymbol{a})\right) - \Phi(\boldsymbol{x})\right] \ , \tag{4.4}$$

where $\boldsymbol{R}_*$ is the location of the center-of-mass, Φ is the potential for external forces, and $\mathcal{E}$ is the specific internal energy which is a prescribed function of the specific volume ρ^{-1} and the specific entropy S. Note that S depends only on the labeling

coordinates $\boldsymbol{a}$.[1] This is, in essence, the perfect fluid approximation:

$$\frac{\partial S}{\partial \tau} = 0 \ .$$

It can be shown that the variation with respect to $\boldsymbol{x}$ of (4.4) yields the Euler equation (see Appendix A).

For computational purposes, it is more convenient to rewrite (4.4) in Eulerian form. This is straightforward to accomplish by noting that the time-dependent map $\boldsymbol{x} = \boldsymbol{x}(\boldsymbol{a}, \tau)$ uniquely determines the inverse map $\boldsymbol{a} = \boldsymbol{a}(\boldsymbol{x}, t)$. Therefore, the requirement that the action be stationary under arbitrary variations $\delta\boldsymbol{x}$ in the forward map is equivalent to the requirement that the action be stationary under variations $\delta\boldsymbol{a}$ in the inverse map. After dropping two total time derivatives, we can now write the fluid Lagrangian as

$$L_* = \frac{1}{2} M_* \dot{\boldsymbol{R}}_*^2 + \int d\boldsymbol{x} \left\{ \rho \left[\frac{1}{2} \boldsymbol{u} \cdot \boldsymbol{u} - \mathcal{E}\left(\rho, S(\boldsymbol{a})\right) - \Phi(\boldsymbol{x}) \right] + \frac{\partial \rho}{\partial t} \boldsymbol{x} \cdot \dot{\boldsymbol{R}}_* \right\} \ , \tag{4.5}$$

where M_* is the total mass of the fluid. However, before we can consider the variation with respect to $\boldsymbol{a}$ of (4.5), we must express the velocity $\boldsymbol{u}$ as a function of $\boldsymbol{a}$ and its derivatives. Alternatively, we can include the relevant relations as constraints in the Lagrangian and then vary $\boldsymbol{u}$ and $\boldsymbol{a}$ independently. The required relations are given by

$$0 = \frac{\partial \boldsymbol{a}}{\partial \tau} = \frac{\partial \boldsymbol{a}}{\partial t} + \left(\boldsymbol{u} \cdot \nabla\right) \boldsymbol{a} \tag{4.6}$$

which are the so-called *Lin constraints*. We may also include mass conservation (4.2) as a constraint in the Eulerian form (4.5) of the Lagrangian. This gives us

$$\begin{aligned} L_* = \frac{1}{2} M_* \dot{\boldsymbol{R}}_*^2 + \int d\boldsymbol{x} \Bigg\{ & \rho \left[\frac{1}{2} \boldsymbol{u} \cdot \boldsymbol{u} - \mathcal{E}\left(\rho, S(\boldsymbol{a})\right) - \Phi(\boldsymbol{x}) - \boldsymbol{\zeta} \cdot \frac{\partial \boldsymbol{a}}{\partial \tau} \right] \\ & + \phi \left[\frac{\partial \rho}{\partial t} + \nabla \cdot (\rho \boldsymbol{u}) \right] + \frac{\partial \rho}{\partial t} \boldsymbol{x} \cdot \dot{\boldsymbol{R}}_* \Bigg\} \ , \end{aligned} \tag{4.7}$$

[1] It follows that any transformation of the labeling coordinates which leaves the density and the entropy unchanged is a symmetry of the system. Vorticity conservation can be shown to follow as a consequence of this 'particle re-labeling' symmetry. See Salmon (1988) for details.

where $\boldsymbol{\zeta}$ and ϕ are Lagrange multipliers, and we now consider the independent variations $\delta\boldsymbol{u}$, $\delta\boldsymbol{a}$, $\delta\boldsymbol{\zeta}$, $\delta\rho$, and $\delta\phi$.

The $\boldsymbol{u}$ variation of (4.7) yields

$$\boldsymbol{u} = \zeta_i \nabla a_i + \nabla\phi \ , \tag{4.8}$$

which can be used to eliminate $\boldsymbol{u}$ from the Lagrangian. After dropping a time derivative and integrating one term by parts, (4.7) becomes

$$\begin{aligned} L_* = \frac{1}{2} M_* \dot{\boldsymbol{R}}_*^2 - \int d\boldsymbol{x} \left\{ \rho \left[\boldsymbol{\zeta} \cdot \frac{\partial \boldsymbol{a}}{\partial t} + \frac{\partial \phi}{\partial t} + \frac{1}{2} \boldsymbol{u} \cdot \boldsymbol{u} + \mathcal{E}\left(\rho, S(\boldsymbol{a})\right) + \Phi \right] \right. \\ \left. - \frac{\partial \rho}{\partial t} \boldsymbol{x} \cdot \dot{\boldsymbol{R}}_* \right\} \ , \end{aligned} \tag{4.9}$$

where $\boldsymbol{u}$ is now just an abbreviation for (4.8), and the independent variations $\delta\boldsymbol{a}$, $\delta\boldsymbol{\zeta}$, $\delta\rho$ and $\delta\phi$ are to be considered.

So far, we have neglected the effects of self-gravitation, considering Φ to be an externally imposed potential. We may now incorporate self-gravity in our formalism by including the Lagrangian for Newtonian gravitation. Our most general perfect-fluid Lagrangian is then

$$\begin{aligned} L_* = \frac{1}{2} M_* \dot{\boldsymbol{R}}_*^2 - \int d\boldsymbol{x} \left\{ \rho \left[\boldsymbol{\zeta} \cdot \frac{\partial \boldsymbol{a}}{\partial t} + \frac{\partial \phi}{\partial t} + \frac{1}{2} \boldsymbol{u} \cdot \boldsymbol{u} + \mathcal{E}\left(\rho, S(\boldsymbol{a})\right) + \Psi + \Phi \right] \right. \\ \left. + \frac{1}{8\pi G} \nabla\Psi \cdot \nabla\Psi - \frac{\partial \rho}{\partial t} \boldsymbol{x} \cdot \dot{\boldsymbol{R}}_* \right\} \ , \end{aligned} \tag{4.10}$$

where Ψ is the self-gravitational potential, and the independent variations are $\delta\boldsymbol{a}$, $\delta\boldsymbol{\zeta}$, $\delta\rho$, $\delta\phi$, and $\delta\Psi$. If the external potential Φ is due to the gravitational field of a point-mass M_0, then the Lagrangian for the whole system, in the center-of-momentum

frame, becomes

$$L = \frac{1}{2}\mu\dot{\boldsymbol{R}}^2 + \int d\boldsymbol{x}\,\rho\frac{GM_0}{|\boldsymbol{x}-\boldsymbol{R}|} - \int d\boldsymbol{x}\left\{\rho\left[\boldsymbol{\zeta}\cdot\frac{\partial\boldsymbol{a}}{\partial t} + \frac{\partial\phi}{\partial t} + \frac{1}{2}\boldsymbol{u}\cdot\boldsymbol{u} + \mathcal{E}\left(\rho, S(\boldsymbol{a})\right) + \Psi\right] + \frac{1}{8\pi G}\nabla\Psi\cdot\nabla\Psi + \frac{M_0}{M}\frac{\partial\rho}{\partial t}\boldsymbol{x}\cdot\dot{\boldsymbol{R}}\right\}, \tag{4.11}$$

where $\boldsymbol{R} \equiv \boldsymbol{R}_0 - \boldsymbol{R}_*$ is the orbital separation vector, $M \equiv M_0 + M_*$ is the total mass, and $\mu \equiv M_0 M_*/M$ is the reduced mass. This Lagrangian is valid for arbitrary perfect fluid flows.[2]

4.1.2 Homentropic Potential Flow

The variation of (4.11) with respect to $\boldsymbol{a}$ gives us

$$\frac{\partial\boldsymbol{\zeta}}{\partial\tau} = \frac{\partial\mathcal{E}}{\partial S}\frac{\partial S}{\partial\boldsymbol{a}}\ . \tag{4.12}$$

We now derive the conditions on $\boldsymbol{\zeta}$ for a homentropic potential flow. By definition, the velocity field for a potential flow has the representation $\boldsymbol{u} = \nabla\chi'$ for some arbitrary scalar potential χ'. Defining a new potential χ such that $\chi' = \chi + \phi$, the velocity field can be written as

$$\boldsymbol{u} = \nabla\chi + \nabla\phi = \frac{\partial\chi}{\partial a_i}\nabla a_i + \nabla\phi\ .$$

Comparing this expression with (4.8), we find that, for a potential flow,

$$\zeta_i = \frac{\partial\chi}{\partial a_i}\ . \tag{4.13}$$

[2]It is, in fact, possible to generalize our variational formulation to include non-adiabatic flows. One way to achieve this is by considering the entropy content as a separate fluid constituent with its own velocity. Thus, effectively, entropy is treated as a gas whose particles correspond to thermal excitations (e.g., phonons). It is precisely the possibility of different velocities for the matter and entropy constituents that allows non-adiabaticity in the flow. We do not consider this possibility to avoid being overly general. More details and references may be found in Prix (2004).

We now note that for a homentropic fluid it follows from (4.12) that $\chi(\boldsymbol{a},\tau)=\chi_1(\boldsymbol{a})+\chi_2(\tau)$. Therefore, after substituting (4.13), we find that the Lagrangian (4.11) takes the form

$$\begin{aligned}L=&\frac{1}{2}\mu\dot{\boldsymbol{R}}^2+\int d\boldsymbol{x}\,\rho\frac{GM_0}{|\boldsymbol{x}-\boldsymbol{R}|}\\&-\int d\boldsymbol{x}\left\{\rho\left[\frac{\partial(\chi_1+\phi)}{\partial t}+\frac{1}{2}[\nabla(\chi_1+\phi)]^2+\mathcal{E}(\rho)+\Psi\right]\right.\\&\left.+\frac{1}{8\pi G}\nabla\Psi\cdot\nabla\Psi+\frac{M_0}{M}\frac{\partial\rho}{\partial t}\boldsymbol{x}\cdot\dot{\boldsymbol{R}}\right\}.\end{aligned}$$

Since χ_1 and ϕ only appear as the combination $\chi_1+\phi$, we can re-define $\chi_1+\phi\to\phi$ to obtain

$$\begin{aligned}L=&\frac{1}{2}\mu\dot{\boldsymbol{R}}^2\\&-\int d\boldsymbol{x}\left\{\rho\left[\frac{\partial\phi}{\partial t}+\frac{1}{2}\nabla\phi\cdot\nabla\phi+\mathcal{E}(\rho)+\Psi-\frac{GM_0}{|\boldsymbol{x}-\boldsymbol{R}|}\right]\right.\\&\left.+\frac{1}{8\pi G}\nabla\Psi\cdot\nabla\Psi+\frac{M_0}{M}\frac{\partial\rho}{\partial t}\boldsymbol{x}\cdot\dot{\boldsymbol{R}}\right\}.\end{aligned}\tag{4.14}$$

It follows from our method of construction that all homentropic potential flows can be derived from (4.14) with ϕ as the velocity potential.

The conservative nature of gravitational forces guarantees that, in the absence of dissipation, tidal excitation will not generate vorticity. Therefore, if the fluid starts out with zero vorticity then the flow will always remain irrotational. We can therefore use (4.14) for problems involving non-rotating, homentropic stars such as cold white dwarfs. From here onwards we shall assume this to be the case.

4.2 Equations of Motion and Normal Modes

4.2.1 Equations of Motion

We consider the perturbations to ϕ, Ψ, and ρ around a static, spherically symmetric equilibrium fluid configuration:

$$\begin{aligned}\phi(\boldsymbol{x},t) &= \phi_0(r) + \phi_1(\boldsymbol{x},t) \ , \\ \Psi(\boldsymbol{x},t) &= \Psi_0(r) + \Psi_1(\boldsymbol{x},t) \ , \\ \rho(\boldsymbol{x},t) &= \rho_0(r) + \rho_1(\boldsymbol{x},t) \ ,\end{aligned}$$

where $r \equiv |\boldsymbol{x}|$. Retaining terms up to quadratic order in the perturbations, we can separate the Lagrangian as

$$L = L_0 + L_1 + L_2 \ , \tag{4.15}$$

where L_0 describes the equilibrium configuration, L_2 describes the structure of the perturbations, and L_1 describes the orbit-perturbation interaction. After making the perturbative expansion, we obtain

$$\begin{aligned}L_0 = &\frac{1}{2}\mu\dot{\boldsymbol{R}}^2 + \frac{GM_0M_*}{R} \\ &- \int d\boldsymbol{x} \left[\rho_0\mathcal{E}_0 + \rho_0\Psi_0 + \frac{1}{8\pi G}\left(\frac{d\Psi_0}{dr}\right)^2\right] \ ,\end{aligned} \tag{4.16}$$

$$\begin{aligned}L_1 = -\int d\boldsymbol{x} \Bigg\{ &\rho_0\left(\dot{\phi}_1 + \Psi_1\right) \\ &+ \rho_1\left(h_0 + \Psi_0 - \frac{GM_0}{|\boldsymbol{x}-\boldsymbol{R}|}\right) \\ &+ \frac{1}{4\pi G}\frac{d\Psi_0}{dr}\frac{\partial\Psi_1}{\partial r} + \frac{M_0}{M}\dot{\rho}_1\boldsymbol{x}\cdot\dot{\boldsymbol{R}}\Bigg\} \ ,\end{aligned} \tag{4.17}$$

$$\begin{aligned}L_2 = -\int d\boldsymbol{x} \Bigg\{ &\rho_1\left(\dot{\phi}_1 + \Psi_1\right) + \frac{1}{2}\frac{c_s^2}{\rho_0}\rho_1^2 \\ &+ \frac{1}{2}\rho_0\nabla\phi_1\cdot\nabla\phi_1 + \frac{1}{8\pi G}\nabla\Psi_1\cdot\nabla\Psi_1\Bigg\} \ ,\end{aligned} \tag{4.18}$$

where $R \equiv |\boldsymbol{R}|$, and h_0 and c_s are the unperturbed specific enthalpy and adiabatic sound speed, respectively. The variations of L_0 with respect to $\boldsymbol{R}$, ρ_0, and Ψ_0 yield

$$\mu \ddot{\boldsymbol{R}} = -\frac{GM_0M_*}{R^2}\hat{\boldsymbol{R}} \ , \tag{4.19}$$

$$h_0 + \Psi_0 = 0, \tag{4.20}$$

$$\frac{1}{r^2}\frac{d}{dr}\left(r^2\frac{d\Psi_0}{dr}\right) = 4\pi G\rho_0 \ , \tag{4.21}$$

where $\hat{\boldsymbol{R}}$ is a unit vector. Together with the equation of state for the fluid, (4.19)–(4.21) determine the unperturbed configuration.

To determine the equations for the perturbations, we consider the variations of L with respect to ϕ_1, ρ_1 and Ψ_1. These give us

$$\dot{\rho}_1 + \nabla\cdot(\rho_0\nabla\phi_1) = 0 \ , \tag{4.22}$$

$$\dot{\phi}_1 + \frac{c_s^2}{\rho_0}\rho_1 + \Psi_1 = \frac{GM_0}{|\boldsymbol{x}-\boldsymbol{R}|} + \frac{M_0}{M}\boldsymbol{x}\cdot\ddot{\boldsymbol{R}} \ , \tag{4.23}$$

$$\nabla^2\Psi_1 = 4\pi G\rho_1 \ . \tag{4.24}$$

It is straightforward to show that, with $M_0 = 0$, (4.22)–(4.24) are the conventional equations for the normal modes of a non-rotating, homentropic star (see Section 4.2.2 below).

The equation for the orbit, including the back reaction of the perturbations, is obtained by considering the variation of L with respect to $\boldsymbol{R}$:

$$\mu\ddot{\boldsymbol{R}} = -\frac{GM_0M_*}{R^2}\hat{\boldsymbol{R}} + \frac{\partial}{\partial\boldsymbol{R}}\int d\boldsymbol{x}\,\frac{GM_0\rho_1}{|\boldsymbol{x}-\boldsymbol{R}|} \ , \tag{4.25}$$

where we have used the fact that

$$\int d\boldsymbol{x}\ \rho_1\boldsymbol{x} = 0$$

(this is equivalent to choosing the origin of the coordinates $\boldsymbol{x}$ to be the center-of-mass of the fluid).

4.2.2 Normal Modes

We expand $|\boldsymbol{x}-\boldsymbol{R}|^{-1}$, ϕ_1, ρ_1, and Ψ_1 in terms of spherical harmonics:

$$\frac{1}{|\boldsymbol{x}-\boldsymbol{R}|} = \sum_{\ell,m} \frac{4\pi}{2\ell+1}\frac{r^\ell}{R^{\ell+1}} Y^*_{\ell m}(\hat{\boldsymbol{R}}) Y_{\ell m}(\hat{\boldsymbol{x}}) \ ,$$
$$\phi_1(\boldsymbol{x},t) = \sum_{\ell,m} \phi_{\ell m}(r,t) Y_{\ell m}(\hat{\boldsymbol{x}}) \ ,$$

and likewise for ρ_1 and Ψ_1. After inserting the expansions and integrating over angular coordinates, (4.22)–(4.24) become

$$\dot{\rho}_{\ell m} + \frac{1}{r^2}\frac{\partial}{\partial r}\left(r^2\rho_0\frac{\partial\phi_{\ell m}}{\partial r}\right) - \frac{\ell(\ell+1)}{r^2}\rho_0\phi_{\ell m} = 0 \ , \tag{4.26}$$

$$\begin{aligned}\dot{\phi}_{\ell m} + \frac{c_s^2}{\rho_0}\rho_{\ell m} + \Psi_{\ell m} = &-\frac{GM_0}{R}\frac{4\pi}{2\ell+1}\left(\frac{r}{R}\right)^\ell Y^*_{\ell m}(\hat{\boldsymbol{R}}) \\ &+ \delta_{\ell,1}\frac{4\pi}{3}\frac{M_0}{M} r|\ddot{\boldsymbol{R}}| Y^*_{\ell m}(\hat{\ddot{\boldsymbol{R}}}) \ ,\end{aligned} \tag{4.27}$$

$$\frac{1}{r^2}\frac{\partial}{\partial r}\left(r^2\frac{\partial\Psi_{\ell m}}{\partial r}\right) - \frac{\ell(\ell+1)}{r^2}\Psi_{\ell m} = 4\pi G\rho_{\ell m} \ . \tag{4.28}$$

The first term on the right hand side of (4.27) is a forcing term that couples the modes to the gravitational potential of the point-mass. The second term is only present for dipolar modes and cancels the first term for that case. Thus, dipolar modes are not tidally excited. This is to be expected since the origin of the coordinates $\boldsymbol{x}$ is the center-of-mass of the fluid.

The temporal Fourier transforms of (4.26)–(4.28), with $M_0 = 0$, give

$$\left[\frac{1}{r^2}\frac{d}{dr}r^2\rho_0\frac{d}{dr} - \frac{\ell(\ell+1)}{r^2}\rho_0\right]\tilde{\phi}_{\ell m} = -\mathrm{i}\omega\tilde{\rho}_{\ell m}, \tag{4.29}$$

$$\mathrm{i}\omega\tilde{\phi}_{\ell m} + \frac{c_s^2}{\rho_0}\tilde{\rho}_{\ell m} + \tilde{\Psi}_{\ell m} = 0, \tag{4.30}$$

$$\left[\frac{1}{r^2}\frac{d}{dr}r^2\frac{d}{dr} - \frac{\ell(\ell+1)}{r^2}\right]\tilde{\Psi}_{\ell m} = 4\pi G\tilde{\rho}_{\ell m} \ , \tag{4.31}$$

where $\tilde{\rho}_{\ell m}$, $\tilde{\phi}_{\ell m}$ and $\tilde{\Psi}_{\ell m}$ are the temporal Fourier transforms of $\rho_{\ell m}$, $\phi_{\ell m}$, and $\Psi_{\ell m}$, respectively. We can use (4.30) to eliminate $\tilde{\rho}_{\ell m}$ from (4.29) and (4.31). This yields

the two second-order equations

$$\left[\frac{1}{r^2\rho_0}\frac{d}{dr}r^2\rho_0\frac{d}{dr}-\frac{\ell(\ell+1)}{r^2}+\frac{\omega^2}{c_s^2}\right]\tilde{\phi}_{\ell m}=\mathrm{i}\frac{\omega}{c_s^2}\tilde{\Psi}_{\ell m}\ , \tag{4.32}$$

$$\left[\frac{1}{r^2}\frac{d}{dr}r^2\frac{d}{dr}-\frac{\ell(\ell+1)}{r^2}+\frac{4\pi G\rho_0}{c_s^2}\right]\tilde{\Psi}_{\ell m}=-\mathrm{i}\frac{4\pi G\rho_0\omega}{c_s^2}\tilde{\phi}_{\ell m}\ . \tag{4.33}$$

With the definitions

$$\eta_1\equiv\frac{1}{\mathrm{i}\omega r}\frac{d\tilde{\phi}_{\ell m}}{dr}\ , \qquad \eta_2\equiv\frac{\omega}{\mathrm{i}gr}\tilde{\phi}_{\ell m}\ ,$$

$$\eta_3\equiv\frac{1}{gr}\tilde{\Psi}_{\ell m}\ , \qquad \eta_4\equiv\frac{1}{g}\frac{d\tilde{\Psi}_{\ell m}}{dr}\ ,$$

(cf. Dziembowski, 1971) and

$$U\equiv\frac{d\ln\mathcal{M}}{d\ln r}\ , \qquad V\equiv-\frac{d\ln P_0}{d\ln r}\ ,$$

$$\Gamma_1\equiv\left(\frac{\partial\ln P}{\partial\ln\rho}\right)_s\ , \qquad C\equiv\frac{M_*}{\mathcal{M}}\left(\frac{r}{R_*}\right)^3\ ,$$

$$\sigma^2\equiv\frac{R_*^3}{GM_*}\omega^2\ ,$$

where

$$\mathcal{M}(r)\equiv\int_0^r dr'\,4\pi r'^2\rho_0(r')\ ,$$

$$g(r)\equiv\frac{G\mathcal{M}(r)}{r^2}\ ,$$

and after some manipulation, (4.32) and (4.33) give the four first-order equations

$$r\frac{d\eta_1}{dr}=\left(\frac{V}{\Gamma_1}-3\right)\eta_1+\left[\frac{\ell(\ell+1)}{\sigma^2C}-\frac{V}{\Gamma_1}\right]\eta_2+\frac{V}{\Gamma_1}\eta_3\ , \tag{4.34}$$

$$r\frac{d\eta_2}{dr}=\sigma^2C\eta_1+(1-U)\eta_2\ , \tag{4.35}$$

$$r\frac{d\eta_3}{dr}=(1-U)\eta_3+\eta_4\ , \tag{4.36}$$

$$r\frac{d\eta_4}{dr}=\frac{UV}{\Gamma_1}\eta_2+\left[\ell(\ell+1)-\frac{UV}{\Gamma_1}\right]\eta_3-U\eta_4\ . \tag{4.37}$$

These are the conventional equations for the normal mode structure of a non-rotating, homentropic star (cf. Cox, 1980; Kippenhahn & Weigert, 1990).

To have a well-posed problem, we need to specify four boundary conditions. At the center of the star, we require that the variables η_i be well-behaved. Expanding in a power series around $r = 0$, we have

$$\eta_i = \sum_{\alpha=0}^{\infty} A_\alpha^{(i)} r^\alpha \ .$$

Substituting into (4.34)–(4.37), and using the facts that

$$\lim_{r\to 0} U = 3 \ ,$$
$$\lim_{r\to 0} V = 0 \ ,$$
$$\lim_{r\to 0} C = \text{constant} \ ,$$

we find that the only non-vanishing coefficients correspond to $\alpha = \ell - 2$, and

$$\ell\eta_2 = \sigma^2 C\eta_1 \ , \tag{4.38}$$
$$\eta_4 = \ell\eta_3 \ , \tag{4.39}$$

which constitute our boundary conditions at the center. At the surface, we require that $\Psi_{\ell m}$ satisfy the Laplace equation. This gives

$$\eta_4 = -(\ell + 1)\eta_3 \ , \tag{4.40}$$

at $r = R_*$, as our third boundary condition. Finally, from (4.34) and using the condition that

$$\lim_{r\to R_*} V = \frac{GM_*}{R_*} \lim_{r\to R_*} \frac{\rho_0}{P_0} = \infty$$

(cf. Cox, 1980), we get a fourth boundary condition that

$$\eta_2 = \eta_1 + \eta_3 \ , \tag{4.41}$$

at the surface. Together with the boundary conditions (4.38)–(4.41), (4.34)–(4.37) constitute an eigenvalue problem for the normal modes.

We now turn to the problem of determining the physical displacement of fluid elements from the unperturbed configuration in terms of the η_i. Expanding $\tilde{\phi}_1$ (the temporal Fourier transform of the perturbation to ϕ) in terms of the normal modes, we have

$$\tilde{\phi}_1 = \sum_{n,\ell,m} \frac{\tilde{x}_{n\ell m}(\omega)}{R_*} \tilde{\phi}_{n\ell m}(r) Y_{\ell m}(\hat{\boldsymbol{x}}) \ ,$$

where $\tilde{\phi}_{n\ell m}$ is a normalized eigenfunction, and we use the subscript n to distinguish between the various modes corresponding to the same ℓ, m. Using the fact that $\dot{\boldsymbol{\xi}} = \nabla\phi_1$, where $\boldsymbol{\xi}$ is the physical displacement of fluid elements, we find

$$\tilde{\boldsymbol{\xi}}(\boldsymbol{x},\omega) = \sum_{n,\ell,m} \frac{\tilde{x}_{n\ell m}(\omega)}{R_*} \hat{\boldsymbol{\xi}}_{n\ell m}(\boldsymbol{x}) \ , \tag{4.42}$$

where

$$\hat{\boldsymbol{\xi}}_{n\ell m}(\boldsymbol{x}) \equiv \left(r\eta_1 \hat{\boldsymbol{x}} + \frac{r^2}{\sigma^2 C} \eta_2 \nabla \right) Y_{\ell m}(\hat{\boldsymbol{x}}) \ .$$

The displacement field $\boldsymbol{\xi}(\boldsymbol{x},t)$ is just the temporal inverse Fourier transform of (4.42).

Note that by taking the gradient of (4.23), it is straightforward to see that the normal modes $\hat{\boldsymbol{\xi}}_{n\ell m}$ satisfy

$$\left[\nabla \left(\frac{c_s^2}{\rho_0} \rho_1 + \Psi_1 \right) \right] (\hat{\boldsymbol{\xi}}_{n\ell m}) = \omega_{n\ell m}^2 \hat{\boldsymbol{\xi}}_{n\ell m} \ ,$$

where the left hand side is a linear, spatial operator:

$$\mathcal{D}(\boldsymbol{\xi}) \equiv \nabla \left[-\frac{c_s^2}{\rho_0} \nabla \cdot (\rho_0 \boldsymbol{\xi}) + G \int d\boldsymbol{x}' \, \frac{\nabla' \cdot (\rho_0' \boldsymbol{\xi}')}{|\boldsymbol{x}' - \boldsymbol{x}|} \right] \ , \tag{4.43}$$

where we have used (4.47) and (4.24) to write ρ_1 and Ψ_1 in terms of $\boldsymbol{\xi}$. It can be proved that the operator $\mathcal{D}$ is Hermitian with respect to mass (Chandrasekhar, 1964; Cox, 1980). Its eigenvalues are therefore guaranteed to be real, and it is generally assumed that its eigenfunctions (the normal modes) form a complete orthogonal set. One

possible choice of normalization for the eigenfunctions, used by Press & Teukolsky (1977), is to normalize the modes by mass:

$$\int d\boldsymbol{x}\, \rho_0 \hat{\boldsymbol{\xi}}^*_{j'} \cdot \hat{\boldsymbol{\xi}}_j = \delta_{j,j'} \tag{4.44}$$

(we shall often use a single index such as j as shorthand for the set of indices required to specify a mode uniquely). However, for us it is more convenient to choose the normalization so that

$$\eta_1(R_*) = 1 \ , \tag{4.45}$$

and to define an effective mode mass:

$$M_j \equiv \frac{1}{R_*^2} \int d\boldsymbol{x}\, \rho_0 |\hat{\boldsymbol{\xi}}_j|^2 \ . \tag{4.46}$$

With this normalization, the $\hat{\boldsymbol{\xi}}_j$ have dimensions of length, and the mode amplitudes are dimensionless. Furthermore, the amplitude of a mode provides a measure of mode non-linearity.

4.2.3 Displacement Formulation

It is convenient to write the equations for tidal excitation in terms of the normal mode displacements (amplitudes, in common usage). Let $\boldsymbol{\xi}$ be the physical displacement field of fluid elements within the star. Integrating (4.22) with respect to time and setting the integration constant to zero, we get

$$\rho_1 = -\nabla \cdot (\rho_0 \boldsymbol{\xi}). \tag{4.47}$$

Taking the gradient of (4.23), we have

$$\ddot{\boldsymbol{\xi}} + \mathcal{D}(\boldsymbol{\xi}) = \nabla \left(\frac{GM_0}{|\boldsymbol{x} - \boldsymbol{R}|} \right) + \frac{M_0}{M} \ddot{\boldsymbol{R}} \ . \tag{4.48}$$

Expanding $\boldsymbol{\xi}$ as

$$\boldsymbol{\xi}(\boldsymbol{x},t) = \sum_j \frac{x_j(t)}{R_*}\hat{\boldsymbol{\xi}}_j(\boldsymbol{x}) \tag{4.49}$$

in (4.48), and then projecting out a single mode gives

$$\ddot{x}_j + \omega_j^2 x_j = \frac{f_j(\boldsymbol{R})}{M_j} + \frac{M_0}{MM_j}\frac{\ddot{\boldsymbol{R}}}{R_*}\cdot\int d\boldsymbol{x}\,\rho_0\hat{\boldsymbol{\xi}}_j^* \ , \tag{4.50}$$

where

$$f_j(\boldsymbol{R}) \equiv \frac{GM_0}{R_*}\int d\boldsymbol{x}\,\rho_0\hat{\boldsymbol{\xi}}_j^*\cdot\nabla\left(\frac{1}{|\boldsymbol{x}-\boldsymbol{R}|}\right) \ . \tag{4.51}$$

This is just a forced, harmonic oscillator with natural frequency ω_j. The second term on the right side of (4.50) is non-zero only for for monopolar (i.e., radial) modes and cancels the first term for that case. This is a mathematical statement of the fact that monopolar modes are not tidally excited. It is convenient to rewrite the overlap integral f_j by performing an integration by parts and using (4.24):

$$f_j(\boldsymbol{R}) = -\frac{M_0}{R_*}\Psi_j^*(\boldsymbol{R}) \ .$$

Using the solution to the Laplace equation in spherical coordinates with boundary conditions at $r = R_*$ set by the variable η_3 for mode j, we get

$$f_j(\boldsymbol{R}) = -\frac{GM_0M_*}{R_*^2}\eta_{3j}(R_*)\left(\frac{R_*}{R}\right)^{\ell+1}Y_{\ell m}^*(\hat{\boldsymbol{R}}) \ . \tag{4.52}$$

In terms of coordinates in the plane of the orbit, this can be written as

$$f_j(\boldsymbol{R}) = -\frac{GM_0M_*}{R_*^2}\eta_{3j}(R_*)Y_{\ell m}\left(\frac{\pi}{2},0\right)\left(\frac{R_*}{R}\right)^{\ell+1}\mathrm{e}^{-\mathrm{i}mu} \ , \tag{4.53}$$

where u is the angular coordinate.

Expanding Ψ_1 in terms of Ψ_j, the equation for the orbit, (4.25), becomes

$$\mu\ddot{\boldsymbol{R}} = -\frac{GM_0M_*}{R^2}\hat{\boldsymbol{R}} + \sum_j x_j\frac{\partial}{\partial\boldsymbol{R}}f_j^*(\boldsymbol{R}) \ . \tag{4.54}$$

4.3 Conservation Laws

To find the conserved energy E, we calculate the time-time component of the energy-momentum tensor from (4.15) using

$$T^i{}_j = \frac{\partial \mathcal{L}}{\partial(\partial_i q_k)} \partial_j q_k - \delta^i{}_j \mathcal{L} \ , \tag{4.55}$$

where $\mathcal{L}$ is the Lagrangian density, and q_k are the generalized fields. A straightforward evaluation gives

$$\begin{aligned} E &= \int d\boldsymbol{x}\, T^t{}_t \\ &= \frac{1}{2}\mu \dot{\boldsymbol{R}}^2 - \frac{GM_0M_*}{R} - GM_0 \int d\boldsymbol{x}\, \frac{\rho_1}{|\boldsymbol{x}-\boldsymbol{R}|} \\ &+ \frac{1}{2}\int d\boldsymbol{x} \left(\rho_0 \nabla\phi_1 \cdot \nabla\phi_1 + \frac{c_s^2}{\rho_0}\rho_1^2 + \rho_1 \Psi_1 \right) , \end{aligned} \tag{4.56}$$

where we have used (4.24) to eliminate the gravitational self-energy of the perturbations. The total energy is the sum of three components: orbital, perturbation, and coupling. The various pieces are easily identified in (4.56), which, if written in terms of the canonical momenta, also corresponds to the Hamiltonian for the system (e.g., Barut, 1980).

We can, without loss of generality, assume the orbit to be in the equatorial plane. The conserved angular momentum L_z can then be calculated from the appropriate component of the energy-momentum tensor as

$$\begin{aligned} L_z &= \int d\boldsymbol{x}\, T^t{}_\varphi \\ &= \mu R^2 \dot{u} - \int d\boldsymbol{x}\, \rho_1 \frac{\partial \phi_1}{\partial \varphi} \ , \end{aligned} \tag{4.57}$$

where φ and u are the azimuthal coordinates associated with $\boldsymbol{x}$ and $\boldsymbol{R}$, respectively.

It may be noted that the canonical form (4.55) of the energy-momentum tensor is not manifestly symmetric. However, it is well-known that the tensor can be made

symmetric by the addition of a suitable divergence term:

$$T'^{ij} = T^{ij} + \frac{\partial}{\partial x^k}\psi^{ijk} \ , \qquad \psi^{ijk} = -\psi^{ikj} \ .$$

We do not need to do this since integral quantities such as (4.56) and (4.57) are unaffected by such a transformation (Landau & Lifshitz, 1975).

The energy and angular momentum associated with the normal modes also take on relatively simple forms in terms of the time-dependent displacements x_j. From (4.56), we know that the energy associated with perturbations is

$$E_1 = \frac{1}{2}\int d\boldsymbol{x} \ \left[\rho_0 \dot{\boldsymbol{\xi}}\cdot\dot{\boldsymbol{\xi}} + \rho_1\left(\frac{c_s^2}{\rho_0}\rho_1 + \Psi_1\right)\right] \ . \tag{4.58}$$

Substituting (4.47) into (4.58) and then integrating the second term in the integrand by parts gives

$$E_1 = \frac{1}{2}\int d\boldsymbol{x}\, \rho_0 \left[\dot{\boldsymbol{\xi}}\cdot\dot{\boldsymbol{\xi}} + \boldsymbol{\xi}\cdot\nabla\left(\frac{c_s^2}{\rho_0}\rho_1 + \Psi_1\right)\right] \ .$$

Note that the second term in the integrand now involves the same linear operator that we used to define the normal modes. Expanding $\boldsymbol{\xi}$ as in (4.49) and using the orthonormality relation (4.46), we find that the energy associated with mode j is just

$$E_j = \frac{1}{2}M_j^2\left(|\dot{x}_j|^2 + \omega_j^2|x_j|^2\right) \ . \tag{4.59}$$

From (4.57) and (4.47), we know that the angular momentum associated with perturbations is

$$L_z^{\rm pert} = \int d\boldsymbol{x}\, \nabla\cdot(\rho_0\boldsymbol{\xi})\,\frac{\partial\phi_1}{\partial\varphi} \ .$$

Performing an integration by parts, we get

$$L_z^{\rm pert} = -\int d\boldsymbol{x}\, \rho_0\boldsymbol{\xi}\cdot\frac{\partial\dot{\boldsymbol{\xi}}}{\partial\varphi} \ . \tag{4.60}$$

Once again expanding $\boldsymbol{\xi}$ as in (4.49), using (4.46), and the fact that

$$\frac{\partial \hat{\boldsymbol{\xi}}_j}{\partial \varphi} = \mathrm{i}m\hat{\boldsymbol{\xi}}_j \ ,$$

we find that the angular momentum associated with mode j is just

$$L_j = -\mathrm{i}mM_j x_j^* \dot{x}_j \ . \tag{4.61}$$

We shall now derive a simple relation between the energy and angular momentum associated with an isolated mode (i.e., with $f_j = 0$). In that case, from (4.50) we have $x_j(t) \propto e^{\mathrm{i}\omega_j t}$. Therefore, from (4.59) and (4.61) we get

$$\frac{E_j}{L_j} = \frac{\omega_j^2 |x_j|^2}{m\omega_j |x_j|^2} = \frac{\omega_j}{m} \ . \tag{4.62}$$

This relation is to be expected on physical grounds as follows. If we consider tidally exciting the mode at resonance in a circular orbit, then the rate at which energy is transferred to the mode is just

$$\frac{dE_j}{dt} = \tau\Omega = \frac{dL_j}{dt}\frac{\omega_j}{m} \ ,$$

where τ is the torque exerted by the perturbing mass, and Ω is the orbital frequency. Integrating this equation with respect to time and setting the initial mode energy and angular momentum to zero, we obtain (4.62).

Finally, the conserved energy (4.56) and angular momentum (4.57), written in terms of the amplitudes, are

$$E = \frac{1}{2}\mu\dot{\boldsymbol{R}}^2 - \frac{GM_0M_*}{R} - \sum_j x_j f_j^*(\boldsymbol{R}) + \frac{1}{2}\sum_j M_j \left(|\dot{x}_j|^2 + \omega_j^2 |x_j|^2\right) \ , \tag{4.63}$$

and

$$L_z = \mu R^2 \dot{u} - \sum_j \mathrm{i}mM_j x_j^* \dot{x}_j \ . \tag{4.64}$$

4.4 Summary

As the azimuthal 'quantum' number m does not appear anywhere in the eigenvalue problem for the normal modes, modes with the same n and ℓ are degenerate in frequency and have identical radial eigenfunctions. This is a direct consequence of ignoring stellar rotation, which breaks this degeneracy. Thus far, we have been dealing with complex mode displacements because the mode eigenfunctions are complex. Specifically, the complex displacements are necessary because of our use of complex spherical harmonics as the angular eigenfunctions (this is only true for $m \neq 0$; the $m = 0$ displacements are always real). It is cumbersome to expand a real function such as the density perturbation in terms of a complex basis. To avoid this, we will re-formulate our results in terms of real basis functions, which will make the displacements real as well. Because of the degeneracy of the (n, ℓ) subspace, we can rotate our basis within each such subspace to form real combinations of the spherical harmonics:

$$\hat{\boldsymbol{\xi}}^{(\mathrm{e})}_{n,\ell,m} \equiv \begin{cases} \hat{\boldsymbol{\xi}}_{n,\ell,0} \ , & m = 0 \\ \dfrac{1}{\sqrt{2}}(\hat{\boldsymbol{\xi}}_{n,\ell,m} + \hat{\boldsymbol{\xi}}^{*}_{n,\ell,m}) \ , & m > 0 \end{cases} , \tag{4.65}$$

$$\hat{\boldsymbol{\xi}}^{(\mathrm{o})}_{n,\ell,m} \equiv \begin{cases} 0 \ , & m = 0 \\ \dfrac{1}{\mathrm{i}\sqrt{2}}(\hat{\boldsymbol{\xi}}_{n,\ell,m} - \hat{\boldsymbol{\xi}}^{*}_{n,\ell,m}) \ , & m > 0 \end{cases} , \tag{4.66}$$

where now only positive values of m are to be considered. The relations between the real and complex displacements follow from the above definitions:

$$x^{(\mathrm{e})}_{n,\ell,m} = \frac{1}{\sqrt{2}} \left[x_{n,\ell,m} + (-1)^m x_{n,\ell,-m} \right] \ , \tag{4.67}$$

$$x^{(\mathrm{o})}_{n,\ell,m} = \frac{\mathrm{i}}{\sqrt{2}} \left[x_{n,\ell,m} - (-1)^m x_{n,\ell,-m} \right] \ , \tag{4.68}$$

where the factors of $(-1)^m$ enter because of the Condon-Shortley phase convention (e.g., Arfken & Weber, 1995). From now on we shall use the real eigenfunctions

exclusively. For economy of notation, we will only note the $^{(e)}$ (even) and $^{(o)}$ (odd) distinctions when necessary.

It will also be convenient for us to work with dimensionless quantities whenever possible. Therefore, we shall adopt the 'natural' units: M_*, R_*, and ω_*^{-1}, where

$$\omega_* \equiv \sqrt{\frac{GM_*}{R_*^3}} \ . \tag{4.69}$$

Occasionally, we shall also make use of the definition

$$\beta_* \equiv \frac{1}{c}\sqrt{\frac{GM_*}{R_*}} \ . \tag{4.70}$$

Unless stated otherwise, all dynamical quantities will be measured in these units.

In terms of the displacements of the real eigenfunctions, the Hamiltonian (conserved energy) and the conserved angular momentum, in natural units, are:

$$H = \frac{p_R^2}{2\mu} + \frac{p_u^2}{2\mu R^2} - \frac{q}{R} + \sum_j \left(\frac{p_j^2}{2M_j} + \frac{1}{2} M_j \omega_j^2 x_j^2 \right) - \sum_j x_j f_j \ , \tag{4.71}$$

and

$$L_z = p_u + \sum_j m \left[x_j^{(e)} p_j^{(o)} - x_j^{(o)} p_j^{(e)} \right] \ , \tag{4.72}$$

where $q \equiv M_0/M_*$ is the mass ratio, and $p_R = \mu \dot{R}$, $p_u = \mu R^2 \dot{u}$, and $p_j = M_j \dot{x}_j$ are the momenta conjugate to R, u, and x_j, respectively. Note that the reduced mass in the natural units is $\mu = q/(1+q)$. We therefore see that the Hamiltonian is comprised of three pieces: the Keplerian terms for the orbit, a sum of harmonic oscillators for the normal modes, and a sum of terms of the form $x_j f_j$ which couple the modes and the orbit. The overlap integral f_j therefore plays a dual role as a forcing function for tidal excitation, and in the disturbing function for the orbit. This is not surprising, since the system is conservative. Hence, any energy and angular momentum transferred to the tides must necessarily be extracted from the orbit. In natural units, the overlap

integral is

$$f_j(\boldsymbol{R}) = \frac{q\eta_j}{R^{\ell+1}} \left\{ \begin{array}{c} \cos(mu) \\ \sin(mu) \end{array} \right. \quad , \tag{4.73}$$

where we have defined

$$\eta_j \equiv -\eta_{3j}(R_*) Y_{\ell m}\left(\frac{\pi}{2}, 0\right) \quad , \tag{4.74}$$

and the bracket notation denotes that either $\cos(mu)$ or $\sin(mu)$ will be present (corresponding to the even and odd components, respectively).

Chapter 5

Resonances Without Back Reaction

5.1 Preliminaries

5.1.1 Simple Harmonic Oscillator

Consider an undamped simple harmonic oscillator with natural frequency ω_0 and displacement $x(t)$ subject to an external force per unit mass $F(t)$. The equation of motion,

$$\ddot{x} + \omega_0^2 x = F(t) \ , \tag{5.1}$$

can be easily solved to get

$$\dot{x}(t) = \Re\left[\zeta(t)\right] \ , \tag{5.2}$$

$$x(t) = \frac{1}{\omega_0}\Im\left[\zeta(t)\right] \ , \tag{5.3}$$

where

$$\zeta(t) = e^{\mathrm{i}\omega_0 t}\left[\zeta_0 + \zeta_1(t)\right] \ , \tag{5.4}$$

and

$$\zeta_1(t) \equiv \int_{t_0}^{t} dt'\, e^{-\mathrm{i}\omega_0 t'} F(t') \ . \tag{5.5}$$

Choosing $t_0 = -\infty$, and for late times, we have

$$\lim_{t\to\infty} \zeta_1 = \tilde{F}(\omega_0) \ , \tag{5.6}$$

where $\tilde{F}(\omega_0)$ is the Fourier transform of $F(t)$ evaluated at the resonant frequency. It follows from the expressions for x and $\dot{x}$ in terms of ζ that the total energy per unit mass of the oscillator as a function of time is given by

$$E(t) = \frac{1}{2}\left|\zeta(t)\right|^2 = \frac{1}{2}\left[\left|\zeta_0\right|^2 + \left|\zeta_1\right|^2 + 2\left|\zeta_0\right|\left|\zeta_1\right|\cos(\phi - \phi_0)\right] \ , \tag{5.7}$$

where ϕ_0 and ϕ are the phases of ζ_0 and ζ_1, respectively. Hence, asymptotically,

$$E = E_0 + \varepsilon + 2\sqrt{E_0\varepsilon}\cos\psi \ , \tag{5.8}$$

where $E_0 \equiv \left|\zeta_0\right|^2/2$ is the initial energy, $\varepsilon \equiv |\tilde{F}(\omega_0)|^2/2$, and ψ is an initial phase. The presence of the ψ-dependent term reflects the fact that the oscillator may gain or lose energy, depending upon its initial energy and the relative phasing with the driver near resonance. If we perform an ensemble average over initial phases , assuming a uniform distribution, we find that the average energy transfer is given by

$$\langle \Delta E \rangle = \varepsilon \ . \tag{5.9}$$

It is also clear that, for $E_0 \ll \varepsilon$, the initial phase is unimportant and the actual energy transfer will be very close to the average. The possibility of negative energy transfer only exists when

$$E_0 > \frac{\varepsilon}{4\cos^2\psi} \ .$$

Note that, since the energy of the oscillator cannot be negative, it must be true that $\Delta E \geqslant -E_0$. It can be shown that (5.8) complies with this constraint.

Let the external force per unit mass now be of the form

$$F(t) = F_0(t)\cos\left[\phi(t)\right] \ ,$$

with the amplitude F_0 and frequency $\dot{\phi}$ being slowly varying functions of time, and $\ddot{\phi} > 0$. Resonance occurs when the relative phase of the driver and the oscillator becomes stationary. This gives us the condition $\dot{\phi}(t) = \omega_0$. We assume that there is only one passage through resonance, and restrict our attention to the resonant energy transfer. Let $t_{\rm R}$ be the time when the resonance condition is satisfied, and expand the driver in a Taylor series around this point:

$$F(t_{\rm R}+\tau) \simeq F_0(t_{\rm R}) \cos\left[\phi(t_{\rm R}) + \omega_0\tau + \ddot{\phi}(t_{\rm R})\frac{\tau^2}{2}\right] \ . \tag{5.10}$$

(Since the amplitude varies slowly with time, to lowest order, we can take the amplitude as constant through the resonance.) With the definitions

$$F_{\rm R} \equiv F_0(t_{\rm R}) \ , \quad \phi_{\rm R} \equiv \phi(t_{\rm R}) \ , \quad \alpha \equiv \frac{\ddot{\phi}(t_{\rm R})}{\omega_0^2} \ ,$$

this becomes

$$F(t_{\rm R}+\tau) \simeq F_{\rm R} \cos\left(\phi_{\rm R} + \omega_0\tau + \alpha\frac{\omega_0^2\tau^2}{2}\right) \ . \tag{5.11}$$

The parameter α has the physical interpretation of being a measure of the fractional change in frequency over a characteristic period of oscillation. The requirement that the frequency of the driver is varying slowly therefore implies $\alpha \ll 1$. In other words, the driver can be considered harmonic with a well-defined frequency over several periods of the oscillator. We can also view α as a measure of the phase 'drift'—i.e., a measure of how fast the driver accumulates additional phase. With this interpretation, it is easy to see that the time spent near resonance is given by $(\alpha\omega_0^2)^{-1/2}$, approximately.

Evaluating the Fourier transform of (5.11) at ω_0, we find that the energy per unit mass changes asymptotically by

$$\Delta E = \frac{\pi F_{\rm R}^2}{4\alpha\omega_0^2}\left(1 + 2\sqrt{\frac{E_0}{\pi F_{\rm R}^2/4\alpha\omega_0^2}}\cos\psi\right) \ . \tag{5.12}$$

Qualitatively, the velocity is in quadrature with the force well away from resonance,

Mass ($M_\odot$)	Radius (10^8 cm)	ω_{f2} (ω_*)	M_{f2} ($10^{-2}\ M_*$)	$\eta_{3,f2}(R_*)/\eta_{1,f2}(R_*)$	Θ_{f2}
0.6	8.83	1.53	2.05	-0.169	9.6×10^7
1.0	5.71	1.65	1.28	-0.124	8.0×10^6
1.4	1.98	1.97	0.25	-0.0412	1.5×10^5

Table 5.1: Homogeneous, cold white dwarf models with $\mu_e = 2$, and properties of their quadrupolar f-modes.

but the relative phase of the two becomes approximately stationary near resonance for a time interval $\sim (\alpha\omega_0^2)^{-1/2}$, and there is a velocity change $\sim F_{\rm R}(\alpha\omega_0^2)^{-1/2}$.

Simple, linear damping is conventionally treated by adding a term $2\gamma\dot{x}$ to the left side of (5.1). When $\gamma \ll (\alpha\omega_0^2)^{1/2}$, the development of the oscillation will be uninfluenced by damping, although the energy of the oscillation will be converted steadily into heat. However, when the damping is effective on the time-scale of energy transfer, the amplitude of the oscillation will be reduced. Nonetheless, it can be shown that the energy that appears ultimately as heat is still given by (5.12), independent of γ, as long as $\gamma \ll \omega_0$ (see, for example, Landau & Lifshitz, 1969).

5.1.2 White Dwarf Oscillations

We confine our attention to homogeneous, non-rotating white dwarfs where the pressure is contributed solely by cold, degenerate electrons. Thermal corrections, Coulomb effects, as well as compositional discontinuities are ignored. The relevant equations of stellar structure are described in Kippenhahn & Weigert (1990). We consider three cases with masses 0.6, 1.0, 1.4 $M_\odot$ for $\mu_e = 2$. Some relevant properties are given in Table 5.1.

The linear theory of normal modes for a cold white dwarf has been reviewed in Chapter 4, and more details can be found in standard references (e.g., Cox, 1980; Kippenhahn & Weigert, 1990). The most important modes for our purpose are the quadrupolar f-modes. For a non-rotating star, the five f-modes with $\ell = 2$ are degenerate in frequency. The eigenfrequencies for our three white dwarf models are given in Table 5.1. The radial eigenfunctions for the $0.6\,M_\odot$ model are displayed in

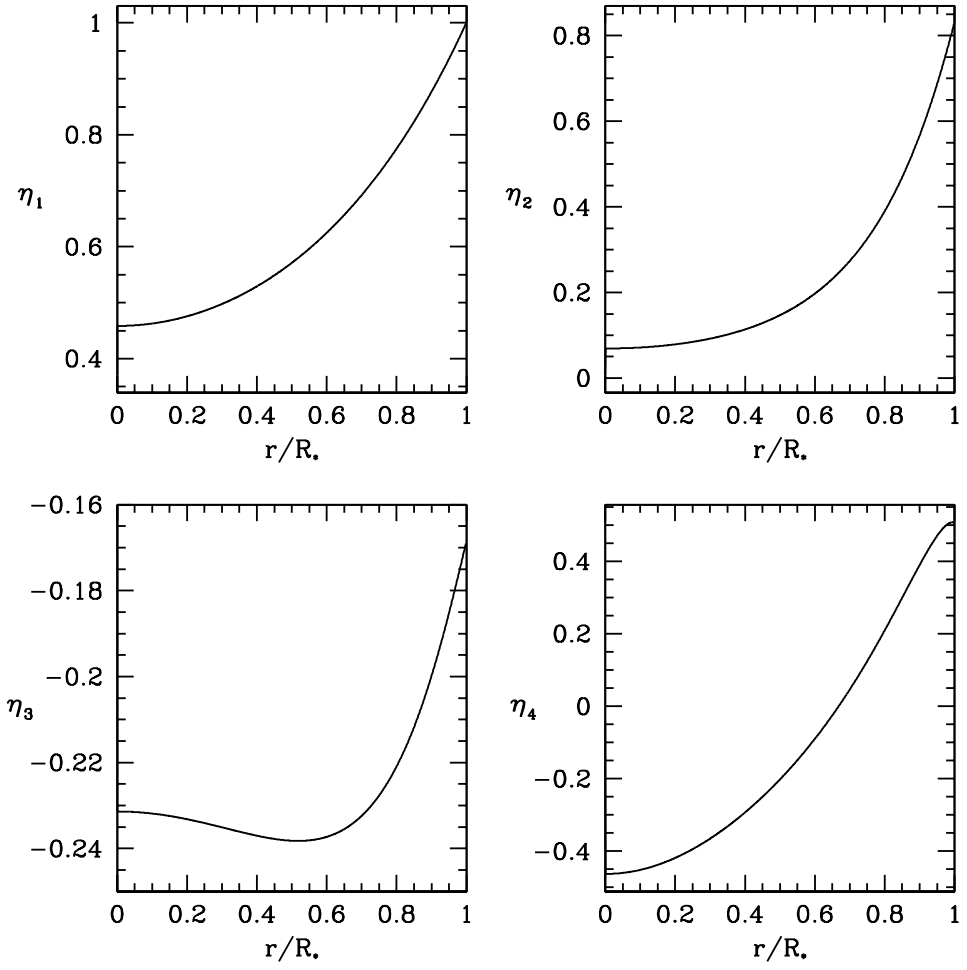

Figure 5.1: Radial eigenfunctions of quadrupolar f-modes for the $0.6\,M_\odot$ model from Table 5.1.

Figure 5.1. The eigenfunctions for the other white dwarf models are qualitatively similar.

5.1.3 Gravitational Radiation

We adopt a Newtonian approach to gravitational radiation reaction in the two-body problem, neglecting all finite-size effects. Namely, we treat the problem as essentially Keplerian with prescribed corrections to the orbital equations. For non-relativistic orbits ($v \lesssim 0.2c$), the secular corrections due to gravitational radiation are provided

to a fair approximation by the orbit-averaged expressions

$$\frac{dE_{\rm orb}}{dt} = -\frac{32}{5} E_* \omega_* \frac{q^2}{(1+q)^{2/3}} \beta_*^5 \left(\frac{n}{\omega_*}\right)^{10/3} \mathcal{F}_1(e) \ , \tag{5.13}$$

$$\frac{dL_{\rm orb}}{dt} = -\frac{32}{5} E_* \frac{q^2}{(1+q)^{2/3}} \beta_*^5 \left(\frac{n}{\omega_*}\right)^{7/3} \mathcal{F}_2(e) \tag{5.14}$$

(Peters, 1964), where $E_{\rm orb}$ and $L_{\rm orb}$ are the orbital energy and angular momentum, q is the ratio of the companion mass to the white dwarf mass, n is the Keplerian orbital frequency, e is the orbital eccentricity, and

$$\mathcal{F}_1(e) \equiv \frac{1}{(1-e^2)^{7/2}} \left(1 + \frac{73}{24} e^2 + \frac{37}{96} e^4\right) \ ,$$

$$\mathcal{F}_2(e) \equiv \frac{1}{(1-e^2)^2} \left(1 + \frac{7}{8} e^2\right) \ .$$

We can re-express the orbital evolution in terms of changes in the orbital frequency and eccentricity:

$$\frac{dn}{dt} = \frac{96}{5} \omega_*^2 \frac{q}{(1+q)^{1/3}} \beta_*^5 \left(\frac{n}{\omega_*}\right)^{11/3} \mathcal{F}_1(e) \ , \tag{5.15}$$

$$\frac{de}{dt} = -\frac{304}{15} \omega_* \frac{q}{(1+q)^{1/3}} \beta_*^5 \left(\frac{n}{\omega_*}\right)^{8/3} \mathcal{F}_3(e) \ , \tag{5.16}$$

where

$$\mathcal{F}_3(e) \equiv \frac{e}{(1-e^2)^{5/2}} \left(1 + \frac{121}{304} e^2\right) \ .$$

If gravitational radiation is the only mechanism for orbital evolution, then it follows from these equations that

$$\dot{e} = -\mathcal{G}(e) \frac{\dot{n}}{n} \ , \tag{5.17}$$

where

$$\mathcal{G}(e) \equiv \frac{19}{18} \frac{\mathcal{F}_3(e)}{\mathcal{F}_1(e)} \ .$$

Finally, we can integrate the above equation to get

$$\frac{n(e)}{n(0.54101)} = \frac{(1-e^2)^{3/2}}{e^{18/19}} \left(1 + \frac{121}{304} e^2\right)^{-1305/2299} \quad . \tag{5.18}$$

As the orbit shrinks, it circularizes, eventually according to $e \propto n^{-1}$, approximately.

For a more accurate treatment of gravitational radiation (especially for high eccentricities), and for the inclusion of other general relativistic effects, corrections to the orbital acceleration can be added directly to the equations of motion. Detailed derivations and discussions of these corrections can be found in the literature (e.g. Iyer & Will, 1995), and we shall not reproduce them here.

It should be noted that it is not necessary to worry about relativistic apsidal precession as it will only affect neglected higher-order terms.

5.1.4 Equations of Motion

Neglecting gravitational radiation, the Hamiltonian for the system is given by (4.71). Hamilton's equations for this system are

$$\ddot{x}_j + \omega_j^2 x_j = \frac{f_j}{M_j} \ , \tag{5.19}$$

$$\dot{p}_R = \frac{p_u^2}{\mu R^3} - \frac{q}{R^2} + x_j \frac{\partial f_j}{\partial R} \ , \tag{5.20}$$

$$\dot{p}_u = x_j \frac{\partial f_j}{\partial u} \ . \tag{5.21}$$

The terms involving the derivatives of f_j give the perturbation of the orbit due to the excitation of tides, and we therefore refer to them as the back reaction terms. As was shown in Chapter 4, the overlap integral f_j can be written as

$$f_j(\boldsymbol{R}) = \frac{q\eta_j}{R^{\ell+1}} \begin{cases} \cos(mu) \\ \sin(mu) \end{cases} \quad . \tag{5.22}$$

It will be useful for us to write f_j in yet another way. From the usual Keplerian relation between the orbital frequency n and the semi-major axis a, it follows that

$$f_j = \frac{q\eta_j}{(1+q)^{(\ell+1)/3}} n^{2(\ell+1)/3} \left(\frac{a}{R}\right)^{\ell+1} \begin{cases} \cos(mu) \\ \sin(mu) \end{cases} .$$

We now make use of the Fourier expansion

$$\left(\frac{R}{a}\right)^p \exp(imv) = \sum_{k=-\infty}^{\infty} X_k^{p,m}(e) \exp(\mathrm{i}kl) ,$$

where v is the true anomaly, l is the mean anomaly (not to be confused with ℓ), and the Fourier coefficients $X_k^{p,m}$ (called Hansen coefficients; see Appendix B) are real functions of the eccentricity. Noting that $u = v + \varpi$, where ϖ is the longitude of periapse, we have

$$\left(\frac{a}{R}\right)^{\ell+1} \begin{cases} \cos(mu) \\ \sin(mu) \end{cases} = \sum_{k=-\infty}^{\infty} X_k^{-(\ell+1),m}(e) \begin{cases} \cos(kl + m\varpi) \\ \sin(kl + m\varpi) \end{cases} . \tag{5.23}$$

The overlap integral f_j is therefore given by

$$f_j = \sum_{k=0}^{\infty} f_{jk} \tag{5.24}$$

where

$$\begin{aligned} f_{jk} = {} & \frac{q\eta_j}{(1+q)^{(\ell+1)/3}} n^{2(\ell+1)/3} \\ & \times \begin{cases} \left[X_{jk}^{+} \cos(kl + m\varpi) + X_{jk}^{-} \cos(kl - m\varpi)\right] \\ \left[X_{jk}^{+} \sin(kl + m\varpi) - X_{jk}^{-} \sin(kl - m\varpi)\right] \end{cases} , \end{aligned} \tag{5.25}$$

and we have used the shorthand $X_{jk}^{\pm} \equiv X_{\pm k}^{-(\ell+1),m}$, for economy of notation. It should be understood in the expression for f_{jk} that, for $k = 0$, only the X_{jk}^{+} terms are present. For $k > 0$, the $X_{jk}^{\pm}$ terms can be combined using trigonometric identities. However, it is simpler to note that, since $X_k^{p,m} \propto e^{|k-m|}$, to lowest order in eccentricity, the

X^-_{jk} terms will be suppressed by $2m$ powers of eccentricity relative to the X^+_{jk} terms. Therefore, for low to moderate eccentricities ($\lesssim 0.6$) and $m > 0$, the X^-_{jk} terms can be neglected to a good approximation. For the case $m = 0$, the $X^\pm_{jk}$ terms are identical. Hence, in all that follows, for $m = 0$ one only needs to make the change $X^+_{jk} \rightarrow 2X^+_{jk}$.

From the preceding discussion, we know that the driving function f_j for the excitation of a particular mode is an infinite sum of f_{jk} terms. The phases that appear in the expression (5.25) for f_{jk} are all of the form $kl \pm m\varpi$. Thus, there exists the possibility of resonance whenever the relative phase of the mode and one of these terms is stationary: $\dot{w}_j = k\dot{l} \pm m\dot{\varpi}$, where w_j is the phase of the mode. As mentioned previously, the $kl - m\varpi$ terms will be suppressed by $2m$ powers of eccentricity relative to the $kl + m\varpi$ terms. Thus, the dominant resonances will occur for $\dot{w}_j = k\dot{l} + m\dot{\varpi}$. It might be thought that the above condition is equivalent to $\omega_j = kn$, but, in general, this is not the case. As the evolution of the orbit is dependent upon the tides via the back reaction terms in the equations of motion, there are complicated, non-linear dependencies implicit in each of the variables in the resonance condition. However, since we expect the orbital corrections to be relatively small, it should be true that, at resonance, $\omega_j \simeq kn$.

5.2 Physical Considerations

5.2.1 The Tidal Limit

Clearly, our formalism for treating the evolution of a WDCO binary as a dynamical interaction between the orbit and the tides is only valid if the white dwarf is not tidally disrupted. In other words, we require that the white dwarf does not fill its Roche lobe. This requirement constrains the harmonics of the orbital frequency that a given mode can interact resonantly with. To quantify the constraint, we use the following approximation to the radius of the Roche lobe:

$$\frac{r_{\rm R}}{R} = \frac{0.49q^{-2/3}}{0.6q^{-2/3} + \ln(1 + q^{-1/3})}$$

(Eggleton, 1983). It then follows that we require

$$k \gtrsim \frac{2.92\omega_j}{(1-e)^{3/2}} \frac{\left[0.6 + q^{2/3}\ln(1+q^{-1/3})\right]^{3/2}}{(1+q)^{1/2}} \ , \tag{5.26}$$

where we have made use of the facts that the orbital separation at periapse is $a(1-e)$, and that $\omega_j \simeq kn$ at resonance. It should be mentioned that we have implicitly assumed that the companion is more compact than the white dwarf, and hence is not disrupted. This is certainly true when the companion is a neutron star or a black hole. However, for the white dwarf-white dwarf case, the actual constraint is provided by the star that is disrupted first, which may be the companion.

It should also be mentioned that the above approximation for the radius of the Roche lobe is for circular, synchronous orbits. A more general treatment of the Roche problem may modify the tidal disruption regime. This is a possibility for future investigation.

5.2.2 Importance of the $\ell = m = 2$ *f*-Mode

The lowest ℓ modes that can be excited tidally are $\ell = 2$. Modes with higher values of ℓ will have smaller overlap integrals, since $f_j \propto R^{-(\ell+1)}$. We may therefore infer that the primary modes that are excited outside the Roche limit are the $\ell = 2$ modes. It is also the case that, with our choice of coordinates, the $m = 1$ modes will not be excited. This is easily seen by remembering that $\eta_j \propto P_\ell^m(0)$, and

$$P_\ell^m(0) = \begin{cases} (-1)^{(\ell-m)/2} \dfrac{(\ell+m-1)!!}{(\ell-m)!!} \ , & \ell+m \text{ even} \\ 0 \ , & \ell+m \text{ odd} \end{cases}$$

(see, for example, Arfken & Weber, 1995). Therefore, the only $\ell = 2$ modes that are excited have $m = 0, 2$. Furthermore, since $X_k^{p,m} \propto e^{|k-m|}$, the $m = 0$ modes will be suppressed by two powers of eccentricity relative to the $m = 2$ modes. Hence, we deduce that the dominant modes for low to moderate eccentricities will have $\ell = m = 2$. Also, since the p-mode frequencies increase monotonically with the radial

order, we can access (before tidal disruption) the lowest harmonic resonances for the modes with lowest radial order–the f-modes.

Putting together the above considerations, we conclude that the mode excited with the largest amplitude in a cold white dwarf will be the $\ell = m = 2$ f-mode. Note that in a warm star, g-modes can also be excited. These will have lower frequencies than the f-modes, and their frequencies will decrease monotonically with the radial order. However, the structure of g-modes is sensitive to assumptions about the stellar model. If the modes are confined to surface layers, then the overlap integrals will be essentially zero, and the modes will not be excited tidally.

5.2.3 Mode Damping

The formalism that we have presented in Section 5.1 does not include any mode damping. In a realistic scenario, white dwarf oscillations will damp out over sufficiently long periods of time. While we shall mention some possible mechanisms through which this might occur, we make no attempt to provide an exhaustive analysis as there is an extensive literature that exists for this problem.

Some possible mechanisms that have been considered for the damping of nonradial white dwarf oscillations include gravitational radiation, neutrino losses due to pycnonuclear reactions, and radiative heat leakage (Osaki & Hansen, 1973). The relative importance of each mechanism depends on the type of mode under consideration, but it was demonstrated by Osaki & Hansen (1973) that the dominant damping mechanism for quadrupolar f- and p-modes, in the linear regime, is gravitational radiation. However, their calculation contains a numerical error. We present a corrected derivation in Appendix C.

Another possible mechanism for the damping of modes with large amplitudes is by non-linear coupling to other modes. This has been explored extensively in various contexts (e.g. Dziembowski, 1982; Kumar & Goodman, 1996; Wu & Goldreich, 2001), and it has been shown that non-linear mode interactions can be important amplitude limiting effects. For now, we ignore this complication because it is, in fact, one of our

goals to study whether such non-linear amplitudes can be excited by passage through a sequence of tidal resonances in a WDCO binary. The non-linear evolution of large amplitude modes on a white dwarf is the subject of Part III.

In stars with compositional discontinuities or solid interiors, turbulence may be excited at boundaries, which can lead to additional dissipation.

5.2.4 Time-Scales

For the long-term evolution of a WDCO binary, there are several time-scales of interest to us. The first of these is the gravitational radiation inspiral time, which, for a circular orbit, is given by

$$T_{\rm GR} = \frac{5}{256}\frac{(1+q)^{1/3}}{q}\beta_*^{-5}n^{-8/3}$$

(Peters, 1964). For an eccentric orbit with a given period, this time is shorter by up to a factor of 1000 for eccentricities up to 0.9. For eccentricities $\lesssim 0.5$, however, the circular orbit inspiral time is a fair approximation.

The second relevant time-scale is the mode damping time. In general, the damping times for quadrupolar f-modes depend upon the white dwarf mass. Assuming gravitational radiation as the mechanism, the damping time (as derived in Appendix C) is given by

$$T_j = 6\pi\beta_*^{-5}\eta_{3j}^{-2}(R_*)M_j\omega_j^{-4}\ .$$

For our 0.6 $M_\odot$ and 1.0 $M_\odot$ models, this gives ~ 3000 and ~ 100 years, respectively. Note that these are necessarily underestimates since our cold white dwarf models are highly centrally condensed. In contrast, the damping times for 'moderately realistic' 0.4 $M_\odot$ and 1.0 $M_\odot$ models used by Osaki & Hansen (1973) are about 2.8×10^5 and 500 years, respectively. The damping times are therefore quite sensitive to the stellar model.

Finally, the third time-scale of interest is the white dwarf cooling time. A rough

estimate for this is provided by

$$T_{\rm cool} = \frac{4.7 \times 10^7 \text{ years}}{A} \left(\frac{M_*/M_\odot}{L_*/L_\odot} \right)^{5/7}$$

(Kippenhahn & Weigert, 1990), where A is the atomic mass, and L_* is the white dwarf luminosity. For typical parameters, this gives a cooling time of $\sim 10^9$ years, which is much longer than any other relevant time-scale. We can therefore ignore the thermal evolution of the white dwarf.

In order for mode damping via gravitational radiation to be physically unimportant during the long-term evolution of a WDCO system, it is necessary that $T_j > T_{\rm GR}$. In other words, we require that the damping between resonances is negligible during the gravitational inspiral. This gives us the following constraint on the harmonics that we can consider for a particular mode:

$$k \lesssim \left[\frac{1536\pi}{5} \frac{q}{(1+q)^{1/3}} \eta_{3j}^{-2}(R_*) M_j \omega_j^{-4/3} \right]^{3/8} , \tag{5.27}$$

where we have used the expressions for T_j and $T_{\rm GR}$ given above, and have also made use of $\omega_j \simeq kn$ at resonance. For our 0.6 $M_\odot$ white dwarf model and mass ratios greater than a few, this constraint evaluates to

$$k \lesssim 11 \left(\frac{M_0}{M_\odot} \right)^{1/4} .$$

Note that, for moderate to high eccentricities, this is overly restrictive, and the actual limit obtained from an evaluation of the inspiral time for eccentric orbits is higher.

5.3 Resonant Energy Transfer

Let us now consider a mode being excited resonantly on a white dwarf in an eccentric orbit around a compact companion. We shall neglect the back reaction terms in the equations of motion, and hence the orbit can be taken to be Keplerian with corrections due to gravitational radiation (the validity of the no back reaction approximation

will be discussed in Section 5.4.1). We assume that we start exciting the mode resonantly at $t = 0$, and limit our analysis to the regime $\dot{n}t/n \ll 1$, where $\dot{n}$ is given by (5.15). This is not particularly restrictive since the gravitational radiation timescale is typically much longer than the resonance time-scale. Finally, we shall also assume low to moderate eccentricities ($\sim 0 - 0.5$), and hence neglect the X^-_{jk} terms in (5.25).

With the above assumptions, we can expand the orbital elements and phases in (5.25) in Taylor series around resonance (retaining only the zeroth-order term in the amplitude) to obtain

$$f_{jk} = \frac{q\eta_j}{(1+q)^{(\ell+1)/3}} n^{2(\ell+1)/3} X^+_{jk} \begin{cases} \cos\left(\phi_{jk} + \omega_j t + k\dot{n}t^2\right) \\ \sin\left(\phi_{jk} + \omega_j t + k\dot{n}t^2\right) \end{cases} , \tag{5.28}$$

where ϕ_{jk} is an initial phase. We now note that (5.28) is exactly of the form of (5.11), with the identifications

$$F_R = \frac{q\eta_j}{M_j(1+q)^{(\ell+1)/3}} n^{2(\ell+1)/3} X^+_{jk} ,$$
$$\omega_0 = \omega_j, \quad \alpha\omega_0^2 = 2k\dot{n}$$

(the division by M_j in F_R is necessary since it is f_j/M_j that appears on the right hand side of (5.19)). We can therefore immediately write down the resonant energy transfer:

$$\langle \Delta E_{jk} \rangle = \frac{5\pi}{768} \frac{q}{(1+q)^{(2\ell+1)/3}} \left(\frac{\eta_j^2}{\beta_*^5 M_j}\right) n^{(4\ell-7)/3} \frac{\left(X^+_{jk}\right)^2}{k\mathcal{F}_1} , \tag{5.29}$$

where we have averaged over initial phases. Using the fact that $\omega_j \simeq kn$ at resonance, we find

$$\langle \Delta E_{jk} \rangle = \frac{q}{(1+q)^{(2\ell+1)/3}} \Theta_j \Xi_{jk}(e) , \tag{5.30}$$

where the parameter

$$\Theta_j \equiv \frac{5\pi}{768} \left[\frac{\eta_j^2 \omega_j^{(4\ell-7)/3}}{\beta_*^5 M_j}\right] \tag{5.31}$$

depends only upon the white dwarf model and the mode, and

$$\Xi_{jk}(e) \equiv \frac{k^{-4(\ell-1)/3}}{\mathcal{F}_1} \left(X_{jk}^{+}\right)^2 \tag{5.32}$$

contains all the dependence upon the eccentricity and the harmonic. The values of the parameter Θ_j for our 0.6 $M_\odot$, 1.0 $M_\odot$, and 1.4 $M_\odot$ white dwarf models are given in Table 5.1. We see that the energy transfer decreases monotonically (relative to the star's binding energy) with the mass. As $\Xi_{jk}(e) \propto e^{2(k-m)}$, to lowest order in eccentricity, the energy transfer is typically a very sensitive function of the eccentricity. Also, for a circular orbit, it is clear that only the fundamental resonance, $k = m$, exists (as would be expected on physical grounds). We remind the reader that, for $m \neq 0$, the energy transfer given by (5.30) is for a particular choice of even or odd component of the mode. It should therefore be multiplied by a factor of two to obtain the total energy transfer to the even-odd mode pair.

5.4 Discussion

5.4.1 Regime of Validity

We now consider in what regime, if any, the no back reaction approximation is valid. Qualitatively, we expect back reaction to change the orbital frequency as a mode is excited resonantly, which will tend to push the system away from resonance. Clearly, this will modulate the energy transfer at some level. However, if the change in orbital frequency is small compared to the resonance width, then we expect that the modulation of energy transfer will not be significant. On the other hand, if the change in orbital frequency is comparable to or larger than the resonance width, then back reaction will play a significant role. Another way of saying this is that the modulation of the energy transfer by back reaction is a second-order effect. Therefore, as long as the energy transfer is small enough, we are justified in ignoring back reaction. We

can quantify this criterion by defining a resonance parameter

$$\chi_{jk} \equiv \frac{\Delta n_{jk}}{\Delta n_k^{\rm res}} \ , \tag{5.33}$$

where Δn_{jk} is what the change in kn would be if the energy given by (5.30) were to be taken out of the orbit, and $\Delta n_k^{\rm res}$ is the resonance width. In general, we expect that for $\chi_{jk} \ll 1$ back reaction will not play a significant role in modulating the energy transfer, where as for $\chi_{jk} \gtrsim 1$ back reaction will be important. Using the estimate $\Delta n_k^{\rm res} \approx (2k\dot{n})^{1/2}$, we find

$$\chi_{jk} = \sqrt{\frac{5}{3}} \frac{5\pi}{2048} \frac{1}{q^{1/2}(1+q)^{(4\ell-1)/6}} \left[\frac{\eta_j^2 \omega_j^{(8\ell-23)/6}}{\beta_*^{15/2} M_j} \right] \frac{k^{-(4\ell-7)/3}}{\mathcal{F}_1^{3/2}} \left(X_{jk}^+ \right)^2 \ . \tag{5.34}$$

Figure 5.2 shows the numerical integration across a particular resonance for various values of χ_{jk}, both with and without back reaction. The first qualitative feature that stands out is that the energy transfer with back reaction tends to be smaller than that without back reaction. This is not surprising since the system with back reaction is expected to spend less time near resonance. Quantitatively, we see that for this particular resonance with $\chi_{jk} \lesssim 0.1$ we obtain nearly identical numerical results with and without back reaction, with $\chi_{jk} \sim 0.1$ the results differ by a factor of order unity (about 2), and with $\chi_{jk} \sim 1$ the energy transfers differ by an order of magnitude.

The delineation of the back reaction and no back reaction regimes in the eccentricity-harmonic plane obtained with the above criterion for a quadrupolar f-mode on a 0.6 $M_\odot$ white dwarf and various companion masses is shown in Figure 5.3. It is seen that the region of parameter space where back reaction may be neglected, according to the χ_{jk} criterion, grows with the companion mass. There is, however, a reason to think that back reaction might actually play an important role in some regions of the parameter space where the χ_{jk} criterion indicates otherwise.

Consider the following thought experiment. Imagine that we are approaching a resonance with an initial phase that would lead to a net negative energy transfer in the no back reaction approximation. As we start removing energy from the mode and

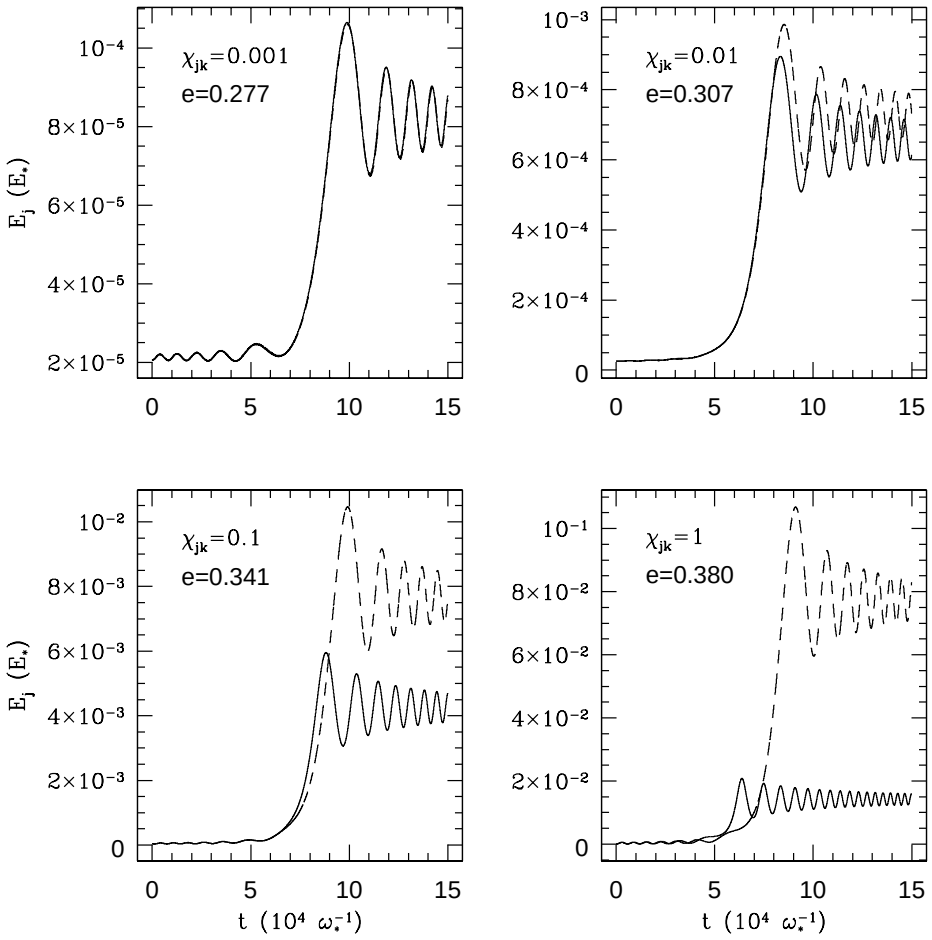

Figure 5.2: The energy in the $\ell = m = 2$ f-mode on a 0.6 $M_\odot$ white dwarf is shown for a passage through the $k = 15$ resonance with different values of the parameter χ_{jk} obtained by varying the eccentricity, and with $q = 10,000$. In each plot, the dashed curve is the system without back reaction, and the solid curve is the system with back reaction. The curves have been smoothed to remove high-frequency components.

depositing it into the orbit, the orbital frequency will necessarily decrease (i.e., the semimajor axis will increase), and the system will get pushed off resonance. It will then have another chance to approach the same resonance. Then, if the phase is such that energy is transferred to the mode, then the system will once again get pushed off resonance, but this time in the opposite direction (since the orbital frequency will increase). Gravitational radiation will then evolve the system away from this resonance and towards the next one. This scenario hints at the possibility that back reaction may force the resonant energy transfer to be always positive. However, this is not necessarily the case. For instance, we have assumed that there is sufficient initial energy in the mode to be able to change the orbital frequency significantly. Also, we have neglected the fact that gravitational radiation will be removing energy from the orbit as we are transferring energy to the orbit from the mode. If the rate of dissipation by gravitational radiation is high enough, then back reaction may not matter. The system will evolve through resonance regardless, on a timescale determined by the rate of dissipation. Hence, we can still get a net negative energy transfer to the mode.

In summary, back reaction may be important in determining both the magnitude and the direction of resonant energy transfer. The χ_{jk} criterion provides, in some sense, only a measure of the correction to the magnitude. In the regime where $\chi_{jk} \gtrsim 1$, the implication is unambiguous: back reaction will be essential in determining the energy transfer. However, when $\chi_{jk} < 1$, things are somewhat uncertain for reasons stated above. A solution of the problem including back reaction is required to determine conclusively whether back reaction is important in that regime.

5.4.2 Long-Term Evolution

In Section 5.3, we calculated the energy transfer for an individual resonance in the absence of back reaction. In general, as the binary shrinks under gravitational radiation, the system will pass through a sequence of resonances for each mode. However, this is only a possibility for an eccentric orbit because, as demonstrated previously,

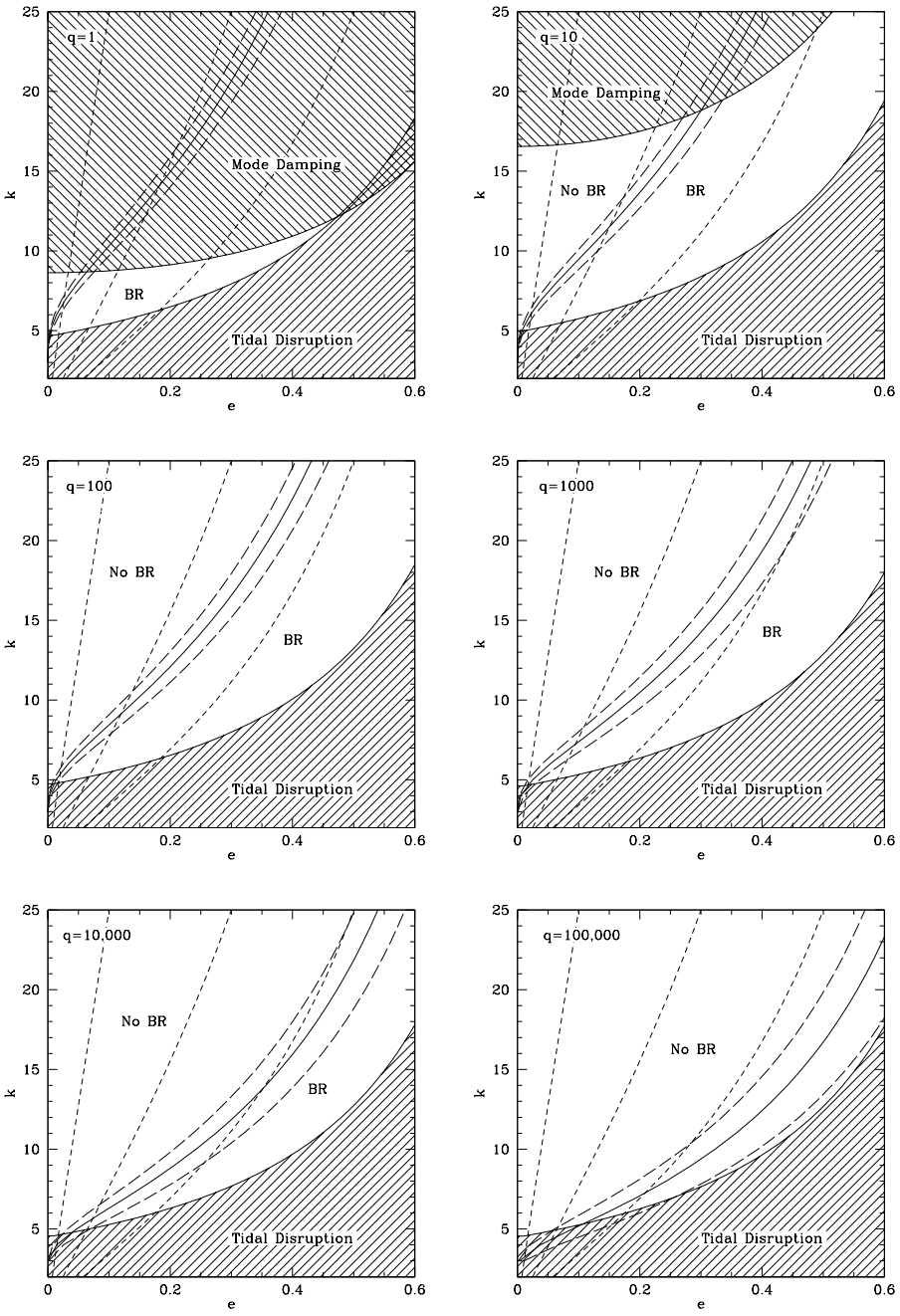

Figure 5.3: The regions in eccentricity-harmonic space where back reaction is and is not important (labelled as 'BR' and 'No BR', respectively) are delineated according to the χ_{jk} criterion for a $\ell = m = 2$ f-mode of a 0.6 $M_\odot$ white dwarf, and various mass ratios. In each plot, the solid curve traces out the contour $\chi_{jk} = 1$, and the long dashed lines to its left and right trace $\chi_{jk} = 0.1$ and $\chi_{jk} = 10$, respectively. The short dashed lines trace three gravitational radiation inspiral trajectories through the plane. For reference, the tidal limit and the region where mode damping via gravitational radiation during inspiral is important are also shown.

only the fundamental resonance exists for a circular orbit. We note that, in the no back reaction approximation, the energy transfer at a resonance can be negative as well as positive, depending on the relative phase of the mode and the driver, and the initial amplitude. Also, there will be negligible average energy transfer between resonances, as long as we are well outside the tidal limit. If we assume (as seems reasonable) that the system has no long term phase memory, then the relative phasing at each resonance will be essentially random, with a uniform distribution. It then follows that, on average, the mode will tend to gain energy over time, and that the average total energy transfer after a sequence of resonances will be simply the sum of the individual average energy transfers given by (5.30).

Let ε_k denote the average energy transfer given by (5.30) for a particular mode at the k-th resonance, and let E_k be the energy in the mode before the k-th resonance. It then follows from (5.12) and our assumptions of random phases and negligible energy transfer between resonances that, for a sequence of resonances in the no back reaction approximation, the evolution of the mode energy will be given by the discrete random walk (with a drift)

$$E_{k-1} = E_k + \varepsilon_k \left(1 + 2\sqrt{\frac{E_k}{\varepsilon_k}} C_k \right) \ , \tag{5.35}$$

where C_k is a random variable drawn from the distribution

$$p(x) = \frac{1}{\pi\sqrt{1-x^2}} \ , \quad x \in [-1, 1] \ .$$

For a derivation of elementary statistical properties of this random walk, see Appendix D.

Figure 5.4 shows the results from calculations of passage through a sequence of resonances performed using the above random walk model for several sets of initial conditions. We have chosen to plot the mode amplitude

$$B_j \equiv \sqrt{\frac{2E_j}{M_j \omega_j^2}} \ , \tag{5.36}$$

rather than the energy, because we want to draw attention to the fact that, for moderate initial eccentricities, the amplitude of a $\ell = m = 2$ f-mode can be driven to values in the range $\sim$0.1–1. (An amplitude of unity for a $\ell = m = 2$ mode corresponds to a maximum physical displacement of the stellar surface of about 55% relative to the unperturbed radius.) We therefore expect that the linear normal mode analysis might not be valid in those cases, and that non-linear effects may in fact determine the actual outcome.

It should be noted that, even if back reaction plays a role in determining the direction of energy transfer, our result that non-linear amplitudes for a $\ell = m = 2$ f-mode can be attained by passage through a sequence of resonances is unlikely to be affected. This is due to the fact that the result depends chiefly upon the allowed magnitude of energy transfer, and as we restricted our calculations to the regime where $\chi_{jk} \ll 1$, back reaction is not expected to change things.

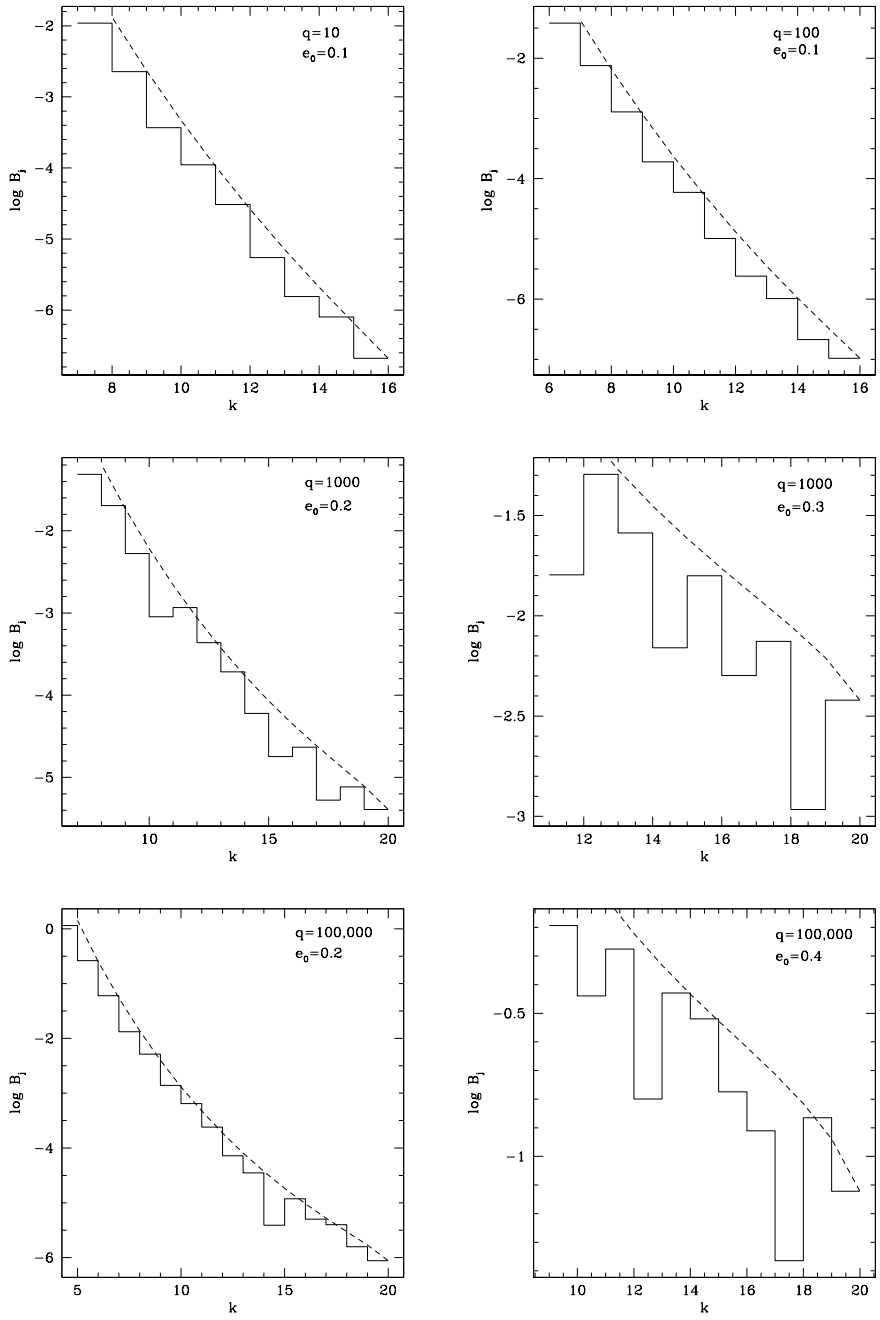

Figure 5.4: The amplitude of the $\ell = m = 2$ f-mode of a 0.6 $M_\odot$ white dwarf during passage through a sequence of resonances in the no back reaction approximation is shown for several sets of initial conditions. All of these lie in regions of the eccentricity-harmonic plane where back reaction is not important according to the χ_{jk} criterion. The calculations were done using our semi-analytical formalism. In each case, the solid line shows a particular realization of the random walk given by (5.35), and the dashed line follows the ensemble average. The random walks were terminated when $\chi_{jk} \sim 0.01$. Note that the scales on the axes are different for each plot.

Chapter 6

Resonances With Back Reaction

As an eccentric white dwarf-compact object (WDCO) binary evolves under gravitational radiation reaction, there will be resonances between harmonics of the orbital frequency and normal mode eigenfrequencies of the white dwarf. In the preceding chapter, the energy transfer at these resonances was considered when the perturbation of the orbit by the excited tides is neglected (the no back reaction approximation). In this limit, the problem can be solved semi-analytically, and it was shown that the energy transfer at a resonance can be either positive or negative, depending upon the initial energy and phase, and that the energy in a mode undergoes a random walk with a drift during passage through a sequence of such resonances. It was speculated that the inclusion of perturbations to the orbit by the excited tides (back reaction) could lead to qualitatively different results, even in the regime where back reaction is not expected to affect the magnitude of the energy transfer significantly. In particular, it was argued that back reaction could be important in determining the sign of the energy transfer at a resonance.

In the present chapter, we consider the problem including back reaction. As before, we ignore stellar rotation, and assume that there is little or no mode damping on a resonance time-scale. In addition, we restrict ourselves to low to moderate eccentricities, and confine our attention to the $\ell = m = 2$ f-mode, which is the dominantly excited mode. However, even with these simplifying assumptions, the problem is a complicated one, owing to its inherent non-linearity. We adopt a Hamiltonian approach because it allows us to maintain self-consistency explicitly, and to exploit

symmetries. The approach is similar in spirit to the Hamiltonian analysis of resonances in the restricted three-body problem (see, for example, Murray & Dermott, 1999), where its power and utility are also manifest. Some aspects of the near-resonant dynamics have been considered previously by Alexander (1987) in a similar language, and the development in Section 6.2 owes much to his account.

It is possible to include gravitational radiation in the formalism via a reaction term in the Hamiltonian (Schäfer, 1990), but, for reasons of simplicity, we choose not to do so. Instead, we impose radiation reaction as an external effect. As the time-scale for orbital evolution under radiation reaction is typically much longer than a resonance time-scale, the system is nearly periodic. This mismatch between the time-scales allows us to exploit the notion of adiabatic invariance to prove the general and elegant result that the energy transfer at a resonance is phase-independent and always positive, to lowest order in the rate of dissipation by gravitational radiation.

6.1 An Overview

In this section, we provide a qualitative outline of the main theoretical developments that follow in Sections 6.2–6.4.

In the presence of gravitational radiation, a WDCO system is clearly not conservative. Nonetheless, if the rate of dissipation is low, the system is nearly conservative over many orbits. This suggests that a conservative, Hamiltonian characterization of the system will be a useful one for understanding the dynamics near a tidal resonance. The Hamiltonian that describes a WDCO system is comprised of a Keplerian piece, and an infinite sum of simple harmonic oscillators, which represent the normal modes of the white dwarf, along with terms that couple the modes to the orbit. The coupling terms are responsible for both the excitation of the modes, and for the back reaction of the modes on to the orbit. In Section 6.2, we start with this Hamiltonian, and consider a series of canonical transformations to different sets of variables in an effort to simplify the description. The power of the Hamiltonian approach becomes evident as we are able to exploit symmetries of the system to reduce the degrees of freedom.

For low to moderate eccentricities, we find that, near a resonance, the Hamiltonian can be reduced to two degrees-of-freedom for the motion of the $\ell = m$ mode variables.

The next simplification comes from the physical insight that the excited tide should take the form of a wave traveling in the azimuthal direction around the star. This leads us to discover the existence of an invariant sub-manifold in the phase space, and for motion on the invariant sub-manifold, the problem is reduced to a single degree-of-freedom. This reduction guarantees integrability and the existence of action-angle variables for the system. We also note the existence of a separatrix in the phase space. It is demonstrated that the system can be described, to a good approximation, by a Hamiltonian with a single parameter, δ. The Hamiltonian thus obtained is nearly identical in form to Hamiltonians encountered in the analysis of first-order eccentricity resonances in the restricted three-body problem (Murray & Dermott, 1999). It is shown that, like the three-body case, a saddle-node bifurcation occurs at the critical value $\delta_{\rm crit} = -3$.

Gravitational radiation is included by imposing the dissipation of energy and angular momentum as external conditions, and we make the reasonable assumption that the rates of dissipation do not change much over the time-scale of a resonance. This allows us to fix the dissipation rates near a resonance, and then ignore the dependence of the rates upon orbital variables during the passage through resonance. The net effect is that gravitational radiation evolves the parameter, δ, of our one degree-of-freedom Hamiltonian. In the regime where the evolution occurs adiabatically, this is an ideal setup for using adiabatic invariant theory. As the action variable is an adiabatic invariant to lowest order in the rate of dissipation, it stays constant during the near-resonant evolution, as long as the adiabatic condition is not strongly violated.

Earlier, we noted the existence of a separatrix in phase space. As the period of the system goes to infinity on the separatrix, the adiabatic condition will be violated near any point where the system's trajectory crosses the separatrix. Therefore, there can be a 'jump' in the adiabatic invariant at a separatrix crossing. This suggests that a resonance passage corresponds to a separatrix crossing, and that the jump in the adiabatic invariant corresponds to the resonant energy transfer, which is confirmed

by numerical evolution. A simple argument, supported by formal results obtained by Cary et al. (1986), allows us to to show that the change in the adiabatic invariant is independent of the phase, to lowest order in the rate of dissipation.

It remains to quantify the change in the action variable at a separatrix crossing, and to determine the relation between the action variable and the mode energy. Fortunately, we are able to leverage results obtained for first-order eccentricity resonances in the restricted three-body problem (Murray & Dermott, 1999, and references therein) for calculating the action variable before and after resonance. It is shown that the action variable always increases at a tidal resonance when the resonance passage is driven by gravitational radiation. As the action variable can be shown to correspond asymptotically to the mode energy (to within a scaling factor), it follows that the energy transfer is always positive. Furthermore, there is no explicit dependence upon any initial phase, to lowest order in the rate of dissipation by gravitational radiation.

6.2 The Hamiltonian Formalism

6.2.1 Two Elementary Systems

It is a well-known result from classical mechanics that action-angle variables are guaranteed to exist for any autonomous, integrable Hamiltonian. It will be convenient for us to work with action-angle variables for tidal excitation; therefore, towards that end, we describe briefly action-angle variables for two elementary systems that are relevant. Details may be found in any standard textbook, such as Goldstein (1980). Note that our convention for the definition of the action variable is

$$J \equiv \frac{1}{2\pi} \oint dq\, p \ , \tag{6.1}$$

which differs from the convention used by Goldstein (1980) by the factor of $1/2\pi$. We also note that a useful property of action variables is their adiabatic invariance.

The Hamiltonian for a simple harmonic oscillator with mass m, natural angular

frequency ω, displacement q and momentum p is

$$\mathcal{H}_{\mathrm{SHO}} = \frac{p^2}{2m} + \frac{1}{2}m\omega^2 q^2 \ . \tag{6.2}$$

The canonical transformation equations relating the coordinates (q, p) to the action-angle variables (w, J) are

$$q = \sqrt{\frac{2J}{m\omega}} \cos w \ , \tag{6.3}$$

$$p = -\sqrt{2m\omega J} \sin w \ , \tag{6.4}$$

and the transformed Hamiltonian is given by

$$\mathcal{H}_{\mathrm{SHO}}(J) = \omega J \ . \tag{6.5}$$

The action variable is, by construction, a constant of the motion, and the angle variable is a linear function of time:

$$w = \omega t + \beta \ , \tag{6.6}$$

where β is an initial phase.

For two-body motion, the Hamiltonian in terms of spherical polar coordinates, the reduced mass μ, and constituent masses M_1 and M_2, is

$$\mathcal{H}_{\mathrm{Kepler}} = \frac{p_r^2}{2\mu} + \frac{p_\theta^2}{2\mu r^2} + \frac{p_\phi^2}{2\mu r^2 \sin^2\theta} - \frac{G_{\mathrm{N}} M_1 M_2}{r} \ , \tag{6.7}$$

where G_{N} is the gravitational constant. In the context of celestial mechanics, action-angle variables for Keplerian motion are often called the Delaunay variables or the Delaunay elements. They are typically denoted as $\{h, g, l, H, G, L\}$. The variable h corresponds to the longitude of the ascending node, g corresponds to the argument of periapse, and l is the mean anomaly. Among the action variables, we note that H is numerically equal to p_θ, and G is equal to p_ϕ. The action variable L is proportional

to $a^{1/2}$, where a is the semi-major axis. For our problem, the orbit will always lie in the equatorial plane. Thus, we discard h and H, and work with the reduced set of Delaunay variables $\{g, l, G, L\}$. The Hamiltonian in terms of these variables is given by

$$\mathcal{H}_{\rm Kepler} = -\frac{(G_{\rm N} M_1 M_2)^2 \mu}{2L^2} \ , \tag{6.8}$$

and the mean orbital angular frequency and eccentricity are given by

$$n = \frac{(G_{\rm N} M_1 M_2)^2 \mu}{L^3} \ , \tag{6.9}$$

$$e = \sqrt{1 - \frac{G^2}{L^2}} \ . \tag{6.10}$$

All the variables are constants of the motion, with the exception of l, which is a linear function of time:

$$l = n(t - T) \ , \tag{6.11}$$

where T is the time of periastron passage.

6.2.2 Resonant Tidal Excitation

In the absence of tidal dissipation and stellar rotation, the Hamiltonian for a white dwarf-compact object binary is

$$\mathcal{H} = \frac{p_R^2}{2\mu} + \frac{p_u^2}{2\mu R^2} - \frac{q}{R} + \sum_j \left(\frac{p_j^2}{2M_j} + \frac{1}{2} M_j \omega_j^2 x_j^2 \right) - \sum_j x_j f_j \ , \tag{6.12}$$

where R is the orbital separation, u is the angular coordinate in the plane of the orbit, q is the ratio of the companion mass M_0 to the white dwarf mass M_*, x_j is the displacement of mode j, M_j is the mass of mode j, and f_j is the overlap integral for mode j. (We remind the reader that we are working in stellar units, where mass, length, and time are measured in terms of M_*, R_*, and $\sqrt{R_*^3/G_{\rm N} M_*}$, respectively.)

As was shown previously, the overlap integral can be written as

$$f_j = \sum_{k=-\infty}^{\infty} f_{jk} \ , \tag{6.13}$$

where

$$f_{jk} = \frac{q\eta_j}{(1+q)^{(\ell+1)/3}} F_{jk}(n,e) \begin{cases} \cos\left(kl + m\varpi\right) \\ \sin\left(kl + m\varpi\right) \end{cases} \ , \tag{6.14}$$

and

$$F_{jk}(n,e) \equiv n^{2(\ell+1)/3} X_k^{-(\ell+1),m}(e)$$

(recall that $X_k^{p,m}$ is a Hansen coefficient; see Appendix B). We now perform a canonical transformation to a new set of variables which consists of Delaunay variables $\{g, l, G, L\}$ for the orbit, and action-angle variables $\{w_j, J_j\}$ for each harmonic oscillator. The Hamiltonian in terms of the new variables is

$$\mathcal{H} = \mathcal{H}_0 + \mathcal{H}_1 \ , \tag{6.15}$$

where the uncoupled part is given by

$$\mathcal{H}_0 = -\frac{q^3}{(1+q)} \frac{1}{2L^2} + \sum_j \omega_j J_j \ , \tag{6.16}$$

and the coupling piece is given by

$$\begin{aligned} \mathcal{H}_1 = & \sum_{j,k} Q_j F_{jk} \\ & \times \left\{ \sqrt{J_j^{(\mathrm{e})}} \left[\cos\left(w_j^{(\mathrm{e})} + kl + mg \right) + \cos\left(w_j^{(\mathrm{e})} - kl - mg \right) \right] \right. \\ & \left. + \sqrt{J_j^{(\mathrm{o})}} \left[\sin\left(w_j^{(\mathrm{o})} + kl + mg \right) - \sin\left(w_j^{(\mathrm{o})} - kl - mg \right) \right] \right\}, \end{aligned} \tag{6.17}$$

where

$$Q_j \equiv -\frac{q}{(1+q)^{(\ell+1)/3}} \frac{\eta_j}{\sqrt{2M_j\omega_j}} \ .$$

In F_{jk}, it should now be understood that n and e are shorthands for the definitions

$$n = \frac{q^3}{(1+q)}\frac{1}{L^3} \ , \tag{6.18}$$

$$e = \sqrt{1 - \frac{G^2}{L^2}} \ . \tag{6.19}$$

The phases that appear in the Hamiltonian are all of the form $w_j - kl \mp mg$. Therefore, there will be resonances whenever

$$\dot{w}_j = k\dot{l} \pm m\dot{g} \tag{6.20}$$

(remember that k can be positive or negative). This corresponds approximately to the condition $\omega_j = kn$.

Let us now consider the dynamics of the system near a resonance for a specific set of modes. After time-averaging the coupling Hamiltonian in the sense that we ignore all rapidly varying (i.e., non-resonant) terms, we find

$$\begin{aligned} \overline{\mathcal{H}_1} = \sum_j^{\mathrm{R}} Q_j \Big[& F_{jk}^{+}\sqrt{J_j^{(\mathrm{e})}}\cos\Big(w_j^{(\mathrm{e})} - kl - mg\Big) \\ & - F_{jk}^{+}\sqrt{J_j^{(\mathrm{o})}}\sin\Big(w_j^{(\mathrm{o})} - kl - mg\Big) \\ & + F_{jk}^{-}\sqrt{J_j^{(\mathrm{e})}}\cos\Big(w_j^{(\mathrm{e})} - kl + mg\Big) \\ & + F_{jk}^{-}\sqrt{J_j^{(\mathrm{o})}}\sin\Big(w_j^{(\mathrm{o})} - kl + mg\Big)\Big] \ , \end{aligned} \tag{6.21}$$

where k is now taken to be positive, the 'R' above the summation indicates that the sum is over the resonant modes only, and we have used the notational shorthand

$$F_{jk}^{\pm} \equiv n^{2(\ell+1)/3} X_{jk}^{\pm} \ , \qquad X_{jk}^{\pm} \equiv X_{\pm k}^{-(\ell+1),m} \ .$$

Following Alexander (1987), we now transform to a new set of variables $\{g',\, l',\, \theta_j^{(\mathrm{e})},$

$\theta_j^{(o)}$, G', L', $P_j^{(e)}$, $P_j^{(o)}\}$ via the generating function[1]

$$\begin{aligned} F_2 &= gG' + lL' \\ &\quad + \sum_j^{\mathrm{R}} \left[(w_j^{(e)} - kl - mg) P_j^{(e)} + (w_j^{(o)} - kl - mg) P_j^{(o)} \right] \end{aligned} \tag{6.22}$$

(there is an implicit identity transformation for all non-resonant modes). The corresponding transformation equations are

$$\begin{aligned} \theta_j^{(e)} &= w_j^{(e)} - kl - mg \ , & J_j^{(e)} &= P_j^{(e)} \ , \\ \theta_j^{(o)} &= w_j^{(o)} - kl - mg \ , & J_j^{(o)} &= P_j^{(o)} \ , \\ l' &= l \ , & L &= L' - k \sum_j^{\mathrm{R}} \left(P_j^{(e)} + P_j^{(o)} \right) \ , \\ g' &= g \ , & G &= G' - \sum_j^{\mathrm{R}} m \left(P_j^{(e)} + P_j^{(o)} \right) \ . \end{aligned}$$

The uncoupled Hamiltonian for the new variables becomes

$$\begin{aligned} \mathcal{H}_0 = &- \frac{q^3}{(1+q)} \frac{1}{2 \left[L' - k \sum_j^{\mathrm{R}} \left(P_j^{(e)} + P_j^{(o)} \right) \right]^2} \\ &+ \sum_j^{\mathrm{R}} \omega_j \left(P_j^{(e)} + P_j^{(o)} \right) \ , \end{aligned} \tag{6.23}$$

and the coupling Hamiltonian is

$$\begin{aligned} \overline{\mathcal{H}_1} = \sum_j^{\mathrm{R}} Q_j \Big[& F_{jk}^{+} \sqrt{P_j^{(e)}} \cos \theta_j^{(e)} - F_{jk}^{+} \sqrt{P_j^{(o)}} \sin \theta_j^{(o)} \\ & + F_{jk}^{-} \sqrt{P_j^{(e)}} \cos \left(\theta_j^{(e)} + 2mg' \right) \\ & + F_{jk}^{-} \sqrt{P_j^{(o)}} \sin \left(\theta_j^{(o)} + 2mg' \right) \Big] \ . \end{aligned} \tag{6.24}$$

Note that we have dropped the terms for the non-resonant modes in $\mathcal{H}_0$. Since the

[1] We follow the notation of Goldstein (1980) in labeling generating functions. Thus, for example, a generating function of type F_2 is given in terms of the old coordinates and new momenta.

Hamiltonian is now cyclic in l', the conjugate momentum L' is conserved. Hence,

$$\frac{d}{dt}\left[L + k\sum_{j}^{\mathrm{R}}\left(J_j^{(\mathrm{e})} + J_j^{(\mathrm{o})}\right)\right] = 0 \ .$$

It may be thought that the conservation of L' corresponds to the conservation of energy, but this is not true. L' is an independent integral of the near-resonant motion. This is most easily seen by rewriting the above expression in terms of the orbital and mode energies, and noting that the resulting relation is non-linear:

$$\frac{d}{dt}\left[\frac{1}{\sqrt{2}}\frac{q^{3/2}}{(1+q)^{1/2}}\left(-E_{\mathrm{orb}}\right)^{-1/2} + k\sum_{j}^{\mathrm{R}}\frac{E_j}{\omega_j}\right] = 0 \ . \tag{6.25}$$

The conservation of energy corresponds to the fact that the Hamiltonian itself is also an integral of the motion.

The uncoupled Hamiltonian $\mathcal{H}_0$ contains an intrinsic degeneracy since $P_j^{(\mathrm{e})}$ and $P_j^{(\mathrm{o})}$ occur only in the combination $P_j^{(\mathrm{e})} + P_j^{(\mathrm{o})}$. We remove this degeneracy by considering the transformation to new variables $\{\overline{g},\, \overline{l},\, \theta_j^{(1)},\, \theta_j^{(2)},\, \overline{G},\, \overline{L},\, P_j^{(1)},\, P_j^{(2)}\}$ generated by

$$F_3 = -\overline{g}G' - \overline{l}L' - \sum_{j}^{\mathrm{R}}\left[\left(P_j^{(\mathrm{e})} + P_j^{(\mathrm{o})}\right)\theta_j^{(1)} + P_j^{(\mathrm{o})}\theta_j^{(2)}\right] \ . \tag{6.26}$$

The corresponding transformation equations are

$$\begin{aligned}
\theta_j^{(\mathrm{e})} &= \theta_j^{(1)} \ , & P_j^{(1)} &= P_j^{(\mathrm{e})} + P_j^{(\mathrm{o})} \ , \\
\theta_j^{(\mathrm{o})} &= \theta_j^{(1)} + \theta_j^{(2)} \ , & P_j^{(2)} &= P_j^{(\mathrm{o})} \ , \\
l' &= \overline{l} \ , & \overline{L} &= L' \ , \\
g' &= \overline{g} \ , & \overline{G} &= G' \ .
\end{aligned}$$

In terms of the new variables, the uncoupled and coupling Hamiltonians become

$$\mathcal{H}_0 = -\frac{q^3}{(1+q)}\frac{1}{2\left[\overline{L} - k\sum_j^{\mathrm{R}} P_j^{(1)}\right]^2} + \sum_{j}^{\mathrm{R}}\omega_j P_j^{(1)} \tag{6.27}$$

and

$$\begin{aligned}\overline{\mathcal{H}_1} = \sum_j^{\mathrm{R}} Q_j \Bigg[& F_{jk}^{+}\sqrt{P_j^{(1)} - P_j^{(2)}}\cos\theta_j^{(1)} \\ & - F_{jk}^{+}\sqrt{P_j^{(2)}}\sin\left(\theta_j^{(1)} + \theta_j^{(2)}\right) \\ & + F_{jk}^{-}\sqrt{P_j^{(1)} - P_j^{(2)}}\cos\left(\theta_j^{(1)} + 2m\overline{g}\right) \\ & + F_{jk}^{-}\sqrt{P_j^{(2)}}\sin\left(\theta_j^{(1)} + \theta_j^{(2)} + 2m\overline{g}\right)\Bigg] ,\end{aligned} \tag{6.28}$$

respectively.

6.2.3 Specialization to a Single Mode

Consider now the particular case when the resonant modes have the same frequency, and differ only in the values of m. Since $X_{jk}^{\pm} \propto e^{|k\mp m|}$, the terms proportional to F_{jk}^{-} in (6.28) are suppressed by $2m$ powers of eccentricity relative to the F_{jk}^{+} terms. Therefore, for low to moderate eccentricities, we can write

$$\begin{aligned}\overline{\mathcal{H}_1} = \sum_j^{\mathrm{R}} Q_j F_{jk}^{+}\Bigg[& \sqrt{P_j^{(1)} - P_j^{(2)}}\cos\theta_j^{(1)} \\ & - \sqrt{P_j^{(2)}}\sin\left(\theta_j^{(1)} + \theta_j^{(2)}\right)\Bigg] .\end{aligned} \tag{6.29}$$

As the Hamiltonian is now cyclic in $\overline{g}$, it follows that the conjugate momentum $\overline{G}$ is an approximate constant of the motion:

$$\frac{d}{dt}\left[L_{\mathrm{orb}} + \sum_j^{\mathrm{R}} m\frac{E_j}{\omega_j}\right] \simeq 0 , \tag{6.30}$$

where L_{orb} is the orbital angular momentum. This expresses the conservation of angular momentum, and we can identify $\overline{G}$ as the total angular momentum of the system. The reason why the conservation holds only approximately is that the expression mE_j/ω_j for the angular momentum in mode j is only exact when the mode takes the form of a pure traveling wave.

It follows from parity considerations that modes with odd $\ell+m$ will not be tidally excited (this is manifested mathematically in the fact that η_j vanishes for odd $\ell+m$). Also, the terms with $m<\ell$ are suppressed by $\ell-m$ powers of eccentricity relative to the terms with $m=\ell$. Therefore, for low enough eccentricities, the total Hamiltonian is given to a good approximation by

$$\begin{aligned}\mathcal{H} = &-\frac{q^3}{(1+q)}\frac{1}{2\left(\overline{L}-kP_j^{(1)}\right)}+\omega_j P_j^{(1)} \\ &+Q_j F_{jk}^{+}\Bigg[\sqrt{P_j^{(1)}-P_j^{(2)}}\cos\theta_j^{(1)} \\ &\qquad -\sqrt{P_j^{(2)}}\sin\left(\theta_j^{(1)}+\theta_j^{(2)}\right)\Bigg]\end{aligned} \tag{6.31}$$

with $m=\ell$.

As $\overline{G}$ and $\overline{L}$ are integrals of the motion, the orbital degrees-of-freedom are completely decoupled from the modes, and the system is reduced effectively to two degrees-of-freedom for the motion of the mode variables. With this perspective, $\overline{G}$ and $\overline{L}$ are parameters of the two degrees-of-freedom system described by (6.31).

6.3 The Dynamics

6.3.1 Fixed Points

Central to the analysis of the dynamics of a non-linear system is an understanding of the fixed point structure of the phase space. Accordingly, we now consider the fixed points of the non-linear system described by the Hamiltonian (6.31). For simplicity of notation, we drop the j subscripts on the mode variables from now on. From (6.31),

we obtain the following equations of motion for the mode variables:

$$\frac{d\theta_1}{dt} = \omega_j - kn + Q_j \left\{ \frac{\partial F^+_{jk}}{\partial P_1} \left[\sqrt{P_1 - P_2} \cos\theta_1 - \sqrt{P_2} \sin\left(\theta_1 + \theta_2\right) \right] + \frac{1}{2} F^+_{jk} \frac{\cos\theta_1}{\sqrt{P_1 - P_2}} \right\} , \tag{6.32}$$

$$\frac{d\theta_2}{dt} = -\frac{Q_j}{2} F^+_{jk} \left[\frac{\cos\theta_1}{\sqrt{P_1 - P_2}} + \frac{\sin\left(\theta_1 + \theta_2\right)}{\sqrt{P_2}} \right] , \tag{6.33}$$

$$\frac{dP_1}{dt} = Q_j F^+_{jk} \left[\sqrt{P_1 - P_2} \sin\theta_1 + \sqrt{P_2} \cos\left(\theta_1 + \theta_2\right) \right] , \tag{6.34}$$

$$\frac{dP_2}{dt} = Q_j F^+_{jk} \sqrt{P_2} \cos\left(\theta_1 + \theta_2\right) \ . \tag{6.35}$$

For non-zero eccentricities, F^+_{jk} will not vanish. Thus, from the conditions $\dot{\theta}_2 = \dot{P}_1 = \dot{P}_2 = 0$, we get

$$\theta_1 = a\pi \ , \tag{6.36}$$

$$\theta_1 + \theta_2 = \left(b + \frac{1}{2} \right) \pi \ , \tag{6.37}$$

$$P_1 = 2P_2 \ , \tag{6.38}$$

where a and b are any integers such that $|a \pm b|$ is odd (i.e., either a or b is odd). Substitution into the fourth condition, $\dot{\theta}_1 = 0$, yields the non-linear equation

$$\omega_j - kn + (-1)^a Q_j \frac{\partial}{\partial P_1} \left(F^+_{jk} \sqrt{2P_1} \right) = 0 \ . \tag{6.39}$$

This equation cannot be solved analytically, in general. Indeed, owing to the non-linear nature of the equation, we cannot even say *a priori* how many real, positive solutions exist. However, as is demonstrated below, the problem admits considerable simplification.

6.3.2 The Invariant Sub-Manifold

Physically, we expect the excited tide to take the form of an azimuthal traveling wave. This leads us to expect the even and odd components of the mode to be excited equally, with a phase difference of $\pi/2$ between them. It is remarkable that this situation actually corresponds to an invariant sub-manifold in phase space. If we set

$$\theta_2 = \left(2c - \frac{1}{2}\right)\pi \ , \tag{6.40}$$

$$P_2 = \frac{1}{2}P_1 \ , \tag{6.41}$$

where c is any integer, on the right hand sides of the equations of motion for θ_2, P_1, and P_2, then we find that the conditions will remain true during evolution in time. This demonstrates that the above conditions describe an invariant sub-manifold. Thus, for motion on this sub-manifold, the system is now reduced to a single degree-of-freedom, with the Hamiltonian

$$\mathcal{H} = -\frac{q^3}{(1+q)}\frac{1}{2(\overline{L} - kP)^2} + \omega_j P + Q_j F^+_{jk}\sqrt{2P}\cos\theta \ , \tag{6.42}$$

and the equations of motion

$$\frac{d\theta}{dt} = \omega_j - kn + Q_j \frac{\partial}{\partial P}\left(F^+_{jk}\sqrt{2P}\right)\cos\theta \ , \tag{6.43}$$

$$\frac{dP}{dt} = Q_j F^+_{jk}\sqrt{2P}\sin\theta \ , \tag{6.44}$$

where $P \equiv P_1$ and $\theta \equiv \theta_1$. Note that the defining relations for the invariant sub-manifold fulfill two of the conditions for fixed points. Hence, at least some (but not necessarily all) of the fixed points may lie on the invariant sub-manifold, and will therefore be fixed points for motion on the sub-manifold.

Interestingly, $\theta_2 = (2c + 1/2)\pi$ does not describe an invariant sub-manifold. This is probably owing to the fact that $\theta_2 = (2c+1/2)\pi$ corresponds to a retrograde wave, where as $\theta_2 = (2c - 1/2)\pi$ corresponds to a prograde wave. Recall that we explicitly

chose to consider only prograde tides and averaged away the retrograde terms when we wrote down the near-resonant Hamiltonian (6.21).

Figure 6.1 shows a sample phase portrait for the Hamiltonian (6.42) as a function of the canonical coordinates:

$$\overline{x} = \sqrt{2P}\cos\theta \ , \qquad \overline{y} = -\sqrt{2P}\sin\theta \tag{6.45}$$

(this is just the transformation relating the displacement and linear momentum to action-angle variables for a one-dimensional harmonic oscillator). These variables have the advantage of making explicit the natural polar structure of the phase space. Note the existence of a separatrix.[2]

Since, typically, $P \ll \overline{L}$ and $P \ll \overline{G}$, we can expand the Hamiltonian (6.42) in powers of $P/\overline{L}$ and $P/\overline{G}$. To second order, we obtain, after dropping a constant offset,

$$\begin{aligned} \mathcal{H}' = & \frac{3}{2}\frac{q^3}{(1+q)}\frac{k^2P^2}{\overline{L}^4} + \sqrt{2}Q_j\frac{\partial F^+_{jk}}{\partial P}P^{3/2}\cos\theta \\ & + \left[\omega_j - \frac{q^3}{(1+q)}\frac{k}{\overline{L}^3}\right]P + Q_jF^+_{jk}(2P)^{1/2}\cos\theta \ , \end{aligned} \tag{6.46}$$

where F^+_{jk} and $\partial F^+_{jk}/\partial P$ are now evaluated at $P = 0$. We now scale the momentum by means of the canonical transformation:

$$\phi = \theta \ , \qquad \Phi = \frac{P}{\lambda} \ , \qquad \mathcal{H}'' = \frac{\mathcal{H}'}{\lambda} \ ,$$

where the scaling parameter λ (defined as real and positive) is to be chosen. The new Hamiltonian is

$$\begin{aligned} \mathcal{H}'' = & \frac{3}{2}\frac{q^3}{(1+q)}\frac{k^2\lambda\Phi^2}{\overline{L}^4} + \sqrt{2}Q_j\frac{\partial F^+_{jk}}{\partial P}\lambda^{1/2}\Phi^{3/2}\cos\phi \\ & + \left[\omega_j - \frac{q^3}{(1+q)}\frac{k}{\overline{L}^3}\right]\Phi + Q_jF^+_{jk}\left(\frac{2\Phi}{\lambda}\right)^{1/2}\cos\phi \ . \end{aligned} \tag{6.47}$$

[2] A separatrix is a contour of $\mathcal{H}$ that passes through a saddle point.

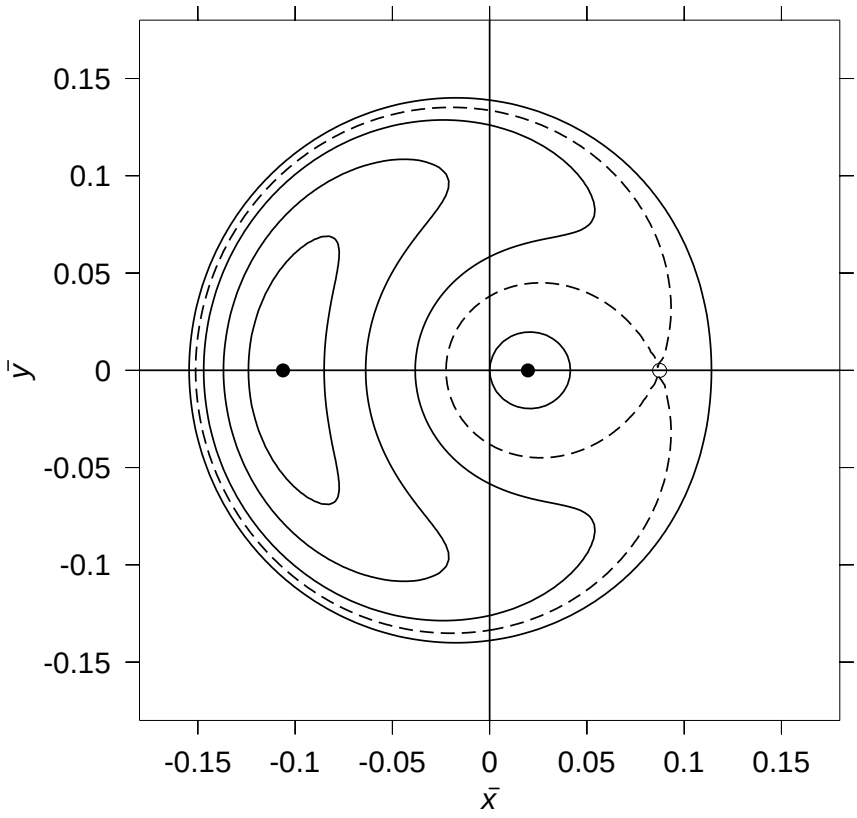

Figure 6.1: A sample phase portrait for the one degree-of-freedom Hamiltonian (6.42), as a function of the canonical coordinates $(\overline{x}, \overline{y})$, defined by (6.45). The fixed points corresponding to extrema of $\mathcal{H}$ are marked with solid circles. Also shown is the separatrix (dashed line). The saddle point of $\mathcal{H}$ is marked with an open circle.

We choose λ such that the coefficients of Φ^2 and $2(2\Phi)^{1/2}\cos\phi$ are identical. That is,

$$\lambda = \left[\frac{1}{3}\frac{(1+q)}{q^3}Q_j F_{jk}^{+}\frac{\overline{L}^4}{k^2}\right]^{2/3} . \tag{6.48}$$

Thus, after dividing out the coefficient of Φ^2 (which amounts to a choice of units), the Hamiltonian becomes

$$\mathcal{H}^{\dagger} = \Phi^2 + \beta(2\Phi)^{3/2}\cos\phi + \delta\Phi + 2(2\Phi)^{1/2}\cos\phi \ , \tag{6.49}$$

where we have defined the coefficients

$$\beta \equiv \frac{1}{F_{jk}^{+}}\frac{\partial F_{jk}^{+}}{\partial P}\lambda \ , \tag{6.50}$$

$$\delta \equiv \frac{2}{Q_j F_{jk}^{+}}\left[\omega_j - \frac{q^3}{(1+q)}\frac{k}{\overline{L}^3}\right]\lambda^{1/2} . \tag{6.51}$$

The Hamiltonian (6.49) resembles Hamiltonians encountered in the analysis of resonances in the restricted three-body problem. In fact, for $\beta = 0$, the above Hamiltonian is identical (apart from a reflection) to the Hamiltonian for first-order eccentricity resonances in the three-body problem (Murray & Dermott, 1999). This mathematical similarity serves as a useful guide for our analysis, and the notation has been chosen to emphasize it.

The fixed points of $\mathcal{H}^{\dagger}$ are given by the solution of the simultaneous equations:

$$2\Phi + 3\beta(2\Phi)^{1/2}\cos\phi + \delta + \frac{2\cos\phi}{(2\Phi)^{1/2}} = 0 \ , \tag{6.52}$$

$$2(\beta\Phi + 1)(2\Phi)^{1/2}\sin\phi = 0 \ . \tag{6.53}$$

A non-trivial solution (i.e., $\Phi \neq 0$) requires $\phi = a\pi$, where a is an integer, and

$$(2\Phi)^{3/2} + (-1)^a 3\beta(2\Phi) + \delta(2\Phi)^{1/2} + (-1)^a 2 = 0 \ , \tag{6.54}$$

which is a cubic equation for $(2\Phi)^{1/2}$. Note that the only effect that a has is to

determine the signs of the roots. Specifically, changing a from even to odd or vice versa simply flips the signs of the roots (which may be complex). Hence, for either choice of a (even or odd), we obtain all the equilibrium solutions. This may appear strange, but it is easily understood when we note that the phase space for (ϕ, Φ) naturally has a polar structure, with $(2\Phi)^{1/2}$ (which is proportional to the mode amplitude) as a radial coordinate, and ϕ as a polar angle. In effect, the choice of a determines the axis which corresponds to $\phi = 0$.

The above considerations are made explicit if we introduce the polar transformation used earlier, which makes the dynamics easier to study:

$$x = \sqrt{2\Phi}\cos\phi \ , \qquad y = -\sqrt{2\Phi}\sin\phi \ . \tag{6.55}$$

The Hamiltonian in terms of these coordinates is

$$\mathcal{H}^{\dagger} = \frac{1}{4}(x^2+y^2)^2 + \beta(x^2+y^2)x + \frac{\delta}{2}(x^2+y^2) + 2x \ . \tag{6.56}$$

The equations for the (non-trivial) equilibrium solutions yield $y = 0$, and

$$x^3 + 3\beta x^2 + \delta x + 2 = 0 \ . \tag{6.57}$$

Setting $x = z - \beta$, the above equation reduces to

$$z^3 + (\delta - 3\beta^2)z + (2 - \delta\beta + 2\beta^3) = 0 \ . \tag{6.58}$$

In general, this equation has three solutions. However, two of those solutions may be complex and, hence, unphysical. To determine where the bifurcation of the roots occurs (that is, where two of the roots coincide and transition between real and complex values), we look at the discriminant:

$$D = \frac{1}{27}(\delta - 3\beta^2)^3 + \frac{1}{4}(2 - \delta\beta + 2\beta^3)^2 \ . \tag{6.59}$$

For $D > 0$, there is one real root and two complex roots, and for $D < 0$, all three roots are real. The bifurcation occurs when $D = 0$, which, for $\beta = 0$, corresponds to $\delta_{\rm crit} = -3$. For $\beta \neq 0$, only a relation between δ and β is determined. To fourth-order in β, this is

$$\delta_{\rm crit} = -3\left(1 + \beta - \frac{1}{4}\beta^2 + \frac{1}{12}\beta^3 - \frac{1}{48}\beta^4\right) \ . \tag{6.60}$$

To lowest order, F^+_{jk} is independent of P, so we can set $\beta = 0$ as a good approximation. Physically, this corresponds to the reasonable approximation that the variations in the mode energy in the near-resonant regime are insufficient to affect the strength of the tidal force significantly.[3] The location of the three equilibrium points is then given by:

$$x_1 = \frac{3^{\frac{1}{3}}\delta - \Delta^{\frac{2}{3}}}{3^{\frac{2}{3}}\Delta^{\frac{1}{3}}} \ , \tag{6.61}$$

$$x_{2,3} = \frac{(-3^{\frac{1}{3}} \pm 3^{\frac{5}{6}}\,{\rm i})\delta + (1 \pm \sqrt{3}\,{\rm i})\Delta^{\frac{2}{3}}}{3^{\frac{2}{3}}2\Delta^{\frac{1}{3}}} \ , \tag{6.62}$$

where

$$\Delta = 9 + \sqrt{3}\sqrt{27 + \delta^3} \tag{6.63}$$

(e.g., Abramowitz & Stegun 1972; cf. Murray & Dermott 1999).

Phase portraits of the Hamiltonian (6.56) with $\beta = 0$ are shown in Figure 6.2 (cf. Murray & Dermott, 1999). For $\delta < -3$, there are three fixed points corresponding to all three roots of (6.57) (cf. Figure 6.1). At $\delta = -3$, one of the nodes and the saddle point (x_2 and x_3, respectively) coincide, and, subsequently, for $\delta > -3$, there is only one fixed point (x_1) corresponding to the single real root of (6.57). The existence of this bifurcation was previously noted by Alexander (1987), and, not surprisingly, a similar bifurcation also exists for first-order eccentricity resonances in the restricted three-body problem (Murray & Dermott, 1999).

Inclusion of higher-order terms in the expansion of the Hamiltonian could lead to

[3]Setting $\beta = 0$ does not amount to ignoring back reaction. Back reaction has two effects: introducing variations in the magnitude of the tidal force, and altering the mode-orbit phase. The approximation $\beta = 0$ reflects the recognition that the latter effect is the dominant one in determining the near-resonant dynamics.

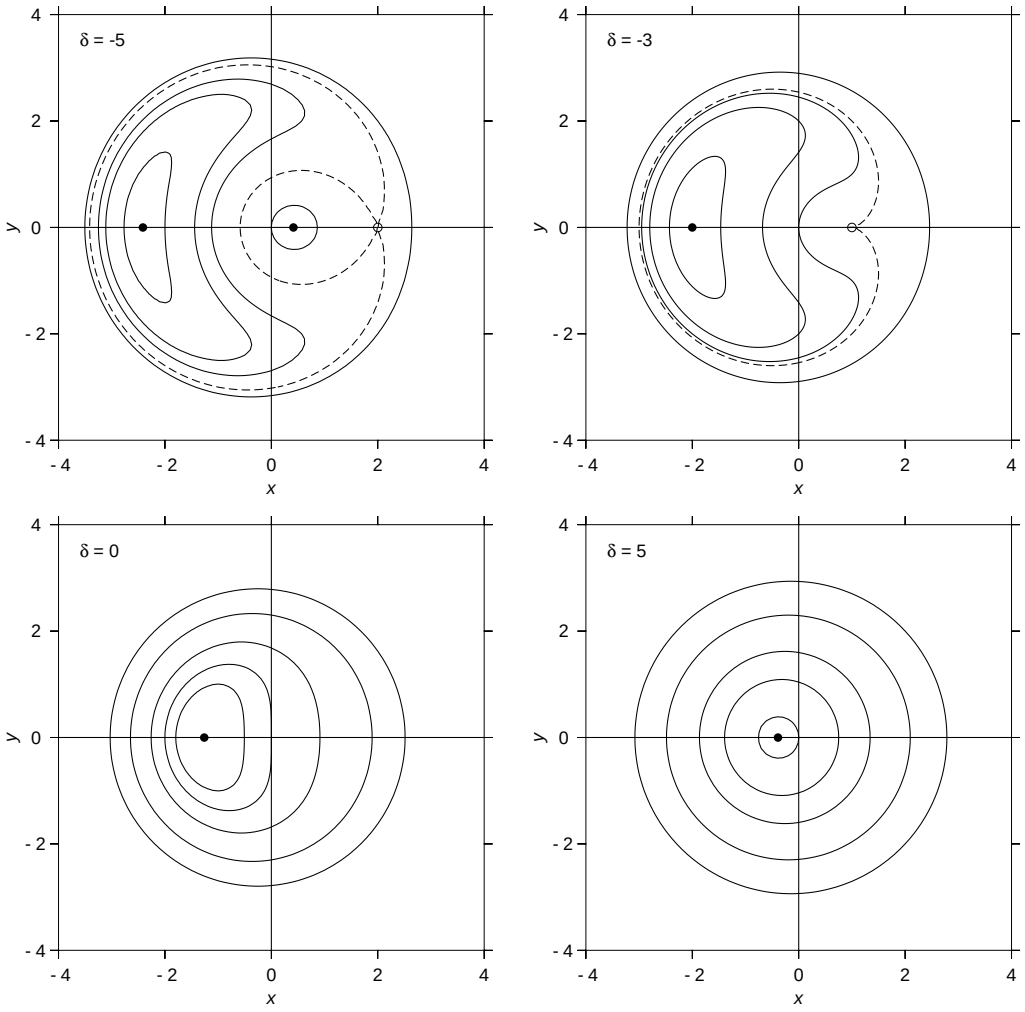

Figure 6.2: Phase portraits of the Hamiltonian given by (6.56), for the case $\beta = 0$. Separatrices are drawn as dashed lines. All the fixed points lie along the x-axis. At $\delta = -3$, there is a saddle-node bifurcation. For $\delta > -3$, there is only one fixed point.

additional bifurcations, but these would necessarily be much smaller effects and are hence negligible.

6.3.3 Approximate Trajectories

As we have seen, the Hamiltonian given by (6.49) (or, equivalently, by (6.56)) describes a variety of possible dynamical behaviors (cf. Figure 6.2). Despite its relative simplicity, the Hamitonian is complicated enough that a general expression for the orbit of the system in phase space is impracticable. It is therefore useful to consider the approximate trajectories in some limited regimes.

When $\Phi \ll 1$, the Φ^2 term in the Hamiltonian can be neglected, and the trajectory of the system obeys

$$\frac{\delta}{2}(x^2 + y^2) + 2x \approx E \ , \tag{6.64}$$

which, after a little algebra, can be written as

$$\left(x + \frac{2}{\delta}\right)^2 + y^2 \approx \frac{2}{\delta}\left(\frac{2}{\delta} + E\right) \ . \tag{6.65}$$

Thus, the trajectory is a circle in the (x, y) plane, centered at $(-2/\delta, 0)$, and with radius $\sqrt{(2/\delta)(2/\delta + E)}$. In Figure 6.2, these orbits are the near-circular ones that lie close to the origin. Note that such orbits can only exist for $(2/\delta)(2/\delta + E) \geqslant 0$. For $\delta < 0$, this requires $E \leqslant -2/\delta$, where as for $\delta > 0$, the requirement is $E \geqslant -2/\delta$. Also, as the value of δ changes from negative to positive values, the center of the circles crosses from the right side of the origin to the left side, which is also seen in Figure 6.2.

When $\Phi \gg 1$, the $\cos\phi$ term in the Hamiltonian can be neglected:

$$\mathcal{H}^\dagger \approx \Phi^2 + \delta\Phi \ . \tag{6.66}$$

It then follows that $\{\phi, \Phi\}$ are action-angle variables for the system:

$$\dot{\phi} \approx \delta + 2\Phi \ , \qquad \dot{\Phi} \approx 0 \ . \tag{6.67}$$

Thus, the orbit is once more a circle in the (x, y) plane, but now centered at the origin. Setting $\mathcal{H}^\dagger = E$, and solving for Φ, we obtain

$$\Phi \approx -\frac{\delta}{2} \pm \sqrt{\frac{\delta^2}{4} + E} \ , \tag{6.68}$$

which implies that no real solutions exist unless $\delta^2/4 + E \geqslant 0$. This is always satisfied for $E \geqslant 0$, but for $E < 0$, such orbits only exist if $E \geqslant -\delta^2/4$. In Figure 6.2, these orbits are easily identified as the near-circular ones that exist at large radii for all values of δ.

Consider now when $\Phi \ll |\delta|$, which is a regime that will be of particular interest to us. The Hamiltonian in this limit is given by

$$\mathcal{H}^\dagger \approx \delta\Phi \ , \tag{6.69}$$

which implies once again that $\{\phi, \Phi\}$ are action-angle variables:

$$\dot{\phi} \approx \delta \ , \qquad \dot{\Phi} \approx 0 \ . \tag{6.70}$$

The system's trajectory in this regime is given by

$$\Phi \approx \frac{E}{\delta} \ , \tag{6.71}$$

which again describes a circle centered at the origin in the (x, y) plane. Note that (6.71) is precisely the action variable for an unforced simple harmonic oscillator with natural frequency δ, and energy E. This makes physical sense because far from the resonance there is little energy transfer to the mode.

6.3.4 Action-Angle Variables

Unfortunately, finding exact expressions for a transformation to action-angle variables for the Hamiltonian (6.49) is not feasible. Instead, we consider a perturbative approach.

For large $|\delta|$ or Φ, the $\cos\phi$ term in the Hamiltonian is relatively small and can be treated as a perturbation. To zeroth-order, $\{\phi, \Phi\}$ are then action-angle variables (cf. (6.67)). From canonical perturbation theory it then follows that the action variable to second-order in the perturbation is given by

$$\overline{\Phi} = \Phi + \frac{2\sqrt{2\Phi}\cos\phi}{(\delta + 2\Phi)} + \frac{2(\delta - 4\Phi\cos^2\phi)}{(\delta + 2\Phi)^3} \tag{6.72}$$

(see Appendix F). Note that the above transformation diverges in the vicinity of $\delta = -2\Phi$, which reflects the failure of the perturbation series to converge near resonance. The Hamiltonian in terms of the action variable is given to second-order by

$$\mathcal{H}^\dagger = \overline{\Phi}^2 + \delta\overline{\Phi} - \frac{2\delta}{(\delta + 2\overline{\Phi})^2} \tag{6.73}$$

(see Appendix F). Note that the shift in the energy only enters at second-order, which is a consequence of the periodic nature of the perturbation. Finally, it should be noted that

$$\lim_{|\delta|\to\infty} \overline{\Phi} = \Phi \ , \tag{6.74}$$

as was shown before.

6.3.5 Gravitational Radiation

Our Hamiltonian treatment of the dynamics assumes that the system is conservative; the actual problem that we are considering is not. The orbit will evolve under gravitational radiation reaction as both energy and angular momentum are dissipated. The lowest-order secular corrections are

$$\dot{E}_{\rm orb} = -\frac{32}{5}\frac{q^2}{(1+q)^{2/3}}\beta_*^5 n^{10/3}\mathcal{F}_1(e) \ , \tag{6.75}$$

$$\dot{L}_{\rm orb} = -\frac{32}{5}\frac{q^2}{(1+q)^{2/3}}\beta_*^5 n^{7/3}\mathcal{F}_2(e) \ , \tag{6.76}$$

where

$$\mathcal{F}_1(e) \equiv \frac{1}{(1-e^2)^{7/2}}\left(1+\frac{73}{24}e^2+\frac{37}{96}e^4\right) ,$$
$$\mathcal{F}_2(e) \equiv \frac{1}{(1-e^2)^{2}}\left(1+\frac{7}{8}e^2\right)$$

(Peters, 1964), and $\beta_* \equiv \sqrt{G_N M_*/R_*}$. To incorporate these corrections into our formalism, we need to write them in terms of the Delaunay variables. Since the Delaunay variable G is just the orbital angular momentum, one of the corrections is already in the required form. The equation for $\dot{E}_{\rm orb}$ can be rewritten as a correction to the Delaunay variable L:

$$\dot{L} = \frac{\dot{E}_{\rm orb}}{n} .$$

Therefore, we have

$$\dot{L}_{\rm GR} = -\frac{32}{5}\frac{q^2}{(1+q)^{2/3}}\beta_*^5 n^{7/3}\mathcal{F}_1(e) , \tag{6.77}$$
$$\dot{G}_{\rm GR} = -\frac{32}{5}\frac{q^2}{(1+q)^{2/3}}\beta_*^5 n^{7/3}\mathcal{F}_2(e) , \tag{6.78}$$

where n and e are now functions of L and G. As δ, defined by (6.51), is also a function of L and G, the above expressions also indirectly describe the evolution of δ with time. In particular, note that gravitational radiation causes δ to drift upwards (i.e., $\dot{\delta} > 0$).

6.4 Resonant Energy Transfer

6.4.1 Resonances as Separatrix Crossings

In Sections 6.2 and 6.3, starting from a Hamiltonian for resonant tidal excitation with four degrees-of-freedom for a $\ell = m = 2$ mode, we have been able to simplify the description to one with a single degree-of-freedom. This is important because

autonomous systems with one degree-of-freedom are always integrable,[4] and, in principle, action-angle variables can be always found for them. The existence of action-angle variables is useful because action variables are known to be adiabatic invariants to lowest order in the rate of change of the system's parameters. In the presence of gravitational radiation, $\overline{G}$ and $\overline{L}$ (considered to be parameters in this context) will change slowly. Assuming the change is slow enough to be considered adiabatic (i.e., the values of $\overline{G}$ and $\overline{L}$ do not change much over a single period of the system's motion), the action variable will stay constant to lowest order in $\dot{\overline{G}}$ and $\dot{\overline{L}}$—provided that the trajectory of the system in phase space does not cross any separatrices (Lichtenberg & Lieberman, 1992). On a separatrix, the period of the system's motion goes to infinity. Therefore, the adiabatic condition necessarily breaks down in some neighborhood of a separatrix, regardless of how small $\dot{\overline{G}}$ and $\dot{\overline{L}}$ are. This violation of adiabatic invariance in the vicinity of a separatrix is the defining feature of our problem, because, as is explicitly shown below, the resonances we are considering correspond to separatrix crossings.[5]

Figure 6.3 shows the phase space trajectory of a sample system during passage through a resonance. Comparing with Figure 6.1, we see that the system crosses the separatrix, and that the crossing occurs from the inner region to the outer region. Since the extent of an orbit in (x, y) space is proportional to $\sqrt{2\Phi}$, the crossing corresponds to a jump in Φ. The same resonance is shown in Figure 6.4, where Φ and ϕ are plotted as functions of time (recall that Φ is proportional to the mode energy: $E_j = \omega_j \lambda \Phi$). The correspondence of the resonance with the separatrix crossing is thus established. Also, note in Figure 6.3 that the one degree-of-freedom Hamiltonian provides a good approximation to the motion of the full system with four degrees-of-freedom.

[4] A sufficient condition for integrability is the existence of N independent constants of the motion, where N is the number of degrees-of-freedom. As the Hamiltonian is itself a conserved quantity for autonomous systems, it follows that autonomous systems with a single degree-of-freedom are always integrable.

[5] In the literature, the term 'resonance' often refers to any fixed point of the motion. To avoid ambiguity, we refrain from using this terminology.

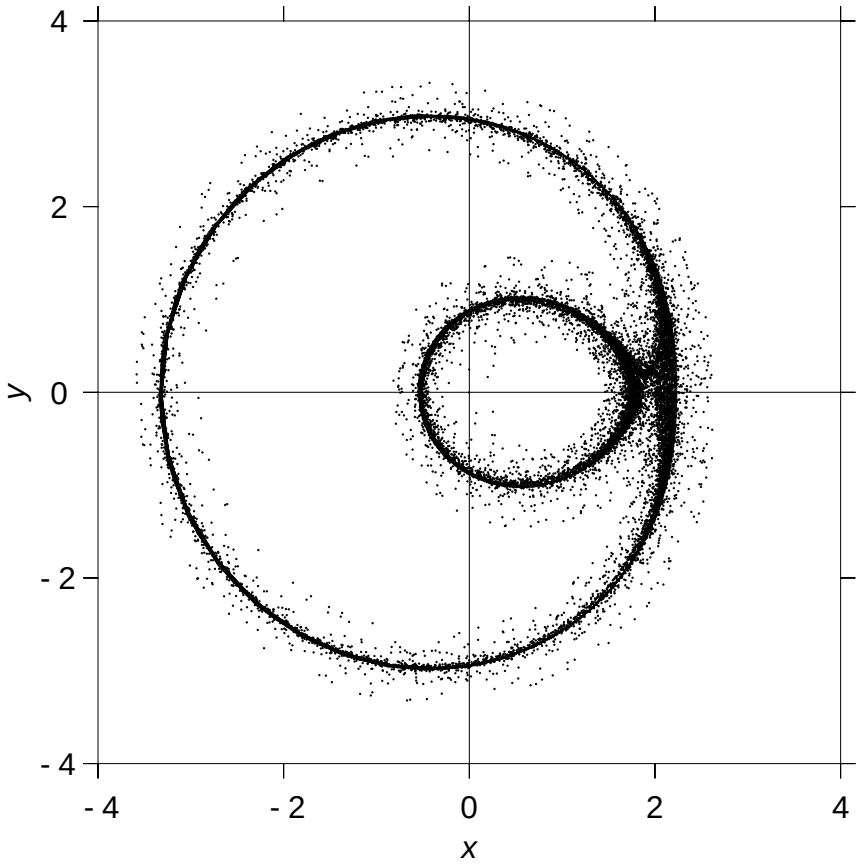

Figure 6.3: A phase space trajectory showing a passage through the $k = 15$ resonance for the $\ell = m = 2$ f-mode of a 0.6 $M_\odot$ white dwarf in a system with $q = 1000$, and an initial eccentricity of 0.4. The solid line traces the trajectory as given by the one degree-of-freedom Hamiltonian, (6.42). The trajectory given by the full Hamiltonian, (6.12), with four degrees-of-freedom is indicated by the dots. The separatrix is crossed from the inner region to the outer region.

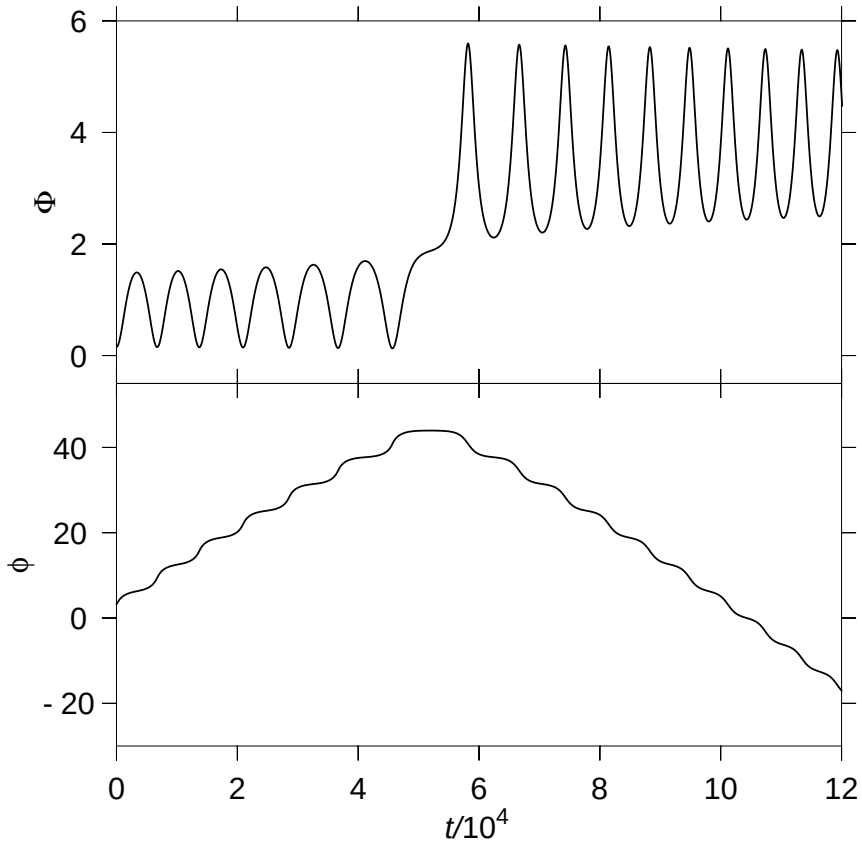

Figure 6.4: The scaled mode energy Φ, and the phase ϕ, are shown as functions of time (as given by the one degree-of-freedom Hamiltonian, (6.42), plus gravitational radiation) for the same resonance as in Figure 6.3.

6.4.2 Change in Adiabatic Invariant at a Separatrix Crossing

We now digress, briefly, to discuss the general problem of quantifying the change in the action variable at a separatrix crossing of a system with a single degree-of-freedom. This problem has been studied previously in the literature; we summarize here some relevant results obtained by Cary et al. (1986).

Consider a separatrix, such as the one shown in Figure 6.5. Suppose that the Hamiltonian depends upon some parameter λ that is varying slowly with time. For trajectories away from the separatrix, standard adiabatic theory holds, and an adiabatic invariant exists that is conserved to all orders in $\epsilon \equiv \dot{\lambda}$ for a time of order $1/\epsilon$ (Cary et al., 1986). However, this is not true for trajectories near the separatrix because, as explained previously, the adiabatic condition must break down there. One way to see this violation of adiabatic invariance is to consider what happens to the action variable, which is the lowest order adiabatic invariant, at a separatrix crossing.

If the system starts in region A of Figure 6.5, then, when the trajectory of the system encounters the separatrix, the action variable is proportional to the area of region A: $J_{\mathrm{A}} \equiv \mathcal{A}_{\mathrm{A}}/2\pi$. If the trajectory of the system were to start in region B, then, at the separatrix encounter, the action variable would be proportional to the area of region B: $J_{\mathrm{B}} \equiv \mathcal{A}_{\mathrm{B}}/2\pi$. Similarly, if the system encountered the separatrix starting from region C, then the action variable would be equal to $J_{\mathrm{A}} + J_{\mathrm{B}}$. Suppose that the system's trajectory crosses from region A to region C. At the time of the crossing, the value of the action variable will change suddenly from J_{A} to $J_{\mathrm{A}} + J_{\mathrm{B}}$, and we expect that this new value of the action variable will then stay constant, because adiabatic theory is valid again after some narrow region in the vicinity of the separatrix has been crossed. This means that, to lowest order, the new value of the adiabatic invarirant is independent of the particular trajectory followed by the system and is therefore phase-independent. As is demonstrated by Cary et al. (1986), this is indeed correct. However, they also show that there are phase-dependent deviations of order $\epsilon \ln \epsilon$ in the invariant change at the crossing. As long as ϵ is sufficiently small, these corrections can be neglected, but for large ϵ the phase-dependent corrections

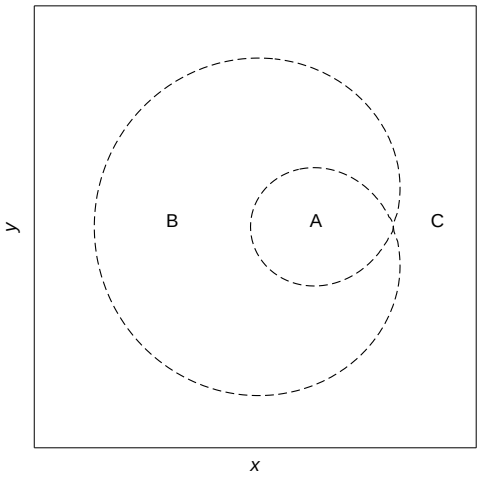

Figure 6.5: A typical separatrix of the kind encountered in tidal resonances.

become important.

It is a small step from the above reasoning to realize that for any number of separatrix crossings, the final value of the adiabatic invariant depends only upon the region where the trajectory of the system ends up, to lowest order in ϵ. The particular trajectory followed is not important.

6.4.3 Energy Transfer at a Tidal Resonance

When the trajectory of a WDCO system crosses a separatrix, there will be a jump in the action variable, which corresponds to the resonant energy transfer. Therefore, if we (i) quantify the change in the action variable at the separatrix crossing, and (ii) determine the relation between the action variable and the mode energy, then we can obtain an estimate for the resonant energy transfer. We will work with the approximate near-resonant Hamiltonian given by (6.49) (or, equivalently, (6.56)), with $\beta = 0$. This makes the problem mathematically equivalent to first-order eccentricity resonances in the restricted three-body problem, and hence allows us to use results from the literature to address (i).

The areas enclosed by the inner and outer branches of the separatrix, in the

notation of Figure 6.5, are given by

$$\mathcal{A}_{\rm A} = 3\left\{\frac{1}{2}\left[\Phi_{\rm max}+\Phi_{\rm min}+2\Phi_3+\frac{2}{3}\delta\right]\left(\frac{\pi}{2}-\gamma\right) - \sqrt{(\Phi_{\rm max}-\Phi_3)(\Phi_3-\Phi_{\rm min})}\right\}, \tag{6.79}$$

$$\mathcal{A}_{\rm C} = -3\left\{\frac{1}{2}\left[\Phi_{\rm max}+\Phi_{\rm min}+2\Phi_3+\frac{2}{3}\delta\right]\left(\frac{\pi}{2}+\gamma\right) + \sqrt{(\Phi_{\rm max}-\Phi_3)(\Phi_3-\Phi_{\rm min})}\right\}, \tag{6.80}$$

where $\Phi_{\rm min,max}$ are points where the separatrix crosses $\phi = 0$:

$$\Phi_{\rm min} = -\delta - \Phi_3 - 2(2\Phi_3)^{1/4}\ , \tag{6.81}$$

$$\Phi_{\rm max} = -\delta - \Phi_3 + 2(2\Phi_3)^{1/4}\ , \tag{6.82}$$

Φ_3 is the location of the saddle point, given by (6.62), and

$$\gamma = \sin^{-1}\left(\frac{\Phi_{\rm max}+\Phi_{\rm min}-2\Phi_3}{\Phi_{\rm max}-\Phi_{\rm min}}\right) \tag{6.83}$$

(Murray & Dermott, 1999, and references therein). The sum of the areas obeys the relation

$$|\mathcal{A}_{\rm A}| + |\mathcal{A}_{\rm C}| = -2\pi\delta\ . \tag{6.84}$$

Gravitational radiation will cause δ to drift with time from negative to positive values. Thus, if the system crosses the separatrix from region A to region C, then the initial and final values of the action variable are related by

$$|\overline{\Phi}_{\rm init}| + |\overline{\Phi}_{\rm final}| = -\delta_{\rm s}\ , \tag{6.85}$$

where $\delta_{\rm s}$ is the value of δ at the separatrix crossing. Note that, since the bifurcation discussed in Section 6.3.2 occurs at $\delta = -3$, it must be true that $\delta_{\rm s} \leqslant -3$.

Because of gravitational radiation, long enough before and after resonance, the condition $\Phi \ll |\delta|$ will inevitably be satisfied. In Section 6.3.3, we observed that in

this regime the trajectory of system is well-approximated by a circle centered at the origin. This is equivalent to the statement that for large $|\delta|$, $\{\phi, \Phi\}$ are action-angle variables for the system. Thus, asymptotically, Φ is an adiabatic invariant, which is also implied by (6.72) in the limit $|\delta| \to \infty$. We can therefore approximate the initial and final values of $\overline{\Phi}$ across the resonance with the initial and final (asymptotic) values of Φ:

$$|\overline{\Phi}_{\rm init}| \approx \Phi_{\rm init} \ , \qquad |\overline{\Phi}_{\rm final}| \approx \Phi_{\rm final} \ . \tag{6.86}$$

The initial and final values of Φ (which is the scaled mode energy) are then related by (6.85), and we have:

$$\Phi_{\rm init} + \Phi_{\rm final} = -\delta_{\rm s} \ , \tag{6.87}$$

or, restoring the scaling factors,

$$E_j^{\rm init} + E_j^{\rm final} = -\delta_{\rm s}\omega_j\lambda \ . \tag{6.88}$$

Writing

$$\overline{L} \simeq \frac{q}{(1+q)^{1/3}} n^{-1/3} \ , \tag{6.89}$$

which is correct to lowest order in $P/\overline{L}$, in (6.48), and using the fact that $\omega_j \simeq kn$ near resonance, λ is given approximately by

$$\lambda \simeq \left[\frac{1}{3}\frac{q}{(1+q)^{1/3}} Q_j \omega_j^{2(\ell-1)/3} k^{-2(\ell+2)/3} X_{jk}^{+}\right]^{2/3} \ . \tag{6.90}$$

Note that the relation (6.88) between the initial and final mode energies does not depend upon the rate of dissipation by gravitational radiation. The radiation reaction is only important in so far as it evolves the system through resonance adiabatically. Furthermore, it is clear that the energy transfer will always be positive, as the area enclosed by the trajectory always increases when crossing from region A to region C (Figure 6.5). There is also no explicit dependence upon where in the phase plane the separatrix is actually crossed.

It remains to find $\delta_{\rm s}$. A limiting case which admits a simple solution is when the

energy of the system at the time of separatrix crossing is zero. This corresponds to when the system's trajectory passes through the point $x = y = 0$, and hence when the initial amplitude of the mode is zero. Instead of solving (6.94) directly for $\delta_{\rm s}$, this case is more easily handled by considering the points where the zero-energy contours intersect the x-axis:

$$\mathcal{H}^{\dagger}(x,0) = \frac{x}{4}(x^3 + 2\delta x + 8) = 0 \ . \tag{6.91}$$

This equation always has one trivial solution at $x = 0$. The alternatives are solutions to

$$x^3 + 2\delta x + 8 = 0 \ . \tag{6.92}$$

This equation has either one or three real solutions, depending upon the sign of its discriminant (cf. the discussion of the bifurcation in Section 6.3.2). The bifurcation of roots occurs when the discriminant vanishes:

$$\frac{8}{27}\delta_{\rm s_0}^3 + 16 = 0 \ ,$$

which has the real solution

$$\delta_{\rm s_0} = -\sqrt[3]{54} = -3.779763\ldots \ . \tag{6.93}$$

The interpretation of this bifurcation is as follows. When there are three real solutions, there are four total intersections of zero-energy contours with the x-axis (including the $x = 0$ intersection). These four intersections correspond to two distinct contours: one in region A and the other in region C of Figure 6.5. Each contour intersects the x-axis twice. As δ approaches $\delta_{\rm s_0}$, these contours converge to the separatrix, which has three intersections with the x-axis. For $\delta > \delta_{\rm s_0}$, there is only one zero-energy contour which is the one that passes through $x = y = 0$ (cf. Figure 6.2). Since at $\delta = \delta_{\rm s_0}$ the zero-energy contour corresponds to the separatrix, it follows that $\delta_{\rm s_0}$ is the value of δ when a system with zero energy crosses the separatrix.

More generally, to find $\delta_{\rm s}$ we need to know when the energy of the system is equal

to the energy of the separatrix. In other words, we have to solve

$$\mathcal{H}^{\dagger}(x_3(\delta_{\rm s}), 0; \delta_{\rm s}) = E_{\rm sys} \tag{6.94}$$

for $\delta_{\rm s}$. As the system's energy is a function of time because of gravitational radiation, it is clear that obtaining an exact solution to the above equation requires solving for the motion of the system, which is cumbersome. Instead, we use the second-order approximation to the system's energy given by (6.73):

$$E_{\rm sys} \approx \Phi^2 + \delta\Phi - \frac{2\delta}{(\delta + 2\Phi)^2} \ , \tag{6.95}$$

which is valid away from resonance. Thus, $\delta_{\rm s}$ can now be estimated as the solution to

$$\frac{1}{4}x_3^4 + \frac{\delta_{\rm s}}{2}x_3^2 + 2x_3 = \Phi_{\rm init}^2 + \delta_{\rm s}\Phi_{\rm init} - \frac{2\delta_{\rm s}}{(\delta_{\rm s} + 2\Phi_{\rm init})^2} \ . \tag{6.96}$$

This is a non-trivial equation, but it can be simplified somewhat with the observation that, by definition, x_3 satisfies

$$x_3^3 + \delta x_3 + 2 = 0 \tag{6.97}$$

(cf. (6.57)). Using this, we can eliminate x_3^4 from (6.96), which gives

$$\frac{\delta_{\rm s}}{4}x_3^2 + \frac{3}{2}x_3 = \Phi_{\rm init}^2 + \delta_{\rm s}\Phi_{\rm init} - \frac{2\delta_{\rm s}}{(\delta_{\rm s} + 2\Phi_{\rm init})^2} \ . \tag{6.98}$$

Though simpler, this equation is still not amenable to analytic solution, but it is straightforward to solve numerically or graphically. The solution for a range of values of $\Phi_{\rm init}$ is shown in Figure 6.6. (See Appendix G for a brief discussion of issues that can arise in the solution.) We note that the magnitude of the slope of the curve in Figure 6.6 is always greater than two, which implies that for each unit of initial energy in the mode, the final energy gains more than one unit. In other words, the energy transfer increases with the initial mode energy.

In summary, the prescription for calculating the energy transfer including back

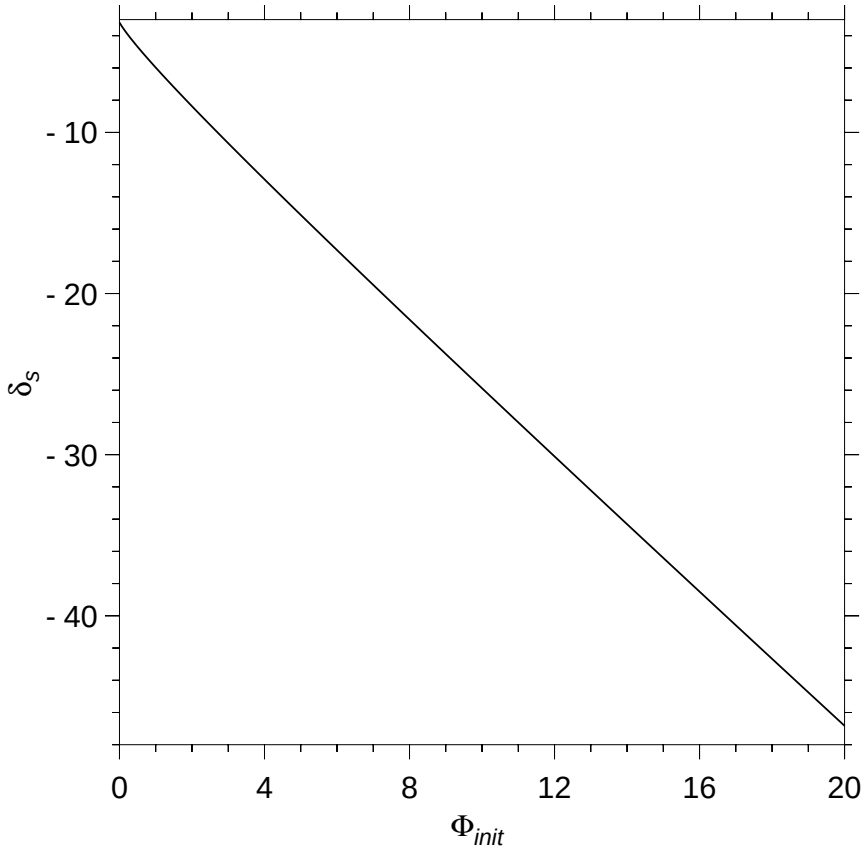

Figure 6.6: The separatrix crossing parameter, δ_s, as a function of the initial asymptotic value of Φ, obtained by solving (6.98).

reaction for a resonance with a given harmonic, eccentricity, and initial mode energy, is as follows:

1. Calculate the scaling parameter λ using (6.90). Then, $\Phi_{\rm init}$ is given by $E_j^{\rm init}/\omega_j\lambda$.

2. Calculate the separatrix crossing parameter $\delta_{\rm s}$ by solving (6.98). From this, $\Phi_{\rm final}$ follows: $\Phi_{\rm final} = -\delta_{\rm s} - \Phi_{\rm init}$.

3. The mode energy after resonance, $E_j^{\rm final}$, is given by $\omega_j\lambda\Phi_{\rm final}$.

A comparison of energy transfers calculated using the above prescription with numerical integrations of the equations of motion from (6.42) are shown in Figure 6.7 for several choices of parameters. Overall, the predicted final energies are accurate to within $\sim 10\%$, with the trend being an over-estimation of the energy transfer. Most of this error results from approximating $\delta_{\rm s}$ by the solution to (6.98). We note that an accuracy of $\sim 10\%$ is quite good when compared to the fact that the energy transfer given by the no back reaction approximation is incorrect in all of these cases by an order of magnitude or more.

6.4.4 Orbital Evolution

As energy is transferred from the orbit to a mode at a tidal resonance, the orbital elements will be affected. Knowing the resonant energy transfer, we can compute the change in the orbital elements by using the fact that, in the near-resonant regime, $\overline{G}$ and $\overline{L}$ are constants of the motion. Using this with the defining relations

$$\overline{G} = G + mP \ , \tag{6.99}$$

$$\overline{L} = L + kP \ , \tag{6.100}$$

it follows that

$$\Delta G = -m\Delta P \ , \tag{6.101}$$

$$\Delta L = -k\Delta P \ . \tag{6.102}$$

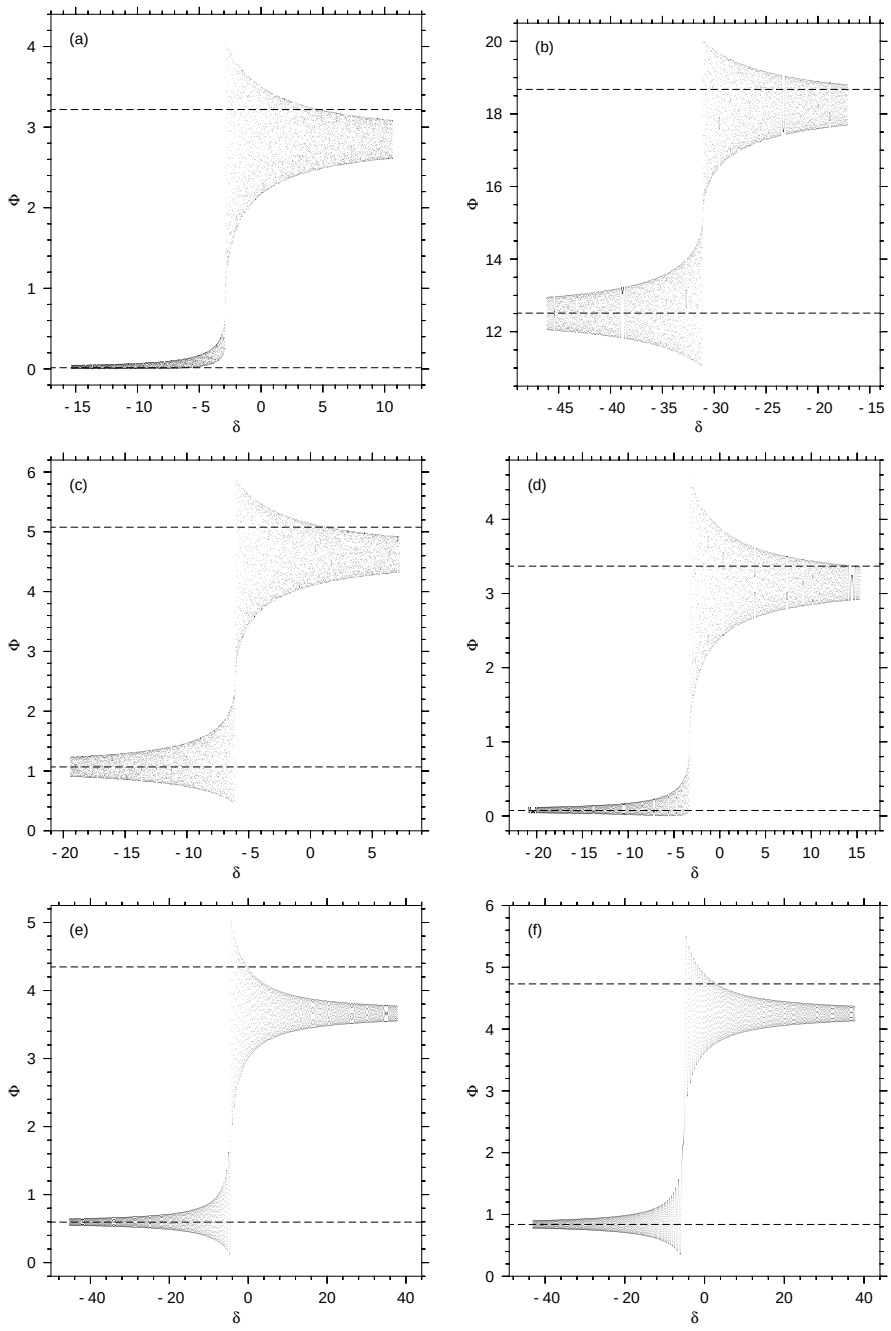

Figure 6.7: A comparison of the energy transfers predicted by (6.87) and (6.98) with the numerical results from direct integration of the equations of motion given by the Hamiltonian (6.42). All plots are for the $\ell = m = 2$ f-mode of a 0.6 $M_\odot$ white dwarf. In each plot, the lower dashed line marks $\Phi_{\rm init}$ and the upper dashed line marks the predicted value for $\Phi_{\rm final}$. The parameters for the plots in the format (q, k, e_0, x_0) are as follows: (a) (1, 7, 0.1, 0.001), (b) (10, 15, 0.3, 0.1), (c) (10^2, 10, 0.3, 0.25), (d) (10^3, 20, 0.5, 0.05), (e) (10^4, 8, 0.2, 0.5), (f) (10^5, 17, 0.5, 1.0). The parameters e_0 and x_0 are the initial orbital eccentricity and mode amplitude, respectively.

Expanding $n(L)$ and $e(G,L)$, given by (6.18) and (6.19), to linear order in $\Delta G/G$ and $\Delta L/L$, and writing $n \simeq \omega_j/k$, we find

$$\Delta n \simeq 3\frac{(1+q)^{1/3}}{q}\frac{\omega_j^{4/3}}{k^{1/3}}\Delta P \ , \tag{6.103}$$

$$\Delta e \simeq \frac{(1+q)^{1/3}}{q}\omega_j^{1/3}\frac{\sqrt{1-e^2}}{k^{1/3}e}(m-k\sqrt{1-e^2})\Delta P \ , \tag{6.104}$$

where ΔP is to be calculated as described in Section 6.4.3. Note that the expression for Δe is not valid for a circular orbit. For the circular case, Δe is identically zero.

It follows from (6.103) and (6.104) that the orbital frequency and eccentricity always increase and decrease, respectively, across a resonance.[6]

6.5 Discussion

6.5.1 Regime of Validity

In order to assess the applicability of the results obtained in the previous section, it is worth considering the various assumptions and approximations made in arriving at (6.88). Perhaps the most important assumption is that of low to moderate eccentricities. This is what allows us to ignore the F_{jk}^- terms relative to the F_{jk}^+ terms in (6.28). This assumption also plays a role in the reduction of the system from two degrees-of-freedom in (6.31) to one degree-of-freedom in (6.42), even though it was not mentioned explicitly. We expect that the approximation of the resonant mode as a pure traveling wave is increasingly inaccurate with higher eccentricities. In the impulse limit, which is relevant for very high eccentricities, the star is essentially 'struck with a hammer' as it swings by periastron in each orbit. The direction of orbital rotation is then unimportant, and the resonant mode is likely to have a significant counter-rotating component. Another place where the low-eccentricity approximation has been used is in the consideration of only the $\ell = m$ mode near resonance,

[6] While (6.104) would seem to imply that the eccentricity can increase across a resonance, it does so in regimes where our formalism is not valid.

by arguing that modes with lower values of m will be suppressed by $\ell - m$ powers of eccentricity relative to the $\ell = m$ modes.

There is, in fact, a reason to think that the consideration of a single near-resonant mode and the pure traveling wave approximation will in reality be more accurate than expected. Consider the set of modes with the same radial order and the same ℓ. These modes are degenerate in frequency only in the absence of stellar rotation. For example, for a star rotating rigidly with an angular frequency Ω that is parallel to the orbital angular momentum, the mode frequencies are split to lowest order as $\omega_j \pm m\Omega$ ($+m$ for a co-rotating component, $-m$ for a counter-rotating component). Therefore, for a rotating star, modes with different values of m will be resonant at different frequencies. In fact, the co-rotating and counter-rotating components of a given mode will also have different frequencies, and the near-resonant Hamiltonian will naturally have a single degree-of-freedom (cf. Alexander, 1988). Thus, a slowly rotating star, such as a realistic white dwarf, is likely to improve rather than diminish the accuracy of our results. Also, note that for $m = 0$ modes ('quasi-static' modes), the single degree-of-freedom description is accurate for arbitrarily high eccentricities as there are no F_{jk}^{-} terms. For a non-rotating star, the resonances of the quasi-static modes overlap with the resonances of modes with higher m (and, hence, our results are not applicable), but for a rotating star the resonances will be separated.

A key assumption that underlies our calculation of the energy transfer is that the adiabatic approximation is valid away from separatrices. In other words, we have assumed that gravitational radiation evolves the orbit on a time-scale longer than the period of the system's orbit in phase space. This condition is expected to be satisfied for most realistic systems. An important exception is a compact object binary during the last few orbits before coalescence. However, in that case, a linear tidal analysis is unlikely to be accurate anyway. In addition, the adiabatic assumption may also break down for companions with very large masses, even before the final stages of coalescence. In such cases, estimates with and without back reaction may be considered as providing limits on the resonant energy transfer.

It may be questioned as to why we have only considered separatrix crossings from

region A to region C (Figure 6.5). That the system will eventually end up in region C is certain because gravitational radiation decreases the area inside the separatrix with time. And as the area enclosed by the inner branch of the separatrix (i.e., the area of region A) for large negative values of δ is nearly equal to the area enclosed by the outer branch of the separatrix, it is reasonably clear that a realistic system will almost always start in region A and then cross to region C.[7]

In addition to the above, there are a number of other issues that can be legitimately raised regarding our analysis. For example, we did not dwell upon the averaging step in going from (6.17) to (6.21), and this 'sleight-of-hand' conceals considerable technical complexity. Strictly speaking, what (6.21) represents is the first-order approximation in a two time-scale expansion, and there are known issues with the convergence of such a perturbation series. In particular, it can be shown to converge only asymptotically. Moreover, by eliminating the 'fast' angle variables in (6.21), we have potentially changed the dynamics of the system in some regimes (Lichtenberg & Lieberman, 1992). Another important point is that by reducing the system to a single degree-of-freedom in the near-resonant regime, the possibility of chaos is precluded, where as in the full system with multiple degrees-of-freedom, chaos is a possibility—indeed, a certainty in a layer around a separatrix. Nonetheless, despite all of these potential issues, we expect and conjecture that our highly-simplified description of the near-resonant dynamics captures the essential features in a coarse-grained sense. Detailed discussions of technical issues such as we have mentioned and others can be found in Lichtenberg & Lieberman (1992).

Finally, we note that the assumption of negligible mode damping on a resonance time-scale is crucial to our analysis. In circumstances where this assumption is strongly violated, the accuracy of our treatment is uncertain.

[7] It is certainly possible to enforce initial conditions that place the system in region B before some resonance. However, it is difficult to imagine in what physically plausible situation this possibility could be realized.

6.5.2 Long-Term Evolution

As an eccentric WDCO binary evolves under gravitational radiation reaction, each white dwarf normal mode will encounter a sequence of resonances with the harmonics of the orbital frequency. Back reaction introduces a qualitative change in the long-term evolution of the mode energies in that the energy transfer to the mode at each resonance is always positive. This is quite different from the no back reaction approximation where the energy transfer can be positive or negative, depending upon the initial phase and initial mode energy. In this sense, back reaction actually simplifies the problem: the evolution of the mode energy is not stochastic or pseudo-stochastic, rather it is monotonic and deterministic.[8]

For a given mode, let P_k be the mode energy divided by the mode frequency before passage through the kth harmonic resonance, and let λ_k and δ_k be the scaling and separatrix crossing parameters for the kth resonance. Assuming negligible energy transfer to the mode between resonances, and also negligible mode damping, it then follows from (6.87) that

$$P_{k-1} = -P_k + \lambda_k |\delta_k| \ . \tag{6.105}$$

Applying this formula repeatedly, we find that after passage through r resonances

$$P_{k-r} = (-1)^r P_k + \sum_{s=0}^{r-1} (-1)^s \lambda_{k-s} |\delta_{k-s}| \ . \tag{6.106}$$

The above deterministic equation replaces the random walk, (5.35), found in the no back reaction approximation.

[8] Technically, the evolution of the mode energy in the no back reaction approximation is also deterministic. However, as the initial phase at successive resonances is typically uncorrelated with the phase at previous resonances, the phase acts more or less like a random variable. Hence the term 'pseudo-stochastic.'

Part III

Non-Linear Evolution of Modes

Chapter 7

A Hydrodynamics Code for Studying Tidal Excitation

Large resonant energy transfers in a WDCO system may result in heating and, possibly, the detonation of the white dwarf, leading to an exotic Type Ia supernova. In order to assess the magnitude and likelihood of such a scenario, it is necessary to understand the mode excitation process in detail. For the linear regime, this has been considered in the preceding chapters, and it was found that, depending upon the initial conditions, it is possible to excite modes with large enough amplitudes that the validity of the linear theory becomes questionable. Therefore, it is necessary to investigate the mode evolution in the non-linear regime. This is most directly done via numerical hydrodynamics simulations.

A number of hydrodynamics codes which may be used for this purpose currently exist. Two such codes, ZEUS (Stone & Norman, 1992) and Flash (Fryxell et al., 2000) have been developed to be generic hydrodynamic engines. Such codes provide access to a sophisticated suite of hydrodynamic simulation tools. However, they also have the disadvantage of being complicated to use and, perhaps, sub-optimal for our specific problem. In addition, to a good approximation, the white dwarf oscillations are adiabatic, and, hence, detailed treatment of shocks and entropy generation are unnecessary.

Motl et al. (2002) have developed an adiabatic hydrodynamics code, primarily for studying binary mass transfer. However, the choice of a cylindrical grid, while useful

for the mass transfer application, is problematic for the case of a pulsating white dwarf, where it is important to maintain uniform resolution throughout the star. Furthermore, a cylindrical coordinate system complicates the numerical advection scheme. These difficulties are avoided with a Cartesian grid, an additional advantage of which is that the Poisson equation can be solved easily and efficiently via spectral methods.

In this chapter, we present a simple hydrodynamics code with some diagnostics and an example application.

7.1 Governing Hydrodynamic Equations

There is considerable freedom in the choice of macroscopic quantities used to describe fluid flows. Our choice was primarily dictated by the numerical convenience of the sourced advective form of the hydrodynamic equations. In addition, since we are restricting ourselves to adiabatic flows, it is convenient to use the entropy rather than the energy as a thermodynamic variable. We therefore chose the following five quantities to describe the fluid flow: mass density (ρ), entropy density (s), and momentum density ($\boldsymbol{J}$).

The equations for ρ and s have a purely advective form,

$$\frac{\partial \rho}{\partial t} + \nabla \cdot (\boldsymbol{v}\rho) = 0 \tag{7.1}$$

$$\frac{\partial s}{\partial t} + \nabla \cdot (\boldsymbol{v}s) = 0\,, \tag{7.2}$$

which correspond to the conservation of mass and entropy.[1] The equation for $\mathbf{J}$ can be written in a sourced advective form,

$$\frac{\partial \boldsymbol{J}}{\partial t} + \nabla \cdot (\boldsymbol{v}\boldsymbol{J}) = -\nabla P - \rho \nabla \Phi + \boldsymbol{f}\ , \tag{7.3}$$

[1]Note that s is the entropy per unit volume and not the specific entropy. Hence, in our notation, the adiabatic condition is

$$\frac{d}{dt}\left(\frac{s}{\rho}\right) = 0\ ,$$

where d/dt is the convective derivative.

where the pressure (P) is given by an equation of state,

$$P = P(\rho, s) \ , \tag{7.4}$$

the self-gravitational potential (Φ) is determined by the Poisson equation,

$$\nabla^2 \Phi = 4\pi G\rho \ , \tag{7.5}$$

and $\boldsymbol{f}$ is any additional external force per unit volume acting on the fluid (e.g., an external gravitational field and/or Coriolis forces).

7.2 Differencing Scheme

In one dimension, the use of a staggered mesh avoids the interpolation of the flow velocities to the cell boundaries. With a zone-centered grid, the velocities would have to be interpolated, which would complicate the advection step in the momentum conservation equation (7.3). However, in multiple dimensions, the interpolation of vector quantities (e.g., the momentum density) cannot be avoided by the use of a staggered mesh. Therefore, we use the conceptually simpler zone-centered grid.

Casting the hydrodynamic equations in a sourced advective form allows the explicit conservation of mass, entropy, and momentum (in so far as the source terms allow).

7.2.1 Advection

The advection steps in equations (7.1–7.3) may be integrated to yield finite-difference equations for a given cell

$$\Delta\lambda = \frac{\Delta t}{\Delta V} \sum_{i=x,y,z} \left(\Lambda_{-i} - \Lambda_{+i}\right) \Delta S_i \ , \tag{7.6}$$

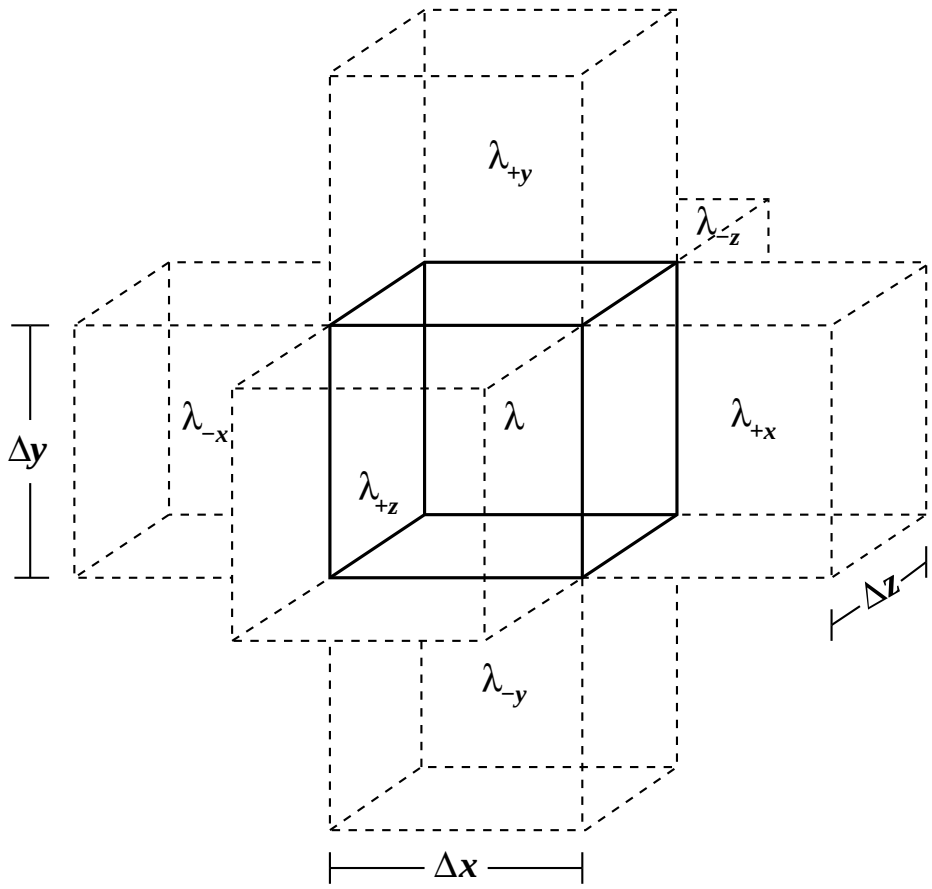

Figure 7.1: The geometry of a zone-centered, uniform Cartesian grid is shown. Here, λ can be any of the five evolved quantities (ρ, s, and $\boldsymbol{J}$) or the gravitational potential (Φ).

where $\Delta\lambda$ is the change in the quantity λ due to fluid advection, Δt is the time step, ΔV is the cell volume, $\Lambda_{\pm i}$ are the fluxes of the quantity λ at the $\pm i$th boundary of the cell, and ΔS_i is the area of the cell surface normal to the ith direction.

In general some interpolation is required to determine the values of the fluxes at the boundaries of the cell. We break the interpolation of the fluxes into an interpolation over the fluid velocity and an interpolation over the advected quantities,

$$\Lambda_{\pm i} = \lambda^*_{\pm i}\overline{v}_{\pm i} \ , \tag{7.7}$$

where $\overline{v}_{\pm i}$ is the interpolated component of the velocity normal to the $\pm i$th cell face at the cell boundary, and λ^* is the interpolated value of the advected quantity. The $\overline{v}_{\pm i}$ are defined by

$$\overline{v}_{\pm i} = \frac{1}{2}(v^i + v^i_{\pm i}) \ , \tag{7.8}$$

where v^i and $v^i_{\pm i}$ are the values of the fluid velocity in the ith direction at the centre of the current cell, and the centres of the neighbouring cells in the $\pm i$th directions, respectively.

A numerical difficulty with the interpolation of the advected quantities is that advecting the volumetric densities tends to generate unphysically high velocities in low cells with low mass density. We circumvent this problem by using consistent transport (Stone & Norman, 1992), in which it is the specific quantities that are interpolated, i.e.,

$$\lambda^*_{\pm i} = \overline{\rho}_{\pm i}(\overline{\lambda/\rho})_{\pm i} \ , \tag{7.9}$$

where $\overline{\rho}_{\pm i}$ and $(\overline{\lambda/\rho})_{\pm i}$ are the interpolated values of ρ and the specific quantity λ/ρ at the $\pm i$th boundary of the cell.

The choice of the method used for interpolating the advected quantities has to be made carefully, so as to avoid introducing instabilities in the finite-difference scheme. Several such methods exist, of which we have chosen to use upwinding methods. These methods provide stability by clipping new local extrema, and limit diffusivity by interpolating quantities to the boundary in a way that accounts for the difference between

the velocities associated with the upwind and downwind characteristics. Upwinding methods of various orders exist, with the the higher-order methods being necessarily more computationally expensive. The three methods we have implemented are the donor cell (zeroth-order), van Leer (first-order), and piecewise parabolic advection (PPA; second-order) methods.

7.2.1.1 Donor Cell Upwinding

The donor cell method is a zeroth-order upwinding scheme, approximating the spatial distribution of a given quantity, q, as a step function. In this method, all information from the downwind cell is ignored, i.e. at the $-i$th cell boundary

$$\overline{q}_{-i} = \begin{cases} q_{-i} & \text{if} \quad \overline{v}_{-i} \geqslant 0 \\ q & \text{if} \quad \overline{v}_{-i} < 0 \end{cases} . \tag{7.10}$$

For a given cell, this only requires information from the nearest neighbors. In practise, donor cell upwinding is highly diffusive (see, e.g., Section 7.4.1), and hence was not used beyond the testing stage.

7.2.1.2 van Leer Upwinding

The van Leer upwinding method is a first-order method first described by its namesake (van Leer, 1977a,b, 1979). In contrast to the donor cell method, the distribution of q is approximated by a piecewise linear function. The slopes of these linear functions are given by the so-called van Leer slopes, defined below for a given cell along the ith direction,

$$dq^i = \begin{cases} \dfrac{2(q_{+i} - q)(q - q_{-i})}{\Delta x^i (q_{+i} - q_{-i})} & \text{if} \quad (q_{+i} - q)(q - q_{-i}) > 0 \\ 0 & \text{otherwise} \end{cases} . \tag{7.11}$$

In terms of the van Leer slopes, the upwinded value of the quantity q at the $-i$th cell boundary is given by

$$\overline{q}_{-i} = \begin{cases} q_{-i} + \frac{1}{2}\left(\Delta x^i - \overline{v}_{-i}\Delta t\right) dq^i_{-i} & \text{if} \quad \overline{v}_{-i} \geqslant 0 \\ q - \frac{1}{2}\left(\Delta x^i + \overline{v}_{-i}\Delta t\right) dq^i & \text{if} \quad \overline{v}_{-i} < 0 \end{cases}, \tag{7.12}$$

where the notation $dq^i_{\pm j}$ denotes the van Leer slope in the ith direction for the neighboring cell in the $\pm j$th direction. The van Leer method prevents the introduction of new local extrema, and hence ensures stability in the advection scheme. When the van Leer slopes vanish, the scheme reduces to the donor cell method. Note that, because van Leer upwinding uses the van Leer slopes of neighboring cells, it requires information from both the nearest and next-nearest neighbors.

7.2.1.3 PPA Upwinding

The PPA method is a second-order upwinding method originally developed by Colella & Woodward (1984). It approximates the distribution of q by a piecewise parabolic function. The essence of the method is the determination of the monotonized left and right interface values, q_L and q_R, which are computed via equations (1.6)–(1.10) in Colella & Woodward (1984). In terms of q_L and q_R, the upwinded value of q at the $-i$th cell boundary is given by

$$\overline{q}_{-i} = \begin{cases} q_{R,-i} + \xi(q_{-i} - q_{R,-i}) & \\ \quad + \xi(1-\xi)(2q_{-i} - q_{R,-i} - q_{L,-i}) & \text{if} \quad \overline{v}_{-i} \geqslant 0 \\ q_L + \xi(q - q_L) & \\ \quad + \xi(1-\xi)(2q - q_R - q_L) & \text{if} \quad \overline{v}_{-i} < 0 \end{cases}, \tag{7.13}$$

where $\xi = \overline{v}_{-i}\Delta t/\Delta x^i$. This requires information from the nearest three neighbors.

The PPA method is substantially less diffusive than the van Leer method. This is especially notable at discontinuities, where the profiles generated by PPA are significantly steeper than those generated by the van Leer scheme. However, the improve-

ment comes with a relatively high computational cost. It has been found by Stone & Norman (1992) that, typically, increasing the grid resolution is a computationally more efficient way to obtain greater accuracy. For this reason, unless explicitly stated otherwise, we use the van Leer upwinding method.

7.2.2 Artificial Viscosity

In Eulerian upwinding schemes, shocks can lead to numerical instabilities. If resolving shocks is critical, the instabilities may be cured via the introduction of Riemann solvers (capable of localising a shock to a single cell boundary). However, if resolving shocks is unnecessary, it is significantly easier to introduce an artificial numerical viscosity to smooth them out. Several prescriptions for implementing numerical viscosity can be found in the literature; we chose to implement the von Neumann-Richtmyer scheme because of its ability to produce the correct shock propagation velocity and its low dissipation far from shocks (a direct result of the fact that it acts only in regions of compression; Stone & Norman, 1992). This scheme takes the form of defining a viscous pseudo-pressure for each direction which is non-vanishing in regions of compression only:

$$Q^i = \begin{cases} l^2 \rho \left(\dfrac{\partial v^i}{\partial x^i} \right)^2 & \text{if} \quad \dfrac{\partial v^i}{\partial x^i} < 0 \\ 0 & \text{otherwise} \end{cases} , \tag{7.14}$$

for $i = x$, y, z, where l is the length scale over which shocks are to be smoothed. The associated source term for equation (7.3) is given by

$$F^i_{\text{visc}} = -\frac{\partial Q^i}{\partial x^i} . \tag{7.15}$$

Typically this will smooth a shock front over a number of cells—a distance that is usually much larger than the natural shock depth. It should also be noted that a strictly correct treatment of shocks is precluded by the adiabatic condition, equation (7.2). This can be remedied by the inclusion of a viscous source term in the entropy equation. However, since for the applications we envision shocks will result

in the rapid thermalization of the kinetic energy of the stellar oscillations, their mere production may make a purely hydrodynamic description inapplicable. In particular, thermonuclear processes could dominate at such a point, and thus neither the added complexity and computational overhead of the Riemann solver methods nor the complication of an entropy source term are required.

7.2.3 Momentum Source Terms

In addition to advection, the momentum density evolves due to pressure gradients, self-gravity, and external forces (if any). We have found that simply finite-differencing ∇P leads to a less stable system than calculating the gradient via partial derivatives of the equation of state, and finite-differencing in ρ and s. In contrast, the gravitational acceleration is obtained directly in terms of a second-order, finite-difference of the gravitational potential (the details of solving for which are presented in Section 7.3). The finite differencing of the viscous force is performed in two steps: (*i*) determining the viscous pseudo-pressure, and (*ii*) finite differencing the viscous pseudo-pressure to obtain the viscous force directly. In finite difference form, the viscous pseudo-pressure is defined by

$$Q^i_{\pm i} = \begin{cases} \eta \dfrac{\rho_{\pm i} + \rho}{2} \left(\dfrac{v^i_{\pm i} - v^i}{\Delta x^i} \right)^2 & \text{if} \quad \pm \left(v^i_{\pm i} - v^i \right) < 0 \\ 0 & \text{otherwise} \end{cases} , \tag{7.16}$$

for $i = x, y, z$. The dimensionless coefficient η is approximately the number of cells over which discontinuities are to be smoothed. Typically, we find $\eta = 2$ to be adequate. The viscous force is then determined by

$$F^i_{\rm visc} = -\frac{Q^i_{+i} - Q^i_{-i}}{\Delta x^i} . \tag{7.17}$$

Therefore, excluding external forces, the source terms in equation (7.3) are given by

$$-\left(\frac{\partial P}{\partial \rho}\right)_s \frac{\rho_{+i}-\rho_{-i}}{2\Delta x^i} - \left(\frac{\partial P}{\partial s}\right)_\rho \frac{s_{+i}-s_{-i}}{2\Delta x^i} - \rho\frac{\Phi_{+i}-\Phi_{-i}}{2\Delta x^i} + F^i_{\rm visc} \ , \quad (7.18)$$

for $i = x, y, z$.

When using a barotropic equation of state, $P(\rho)$, it can be convenient to write the source terms in terms of the specific enthalpy, h,

$$-\rho\left(\frac{h_{+i}-h_{-i}}{2\Delta x^i} + \frac{\Phi_{+i}-\Phi_{-i}}{2\Delta x^i}\right) + F^i_{\rm visc} \ , \quad (7.19)$$

for $i = x, y, z$. An example of when this is useful will be discussed in Section 7.5. Note that in this case, the entropy equation is superfluous.

7.2.4 Courant-Friedrichs-Lewy Time Step

The stability of our explicit finite-difference scheme requires that the time step should satisfy the Courant-Friedrichs-Lewy (CFL) criterion. This corresponds to the physical consideration that, in a single time step, information should only propagate into a given cell from the neighboring cells which are used to compute spatial derivatives at that point. A time step that is too large would require information from more distant cells, which is not available in the differencing scheme. Therefore, for stability,

$$\Delta t \leqslant t_{\rm CFL} \ , \quad (7.20)$$

where the CFL time is defined by

$$t_{\rm CFL} = \min\left(\frac{\Delta x}{c_s + |v^x|}, \frac{\Delta y}{c_s + |v^y|}, \frac{\Delta z}{c_s + |v^z|}\right) \ , \quad (7.21)$$

where c_s is the local adiabatic sound speed (e.g., Motl et al., 2002; Stone & Norman, 1992, and references therein). In addition, the inclusion of an artificial viscosity

imposes the additional requirement that the time step does not exceed the time-scale for diffusion across cell width length-scales:

$$t_{\rm visc} = \min\left(\frac{\Delta x}{4\eta|\Delta v^x|}, \frac{\Delta y}{4\eta|\Delta v^y|}, \frac{\Delta z}{4\eta|\Delta v^z|}\right) \ , \tag{7.22}$$

(e.g., Stone & Norman, 1992). In practice, for many operator split methods, taking the time step to be the CFL time does not ensure stability. Rather, it is necessary to take Δt to be some fraction of $t_{\rm CFL}$ or $t_{\rm visc}$. In practice, we find that a robust choice is

$$\Delta t \leqslant \frac{1}{4}\min\left(t_{\rm CFL}, t_{\rm visc}\right) \ . \tag{7.23}$$

From equation (7.21) it is clear that the cells with the highest velocities (both kinetic and sound) will provide the most stringent limits on the time step. An example is the case of cells constituting the vacuum surrounding a star. In practice, for numerical reasons, no portion of the grid can have vanishing mass density. Therefore, we take 'zero' density to be some small fraction (typically, 10^{-8}) of the initial maximum density. As a result, the vacuum is physically insignificant. Nonetheless, because of their large accretion velocities (though negligible momentum densities), the vacuum cells can be the limiting factor in determining the time step. To avoid this problem, we impose a velocity cap, so that the CFL time is set by only considering cells with densities larger than, say, 10^{-6} of the maximum density.[2] The remaining cells have their velocities capped at

$$v_{\rm cap} = \min\left(\frac{\Delta x}{\Delta t}, \frac{\Delta y}{\Delta t}, \frac{\Delta z}{\Delta t}\right) \ , \tag{7.24}$$

so as to not drive the time step down. While this explicitly violates the hydrodynamic equations presented in Section 7.1, it does so in a physically negligible manner.

We use operator splitting to separate the source and advection contributions to the evolution of the fluid quantities at each time step. However, we do not use directional

[2]What is important is that the density cut-off used for the CFL time is large enough to exclude the vacuum cells.

splitting, making our scheme a variation of the unsplit method of van Leer. Thus, a single time step is taken in two stages: (1) taking the source step, and (2) performing the updates due to advection. The gravitational potential is calculated at each source step.

7.2.5 Boundary Conditions

Because the upwinding methods require information about neighboring cells, it is necessary to provide a boundary of ghost cells along the outer edges of the grid. As these ghost cells are not evolved themselves, they require some prescription for assigning the evolved quantities to them. We have implemented three types of boundary conditions: fixed, replicated, and outflow.

The first, and simplest, is the fixed boundary condition. In this prescription, the boundary cells are fixed to have 'zero' density, entropy density, and momentum flux. This tends to limit the velocity of the 'zero' density vacuum by not providing a boundary momentum flux.

The second set of boundary conditions consists of replicating the last set of cells in the grid. This provides a slightly more realistic set of boundary conditions, allowing the accretion of the 'zero' density vacuum to stabilise through hydrodynamic balance. However, if a physically significant portion of the flow is crossing the boundary, then this is significantly superior to the first scheme.

The third set of boundary conditions implemented are the so-called outflow boundary conditions. In this prescription, fluid is allowed to flow off the grid but not into it. In order to prevent the boundaries from physically affecting the fluid on the grid, the boundary values for density and entropy are chosen to preserve hydrostatic equilibrium in the last grid zone. Note that this does not stop the fluid from advecting off the grid through this zone. As a result, this will minimise the creation of spurious reflections at the boundaries. For a self-gravitating fluid configuration that is initially contained entirely within the grid, this provides the most realistic set of conditions.

7.2.6 Parallelization

The primary purpose for the development of our code is to perform high resolution studies of the non-linear evolution of normal modes in white dwarfs. The resulting computational requirements necessitate high-performance computing. Because the sourced advection step for a given cell depends only upon cells in its immediate neighbourhood, it naturally lends itself to a straightforward parallelization scheme. This takes the form of dividing the entire grid into a number of sub-domains, each of which are handled by a separate process. Because interprocess communication incurs substantial performance penalties, we need to choose a domain decomposition that minimises the communication required. The source of interprocess communication in each sourced advection step is the need for neighbor data around the edges of each sub-domain. Therefore, the time penalties due to interprocess communication are dictated by the surface area of each sub-domain, as well as the depth of neighbors that is necessary (one for donor cell upwinding, two for van Leer upwinding, and three for PPA upwinding). Hence, minimizing the surface area of each sub-domain minimises the interprocess communication.

We have chosen to implement our code in the C++ programming language. This choice is motivated by considerations such as modularity of design, flexibility, efficiency, ease of code reuse, and extensibility. For example, using the object-oriented paradigm in the C++ language has allowed us to maintain a clean separation between interfaces and implementations (e.g., for the equation of state, Poisson equation solver, and initial conditions etc.), and features such as templates have allowed us to write generic code without sacrificing runtime performance.

As standard C++ does not provide facilities for parallel computing, it is necessary to use additional libraries to handle the parallelization. We have chosen to implement parallelisation via the Message Passing Interface (MPI). Since both optimising, ISO-compliant C++ compilers and high quality MPI implementations are available for virtually every major computing platform, our code is highly portable.

7.3 Solving the Poisson Equation

Equation (7.5) is distinct from equations (7.1-7.3) in that it requires global, rather than local, information. There are a number of methods that can be used to solve the Poisson equation. These include general elliptic equation set solvers, multigrid methods, multipole methods, and spectral methods (e.g., Motl et al., 2002; Fryxell et al., 2000; Muller & Steinmetz, 1995; Stone & Norman, 1992). Spectral methods tend to be the most efficient, and implementing them on a regular Cartesian grid is straightforward.

The solution of the Poisson equation requires the specification of a boundary condition on some closed surface. In most physical problems, this surface is chosen to lie at infinity, upon which the potential is chosen to vanish. However, since our computational domain is finite, it is not possible to impose a boundary condition at infinity in a straightforward manner. Instead, we define the value of the potential on the surface of our domain, which we compute via a multipole expansion:

$$\Phi^B(\mathbf{x}) = -\sum_{\ell=0}^{\infty}\sum_{m=-\ell}^{\ell}\frac{4\pi G}{2\ell+1}r^{-\ell-1}Q_{\ell m}Y_{\ell m}(\hat{\boldsymbol{x}}) \ , \tag{7.25}$$

where

$$Q_{lm} = \int d\boldsymbol{x}' \, r'^{\ell}Y^*_{\ell m}(\hat{\boldsymbol{x}}')\rho(\boldsymbol{x}') \ . \tag{7.26}$$

In practice, it is only necessary to include the first few multipoles (for our purposes $\ell_{\max} = 10$) to obtain accurate boundary values. Note that the boundary condition at infinity is built into the multipole expansion.

Given the Dirichlet boundary condition, it is possible to solve Poisson equation via a discrete sine transform (DST) (e.g., Press et al., 1992). Written in its finite-difference form, (7.5) becomes

$$\sum_{i=x,y,z}\frac{\Phi_{+i} - 2\Phi + \Phi_{-i}}{(\Delta x^i)^2} = 4\pi G\rho \ . \tag{7.27}$$

In terms of their discrete sine transforms $\widehat{\Phi}$ and $\widehat{\rho}$, Φ and ρ are given by

$$\Phi_{i,j,k} = \frac{2}{IJK} \sum_{m=1}^{I-1} \sum_{n=1}^{J-1} \sum_{p=1}^{K-1} \widehat{\Phi}_{m,n,p} \sin \frac{\pi i m}{I} \sin \frac{\pi j n}{J} \sin \frac{\pi k p}{K} \tag{7.28}$$

$$\rho_{i,j,k} = \frac{2}{IJK} \sum_{m=1}^{I-1} \sum_{n=1}^{J-1} \sum_{p=1}^{K-1} \widehat{\rho}_{m,n,p} \sin \frac{\pi i m}{I} \sin \frac{\pi j n}{J} \sin \frac{\pi k p}{K} \ , \tag{7.29}$$

where i, j, k, and I, J, K define the location in, and the dimensions of, the computational domain, respectively. Substituting these expansions into (7.27) gives

$$\widehat{\Phi}_{m,n,p} = -4\pi G \frac{\widehat{\rho}_{m,n,p}}{\kappa^2_{m,n,p}} \ , \tag{7.30}$$

where

$$\begin{aligned} \kappa^2_{m,n,p} = & \frac{2}{(\Delta x)^2} \left(1 - \cos \frac{\pi m}{I}\right) \\ & + \frac{2}{(\Delta y)^2} \left(1 - \cos \frac{\pi n}{J}\right) \\ & + \frac{2}{(\Delta z)^2} \left(1 - \cos \frac{\pi p}{K}\right) \ . \end{aligned}$$

The potential $\Phi_{i,j,k}$ is then computed from (7.28).

Expanding Φ in terms of the sine basis functions of the Fourier series ensures that it vanishes at the boundaries of the domain. Non-zero boundary conditions can be incorporated by adding an appropriate source term to the right side of equation (7.27). We may define $\Phi' = \Phi - \Phi^B$ where now Φ^B is determined by equation (7.25) at one zone beyond the boundary and vanishes everywhere else. The resulting equation for Φ' is the same as equation (7.27) in the interior and is given by

$$\sum_{i=x,y,z} \frac{\Phi'_{+i} - 2\Phi' + \Phi'_{-i}}{(\Delta x^i)^2} = 4\pi G\rho - \frac{\Phi^B_{\pm j}}{(\Delta x^j)^2} = 4\pi G\rho' \ , \tag{7.31}$$

on the $\pm j$th boundary. As a result, the effective source terms are given by

$$\begin{aligned} 4\pi G\rho'_{i,j,k} = 4\pi G\rho_{i,j,k} \\ - \frac{1}{(\Delta x)^2}\left(\delta_{i,1}\Phi^B_{0,j,k} + \delta_{i,I-1}\Phi^B_{I,j,k}\right) \\ - \frac{1}{(\Delta y)^2}\left(\delta_{j,1}\Phi^B_{i,0,k} + \delta_{j,J-1}\Phi^B_{i,J,k}\right) \\ - \frac{1}{(\Delta z)^2}\left(\delta_{k,1}\Phi^B_{i,j,0} + \delta_{k,K-1}\Phi^B_{i,j,K}\right) \ . \end{aligned} \tag{7.32}$$

To summarize, our procedure for solving the Poisson equation is:

1. Calculate Φ^B via the multipole expansion (7.25).
2. Calculate the effective source terms for Φ' from (7.32).
3. Perform a DST on the effective source terms.
4. Calculate $\widehat{\Phi}'$ from (7.30).
5. Perform a DST on $\widehat{\Phi}'$ to determine Φ'.

We do not actually need to add Φ^B to our final answer since it only affects the ghost points outside our grid. Note that, because we use a second-order finite-difference to determine the gravitational acceleration in equation (7.18), it is necessary to define Φ on an extra surface of ghost cells on each edge of the domain.

The DST is most efficiently parallelized in terms of a slab decomposition of the grid, as opposed to the ideal decomposition for the sourced advection step (which is cubical). As a result, a significant amount of interprocess communication is required to prepare for the solution of the Poisson equation at each source sub-step. However, we have found that the time saved by using the DST more than outweighs the penalty incurred by the communication overhead compared to alternative methods.

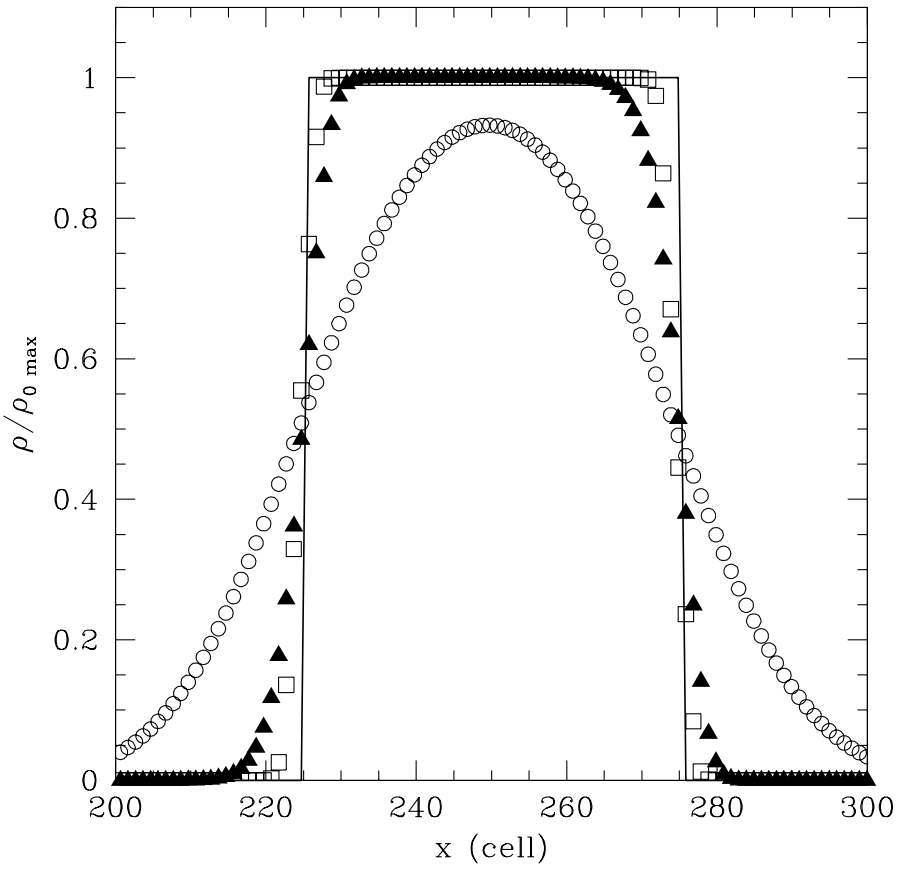

Figure 7.2: A square pulse that has been advected five times its initial width (50 cells) using the donor cell (open circles), van Leer (filled triangles), and PPA (open squares) upwinding schemes. For reference, the original pulse profile is also shown.

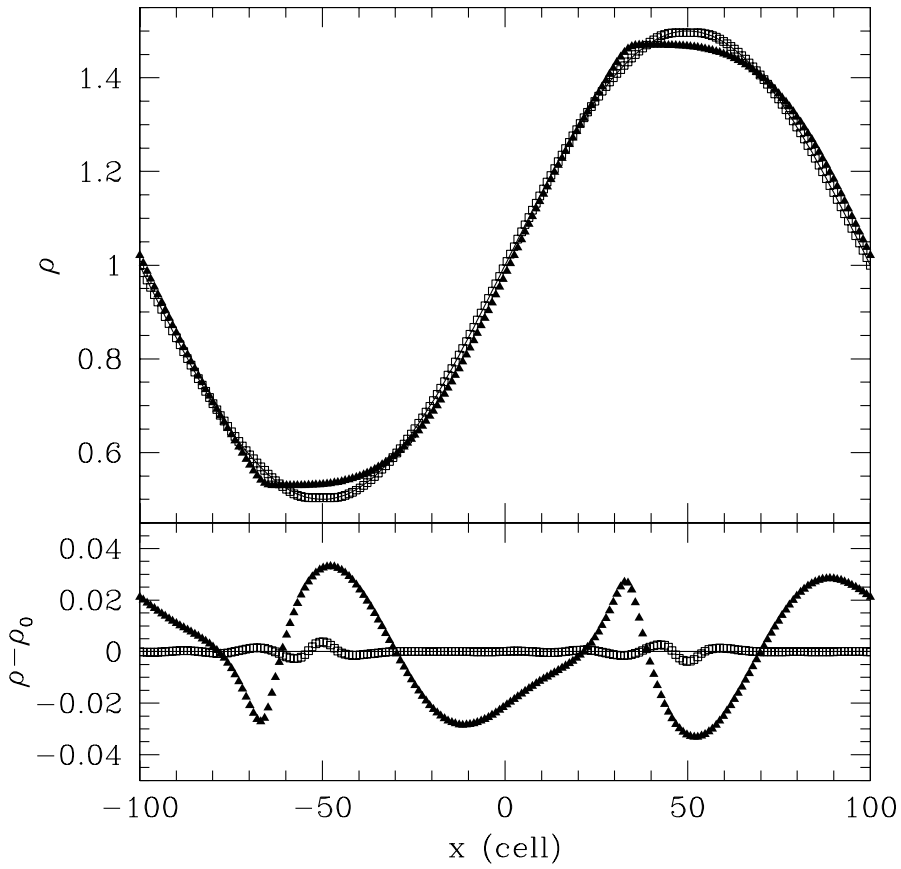

Figure 7.3: A sine wave is advected with periodic boundary conditions for 100 times its wavelength (200 cells) using the van Leer (filled triangles) and PPA (open squares) upwinding schemes. In the top panel the density profile is shown explicitly, while in the bottom the residuals are plotted. For reference the analytical result is also shown.

7.4 Test Problems

7.4.1 Advection

In order to test the advection scheme, we considered the advection of a square pulse (without source terms). In Figure 7.2, the pulse is shown after being advected five times its initial width (50 cells) using both the donor cell and van Leer upwinding methods. It is clear that both methods are diffusive, with the donor cell method substantially more so.

In general, diffusion will lead to errors in both the amplitude and the phase of

an advected pulse. In order to quantify these errors for diffusion resulting from the upwinding scheme, a sine wave was advected with periodic boundary conditions for 100 times its wavelength. By this time, the donor cell upwinding scheme has diffused the sine wave completely, hence only the van Leer and PPA methods are shown in Figure 7.3. The errors are at the 4% and 0.4% levels, respectively, with deviations becoming most significant at extrema. In both the square pulse and the sine wave, a noticeable asymmetry (which is determined by the direction of propagation) develops as a result of higher-order effects in the upwinding schemes.

7.4.2 Sod Shock Tube

The pressure source term in equation (7.3) was tested by the Sod shock tube problem. The Sod shock tube consists of an initial density and pressure discontinuity, and its subsequent evolution for an ideal gas ($\Gamma = 1.4$) and a specific set of initial conditions. For $x > 0$, $\rho = 0.125$ and $P = 0.1$, while for $x \leqslant 0$, $\rho = 1$ and $P = 1$. Because it is the entropy density and not the pressure that is evolved, it is necessary to find s as a function of ρ and P for an ideal gas:

$$s = \ln\left(\frac{P^n}{\rho^{n+1}}\right) \quad \text{where} \quad n = \frac{1}{\Gamma - 1} \ . \tag{7.33}$$

The Sod shock tube is useful as a test because the resulting ρ and P profiles for any given time can be calculated analytically (e.g., Sod, 1978; Hawley et al., 1984).

In Figure 7.4, the numerical results from our code are compared to the analytical solutions. Overall, they are in good agreement, with the exception of two minor discrepancies. The most notable discrepancy is the entropy deficit in the post-shock fluid ($0.184 < x < 0.35$). This is a result of using the adiabatic condition, and thus ignoring entropy production at shocks. Hence, the higher analytical value is easy to understand. Because we intend to apply the code to scenarios in which the adiabatic condition holds to a very good approximation, we expect the entropy deficit to be physically insignificant. The second discrepancy is the presence of overshoots at points where the slopes of quantities change discontinuously. As discussed in Stone &

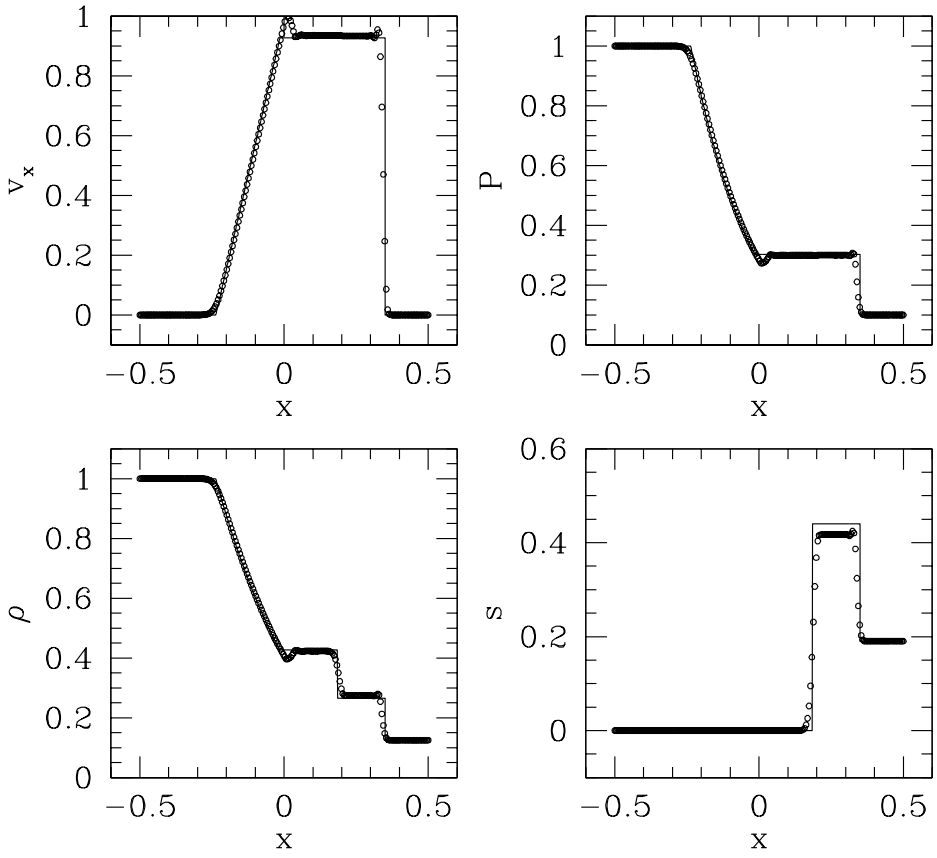

Figure 7.4: The density, pressure, velocity, and entropy are shown for the Sod shock tube at $t = 0.2$ (the units of which depend upon the units chosen for the pressure and density). 200 cells were used with van Leer upwinding. The head and tail of the rarefaction wave are located at $x = -0.235$ and $x = -0.014$, respectively. The contact and shock discontinuities are at $x = 0.184$ and $x = 0.35$, respectively.

Norman (1992), this is a real result, originating from the numerical viscosity inherent in any finite-difference code. The most important result, however, is the fact that the artificial viscosity causes the shock fronts to be well behaved in our code.

7.4.3 Pressure-Free Collapse

The gravitational source term in equation (7.3) was tested via the pressure-free collapse of a uniform density sphere. Once again, there is an analytical solution:

$$\begin{aligned} r &= r_0 \cos^2 \beta \\ \rho &= \rho_0 \cos^{-6} \beta \\ t &= \left(\beta + \frac{1}{2}\sin 2\beta\right)\left(\frac{8\pi}{3} G\rho_0\right)^{-1/2} , \end{aligned} \tag{7.34}$$

(see, e.g., Stone & Norman, 1992). Figure 7.5 depicts the result after allowing the radius to halve (at $t = 0.909$ for $G = 1$), for a $256 \times 256 \times 256$ cell grid. There is a small excess on the edges resulting from our implementations of viscosity and consistent transport (which necessarily treats the advection of velocity into the edges differently due to the density gradients). Overall, it does show good agreement with the analytical prediction.

7.5 Application to a Pulsating White Dwarf

7.5.1 Hydrostatic Equilibrium

The problem of choosing an equilibrium fluid configuration is made non-trivial by the finite differencing of the the dynamical equations. Consequently, a method to produce an equilibrium solution for the finite difference equations is required. For a barotropic equation of state, we have chosen to make use of the self-consistent field (SCF) method (e.g., Motl et al., 2002; Hachisu, 1986; Ostriker & Mark, 1968). Because it is well described elsewhere, we will only summarize the procedure here.

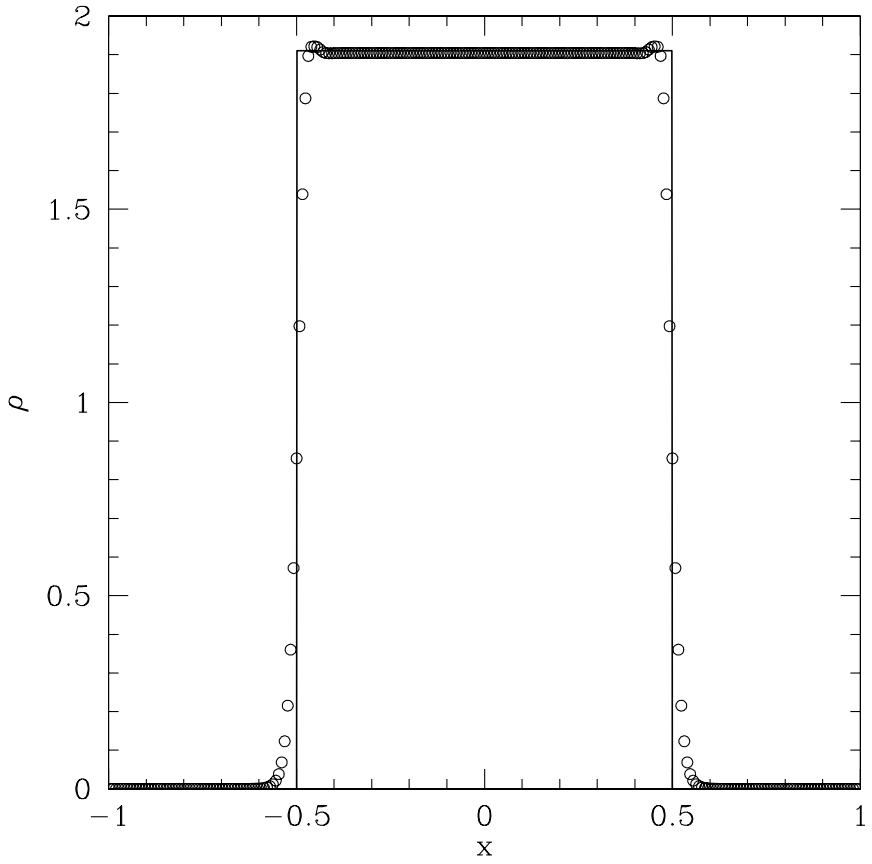

Figure 7.5: The numerical (open circles) and analytical (solid line) solutions for the density as a function of distance along a radial section for the pressure-free collapse of a uniform density sphere are shown. The initial radius and total mass of the sphere was unity. A $256 \times 256 \times 256$ cell grid was used. With Newton's constant given by $G = 1$, this occurs at $t = 0.909$.

Model	$M\,(M_\odot)$	$R\,(10^6\mathrm{m})$	$\omega_*\,(\mathrm{Hz})$	$\omega_{f2}\,(\mathrm{Hz})$	$\omega_{p2}\,(\mathrm{Hz})$
CWD	0.632	8.56	0.365	0.562	1.15
HWD	0.632	11.2	0.243	0.560	0.749

Table 7.1: Stellar properties for a cold white dwarf with (CWD) and without (HWD) an isothermal envelope. Specifically, the mass, radius, fiducial stellar frequency $\omega_* = \sqrt{GM/R^3}$, frequency of the adiabatic quadrupolar fundamental mode, and the frequency of the lowest order adiabatic quadrupolar p-mode. Note that the inclusion of the isothermal envelope does not change the mass appreciably while significantly increasing the radius.

1. An initial guess for the density (taken from the continuous solution) is used to generate the gravitational potential via the method described in Section 7.3.

2. The new gravitational potential and the initial density guess are then used to calculate the Bernoulli constant at the center of the star.

3. the Bernoulli constant and the new gravitational potential are used to calculate the enthalpy at all points on the grid, which is then subsequently inverted to yield the new density guess.

This procedure is iterated until the Bernoulli constant converges to some specified tolerance—i.e., when the fractional change is less than some small value (say, 10^{-12}). The resulting density distribution is a solution to

$$\frac{h_{+i} - h_{-i}}{2\Delta x^i} + \frac{\Phi_{+i} - \Phi_{-i}}{2\Delta x^i} = 0 \,, \tag{7.35}$$

and, hence, no net momentum flux is generated if the source terms are given by equation (7.19). Note that, if the source terms are given by equation (7.18), this *may* still produce a net momentum flux, and is not necessarily a good approximation to equilibrium in that case.

When

$$\left|\frac{\partial P}{\partial x^i}\right| > \frac{P}{\Delta x^i} \,, \tag{7.36}$$

the pressure gradient required to preserve hydrostatic equilibrium cannot be resolved on the grid. For a star, this can result in strong, inwardly directed forces at the

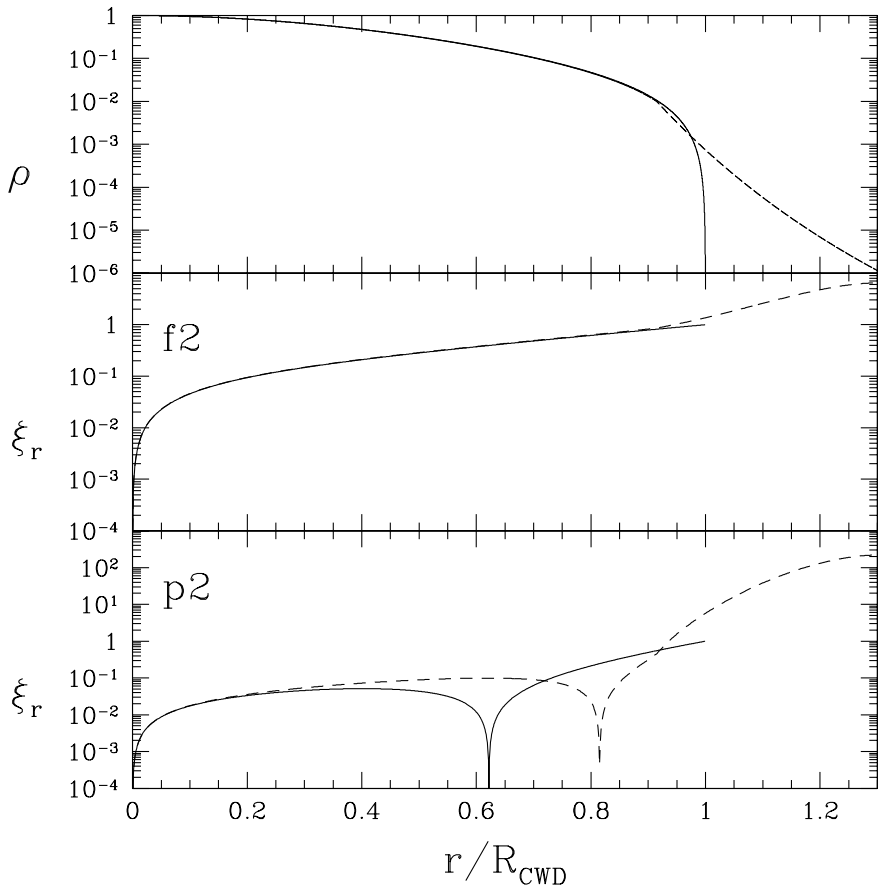

Figure 7.6: Shown in the top panel are the density profiles for the cold white dwarf with (solid) and without (dashed) the isothermal envelope. The two lower panels are the radial displacement profiles for the quadrupolar fundamental mode ($f2$) and the lowest order quadrupolar p-mode ($p2$) for the two models. Note that the density and $f2$ mode profiles are very nearly the same for the two cases. However, the mode profiles differ substantially for the $p2$ mode.

surface, driving shocks into the interior. We have found that adding an isothermal envelope can mitigate this problem by pushing the region where this inequality is true off the grid, while adding an insignificant amount of mass to the star itself. This is done explicitly by setting a fiducial density (which we chose to be 10^{-2} of the central density) at which the equation of state changes from that of a cold white dwarf to a $\Gamma = 1$ polytrope. The polytropic constant is chosen such that $P(\rho)$ remains continuous across the transition. Table 7.1 compares the properties of the cold white dwarf with (HWD) and without (CWD) the isothermal envelope. Note that while the isothermal envelope increases the radius significantly, it does not change the mass or the frequency of the quadrupolar fundamental mode (ω_{f2}). The reason for this can be seen in Figure 7.6. The $f2$ mode is more strongly weighted in the core where the addition of the isothermal envelope makes no difference. In contrast, the lowest-order quadrupolar p-mode is substantially affected by the presence of the envelope. This probably results from the fact that the radial wavelength of the $p2$ is much closer to the height of the isothermal envelope. Henceforth, all evolutions were begun with the HWD model listed in Table 7.1.

The quality of the equilibrium generated by the SCF method may be explicitly demonstrated. Figure 7.7 shows the evolution of the centre-of-mass position, net momentum, and the fraction of the total energy that is converted into kinetic energy for a star initially in hydrostatic equilibrium. The last quantity is given in terms of the kinetic, internal, and gravitational components:

$$K = \int \frac{1}{2}\rho v^2 \, d^3x \ , \quad \Pi = \int p \, d^3x \ , \quad W = \int \rho\Psi \, d^3x \ . \tag{7.37}$$

Despite an initial exponential rise, these quantities saturate at relatively low levels for all resolutions shown. Note that all times are measured in dynamical times of the cold white dwarf, $t_{\rm CWD} \equiv 1/\omega_*$, which is approximately the time it takes for a disturbance to cross the star.

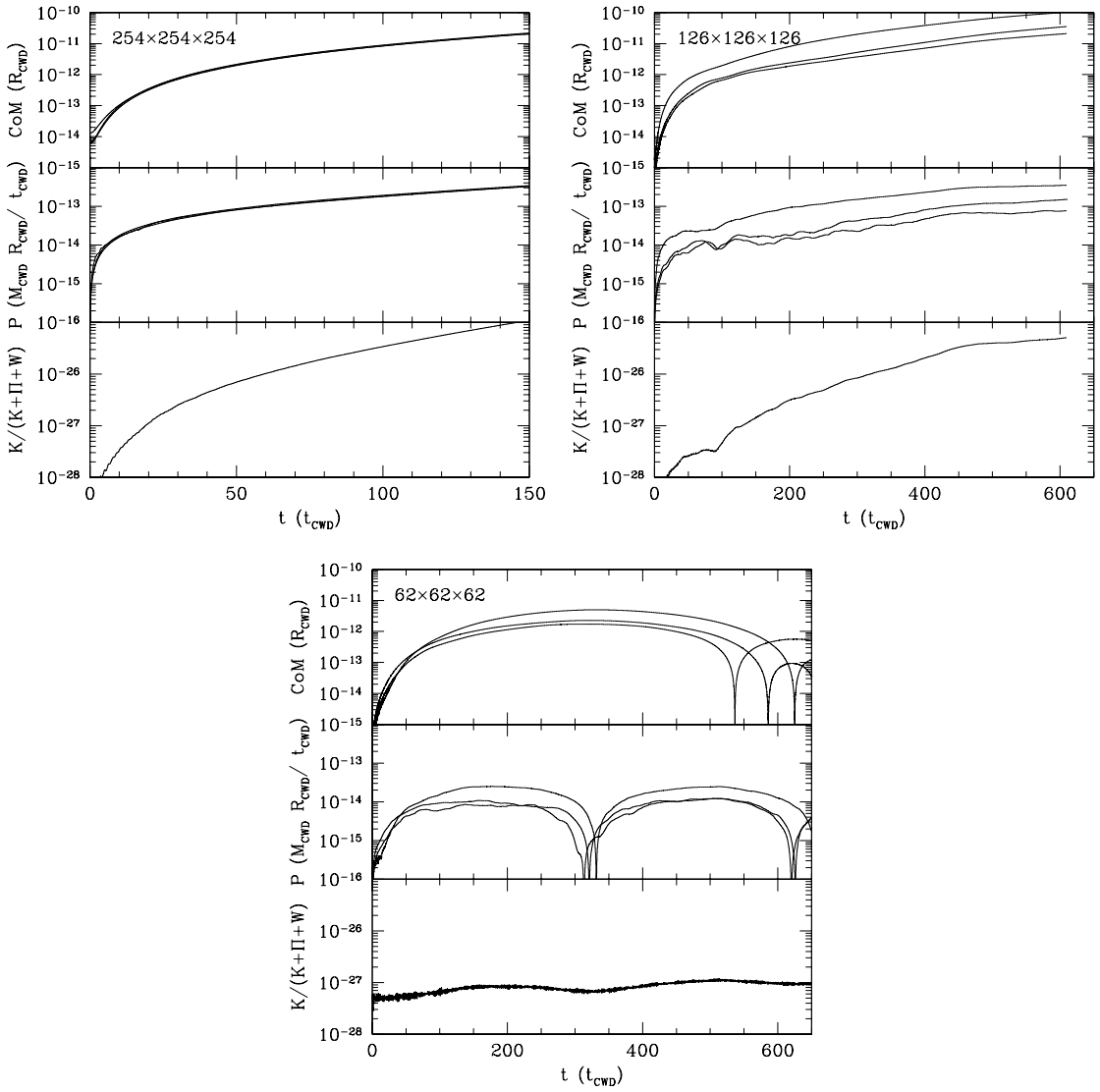

Figure 7.7: Shown are the center-of-mass (top panels), net momentum (middle panels), and fraction of the total energy converted into kinetic energy (bottom panels) for a number of grid resolutions (note the different time scales). In all cases these quantities saturate well below significant levels (e.g., for the worst case, the center-of-mass moves by less than 10^{-8} cell widths in the 150 dynamical times shown, thus it would require roughly 10^{13} dynamical times before the center-of-mass moves one stellar radius. Typically, these appear to turn over, implying that they may never rise significantly above 10^{-7} cell widths.)

7.5.2 Oscillation Modes

In general, the problem of interest is dynamical. Specifically, we are interested in the non-linear evolution of the oscillation modes of a cold white dwarf which are being excited resonantly by tidal forces. Towards this end, it is important to obtain a measure of the numerical quality factor (Q; the e-folding time of the energy in the oscillation), and the oscillation frequencies themselves. That the latter may be different from the frequencies in Table 7.1 is a result of both the approximation of discrete cells *and* the fact that the finite-difference equations are distinct from the continuous equations. However, we expect the deviation to be small, and therefore a close agreement between the predicted and observed frequencies serves as yet another test for the correctness of our code. Both the quality factor and the oscillation eigenfrequencies can be obtained by deforming the star in a particular way, and analyzing the subsequent oscillations.

We deformed the star by adding a fractional quadrupolar perturbation to the density, i.e.,

$$\Delta\rho(\boldsymbol{r}) = A\rho(r)Y_{22}^{e}(\theta,\varphi)\ , \tag{7.38}$$

where the amplitude, A, was chosen to be small (10^{-4}) so that the resulting oscillation occurred in the linear regime. This initiated an even $m = 2$ standing wave on the star. Figures 7.8 and 7.9 show the resulting evolutions for a number of grid resolutions. The same diagnostics as those used to demonstrate hydrostatic equilibrium are shown in Figure 7.7. In this case as well, the center-of-mass and momentum drift saturate at levels well below those of interest. Unlike hydrostatic equilibrium, there now exists a non-vanishing kinetic energy. It is strongly harmonic and decays exponentially. Because the initial perturbation excited all of the even quadrupolar modes with $m = 2$, there are a number of distinct decay constants, with the slowest being due to the $f2$ mode. This exponential decay at late times may be fit to estimate the numerical Q, found here to be on the order of 6000.

In Figure 7.9, the quadrupolar moments are shown. The even $m = 2$ moment is strongly dominant as expected. It also has a very clear harmonic structure. This may

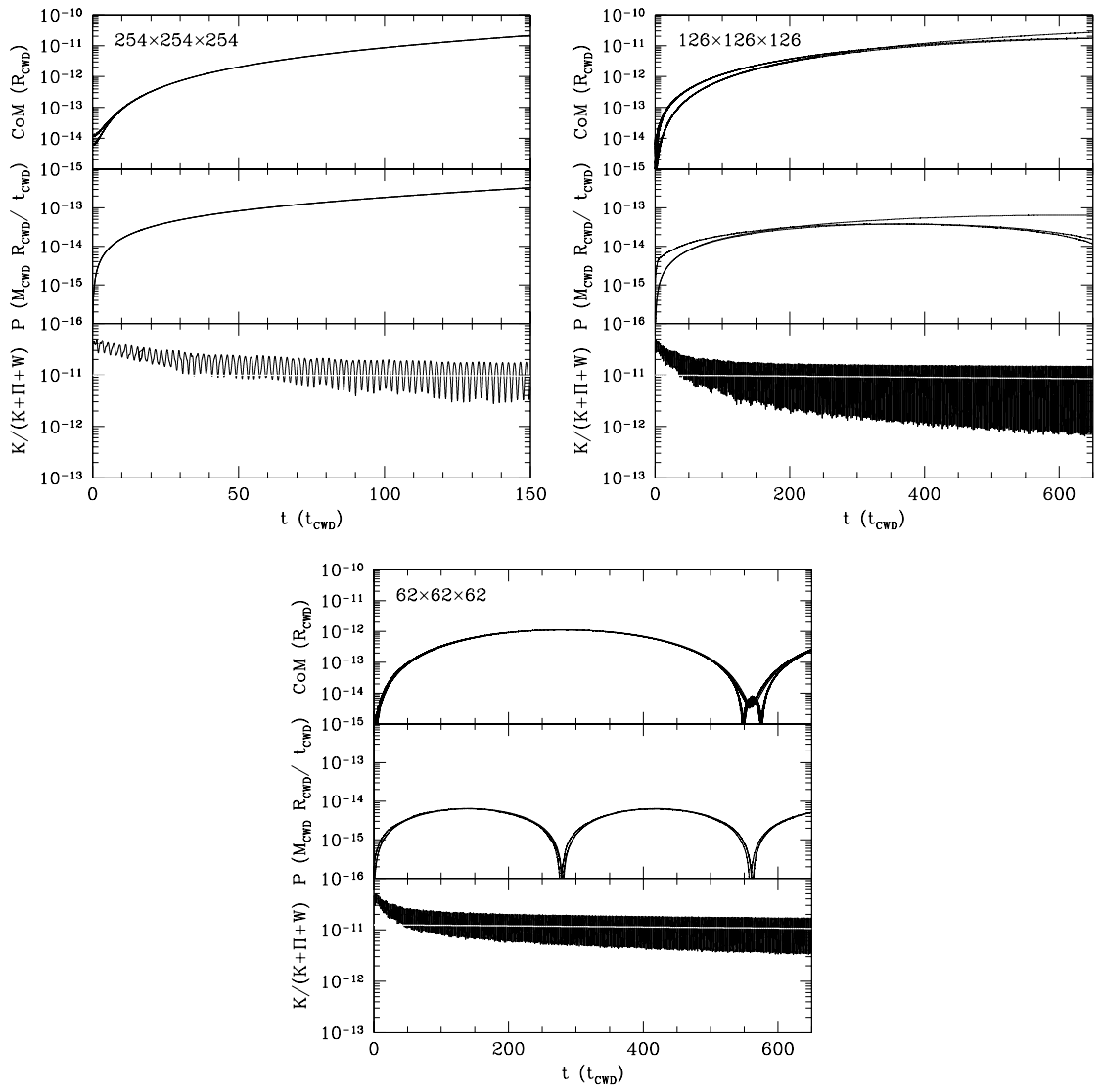

Figure 7.8: Same as Figure 7.7 for the case when a quadrupolar perturbation is present (note the difference in scales in comparison to that figure). The white line drawn through the oscillations is for a Q of approximately 6000.

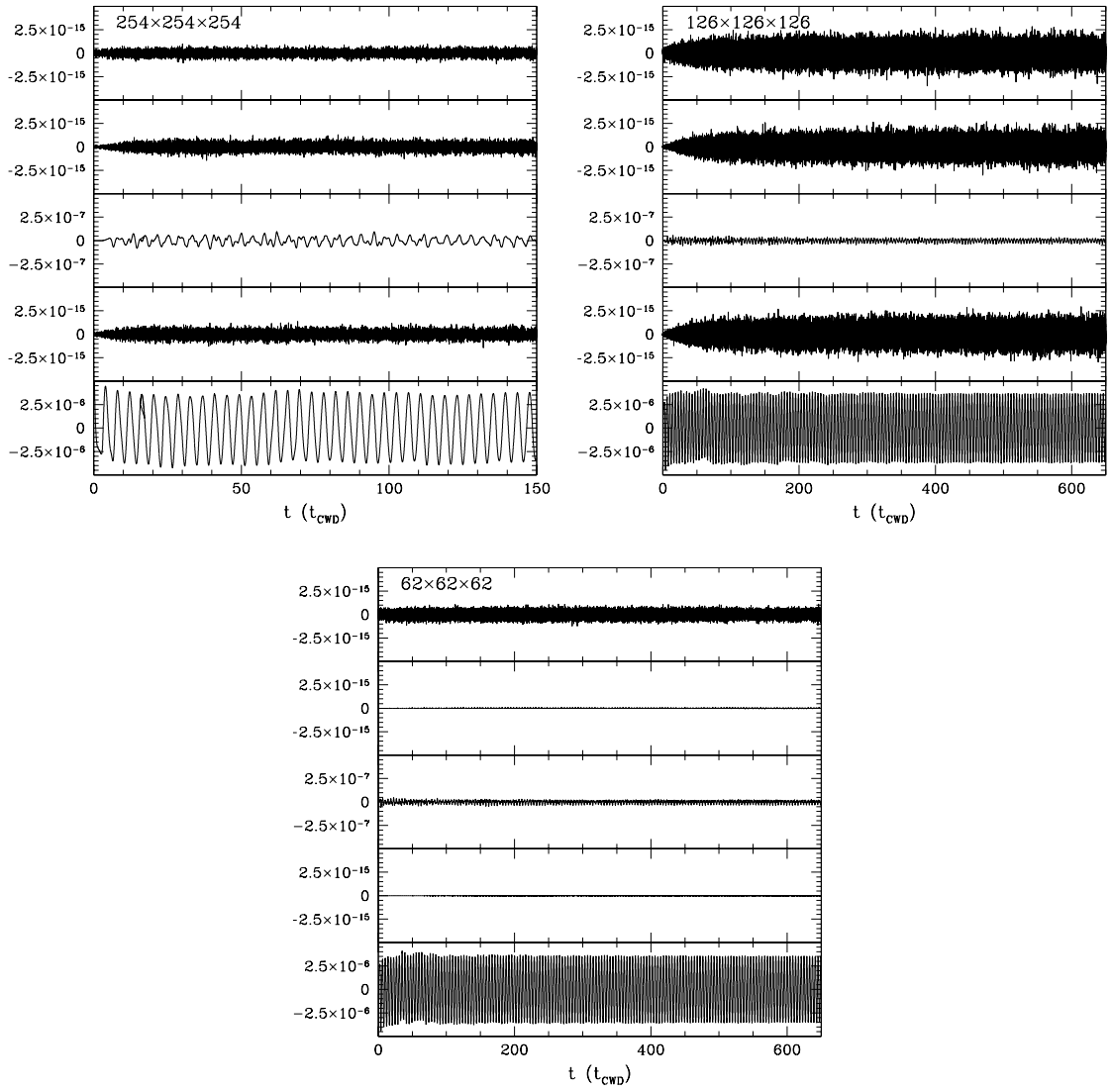

Figure 7.9: The quadrupolar moments of the perturbed star for each of the resolutions considered in Figure 7.8. From top to bottom, the panels are the odd $m = 2$, odd $m = 1$, $m = 0$, even $m = 1$, and even $m = 2$ moments. Note the difference in scales of the different moments, namely that the even $m = 2$ moment is two orders of magnitude larger than the $m = 0$ moment and nine orders of magnitudes larger than the others.

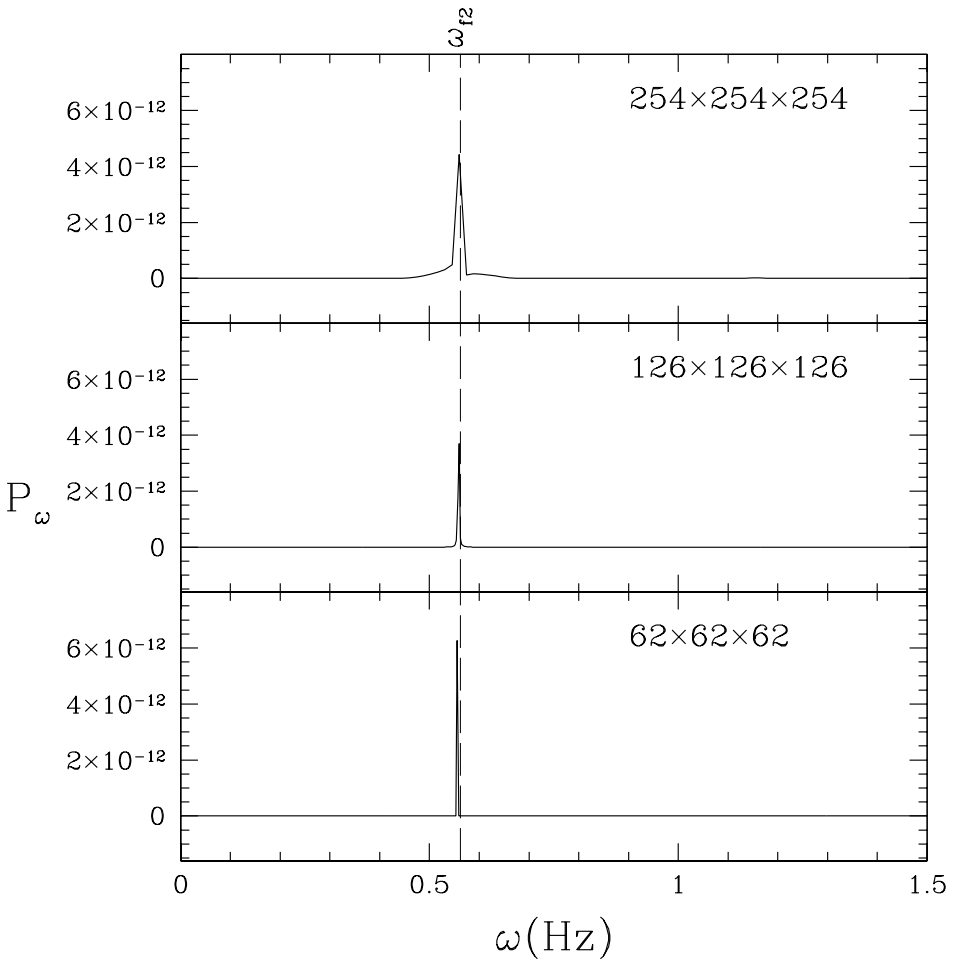

Figure 7.10: Shown are the power spectra of the even $m = 2$ quadrupolar moment as a function of angular frequency (using the mean squared amplitude normalization). As expected, for each grid resolution there is a strong spike coincident with the $f2$ mode frequency predicted for the HWD model.

be Fourier analyzed to produce the dominant oscillation mode, as shown in Figure 7.10. In the power spectrum of the even $m = 2$ quadrupolar moment, there is a peak which extends five orders of magnitude above the rest of the spectrum. This peak is clearly identifiable with the $f2$ mode, and appears to have very nearly the frequency predicted by the HWD model.

Chapter 8

Non-Linear Evolution of White Dwarf Oscillations

8.1 Mode Projection

To look for non-linear effects with large amplitude modes, a numerical procedure to determine the displacement of a given linear normal mode is needed. The fluid displacement field inside the star can be expanded in terms of the modes:

$$\boldsymbol{\xi}(\boldsymbol{x},t) = \sum_j x_j(t)\hat{\boldsymbol{\xi}}_j(\boldsymbol{x}) \ , \tag{8.1}$$

and the modes obey the orthonormality relation

$$\frac{1}{\sqrt{M_j M_j'}} \int d\boldsymbol{x}\, \boldsymbol{\xi}_j^* \cdot \boldsymbol{\xi}_j = \delta_{j,j'} \ . \tag{8.2}$$

(In this section, we temporarily revert to using complex eigenfunctions. This choice is merely for convenience; the final result will carry over trivially to the case of real eigenfunctions.) Thus, in principle, the displacement of mode j is obtained by

$$x_j = \frac{1}{M_j} \int d\boldsymbol{x}\, \boldsymbol{\xi}_j^* \cdot \boldsymbol{\xi} \ . \tag{8.3}$$

However, with an Eulerian computational grid, the fluid displacement field $\boldsymbol{\xi}$ is not available directly to us. A different computational scheme is therefore required which

can project out the displacement for a given mode using Eulerian quantities such as the density perturbation ρ'.

From the equation for mass conservation,

$$\rho' = \nabla \cdot (\rho_0 \boldsymbol{\xi}) \ , \tag{8.4}$$

and the eigenfunction expansion of $\boldsymbol{\xi}(\boldsymbol{x}, t)$,

$$\boldsymbol{\xi}(\boldsymbol{x}, t) = \sum_j x_j(t) \hat{\boldsymbol{\xi}}_j(\boldsymbol{x}) \ , \tag{8.5}$$

it follows that

$$\rho'(\boldsymbol{x}, t) = \sum_j x_j(t) \rho_j(\boldsymbol{x}) \ , \tag{8.6}$$

where

$$\rho_j(\boldsymbol{x}) = -\nabla \cdot [\rho_0 \hat{\boldsymbol{\xi}}_j(\boldsymbol{x})] \ . \tag{8.7}$$

We are looking for a function $\mathcal{F}_j$ such that

$$\int d\boldsymbol{x} \, \rho_j \mathcal{F}_{j'} = \delta_{j,j'} \ . \tag{8.8}$$

Using the expression for ρ_j, integrating the above integral by parts, and dropping the surface term, we get

$$\int d\boldsymbol{x} \, \rho_0 \hat{\boldsymbol{\xi}}_j \cdot \nabla \mathcal{F}_{j'} = \delta_{j,j'} \ . \tag{8.9}$$

Consider the case when $\mathcal{F}_j = \mathrm{i}\phi_j^*/\omega_j$, where ϕ_j is the jth component of the velocity potential, such that $\nabla \phi_j = \mathrm{i}\omega_j \hat{\boldsymbol{\xi}}_j$. It then follows that

$$\int d\boldsymbol{x} \, \rho_0 \boldsymbol{\xi}_j \cdot \nabla \mathcal{F}_{j'} = \int d\boldsymbol{x} \, \rho_0 \boldsymbol{\xi}_j \cdot \boldsymbol{\xi}_{j'}^* = \sqrt{M_j M_{j'}} \, \delta_{j,j'} \ , \tag{8.10}$$

which is what we want. Therefore, if we know ρ', then we can use ϕ_j^* to project out

the displacement of mode j:

$$x_j = \frac{\mathrm{i}}{\omega_j} \int d\boldsymbol{x}\, \phi_j^* \rho' \ . \tag{8.11}$$

In terms of the Dziembowski variables defined in Section 4.2.2, ϕ_j is given by

$$\phi_j = \frac{\mathrm{i}gr}{\omega_j} \eta_2(r) Y_{\ell m}(\hat{\boldsymbol{x}}) \ . \tag{8.12}$$

Hence, we have

$$x_j = \frac{1}{M_j \omega_j^2} \int d\boldsymbol{x}\, \frac{r^2 \eta_2}{C} Y_{\ell m}^* \rho' \ . \tag{8.13}$$

With real eigenfunctions, the above equation is still valid: we simply replace $Y_{\ell m}^*$ with $Y_{\ell m}^{(\mathrm{e})}$ or $Y_{\ell m}^{(\mathrm{o})}$, defined similarly to (4.65) and (4.66).

It should be mentioned that (8.13) can only be used to project out the displacements if the only modes excited are poloidal. As tidal forces are conservative, in the absence of viscosity, toroidal modes will not be excited. While the presence of a finite viscosity due to the differencing scheme in our code would seem to violate this, the effects are negligibly small. We can therefore use (8.13) to calculate the mode displacements numerically. In general, however, we cannot expect mode orthogonality to hold identically on a discrete grid. Therefore, we are faced with the problem of distinguishing physical effects from by-products of the numerical scheme. A good way to check for this is to run a given simulation at different resolutions and look for convergence.

We can also gain some sense of the level at which finite-resolution effects enter into the mode projection by evaluating the projection integral (8.13) between the $\ell = m = 2$ f-mode, and several other modes. Note that a discretized star will necessarily possess a finite spectrum of modes; it is clearly impossible for a wavelength shorter than the grid separation to be resolved. And, generally, the shorter the mode wavelength, the lower will be the effective resolution on a given grid. Thus, for example, we expect that for varying radial order n, the violation of mode orthogonality should scale monotonically with the parameter $n\Delta x/R_*$. Typically, we find that

orthogonality between modes with different ℓ, m is not affected by the finite resolution. For modes with the same ℓ, m and different n, the grid introduces a small coupling. However, the coupling is at a level well below that of interest, and scales down as expected with increasing resolution.

8.2 Resonant Excitation of Modes

We ran several simulations of the resonant excitation of the $\ell = m = 2$ f-mode in a 0.6 $M_\odot$ white dwarf. The simulations were run at several different orbital separations with a circular orbit, and with the orbital period fixed at 24.06 s (the fundamental resonant period of the $\ell = m = 2$ f-mode). The white dwarf model used was a hybrid, with a degenerate core, and an isothermal envelope, with the transition from the core to the envelope occurring at 10^{-4} of the central density. The companion mass was fixed at 10^3 M_* (hence, 6×10^2 $M_\odot$). The simulations were run at separations of 3.5 (run A), 4.5 (run B), 5.5 (run C), and 6.5 (run D) times the Keplerian separation (11.9 R_*). In terms of the estimated Roche separation for a 10^3 M_* companion, these correspond to 2.0, 2.6, 3.2, and 3.8 $R_{\rm Roche}$, respectively. No back reaction effects were included, and the orbital elements were not evolved in any way. The resulting mode amplitudes are shown as functions of time in Figures 8.1–8.3, and Figure 8.4 shows the total mass contained within the computational grid and the center-of-mass motion for the same runs. An interesting feature is the onset of mass loss at a different point in each run. For example, there is a noticeable downturn in the mass for run A around $t = 120$. This is an important observation which we will revisit later. For the moment it is sufficient to note that the maximum fractional mass loss in 400 dynamical times is only about 0.5%. Still, the onset of mass loss means that any long-term conclusions regarding mode behavior based upon the results of these runs should be considered tentative, pending further confirmation.

As Figures 8.1–8.3 show, the evolutions of the mode amplitudes are complicated. Nonetheless, some information can still be extracted from these figures visually. In general, the multipolar components of the tidal overlap integrals scale with orbital

separation, R, as $\propto 1/R^{\ell+1}$. Thus, for quadrupolar modes the scaling is $\propto 1/R^3$. As the rate of excitation of a mode in the linear approximation is proportional to its overlap integral, we expect that the rates at which the quadrupolar mode amplitudes rise should scale as $\propto 1/R^3$. Hence, the initial rise in the amplitudes of quadrupolar modes for run A should be about twice as fast as for run B. The results in Figure 8.1 are in satisfactory agreement with this prediction.

The amplitude of the $f22$ mode exhibits a puzzling behavior in all of the runs: in the long-term it starts declining, despite continued resonant excitation. As the decline seems to correspond roughly with the onset of mass loss, we speculate that the two are related. The nature of this relationship is unclear at the moment. For run A, however, the amplitude of the $f22$ mode shows some signs of saturating around a value of 0.5 before the mass loss sets in and the mode amplitude starts declining for the remainder of the run. This saturation, if it is real, has a natural interpretation as follows. Tidal coupling transfers energy resonantly to the $f22$ mode at some rate which is determined by the overlap integral and the orbital parameters. If the mode couples non-linearly to other modes, then the coupling constants set the rate of damping (the 'transition rate' in quantum mechanical terminology). An equilibrium is then achieved when the rates of excitation and non-linear damping are equal. As the damping rate is expected to depend upon the mode amplitude, the point at which equilibrium is achieved determines the saturation amplitude. In such a 'steady' state, the energy cascades from the resonant $f22$ mode to other modes. This energy cannot accumulate indefinitely in the other modes, and they, in turn, transfer energy to still other modes via non-linear couplings. At some point along this chain of coupling, modes of sufficiently high order will be reached so that the dominant damping mechanism is microscopic viscosity, which will then thermalize the energy. Thus, in this scenario, we have a Kolmogorov-type cascade of energy down to small scales, and a steady heating of the star. Despite its appealing simplicity, we do not consider the hint of amplitude saturation in run A as providing compelling evidence for the correctness of this description of non-linear damping. Additional runs at higher resolutions and with different parameters are needed before a definite conclusion can

be drawn.

As we have noted above, the tidal overlap integrals for modes with a given ℓ scale as $1/R^{\ell+1}$. For $\ell = 4$ modes, we therefore expect the initial rise in the mode amplitudes to scale as $\propto 1/R^5$, in the linear approximation. However, in Figure 8.3, this is clearly not the case. The mode amplitudes for many of the $\ell = 4$ modes appear to rise similarly to the $\ell = 2$ modes, and seem to track their general evolution with time. This suggests the existence of a coupling between the $\ell = 2$ and $\ell = 4$ modes. The case for a coupling becomes more plausible with the observation that the $\ell = 3$ modes do not exhibit a similar behavior, which would be accounted for by the existence of selection rules for the lowest-order two-mode couplings (e.g., Van Hoolst, 1994). A useful calculation to be done in the future would be to compare the couplings observed in simulations with theoretical calculations for coupling in the weakly non-linear regime.

Earlier, we drew attention to the long-term mass loss exhibited by runs A through D. This feature seems to imply some instability in the numerical simulations, the nature of which is not yet understood. One way to avoid this problem may be to run simulations with eccentric orbits and higher-harmonic resonances.

Figures 8.5 and 8.6 show results from another set of runs with parameters identical to runs A through D, but with the difference that mode excitation was turned off at time $t = 50$. The sole reason for this was to observe the damping behavior of the $f22$ mode with different amplitudes. It would be of interest to obtain an empirical scaling relation for the damping rate as a function of the amplitude. Unfortunately, the onset of mass loss prohibits a simple interpretation of the observed long-term decline in the mode amplitude. We therefore limit ourselves to a qualitative observation. Generally, we expect the rate of damping to increase with the mode amplitude. In the regime $t \lesssim 100$, the results shown in Figure 8.5 are in satisfactory agreement with this expectation.

The results we have presented above are tentative, and a number of things can be done in the future to obtain more definite and quantitative conclusions. Simulations with higher resolution will be useful for mitigating short-term variability in

the mode amplitudes which can be seen in Figures 8.1–8.3 and Figure 8.5. This variability is a finite-resolution artifact, and scales down with increasing resolution. Insight into the non-linear mode evolution could also be obtained by comparing the results of simulations with theoretical predictions of two-mode and three-mode couplings in the weakly non-linear regime (e.g., Dziembowski, 1982; Van Hoolst, 1994). Also, runs with eccentric orbits and higher-harmonic resonances may alleviate the problem of mass loss, which will simplify the interpretation of long-term trends in the mode amplitudes. In addition, simulations which have cut-offs in the mode excitation (similar to Figure 8.5), but are unhampered by mass loss, will allow an empirical determination of the how the non-linear damping rate of the $f22$ mode scales with the amplitude. Such simulations will have to be run at multiple resolutions to ensure that the damping rates being measured are due to non-linear effects and not numerical dissipation.

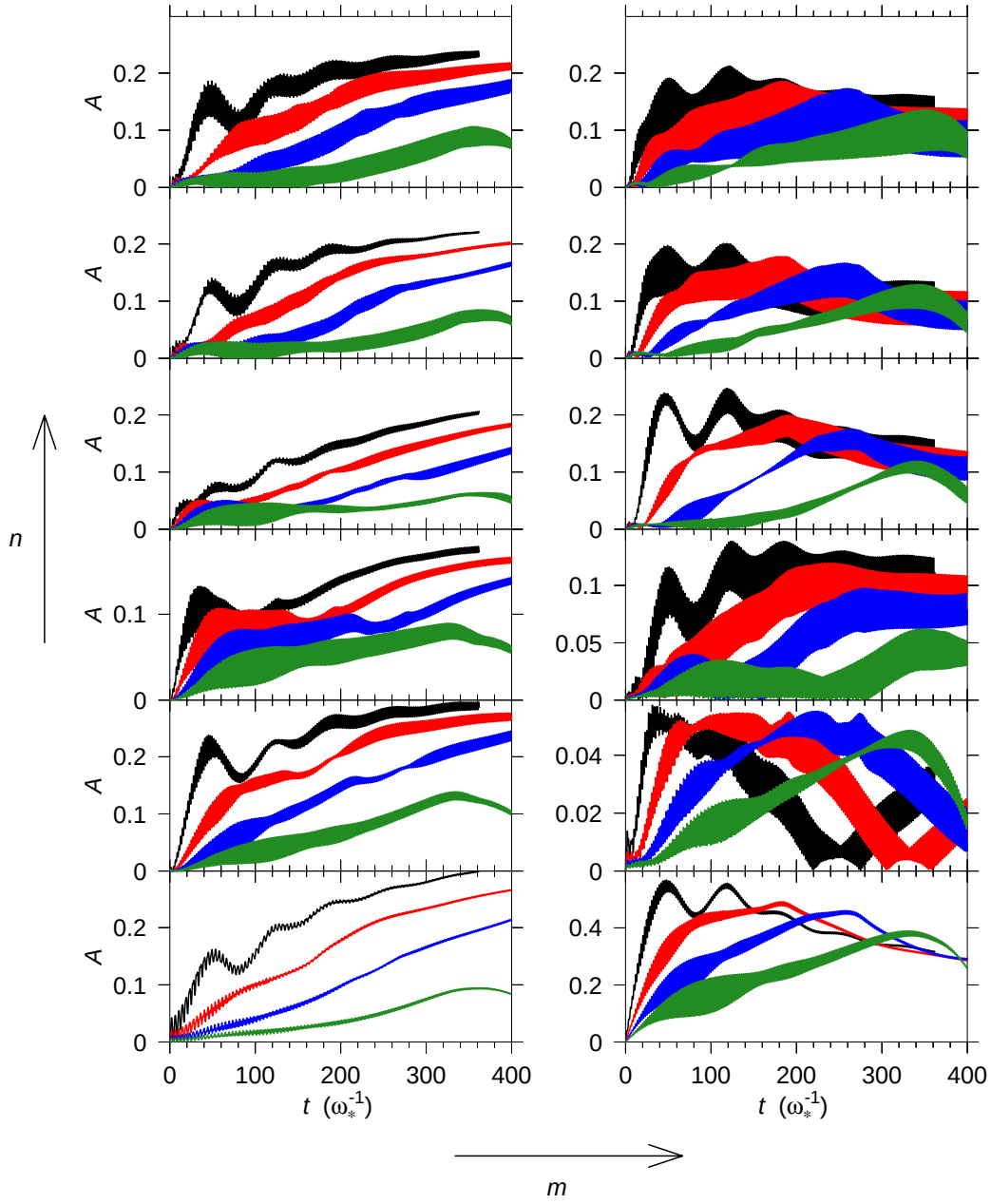

Figure 8.1: Amplitudes as functions of time of $\ell = 2$ modes with a $60 \times 60 \times 60$ grid, a white dwarf mass of 0.6 $M_\odot$, companion mass of 10^3 M_*, and several orbital separations. The orbital period is the fundamental resonant period for the $\ell = m = 2$ f-mode (24.06 s). The orbital separations are 41.8 R_* (2.0 $R_{\rm Roche}$) for the black curve, 53.8 R_* (2.6 $R_{\rm Roche}$) for the red curve, 65.7 R_* (3.2 $R_{\rm Roche}$) for the blue curve, and 77.6 R_* (3.8 $R_{\rm Roche}$) for the green curve. Modes with increasing radial order are stacked vertically, and modes with increasing azimuthal order are laid out horizontally. Only modes with even $|\ell + m|$ are shown ($m = 0, 2$), as modes with odd $|\ell + m|$ are excited negligibly. Radial orders (n) from 0 to 5 are shown.

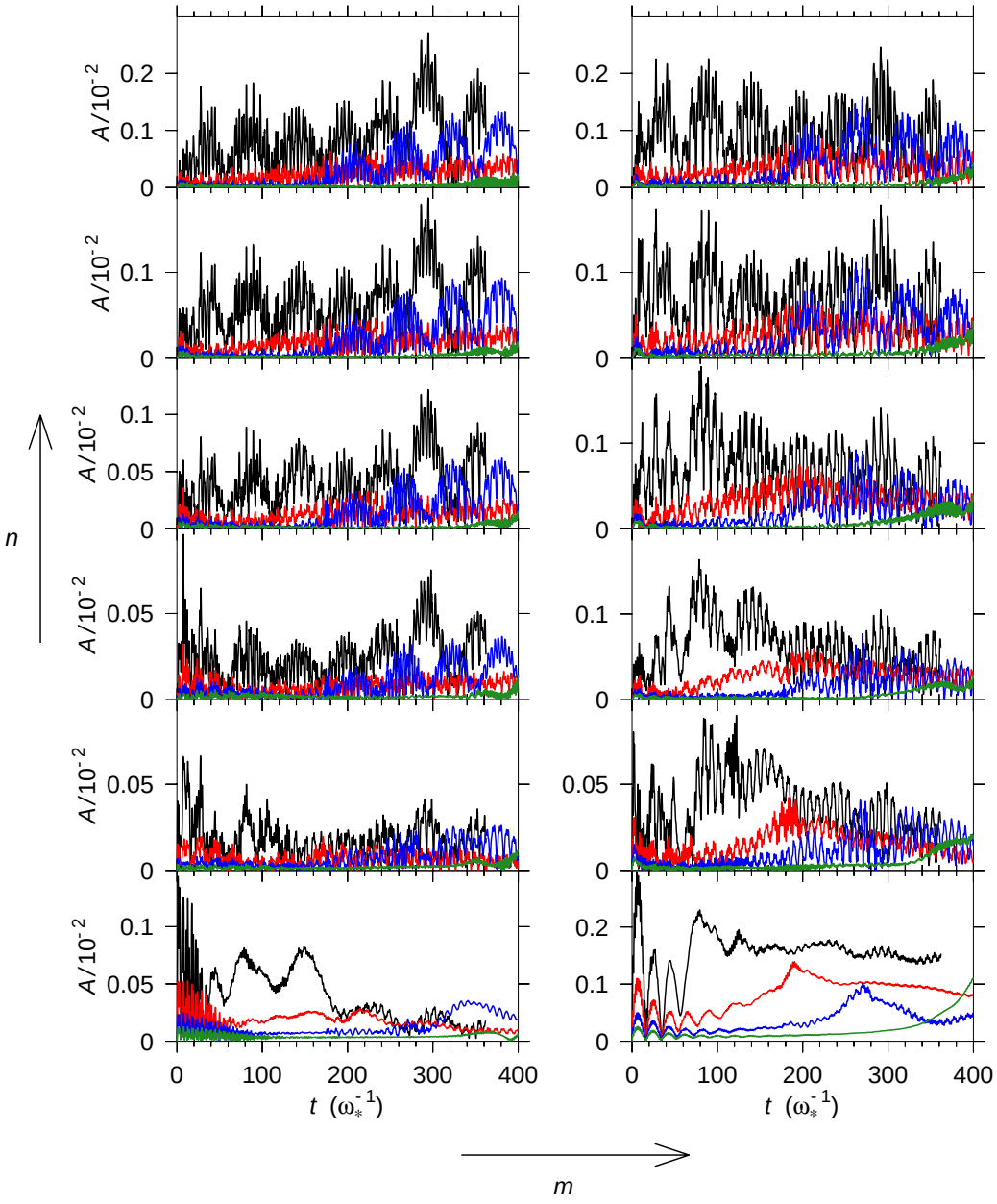

Figure 8.2: Amplitudes as functions of time for $\ell = 3$ modes for the same runs as Figure 8.1. Modes with radial orders $n = 0 \ldots 5$, and $m = 1, 3$ are shown.

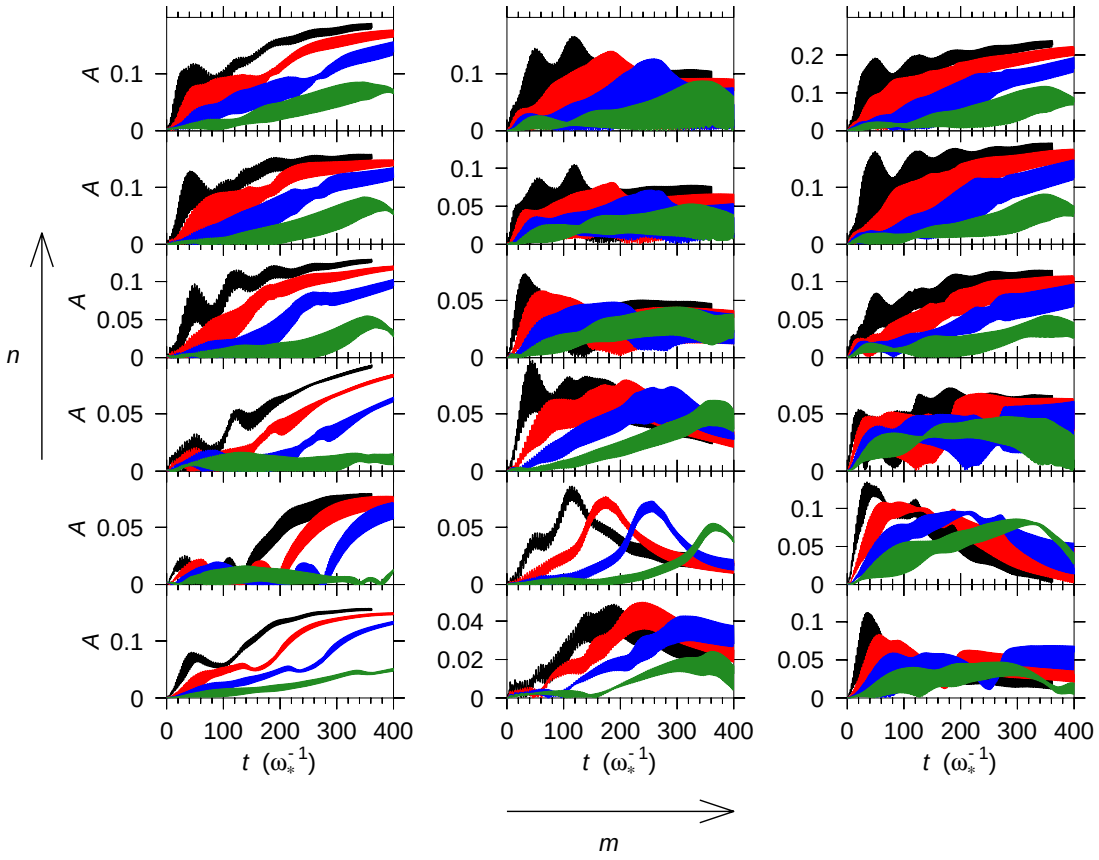

Figure 8.3: Amplitudes as functions of time for $\ell = 4$ modes for the same runs as Figure 8.1. Modes with $n = 0 \ldots 5$, and $m = 0, 2, 4$ are shown.

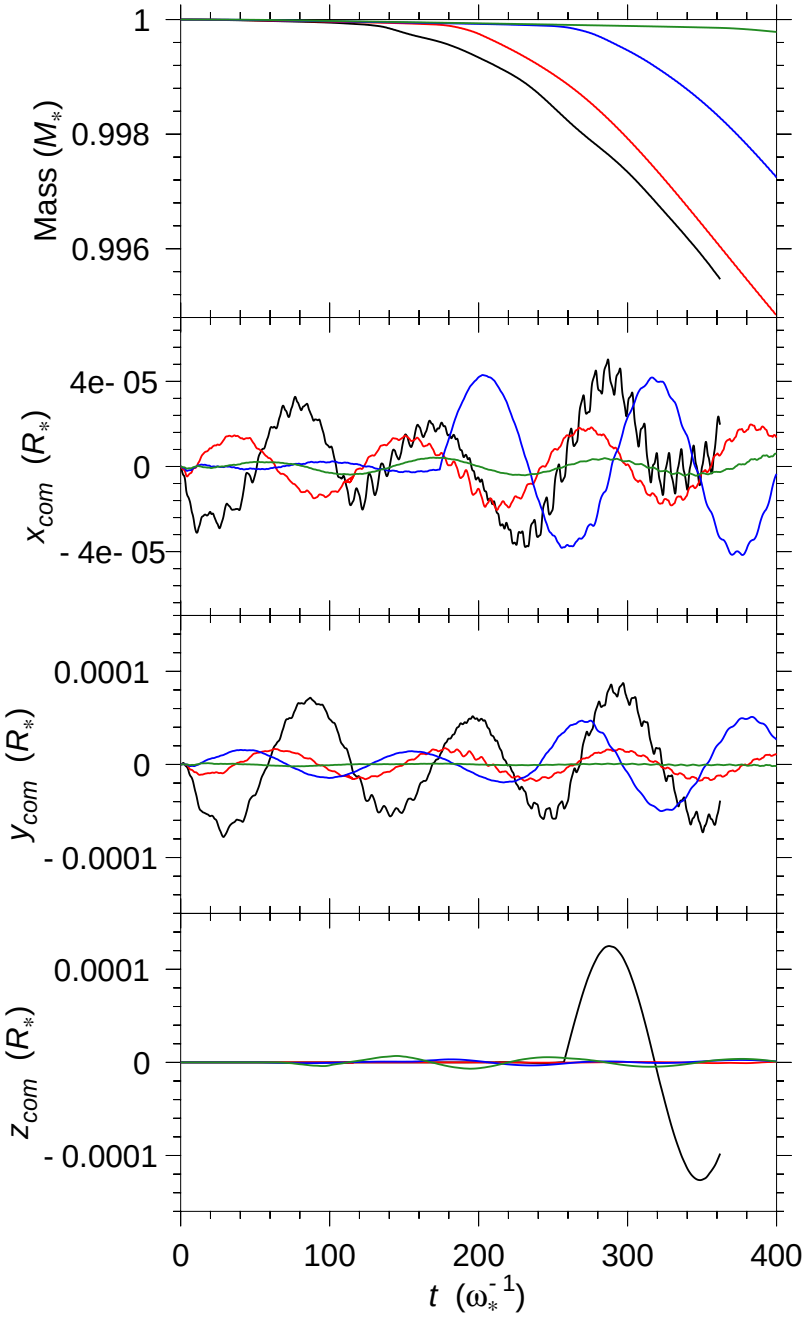

Figure 8.4: The total mass contained within the computational grid, and the x, y, z locations of the center-of-mass as a function of time for the runs shown in Figures 8.1–8.3.

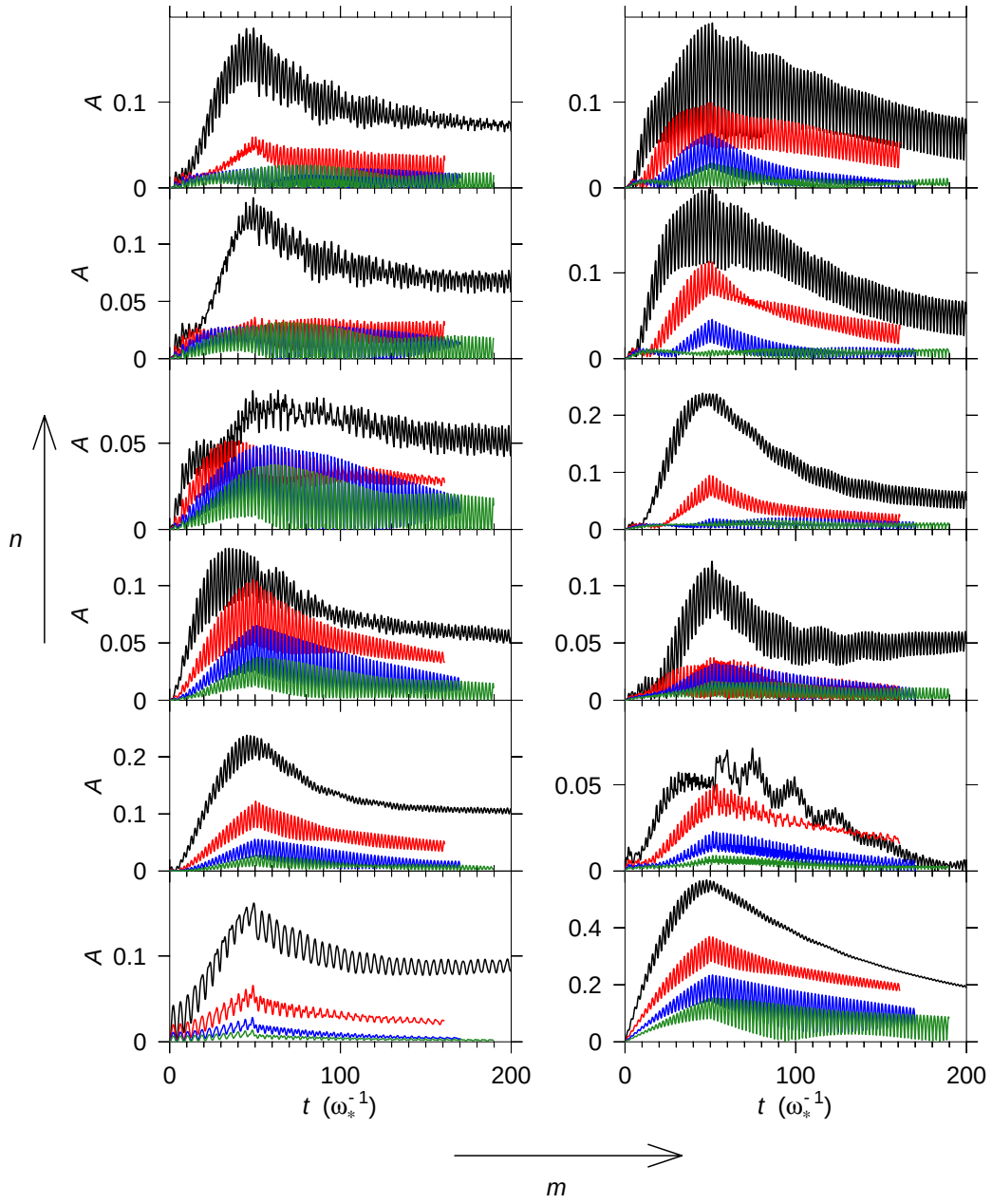

Figure 8.5: Ampltiudes as functions of time for $\ell = 2$ modes for runs identical to Figure 8.1 except for the difference that mode excitation was turned off at $t = 50$.

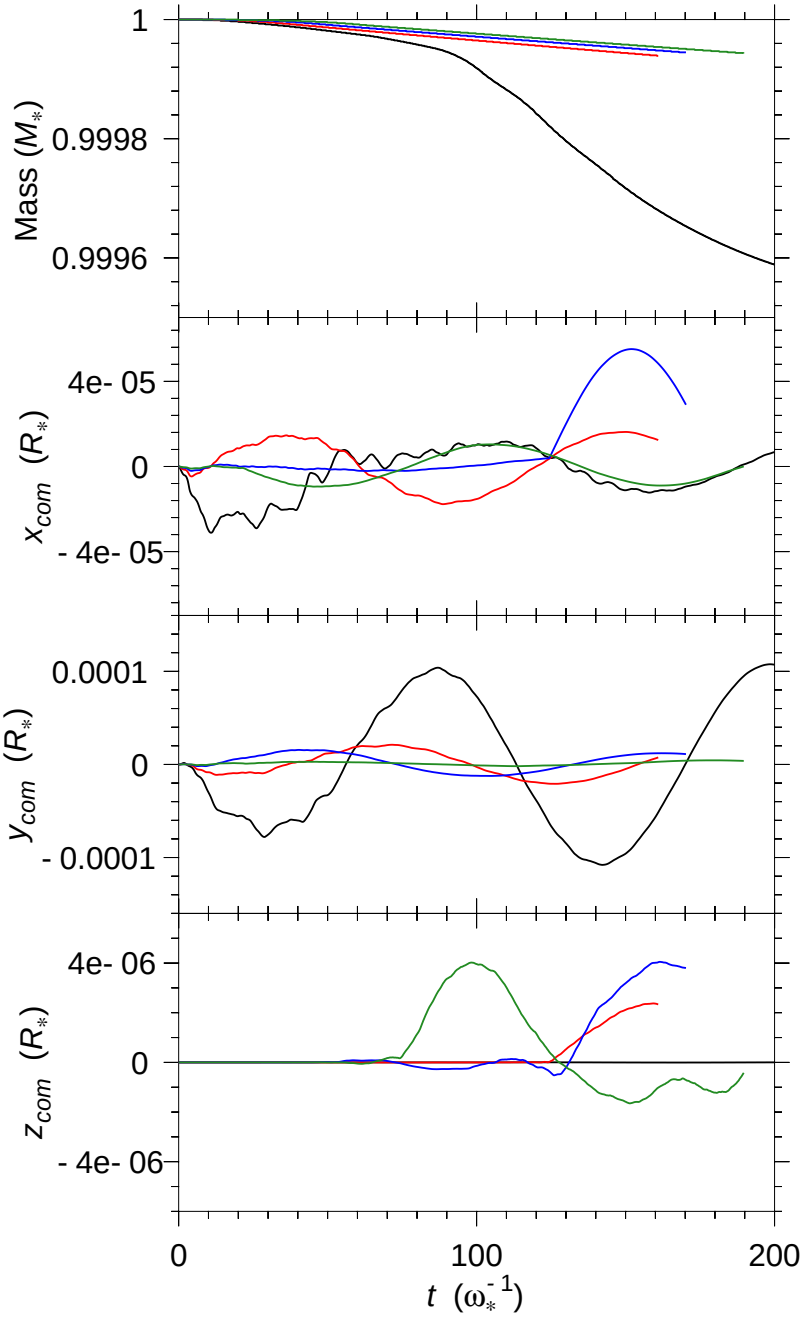

Figure 8.6: The total mass contained within the computational grid, and the x, y, z locations of the center-of-mass as a function of time for the runs shown in Figure 8.5.

Chapter 9

Applications

Much of the present work is devoted to the development of formalism. While this may be considered as valuable in itself, a formalism with relevance to observations is always preferable. This chapter therefore focuses on observable consequences of results obtained in the previous chapters. While we consider only two specific applications, it is worth mentioning that we have attempted to maintain some generality in our development of formalism. In particular, the results of Chapter 6 are general enough to be applicable to other systems, which need not be composed of compact objects. For example, a planet migrating through a circumstellar disk may well experience resonant tidal excitation, and our formalism could be employed in that context.

9.1 Exotic Supernovae

9.1.1 Progenitors

In dense environments such as galactic centers and globular clusters, eccentric white dwarf-compact object binaries can form in several ways. One possibility is tidal capture. Here, the initial orbit of the system will be highly eccentric, and its evolution is somewhat uncertain (cf. the discussion in Section 1.1.2). However, for binaries that survive in the long-term, the initial evolution will be driven tidally rather than by gravitational radiation (for systems with masses less than a few times $10^5\ M_\odot$), with modes being excited non-resonantly at each periastron passage. This initial period

of evolution will lead to faster changes in the orbital energy than the orbital angular momentum, as the mode excitation will be close to the impulse limit. As the orbit shrinks and circularizes, there will come a point when its evolution will cease to be driven by non-resonant excitation of tides, and gravitational radiation will become the dominant evolution mechanism. The system will then be in a regime where the tidal interactions are best treated as a sequence of resonance passages, with a negligible amount of energy being transferred between resonances. At this point, the system will still have a moderate amount of eccentricity, with ~ 0.5 being a canonical value. In principle, the formalism of Press & Teukolsky (1977) can be used to calculate the initial evolution of the orbit, assuming that the oscillations are damped on an orbital time-scale. However, we note that tidally captured white dwarfs are likely to be quite close to the Roche limit at capture. The tidal interaction is therefore expected to be strong, and numerical simulations will be necessary to check the results from linear calculations.

Alternatively, an eccentric white dwarf-compact object binary may form through three-body processes. Typically, in an exchange, the lightest body is ejected. As we noted previously in Section 1.1.3, the average eccentricity of the remaining binary is insensitive to the initial configuration, and is given approximately by $1-M_{\rm e}/M_{\rm f}$, where $M_{\rm e}$ is the mass of the ejected body, and $M_{\rm f}$ is the mass of the intruder (Sigurdsson & Phinney, 1993). As values of ~ 2 for the ratio $M_{\rm e}/M_{\rm f}$ are not atypical, initial eccentricities of ~ 0.5 seem reasonable for systems formed in this way.

9.1.2 Tidal Heating: Bombs vs. Duds

As modes are excited resonantly during the inspiral of an eccentric white dwarf-compact object binary, the energy transfer to the white dwarf may be sufficient to raise its temperature to the point where runaway thermonuclear burning disassembles the star, producing a Type Ia supernova. For this to occur, the modes must damp on a time-scale shorter than the inspiral time to tidal disruption. We shall revisit this point later, but for the moment we take it as given. In addition, sufficient energy

must be transferred during passage through a sequence of resonances to attain the relevant temperatures. To investigate the plausibility of this scenario, we consider the resonant excitation of the $\ell = m = 2$ f-mode during inspiral, with orbital eccentricities of less than 0.5. There are two reasons for this: (i) as we have argued above, initial eccentricities of ~ 0.5 are typical of what we expect from binary formation mechanisms, and (ii) our formalism, as developed in Chapter 6, is not valid for high eccentricities. In addition, the resonant excitation of f-modes is unimportant for companion masses $\gtrsim 10^6\ M_\odot$, as the last stable orbits then correspond to high-order harmonics ($\gtrsim 40$; see Section 9.2 below). Because the location of the last stable orbit is proportional to the companion mass (for large q), it follows that the excitation of f-modes is only of interest for companion masses $\lesssim 10^5\ M_\odot$. Accordingly, we focus on this regime.

The heat capacity of a white dwarf is essentially dominated by the ions (e.g., Hansen & Kawaler, 1994), and is therefore given approximately by the ideal gas heat capacity:

$$C_V = \frac{3}{2} k_{\rm B} \frac{M_*}{\mu m_{\rm u}} \ , \tag{9.1}$$

where μ is the molecular mass.[1] The heat capacities and binding energies for several white dwarfs are shown in Table 9.1. We note that to raise the temperature by $\sim 10^8$ K requires $\sim$ 1–5 percent of the binding energy. The heat capacities allow us to identify mode amplitudes with effective temperature differences, which is a convenient characterization for the present application:

$$\Delta T = \frac{M_j \omega_j^2}{C_V} A_j^2 \tag{9.2}$$

(for modes with $m = 0$, the right hand side of the above equation has a factor of $1/2$). Figure 9.1 shows the correspondence for the $\ell = m = 2$ f-mode. An important observation is that a temperature difference of about 10^8 K corresponds to mode amplitudes of around 0.45–0.65, which are expected to be in the non-linear regime.

[1]For low temperatures ($\lesssim 10^7$ K), crystallization of the ions changes the heat capacity significantly, but this does not affect our calculations as the temperatures we are concerned with are quite

Mass ($M_\odot$)	Radius (10^8 cm)	B.E. (10^{50} erg)	C_V (10^{40} erg K^{-1})
0.6	8.83	0.43	2.12
1.0	5.71	1.6	3.52
1.4	1.98	5.1	4.93

Table 9.1: The binding energies (B.E.) and heat capacities (C_V) for several Chandrasekhar white dwarfs, assumed to be equal carbon-oxygen mixtures. For helium, the heat capacities are a factor of 7/2 higher.

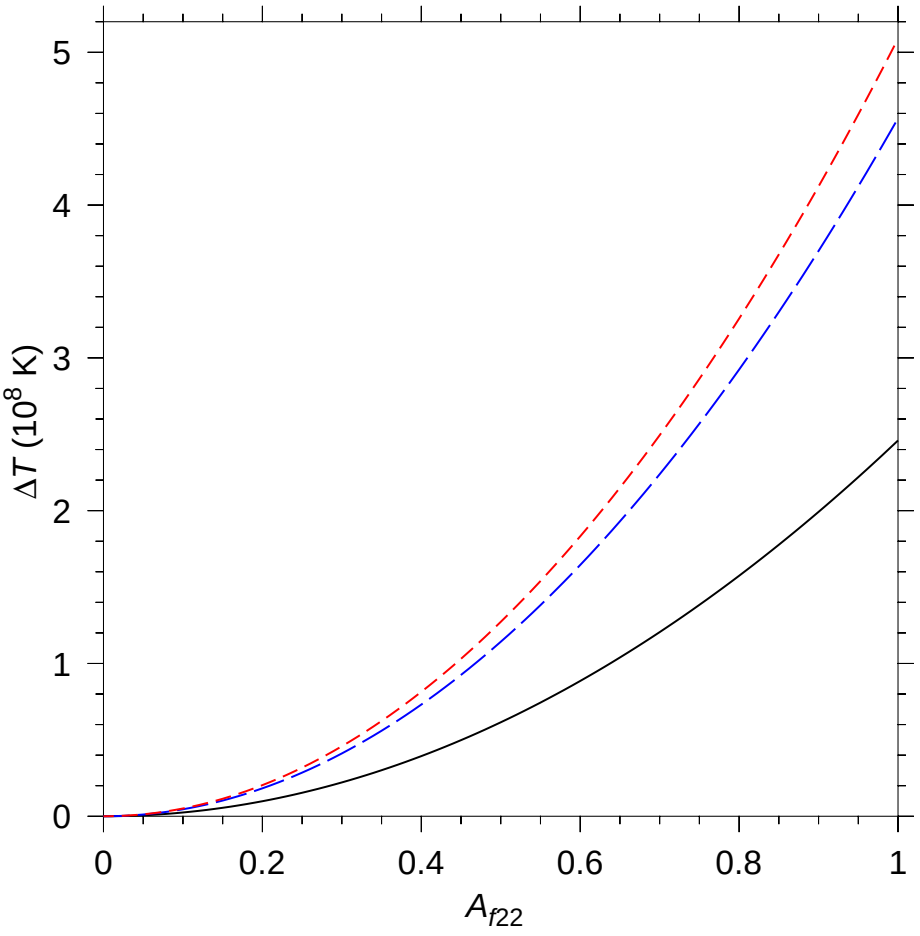

Figure 9.1: The correspondence between $\ell = m = 2$ f-mode amplitudes and effective temperature differences for the white dwarf models listed in Table 9.1. The solid line corresponds to the 0.6 $M_\odot$ model, and the long and short dashed lines correspond to the 1.0 and 1.4 $M_\odot$ models, respectively.

Figure 9.2 shows plots of several gravitational inspiral trajectories in the eccentricity-harmonic plane for the $\ell = m = 2$ f-mode with different white dwarf and companion masses. The resonant energy transfer, assuming a zero initial mode amplitude at each resonance, has been used to plot contours of constant ΔT. Also shown are the tidal limit and contours corresponding to constant inspiral times to tidal disruption. Stellar evolution calculations indicate ignition temperatures of about 2.5×10^8 K and 8×10^7 K for thermonuclear burning of carbon and helium, respectively (Kippenhahn & Weigert, 1990). Thus, we expect that the probability of a detonation becomes significant for a carbon-oxygen white dwarf if its temperature approaches 2.5×10^8 K. It is interesting to note that for a helium white dwarf of identical mass, the ignition temperature is lower, but the heat capacity is higher by a factor of 7/2, so that the required amount of energy for ignition is only a factor of about 1.1 higher than for the carbon-oxygen case.

If we assume that the mode is damped completely between resonances, then the heating of the white dwarf along an inspiral trajectory is given simply by adding up the values of ΔT for each resonance before tidal disruption. In this way, we can identify trajectories which are potentially viable for detonating the white dwarf. It is immediately obvious from Figure 9.2 that, regardless of the white dwarf mass, tidal detonation through resonant excitation of f-modes is not a possibility with a companion mass of 1.4 $M_\odot$ or less, as the required rise in the temperature cannot be attained before tidal disruption. Therefore, when the companion is either a neutron star or another white dwarf, we can assert that we have a 'dud' rather than a 'bomb.'[2]

For companion masses of 10^3 and 10^5 $M_\odot$, Figure 9.2 provides a rough estimate of the limiting inspiral tracks that separate trajectories for which detonation is a theoretical possibility from those where detonation can be ruled out. We parametrize the limiting trajectories by their orbital periods at an eccentricity of 0.5. The results are summarized in Table 9.2 (companion masses of 10 and 100 $M_\odot$ are also provided for reference). Trajectories with periods longer than those listed in Table 9.2 at an eccen-

a bit higher.

[2]One can argue that the possibility of detonation with a 1.4 $M_\odot$ companion still exists if the white dwarf is initially very hot. We assume that this is not the case.

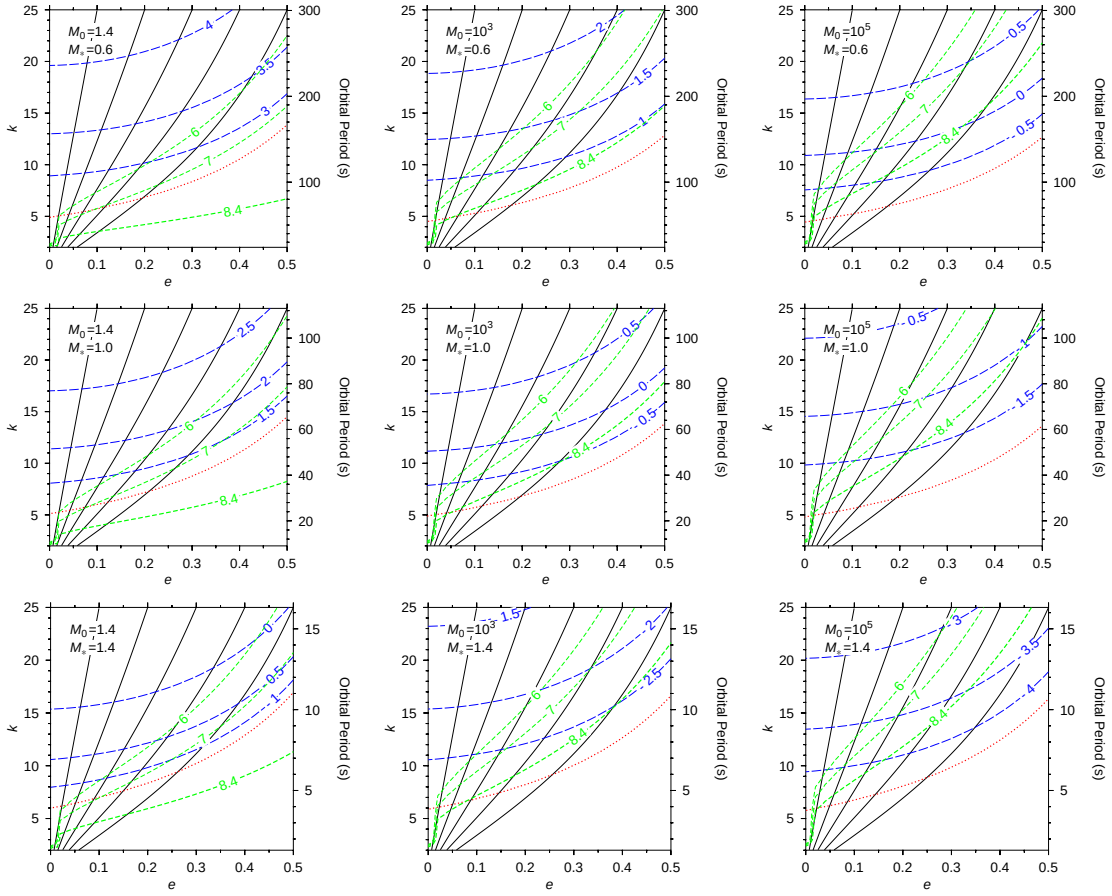

Figure 9.2: Several inspiral trajectories for different white dwarf and companion masses (in units of $M_\odot$) are shown in the eccentricity-harmonic plane. In each plot, the solid lines correspond to the trajectories, the short dashed lines are contours of constant ΔT (in Kelvins, and labeled with base-10 logarithms), and the long dashed lines are contours of constant inspiral time to tidal disruption (measured in years, and also labeled with base-10 logarithms). The tidal disruption limit is denoted by the dotted line. The curve corresponding to our assumed threshold for carbon ignition is $\log(\Delta T/\mathrm{K}) = 8.4$ (i.e., $\Delta T = 2.5 \times 10^8$ K).

M_* \ M_0	1.4 $M_\odot$	10 $M_\odot$	10^2 $M_\odot$	10^3 $M_\odot$	10^5 $M_\odot$
0.6 $M_\odot$	-	253 s	415 s	571 s	2008 s
1.0 $M_\odot$	-	113 s	198 s	265 s	517 s
1.4 $M_\odot$	-	19 s	27 s	43 s	72 s

Table 9.2: Approximate orbital periods at an eccentricity of 0.5 for gravitational radiation inspiral tracks that delineate trajectories for which detonation via resonant excitation of quadrupolar f-modes is a theoretical possibility. For a given pair of white dwarf and companion masses, trajectories with longer periods than the given value are expected to be 'duds.' Most trajectories with shorter periods are potential 'bombs.' For a companion mass of 1.4 $M_\odot$, tidal detonation is ruled out.

tricity of 0.5 are expected to be duds, where as most trajectories with shorter periods are potential bombs. We say 'most' rather than 'all' because the variation in the tidal limit for different trajectories can introduce strips in the eccentricity-harmonic plane which are duds despite meeting the criterion of Table 9.2. For reference, Figure 9.3 shows the orbital period as a function of eccentricity for gravitational inspiral. The period is shown in units of the period at an eccentricity of 0.5. Note that this plot is scale-free in the sense that it applies to all inspiral trajectories.

9.1.3 Detonation and Aftermath

Assuming that the carbon in the white dwarf is ignited, the result may be a runaway detonation that disassembles the entire star—in other words, a Type Ia supernova. If the ejecta from the explosion remain bound in orbit around the companion, then an even larger amount of energy will be released when this matter is accreted onto the companion. This is quite different from conventional scenarios for Type Ia supernovae.

We can evaluate the plausibility of the star being disassembled by a calculation of the energy budget. The energy yield from thermonuclear burning of carbon in an equal carbon-oxygen mixture yields $Q = 2.5 \times 10^{17}$ erg g^{-1} (Kippenhahn & Weigert, 1990). Assuming that all this energy goes into heat, if the total energy yield exceeds the binding energy of the star then there is a significant probability that the star will not survive. The minimum fraction of the stellar matter that must be burned for the

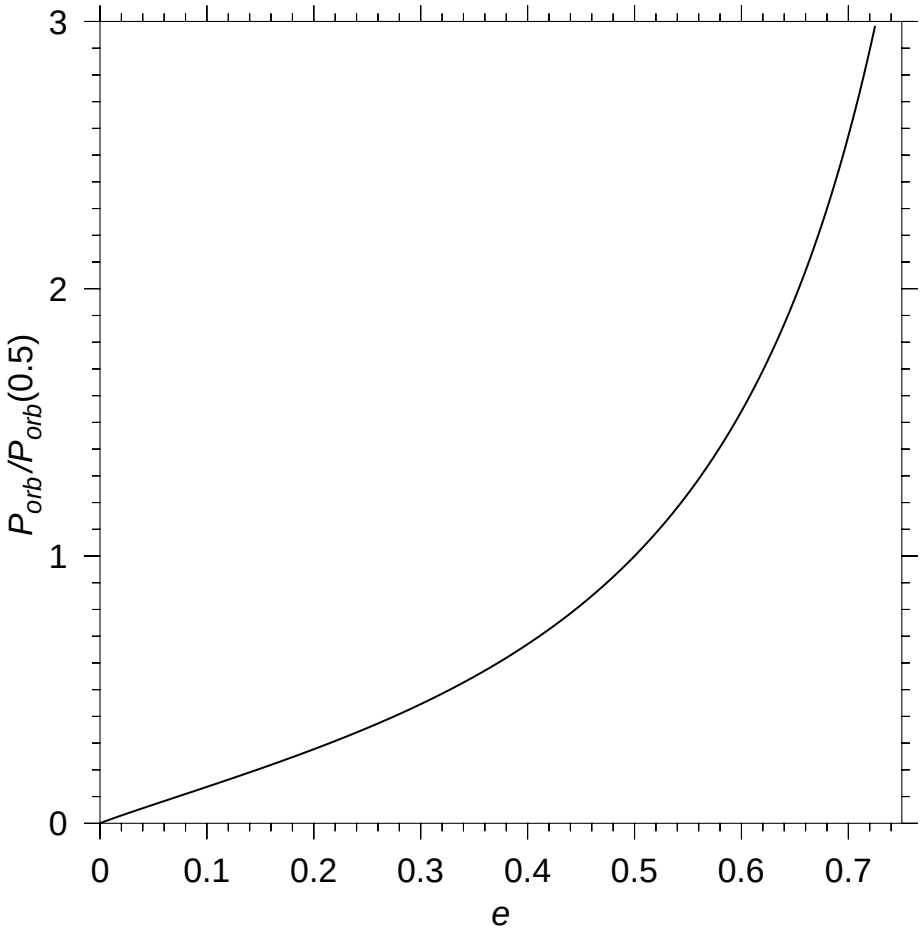

Figure 9.3: The orbital period as a function of eccentricity for gravitational inspiral. The period is shown in units of the period at an eccentricity of 0.5. This makes the plot scale-free and applicable to all inspiral trajectories.

star to disassemble by carbon detonation is roughly 0.14 for a 0.6 $M_\odot$ white dwarf, 0.32 for a 1.0 $M_\odot$ white dwarf, and 0.73 for a 1.4 $M_\odot$ white dwarf. We denote this fraction by α, and let β be the fraction of the stellar matter that is actually burned. Assuming that $\beta > \alpha$ (i.e., the star is disassembled), the specific kinetic energy of the ejecta from the explosion is given by $(\beta - \alpha)Q$. If this energy exceeds the specific orbital binding energy, $GM_0/2a$, then we can expect the ejecta to become mostly unbound (from the orbit). However, if the orbital binding energy is larger, then most of the ejecta will remain trapped in orbit around the companion. Using this criterion, the conditions for the ejecta to be trapped are found to be:

$$(\beta - 0.14) - 0.21\frac{q}{(1+q)^{1/3}}k^{-1/3} < 0 \qquad (\text{for } 0.6\ M_\odot)\ , \tag{9.3}$$

$$(\beta - 0.32) - 0.55\frac{q}{(1+q)^{1/3}}k^{-1/3} < 0 \qquad (\text{for } 1.0\ M_\odot)\ , \tag{9.4}$$

$$(\beta - 0.73) - 2.3\frac{q}{(1+q)^{1/3}}k^{-1/3} < 0 \qquad (\text{for } 1.4\ M_\odot)\ . \tag{9.5}$$

For the limiting case, $\beta = 1$, the resulting conditions on the orbital period at the time of detonation for the ejecta to remain bound are

$$P_{\rm orb} \lesssim (0.18\ {\rm s})\, q^2 \qquad (\text{for } 0.6\ M_\odot)\ , \tag{9.6}$$

$$P_{\rm orb} \lesssim (2.4\ {\rm s})\, q^2 \qquad (\text{for } 1.0\ M_\odot)\ , \tag{9.7}$$

$$P_{\rm orb} \lesssim (420\ {\rm s})\, q^2 \qquad (\text{for } 1.4\ M_\odot)\ . \tag{9.8}$$

The detonation is likely to occur close to the tidal limit, if at all. As the orbital period at the tidal limit for eccentricities 0–0.5 is never larger than about 150 s for the 0.6 $M_\odot$ white dwarf, 60 s for the 1.0 $M_\odot$ white dwarf, and 11 s for the 1.4 $M_\odot$ white dwarf (cf. Figure 9.2), the ejecta should remain bound in the majority of cases, with a 0.6 $M_\odot$ star and a $\sim 10\ M_\odot$ companion being an exception.

9.1.4 Comments and Caveats

The estimates for the carbon and helium ignition temperatures that we have quoted are taken from calculations of helium and carbon flashes in evolving stars presented in Kippenhahn & Weigert (1990). Other references quote somewhat different temperatures. Indeed, Kippenhahn & Weigert (1990) themselves state elsewhere that the temperatures for helium and carbon ignition are $\gtrsim 10^8$ K and ~ 5–10×10^8 K, respectively. Hansen & Kawaler (1994) state a temperature of about 1.2×10^8 K for helium ignition, and a range ~ 5–10×10^8 K for carbon ignition. Rose (1998) states the corresponding temperatures as $\gtrsim 10^8$ K and ~ 4–8×10^8 K, respectively. Bisnovatyi-Kogan (2002) states a maximum temperature of about 2×10^8 K for a helium flash, and $\geqslant 3 \times 10^8$ K for carbon burning. The actual ignition temperatures may depend upon details of the white dwarf model, and full evolutionary calculations are required to determine this. Nonetheless, in view of the numbers quoted above, the ones we have chosen to use are perhaps the most optimistic. Note, however, that all of the quoted temperatures are attainable through tidal excitation. Higher temperature thresholds will lower the periods listed in Table 9.2, and therefore decrease the number of viable trajectories. For example, a carbon ignition threshold of 5×10^8 K lowers the limiting period for a 1.0 $M_\odot$ white dwarf with a 10^3 $M_\odot$ companion by ~ 20 percent to about 214 s.

The assumption of mode damping between resonances was adopted as an *ansatz*. If the dominant mode damping mechanism is gravitational radiation, as is probably the case for linear mode amplitudes, then the full damping assumption is incorrect. Moreover, with gravitational radiation as the damping mechanism, the energy in oscillations is not available for heating. However, if the mode amplitudes are large enough, then non-linear processes may dominate the damping. It was observed previously that the quadrupolar f-mode amplitudes corresponding to a temperature of about 10^8 K are around ~ 0.5. As an amplitude of 0.5 for a quadrupolar f-mode represents a maxmimum radial displacement at the stellar surface of about $0.27\,R_*$, we can expect non-linear processes to be relevant. It is interesting to note that for

different companion masses, there is a trade-off between the resonant energy transfer and the time available for mode damping before tidal disruption: higher masses mean more energy, but less time because the binary coalesces more rapidly.

Suppose that the mode does not damp by non-linear processes completely between resonances, but is instead damped until its amplitude is in the linear regime, where gravitational radiation then becomes the dominant damping mechanism. We can obtain some sense of how this would affect the heating of the white dwarf along an inspiral trajectory by assuming that the mode damps to some non-zero fiducial amplitude between resonances, which we take to be 0.2. Thus, only part of the mode energy is assumed to be available for heating. If we evaluate the temperatures attained during inspiral for the marginal bomb trajectories listed in Table 9.2, then we find that the temperatures attained before tidal disruption are, in fact, higher than for the full mode damping case. The reason for this is that the energy transfer at a resonance increases with the initial mode amplitude (cf. Section 6.4.3). Therefore, for partial mode damping, the region of bomb trajectories in the eccentricity harmonic plane appears to be larger rather than smaller. However, this conclusion is subject to the following caveat.

The formalism developed in Chapter 6 assumes that the mode amplitude is in the linear regime. If the mode is even marginally non-linear, then it is unclear whether the energy transfer calculated with our formalism is accurate. For want of a better answer, we assume that the energy transfer including non-linear effects does not change by more than a factor of order unity. A more definite answer requires further investigation.

We have treated the orbit as being non-relativistic in all cases. For high-mass binaries and low-harmonic resonances, the orbital velocities become a significant fraction of the speed of light. Relativistic effects are therefore expected to be important in such systems. A more accurate treatment of the problem would be obtained by incorporating post-Newtonian terms in the equations of motion.

Our estimate of the tidal disruption limit is the application of an analytic fit to the tidal limit in circular, synchronous binaries. We have simply treated the periastron

separation as the effective radius of the orbit. The resulting estimate is probably conservative in that the white dwarf is likely to be able to maintain its structural integrity (perhaps with some mass loss from the outer layers) for smaller separations in an eccentric orbit, as the system does not spend most of its time at periastron. Thus, the net energy transfer before disruption may be quite a bit larger than we have calculated (perhaps by a factor of two or more).

Of the companion masses we have considered, 10^3 and 10^5 $M_\odot$ are purely speculative (save, perhaps, for some galaxies which may have black holes with masses a few times 10^5 $M_\odot$ at their centers). However, 10^3 $M_\odot$ is about what is predicted for objects formed by runaway collisions in globular cluster dynamics simulations (Portegies Zwart & McMillan, 2002; Portegies Zwart et al., 2004). Less speculative companion masses are 10 and 100 $M_\odot$, which may be expected for black holes formed from massive stars.

Finally, we note that even if carbon is ignited in a white dwarf (or helium in a helium white dwarf), the result may be a flash rather than a supernova for stellar masses lower than the Chandrasekhar limit. In a flash, the temperature in the core increases at nearly constant density until the degeneracy is removed, and the core then expands and the central burning becomes stable. For near-Chandrasekhar mass white dwarfs, a supernova is more likely to be the outcome if carbon ignition occurs in the center (Kippenhahn & Weigert, 1990). Once again, detailed evolutionary calculations are required to obtain a more definite answer.

9.2 Gravitational Wave Sources

Supermassive black holes with masses $\sim 10^6$ $M_\odot$ or greater are thought to reside at the centers of most, if not all, nucleated galaxies. Within the central cusp of such a galaxy, the dynamics are dominated by the gravitational field of the central black hole, and the mass of the stars inside the cusp is typically comparable to the black hole mass. When two of these stars undergo a scattering event, one of them can be captured into a close, highly eccentric orbit around the central black

hole. This orbit subsequently inspirals under gravitational radiation reaction, and also evolves due to other relativistic effects such as periastron advance and Lense-Thirring precession of the orbital plane. These extreme-mass-ratio capture events are expected to be important potential sources for the proposed space-based gravitational wave detector, LISA (Barack & Cutler, 2004). LISA's sensitivity band is centered around a frequency of $\sim 3 \times 10^{-3}$ Hz. Most main-sequence stars are not expected to be able to sustain the strong tidal forces in this regime, and are therefore unlikely to be observable by LISA. For the star to be able to survive in the LISA band, it would have to be a white dwarf, neutron star, black hole or a very low-mass main-sequence star (Barack & Cutler, 2004). Note that, for a stellar-mass companion, the center of LISA's sensitivity band corresponds to a black hole mass of $\sim 10^6\ M_\odot$.

The proposed algorithms for parameter estimation from gravitational wave signals observed by LISA are based upon the technique of 'matched filtering' (e.g., Buonanno et al., 2003; Barack & Cutler, 2004). The basic idea is that a theoretical gravitational waveform can be calculated for a binary system, in the point-mass approximation, for a given set of parameters such as an initial time, the masses of the two components, the spins, the relative orientations of the spins and the orbital angular momentum, the initial longitude of periastron, and the initial orbital phase.[3] The output from the detector can then be filtered through such a theoretical waveform to look for a signal. A detection is claimed when the signal-to-noise ratio is larger than some threshold. Details of the matched filtering technique can be found in Buonanno et al. (2003) or Barack & Cutler (2004), and references therein.

An important property of the extreme-mass-ratio capture events is that the orbits can remain moderately eccentric up until the final 'plunge' beyond the innermost stable orbit. The initial eccentricity of the orbits is extremely high: $1 - e_{\rm init} \sim 10^{-6}$–$10^{-3}$, typically, and the initial periastron separation is only $r_{\rm p}^{\rm init} \sim 8$–$100\ M_0$. At the innermost stable orbit, $e > 0.1$ for $r_{\rm p}^{\rm init} \lesssim 20.0\ M_0$, $e > 0.2$ for $r_{\rm p}^{\rm init} \lesssim$

[3]These are the so-called *intrinsic* parameters: they describe properties of the source and are independent of the observer. For the actual detection algorithm, the location and orientation of the observer relative to the source have to be accounted for as well. These comprise the *extrinsic* parameters (Buonanno et al., 2003; Barack & Cutler, 2004).

12.8 M_0, and $e > 0.3$ for $r_{\rm p}^{\rm init} \lesssim 9.2\ M_0$ (Barack & Cutler, 2004). Therefore, during the inspiral, the tidal force exerted by the central black hole upon the stellar-mass compact object has non-zero amplitudes for harmonic components at integer multiples of the orbital frequency (recall that the Hansen coefficients scale as $\sim e^{|k-|m||}$). This is the kind of scenario in which resonant tidal effects, which are finite-size effects, may be interesting. The presence of a non-zero orbital eccentricity means that f-modes, which have the largest tidal overlap, can be excited resonantly during the inspiral. It is interesting to investigate whether this can have noticeable consequences for the gravitational waveform when the inspiraling compact object is a white dwarf.

Typical orbital periods at the innermost stable orbit for a white dwarf are $\sim$ 500–600 s, with typical eccentricities at the innermost orbit being less than ~ 0.5 (see Figure 2 in Barack & Cutler, 2004). Thus, the harmonics available for resonance with the $\ell = m = 2$ f-mode of a 0.6 $M_\odot$ Chandrasekhar white dwarf are $k \gtrsim$ 42–50. The high orders of these harmonics suggest that resonant excitation of f-modes will be unimportant, which is confirmed by direct calculation: for $k = 50$ and $e = 0.5$, and zero initial mode energy, the energy transfer to the $\ell = m = 2$ f-mode, calculated using (6.88), is of order $\sim 10^{-5}\ GM_*^2/R_*$. The corresponding fractional changes in the orbital frequency and eccentricity are of order $\sim 10^{-8}$. By contrast, over the time-scale of resonance passage (estimated as $\sim (2k\dot{n})^{-1/2}$, where $\dot{n}$ is given by (5.15) with $n \simeq \omega_j/k$), the fractional change in the orbital frequency due to gravitational radiation is about $\sim 10^{-5}$.[4] Thus, resonant excitation of f-modes is completely negligible in this case. However, the excitation of g-modes, which have longer periods, may be of interest. Depending on the mode periods, these can be excited at low harmonic or fundamental resonances. As the dominant restoring force for g-modes is buoyancy (which depends upon the entropy gradient), a realistic calculation of g-mode frequencies and eigenfunctions requires accurate modeling of the thermal properties of white dwarfs. This is an industry in itself, but we can obtain a rough estimate by using the following model for a "poor man's" warm white dwarf, adapted from

[4] In this chapter, the symbol n is used to denote both the orbital angular frequency and the radial order of a mode. There should be little room for confusion, as the meaning is usually obvious from the context.

n,ℓ,m	$\omega_{n\ell}$ (ω_*)	Period (s)	$M_{n\ell}$ (M_*)	$\eta_{3,n\ell}/\eta_{1,n\ell}$
0,2,2	1.61	12	0.0176	-1.51×10^{-1}
1,2,2	0.205	95	0.129	-1.46×10^{-3}
2,2,2	0.178	110	0.126	1.01×10^{-3}
3,2,2	0.144	135	0.318	3.83×10^{-4}
4,2,2	0.120	163	0.517	9.32×10^{-5}
5,2,2	0.102	191	0.731	2.19×10^{-4}
6,2,2	0.0894	218	0.932	2.52×10^{-4}
7,2,2	0.0792	246	1.20	2.56×10^{-4}
8,2,2	0.0713	274	1.55	2.33×10^{-4}
9,2,2	0.0647	301	2.16	2.35×10^{-4}
10,2,2	0.0592	330	3.05	2.36×10^{-4}

Table 9.3: Properties of quadrupolar f- and g-modes for a 0.6 $M_\odot$ helium white dwarf, with a core temperature of 10^7 K, and radius 9.22×10^8 cm. The corresponding value for ω_* is 0.322 s^{-1}.

Kippenhahn & Weigert (1990).

In the core of the star, the electrons are almost fully degenerate, and their long mean free paths provide an efficient conduction mechanism that keeps the core virtually isothermal. However, near the surface layers, the electrons are no longer degenerate and act nearly like an ideal gas. Conduction then ceases to be efficient, and the energy transfer is dominated by radiation. The absorption in these layers is mainly due to bound-free and free-free processes, and is well-approximated by the Kramers opacity. Thus, we describe the electrons with a relativistic Fermi-Dirac equation of state in the core (which is set to be isothermal with a specified temperature), and at the point where the Fermi-Dirac pressure equals the ideal gas pressure, we switch to the ideal gas equation of state, and enforce the temperature profile given by the Kramers opacity: $d\log T/d\log P = 4/17$. In order to avoid unphysical discontinuities in the temperature profile at the transition from the isothermal core to the radiative envelope, we smooth the profile in a narrow region across the transition point. The nuclei are modeled as an ideal gas throughout the star.

For a 0.6 $M_\odot$ model calculated with the above prescription using a core temperature of 10^7 K, properties of the quadrupolar f- and several quadrupolar g-modes

n,ℓ,m	$\omega_{n\ell}$ (ω_*)	Period (s)	$M_{n\ell}$ (M_*)	$\eta_{3,n\ell}/\eta_{1,n\ell}$
0,2,2	1.57	12	0.0191	-1.60×10^{-1}
1,2,2	0.137	138	0.135	-3.21×10^{-4}
2,2,2	0.111	171	0.571	1.22×10^{-3}
3,2,2	0.0907	209	0.514	9.32×10^{-6}
4,2,2	0.0765	247	0.527	5.72×10^{-5}
5,2,2	0.0664	285	0.570	1.56×10^{-4}
6,2,2	0.0586	323	0.856	1.25×10^{-4}
7,2,2	0.0521	363	1.47	1.16×10^{-4}
8,2,2	0.0467	405	2.33	1.26×10^{-4}
9,2,2	0.0423	448	3.34	1.26×10^{-4}
10,2,2	0.0386	490	4.48	1.07×10^{-4}

Table 9.4: Properties of quadrupolar f- and g-modes for a 0.6 $M_\odot$ carbon white dwarf, with a core temperature of 10^7 K, and radius 9×10^8 cm. The corresponding value for ω_* is 0.332 s^{-1}.

are given in Table 9.3 for a pure helium white dwarf, and in Table 9.4 for a pure carbon white dwarf. Note that the f-mode is relatively insensitive to the model, but the g-modes vary significantly. We consider a few illustrative cases to evaluate the importance of g-modes during the inspiral of LISA capture sources. From Figure 2 of Barack & Cutler (2004), we see that on one of the inspiral trajectories, g-modes with periods ~ 250 s ($n=7$ in Table 9.3, $n=4$ in Table 9.4) have fundamental resonances with an eccentricity of about ~ 0.1 just before the final plunge (for fundamental resonance, low eccentricities are better, as less power is then distributed among other harmonics). The resulting energy transfers are of order $\sim 0.01\ GM_*^2/R_*$. The fractional changes to the orbital frequency and eccentricity due to the resonant energy transfer are of order $\sim 10^{-5}$, where as the fractional changes due to gravitational radiation are of order $\sim 10^{-4}$. The typical resonance passage time is $\sim 10^5$ s. In addition to fundamental resonances, it is also possible to excite g-modes at low harmonic resonances for inspiral trajectories with larger eccentricities. For example, one of the trajectories in Figure 2 of Barack & Cutler (2004) passes close to the point with period ~ 1000 s and eccentricity ~ 0.5. Thus, near this point, from Table 9.3, the $n=1$ mode has a resonance with the $k=10$ harmonic, and, from Table 9.4, the $n=4$

mode has a resonance with the $k = 4$ harmonic. Once again, the energy transfers are of order $\sim 0.01\ GM_*^2/R_*$, and the fractional changes to the orbital frequency and eccentricity are of order $\sim 10^{-5}$, where as the fractional changes due to gravitational radiation are of order $\sim 10^{-4}$. The typical resonance passage time is again $\sim 10^5$ s.

The net result of g-mode resonances is to cause the system's inspiral trajectory in the orbital frequency-eccentricity plane to deviate from the point-mass trajectory. The passage of a system through a sequence of such resonances will effectively change the slope of the trajectory (each individual 'step' corresponding to a resonance passage only lasts about a day, and so, over an integration time of several years, the steps themselves will average out). While this should not affect LISA's ability to detect such signals, it will introduce errors in the parameter estimation if the fitting algorithms use a point-mass approximation. The exact magnitude of such errors depends upon the number of resonances in the LISA frequency band and the resonant energy transfer, and its evaluation therefore requires realistic white dwarf models, but we may expect the deviations to be potentially as large as few tens percent. In contrast, Barack & Cutler (2004) claim that LISA will be able to determine the constituent masses of a capture source to better than ~ 0.1 percent accuracy, in the point-mass approximation.

It is interesting to note that the energy transfers seen above for the g-modes are more than adequate to drive the mode amplitudes to over unity. This suggests that non-linear processes will likely damp the oscillations and thermalize the energy (non-adiabatic processes in the outer layers of the star may also be limiting effects). With a net energy transfer of $\sim 0.01\ GM_*^2/R_*$, the temperature of the star can be raised to $\sim 10^8$ K (cf. Section 9.1). We can therefore expect the white dwarf's structure to be altered significantly.

The main caveat to our results is the crudeness of our warm white dwarf model. For more realistic models, the energy transfer and, consequently, the impact upon the gravitational wave signal and the heating of the white dwarf could change significantly. Therefore, our results should not be considered definitive, but, rather, illustrative of the fact that tidal resonant effects are potentially important in the evolution of LISA

capture sources with white dwarfs. However, we can state with reasonable confidence that the excitation of f-modes is unimportant in this context.

One of the limitations to LISA's sensitivity is expected to be confusion noise from short-period Galatic and extra-Galactic binaries (e.g., Nelemans et al., 2001; Hughes, 2002; Barack & Cutler, 2004). Many of these systems are double degenerates, and, for evolutionary reasons, are expected to be mostly circular (cf. Section 1.1.1). The resonant excitation of f-modes is therefore not possible in such systems. However, g-modes, with their longer periods, can be excited at fundamental resonance. It would be of interest to determine whether the excitation of g-modes in this context is of any importance for the limitations to LISA's sensitivity. This could be the subject of a future study.

Part IV

Conclusions

A complete formalism for describing the excitation of dynamic tides in stars has been developed. The formalism starts from a variational description of perfect fluids and systematically develops the theory of normal modes and tidal excitation, which allows for easy identification of conserved quantities and ensures self-consistency in the equations of motion. Although only the specific case of a non-rotating homentropic star is treated in detail, an effort has been made to maintain generality whenever possible, and to indicate points of specialization explicitly.

From the equations of motion, the energy transfer at a tidal resonance in a white dwarf-compact object binary during gravitational inspiral has been calculated in the approximation when the back reaction of the tides on the orbit is neglected, and the orbital eccentricity is not too high ($\lesssim 0.5$). It was found in this no back reaction approximation that the energy in a stellar mode of oscillation executes a random walk with a net positive drift during passage through a sequence of resonances. It was also demonstrated that the no back reaction approximation is incorrect in a significant portion of the parameter space, and an attempt was made to delineate the region of the parameter space where back reaction modulates the magnitude of resonant energy transfer significantly. It was then argued that back reaction, in fact, determines the direction of energy transfer in most cases as well.

A detailed treatment of the problem including back reaction has been developed from a Hamiltonian perspective, assuming negligible damping on a resonance time-scale. It was demonstrated that, in the near-resonant regime, the problem can be reduced from four to two, and then one degree-of-freedom. This reduction guarantees integrability. The mathematical similarity of the one degree-of-freedom Hamiltonian to Hamiltonians encountered in the treatment of first-order eccentricity resonance in the circular, restricted three-body problem was also established. A resonance passage was shown to correspond to a separatrix crossing in phase space, and the problem of calculating the resonant energy transfer was shown to correspond to the calculation of the change in an adiabatic invariant at the separatrix crossing. By leveraging results for the similar three-body resonance problem, an expression for the resonant energy transfer including back reaction was found, which was shown to be accurate

to within $\sim$ 10 percent for orbital eccentricities $\lesssim 0.5$, and a wide range of other parameters. Two important qualitative results obtained were: (i) the energy transfer at a resonance is always positive, and is independent of the phase to lowest order in the rate of dissipation by gravitational radiation, and (ii) the energy transfer at a resonance increases with the initial mode energy. While the explicit treatment of the back reaction problem was specialized to the specific case of an $\ell = m$ mode in a non-rotating star, it was argued that the results obtained have more general validity.

The design and implementation of a simple, fast, and parallel numerical code to study the excitation of tides and the non-linear evolution of the excited tides have been described. The described code is an adiabatic, explicit, Eulerian finite-difference scheme on a uniform Cartesian mesh. Special attention was paid to the fast solution of the Poisson equation for the self-gravitational potential via a discrete sine transform method. The results of several test problems were used to establish the stability and accuracy of the code, as well as its suitability for studying the evolution of tides on white dwarfs. The problem of maintaining hydrostatic equilibrium on the finite-difference grid was discussed, and a solution using the so-called self-consistent field method was described, which is valid for homentropic stars.

The results of several simulations of resonant excitation of the $\ell = m = 2$ f-mode on a white dwarf have been presented. Due to problems with long-term mass loss from the grid, quantitative results were not obtained. However, several qualitative observations were discussed. It was shown that a significant coupling between modes with $\ell = 2$ and $\ell = 4$ seems to exist. Modes with $\ell = 3$, on the other hand, did not seem to couple directly with $\ell = 2$ modes. Directions for future work were described, which would allow for more quantitative results such as the non-linear damping rate for the $\ell = m = 2$ mode, and its scaling with the mode amplitude.

Two specific applications of the work presented have been considered. The first is the possibility of tidally triggered Type Ia supernovae. It was argued that likely progenitors for such systems would be eccentric white dwarf-compact object binaries formed through tidal capture or three-body processes in dense environments such as galactic centers and globular clusters. It was then studied whether, for such binaries

with carbon-oxygen white dwarfs with masses 0.6, 1.0, and 1.4 $M_\odot$, there exist regions in the parameter space where sufficient energy can be transferred resonantly to the $\ell = m = 2$ f-mode during gravitational inspiral to raise the star's temperature to the ignition point for carbon. A 1.4 $M_\odot$ companion such as a neutron star or another white dwarf was found to be not viable. However, for companion masses ~ 10 $M_\odot$ or higher, regions in the parameter space were shown to exist where the relevant temperatures can be attained before tidal disruption. It was noted that the assumption of mode damping on the gravitational inspiral time-scale is necessary to heat the star. Moreover, the damping mechanism must thermalize the energy rather than radiate it away, which would be the case if the damping mechanism is gravitational radiation. If the energy is thermalized, then the ignition of carbon is possible. It was shown that sufficient energy can be released by the thermonuclear burning to disassemble the entire star and generate a Type Ia supernova. In addition, the ejecta from such a detonation were shown to be likely to remain trapped in orbit around the companion, with the exception of a 0.6 $M_\odot$ white dwarf with a ~ 10 $M_\odot$ companion. This then implies that the ejecta would eventually be accreted by the companion, which would potentially result in the release of even more energy than was released in the detonation. A number of caveats to the tidal detonation picture were also discussed, with the main issues being the need for full evolutionary calculations to determine the correct ignition temperatures, an understanding of mode damping time-scales, and the validity of the resonant energy transfer calculation when the mode amplitudes are either non-linear or nearly non-linear.

A second application considered was a preliminary evaluation of the importance of resonant tidal effects for gravitational wave observations of white dwarf-compact object binaries. The particular systems considered were LISA capture sources with white dwarfs as the captured objects and a $\sim 10^6$ $M_\odot$ central object. The focus was on determining whether tidal resonances can complicate detection and parameter estimation for such sources. The resonant excitation of f-modes on the white dwarf was shown to be unimportant in this context because of the large orbital periods at the last stable orbits. A rough estimate of the importance of g-modes was made using

a crude warm white dwarf model, and it was found that, for typical parameters, a resonance with a quadrupolar g-mode can affect the orbital elements at a ~ 10 percent level relative to gravitational radiation on a resonance passage time-scale (estimated to be of the order of a day). It was argued that this will not affect LISA's ability to detect such systems, but could introduce significant errors in the parameter estimation if point-mass waveform templates are used, as the effective inspiral trajectory in the eccentricity-frequency plane would deviate from the point-mass track. The exact size of the errors depends upon the white dwarf model and orbital parameters. Also, for LISA, it was suggested that the resonant excitation of g-modes could be important for determing the confusion noise limit imposed by Galactic and extra-Galactic double degenerate systems.

Appendix A

Variational Derivation of the Euler Equation

We shall assume, for simplicity, that the centre-of-mass frame of the fluid is inertial. Then, in the centre-of-mass frame, the Lagrangian (4.4) becomes

$$L_* = \int d\mathbf{a} \left[\frac{1}{2}\left(\frac{\partial \mathbf{x}}{\partial \tau}\right)^2 - E\left(\alpha, S(\mathbf{a})\right) - \Phi(\mathbf{x})\right],$$

where $\alpha \equiv \rho^{-1}$ is the specific volume. The variation with respect to $\mathbf{x}$ yields

$$\frac{\partial^2 x_i}{\partial \tau^2} - \frac{\partial E}{\partial \alpha}\frac{\partial}{\partial a_j}\left[\frac{\partial \alpha}{\partial(\partial x_i/\partial a_j)}\right] - \frac{\partial \alpha}{\partial(\partial x_i/\partial a_j)}\frac{\partial}{\partial a_j}\left(\frac{\partial E}{\partial \alpha}\right) = -\frac{\partial \Phi}{\partial x_i}. \tag{A.1}$$

We can show that the second term on the left hand side of (A.1) is zero as follows. From the definition of α, we know that

$$\alpha = \frac{\partial(\mathbf{x})}{\partial(\mathbf{a})} = \frac{1}{6}\epsilon_{ijk}\epsilon_{lmn}\frac{\partial x_i}{\partial a_l}\frac{\partial x_j}{\partial a_m}\frac{\partial x_k}{\partial a_n},$$

where ϵ_{ijk} is the three-dimensional Levi-Civita symbol (cf. Arfken & Weber, 1995). Taking the derivative of both sides with respect to $\partial x_i/\partial a_j$, we get

$$\frac{\partial \alpha}{\partial(\partial x_i/\partial a_j)} = \frac{1}{2}\epsilon_{ijk}\epsilon_{lmn}\frac{\partial x_j}{\partial a_m}\frac{\partial x_k}{\partial a_n}.$$

And, finally, taking a derivative with respect to a_j gives us

$$\frac{\partial}{\partial a_j}\left[\frac{\partial \alpha}{\partial(\partial x_i/\partial a_j)}\right] = \epsilon_{ijk}\epsilon_{lmn}\frac{\partial^2 x_j}{\partial a_l \partial a_m}\frac{\partial x_k}{\partial a_n} = 0.$$

Next, using the definition of α and the identity (4.3), we note that

$$\frac{\partial \alpha}{\partial(\partial x_i/\partial a_j)}\frac{\partial}{\partial a_j} = \alpha\frac{\partial a_j}{\partial x_i}\frac{\partial}{\partial a_j} = \alpha\frac{\partial}{\partial x_i}.$$

Therefore, (A.1) now becomes

$$\frac{\partial^2 x_i}{\partial \tau^2} = -\alpha\frac{\partial P}{\partial x_i} - \frac{\partial \Phi}{\partial x_i},$$

where $P \equiv -\partial E/\partial\alpha$ is the pressure. Recalling that $\partial/\partial\tau$ corresponds to a convective derivative in the Eulerian description, we see that this is just the Euler equation.

Appendix B

Hansen Coefficients

The Hansen coefficients $X_k^{p,m}$ for the two-body problem are defined by

$$\left(\frac{R}{a}\right)^p \exp(imv) = \sum_{k=-\infty}^{\infty} X_k^{p,m}(e) \exp(ikl) \ ,$$

where R is the orbital separation, a is the semi-major axis, v is the true anomaly, e is the orbital eccentricity, and l is the mean anomaly. The Hansen coefficients are real functions of the eccentricity, and it can be shown that, to lowest order in eccentricity,

$$X_k^{p,m}(e) \propto e^{|k-m|}$$

(Murray & Dermott, 1999, and references therein). The coefficients can be calculated to any desired order in eccentricity as a series in terms of Newcomb operators:

$$X_k^{p,m}(e) = e^{|k-m|} \sum_{\nu=0}^{\infty} X_{\nu+\lambda,\nu+\zeta}^{p,m} e^{2\nu} \ ,$$

where $\lambda = \max(0, k-m)$, $\zeta = \max(0, m-k)$, and the Newcomb operators $X_{c,d}^{a,b}$ are defined via recursion relations (see Murray & Dermott, 1999). Alternatively, for quantitative work, the Hansen coefficients can be evaluated for a given eccentricity by calculating the integral

$$X_k^{p,m}(e) = \frac{1}{2\pi} \int_0^{2\pi} dl \left(\frac{R}{a}\right)^p \cos(mv - kl)$$

numerically.

Appendix C

Damping of Quadrupolar Modes by Gravitational Radiation

The average power radiated in gravitational waves due to a time-dependent mass quadrupole moment is given, in the weak-field limit of general relativity, by

$$\frac{dE_{\rm GW}}{dt} = \frac{G}{45c^5}\langle \dddot{Q}_{ij}\dddot{Q}_{ij}\rangle$$

(Misner et al., 1973), where Q_{ij} is the mass quadrupole moment as defined conventionally in classical physics:

$$Q_{ij} = \int d^3x \, \left(3x_i x_j - r^2\delta_{ij}\right)\rho(\mathbf{x},t) \ .$$

It can be shown that the power radiated by a quadrupolar mode is independent of m (this is a consequence of the Wigner-Eckart theorem). Hence, we can restrict ourselves to the $m = 0$ case for simplicity. It then follows that $Q_{11} = Q_{22} = -Q_{33}/2$, and that the off-diagonal terms vanish. Therefore, noting that the time dependence is sinusoidal, we have

$$\frac{dE_j^{\rm GW}}{dt} = -\frac{G}{60c^5}\omega_j^6 \dddot{Q}_{33}^2 \ , \tag{C.1}$$

where Q_{33} should now be understood to mean the time-independent amplitude of the mass quadrupole moment. Writing the mass density as

$$\rho(\mathbf{x}) = \rho_0(r) + A_j\delta\rho_j(r)Y_{20}(\hat{\mathbf{r}}) \ ,$$

where A_j is the amplitude of the mode and $\delta\rho_j$ is the normalized density perturbation associated with the mode, we find

$$Q_{33} = 4\sqrt{\frac{\pi}{5}} A_j \int_0^{R_*} dr\, r^4 \delta\rho(r) \ .$$

The above integral can be simplified by using the linearized Poisson equation, integrating by parts twice, and using the surface boundary condition $\eta_4 = -(\ell+1)\eta_3$. The result is

$$Q_{33} = \sqrt{\frac{5}{\pi}} M_* R_*^2 \eta_{3j}(R_*) A_j \ .$$

Substituting the above expression into (C.1), we get

$$\frac{dE_j^{\rm GW}}{dt} = -\frac{G M_*^2 R_*^4}{12\pi c^5} \eta_{3j}^2(R_*) \omega_j^6 A_j^2 \ .$$

Finally, noting that the total energy for an isolated mode is given by

$$E_j = \frac{1}{2} M_j R_*^2 \omega_j^2 A_j^2 \ ,$$

we arrive at the e-folding time for the mode energy under damping by gravitational radiation:

$$T_j = \frac{6\pi}{\omega_*} \beta_*^{-5} \eta_{3j}^{-2}(R_*) \left(\frac{M_j}{M_*}\right) \sigma_j^{-4} \ .$$

Appendix D

Statistical Properties of Resonant Energy Transfer in the No Back Reaction Approximation

In this appendix, we derive some statistical properties of the random walk given by (5.35), which we rewrite as

$$E_{k-1} = E_k + \varepsilon_k + Z_k \ , \tag{D.1}$$

where

$$Z_k \equiv 2\sqrt{\varepsilon_k E_k} C_k \ .$$

Recall that ε_k is known in advance, and that C_k is a random variable drawn from the distribution

$$p(x) = \frac{1}{\pi\sqrt{1-x^2}} \ , \quad x \in [-1, 1] \ .$$

Note that

$$\langle C_k \rangle = 0 \ , \quad \langle C_k^2 \rangle = \frac{1}{2} \ .$$

Since E_k will only depend upon C_α, for $\alpha > k$, Z_k is linear in C_k. As all the C_k are independent random variables (by assumption), it follows that

$$\langle Z_k \rangle = 0 \ , \quad \langle Z_k^2 \rangle = 2\varepsilon_k \langle E_k \rangle \ . \tag{D.2}$$

Given an initial mode energy E_k before the k-th resonance, we wish to determine the average mode energy $\langle E_{k-p} \rangle$, and its variance σ_p^2, after passage through p resonances. From (D.1), we have

$$E_{k-p} = E_k + \sum_{\alpha=k-p+1}^{k} \varepsilon_\alpha + \Delta_p \ , \tag{D.3}$$

where we have defined

$$\Delta_p \equiv \sum_{\alpha=k-p+1}^{k} Z_\alpha \ .$$

Using (D.2), it follows immediately that

$$\langle E_{k-p} \rangle = E_k + \sum_{\beta=k-p+1}^{k} \varepsilon_\beta \ . \tag{D.4}$$

Note that, since $\varepsilon_\beta > 0$, $\langle E_{k-p} \rangle$ increases monotonically as we pass through a sequence of resonances. Hence, we say that the random walk (D.1) has a drift. To calculate the variance, we need to find $\langle E_{k-p}^2 \rangle$. Writing

$$E_{k-p}^2 = \left(E_k + \sum_{\alpha=k-p+1}^{k} \varepsilon_\alpha \right)^2 + \Delta_p^2 + O(\Delta_p) \ ,$$

we see that

$$\langle E_{k-p}^2 \rangle = \langle E_{k-p} \rangle^2 + \langle \Delta_p^2 \rangle \ , \tag{D.5}$$

as all the terms linear in Δ_p will vanish when averaged. To calculate $\langle \Delta_p^2 \rangle$, we write

$$\Delta_p^2 = \sum_{\alpha=k-p+1}^{k} Z_\alpha^2 + 2 \sum_{\alpha=k-p+1}^{k-1} \sum_{\beta=\alpha+1}^{k} Z_\alpha Z_\beta \ ,$$

and note that, since $\beta > \alpha$ in the above double sum, each term of the double sum will be linear in C_α, and will, hence, vanish upon averaging. Therefore, we have

$$\langle \Delta_p^2 \rangle = 2 \sum_{\alpha=k-p+1}^{k} \varepsilon_\alpha \langle E_\alpha \rangle \ .$$

Substituting into (D.5), and then using (D.4), we find

$$\sigma_p^2 = 2 \sum_{\alpha=k-p+1}^{k} \varepsilon_\alpha \left(E_k + \sum_{\beta=\alpha+1}^{k} \varepsilon_\beta \right) \ . \tag{D.6}$$

It should be noted that (D.1) is not Gaussian, nor will it become Gaussian after many resonances. That the process is not Gaussian is clear from the fact that the random walk is bounded from below. Furthermore, the central limit theorem is not applicable because, typically, the probability distribution of Δ_p is dominated by the most recent few harmonics, and hence the effective number of variables never becomes large.

Appendix E

Time-Dependent Scalings of a Hamiltonian System

In Section 6.3.2, we use a pair of canonical transformations to obtain a Hamiltonian with a single free parameter starting from a Hamiltonian with three parameters. The two transformations are: a scaling of the momentum, and an overall scaling of the Hamiltonian. Since the scale factors were constant for the case of a conservative system, the transformations were easily seen to be canonical. However, with gravitational radiation, the scale factors are no longer constant. It is unclear whether the two transformations are still canonical in this case. Note that the Hamiltonian given by (6.49) describes a perfectly valid system, regardless. The issue is whether the system described by this Hamiltonian is the same as that described by (6.46). This question is addressed below.

The modified Hamilton's principle asserts that, for a system with the Hamiltonian $\mathcal{H}(q, p, t)$,

$$\Delta \int_{t_1}^{t_2} dt \, \left(p\frac{dq}{dt} - \mathcal{H} \right) = 0 \, , \tag{E.1}$$

where Δ denotes the usual first-order variation of the integral, and variations of q and p are considered independent (see, for example, Goldstein, 1980). Hamilton's equations follow as the Euler-Lagrange equations for this variational principle. Therefore, any transformation which preserves the form of the modified Hamilton's principle is canonical.

We first consider an overall scaling of the Hamiltonian by some time-dependent

scale factor $\lambda(t)$. Pulling out a factor of λ in the integrand of the modified Hamilton's principle, we obtain

$$\Delta \int_{t_1}^{t_2} dt\, \lambda \left(\frac{p}{\lambda} \frac{dq}{dt} - \frac{\mathcal{H}}{\lambda} \right) = 0 \ . \tag{E.2}$$

Defining a new time parameter τ by the differential relation

$$d\tau \equiv \lambda dt \ , \tag{E.3}$$

and changing the integration variable from t to τ, we get

$$\Delta \int_{\tau_1}^{\tau_2} d\tau \, \left(p \frac{dq}{d\tau} - \frac{\mathcal{H}}{\lambda} \right) = 0 \ , \tag{E.4}$$

which is just the modified Hamilton's principle for a system with the Hamiltonian H/λ and time parameter τ. The only consequence of λ not being constant is that the relation between τ and t is non-linear:

$$\tau(t) = \int^{t} dt' \, \lambda(t') \ . \tag{E.5}$$

Thus, an overall scaling of the Hamiltonian by a function of time amounts to a time re-parametrization, and is always canonical.

The second transformation we are concerned with is a scaling of the momentum. Once again, we pull out an overall factor of λ in the modified Hamilton's principle, as in (E.2). Expanding λ to linear order around some time t_0, and dividing out the constant factor $\lambda_0 = \lambda(t_0)$, we have

$$\Delta \int_{t_1}^{t_2} dt \, \left[1 + \frac{\dot{\lambda}}{\lambda_0}(t - t_0) \right] \left(\frac{p}{\lambda} \frac{dq}{dt} - \frac{\mathcal{H}}{\lambda} \right) = 0 \ . \tag{E.6}$$

As long as $\dot{\lambda}(t - t_0)/\lambda_0 \ll 1$, the above variational principle corresponds approximately to Hamilton's modified principle for a system with momentum p/λ and Hamiltonian $\mathcal{H}/\lambda$. In other words, the momentum-scaling transformation is canonical to lowest order for a time interval $\Delta t \ll \lambda/\dot{\lambda}$.

The above results imply that, with gravitational radiation, the Hamiltonian (6.49) is only valid for time intervals

$$\Delta t \ll \frac{\lambda}{\dot{\lambda}} \ . \tag{E.7}$$

Fortunately, this requirement does not impose any restrictions in addition to those already imposed by our treatment of gravitational radiation as being characterized by constant dissipation rates in the near-resonant regime. In general, we expect the above condition to be satisfied because the gravitational radiation time-scale is typically much longer than a resonance time-scale.

Appendix F

Perturbative Calculation of Action-Angle Variables

The development of the canonical perturbation series for a Hamiltonian system with a time-independent perturbation can be found in any standard reference on classical mechanics, such as Goldstein (1980). Consider a system with the Hamiltonian

$$\mathcal{H}(\theta, J) = \mathcal{H}_0(J) + \epsilon \mathcal{H}_1(\theta, J) \ , \tag{F.1}$$

where $\mathcal{H}_0$ is the unperturbed part, and $\mathcal{H}_1$ is the perturbation. For the unperturbed system, $\{\theta, J\}$ are action-angle variables. For the perturbed system, the new action variable is given by

$$\overline{J} = J + \epsilon \frac{\{\mathcal{H}_1\}}{\omega_0} + \epsilon^2 \left[\frac{1}{2} \frac{\partial}{\partial J} \left(\frac{\{\mathcal{H}_1\}}{\omega_0} \right)^2 + \frac{\{\Phi_2\}}{\omega_0} \right] + O(\epsilon^3) \ , \tag{F.2}$$

and the Hamiltonian by

$$\mathcal{H}(\overline{J}) = \mathcal{H}_0(\overline{J}) + \epsilon \langle \mathcal{H}_1 \rangle + \epsilon^2 \langle \Phi_2 \rangle + O(\epsilon^3) \ , \tag{F.3}$$

where

$$\omega_0(\overline{J}) \equiv \frac{\partial \mathcal{H}_0(\overline{J})}{\partial \overline{J}} \ , \tag{F.4}$$

$$\Phi_2(\overline{\theta}, \overline{J}) \equiv \frac{\{\mathcal{H}_1\}}{\omega_0} \left[\frac{1}{2} \frac{\partial^2 \mathcal{H}_0}{\partial \overline{J}^2} \frac{\{\mathcal{H}_1\}}{\omega_0} - \frac{\partial \mathcal{H}_1}{\partial \overline{J}} \right] \ , \tag{F.5}$$

and the notations $\langle\cdot\rangle$ and $\{\cdot\}$ denote the secular and periodic parts of a quantity:

$$\langle A\rangle \equiv \frac{1}{2\pi}\int_0^{2\pi} d\overline{\theta}\, A(\overline{\theta},\overline{J}) \ , \tag{F.6}$$

$$\{A\} \equiv A - \langle A\rangle \ . \tag{F.7}$$

For the Hamiltonian (6.49), we identify

$$\mathcal{H}_0 = \Phi^2 + \delta\Phi \ , \tag{F.8}$$

$$\mathcal{H}_1 = 2\sqrt{2\Phi}\cos\phi \ , \tag{F.9}$$

from which it follows that

$$\omega_0(\overline{\Phi}) = \delta + 2\overline{\Phi} \ , \tag{F.10}$$

$$\Phi_2(\overline{\phi},\overline{\Phi}) = -\frac{4\delta\cos^2\overline{\phi}}{(\delta+2\overline{\Phi})^2} \ . \tag{F.11}$$

Substituting into (F.2) and (F.3), the new action variable and the Hamiltonian to second-order are found to be

$$\overline{\Phi} = \Phi + \frac{2\sqrt{2\Phi}\cos\phi}{(\delta+2\Phi)} + \frac{2(\delta-4\Phi\cos^2\phi)}{(\delta+2\Phi)^3} \ , \tag{F.12}$$

$$\mathcal{H}^\dagger = \overline{\Phi}^2 + \delta\overline{\Phi} - \frac{2\delta}{(\delta+2\overline{\Phi})^2} \ . \tag{F.13}$$

Appendix G

Determining the Separatrix Crossing Parameter

A subtlety arises in the numerical solution of (6.98) when, for certain values of $\Phi_{\rm init}$, multiple roots exist. The situation is depicted in Figure G.1 for a particular example. In such a case the question of which root should be chosen arises. Also, it may not be obvious what the interpretation of the other roots is.

The simple rule-of-thumb is this: for a passage through a tidal resonance that is driven by gravitational radiation, the most negative root is always chosen. This is justified by noting that the most negative root is the first one that is encountered as δ drifts from negative values to positive values. It then remains to determine what the interpretation of the other roots is. The key observation is that the relation between the initial and final values of the action variables does not depend upon the direction of the crossing: (6.85) is equally valid whether the direction of the crossing is from region A to region C in Figure 6.5, or from region C to region A. In the former case $\dot{\delta} > 0$ and the most negative root of (6.98) is encountered first, and in the latter case $\dot{\delta} < 0$ and the most positive root of (6.98) is encountered first. Also, it should be noted that when the most positive root lies outside the interval $(-\infty, -3]$, as it does for $\Phi_{\rm init} \lesssim 3.186$, the C$\rightarrow$A crossing is impossible (see the discussion of the bifurcation at $\delta = -3$ in Section 6.3.2). For $\Phi_{\rm init} \geqslant 0$, the most negative root always lies in the interval $(-\infty, -3]$, and hence the A$\rightarrow$C crossing is always possible.

The roots intermediate between the most negative and the most positive ones

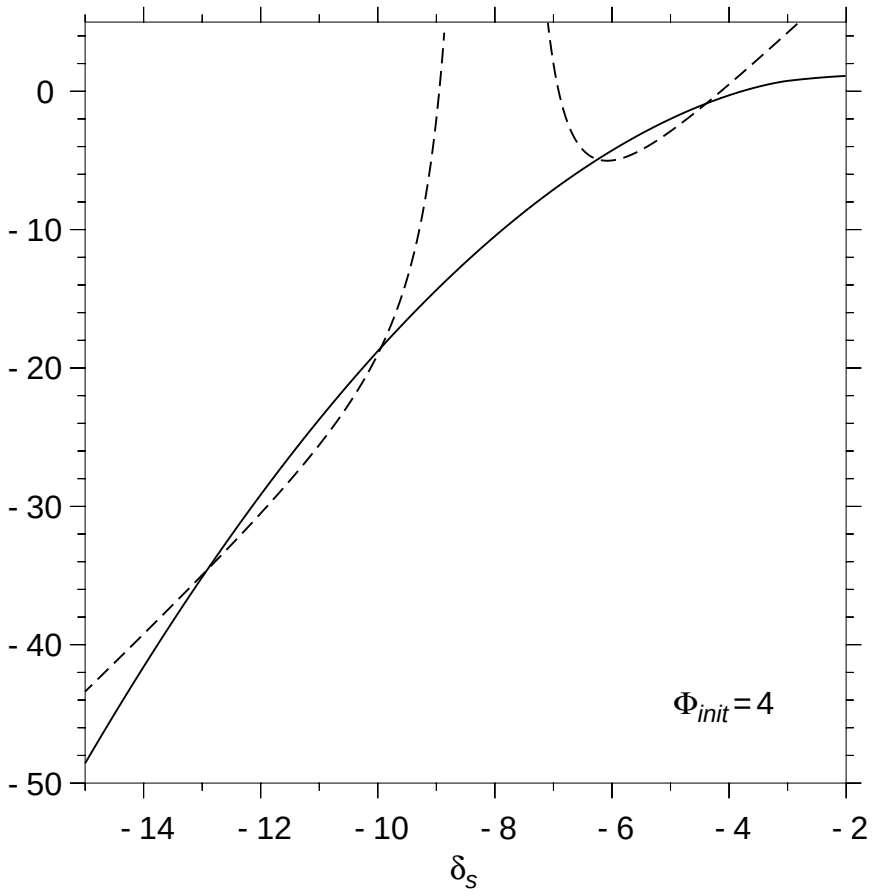

Figure G.1: Shown are curves for the left hand side (solid line) and the right hand side (dashed line) of (6.98) for the particular case $\Phi_{\rm init} = 4$. The roots of (6.98) are the values of $\delta_{\rm s}$ where the curves intersect.

in Figure G.1 arise from the failure of the canonical perturbation series to converge in that region. As such, these roots are spurious and do not have any physical significance.

Bibliography

Abramowicz M. A., Kluźniak W., McClintock J. E., Remillard R. A., 2004, ApJL, 609, L63

Abramowitz M., Stegun I. A., eds, 1972, Handbook of Mathematical Functions. Dover, New York

Alexander M. E., 1987, MNRAS, 227, 843

Alexander M. E., 1988, MNRAS, 235, 1367

Arfken G. B., Weber H. J., 1995, Mathematical Methods for Physicists. Academic Press, San Diego

Bahcall J. N., 1978, ARA&A, 16, 241

Barack L., Cutler C., 2004, Phys. Rev. D, 69, 082005

Barut A. O., 1980, Electrodynamics and Classical Theory of Fields and Particles. Dover, New York

Bildsten L., Cutler C., 1992, ApJ, 400, 175

Bisnovatyi-Kogan G. S., 2002, Stellar Physics. Vol.2: Stellar Evolution and Stability. Berlin: Springer

Blumenthal G. R., Tucker W. H., 1974, ARA&A, 12, 23

Bradt H. V. D., McClintock J. E., 1983, ARA&A, 21, 13

Brown G. E., Bethe H. A., 1994, ApJ, 423, 659

Brown G. E., Lee C.-H., Portegies Zwart S. F., Bethe H. A., 2001, ApJ, 547, 345

Buonanno A., Chen Y., Vallisneri M., 2003, Phys. Rev. D, 67, 024016

Burke J. A., 1967, MNRAS, 136, 389

Camilo F., Lyne A. G., Manchester R. N., Bell J. F., Stairs I. H., D'Amico N., Kaspi V. M., Possenti A., Crawford F., McKay N. P. F., 2001, ApJL, 548, L187

Carter B., Luminet J. P., 1985, MNRAS, 212, 23

Cartwright D. E., 1999, Tides: A Scientific History. Cambridge, New York

Cary J. R., Escande D. F., Tennyson J. L., 1986, Phys. Rev. A, 34, 4256

Chandrasekhar S., 1963, ApJ, 138, 896

Chandrasekhar S., 1964, ApJ, 139, 664

Chandrasekhar S., 1969, Ellipsoidal figures of equilibrium. The Silliman Foundation Lectures, New Haven: Yale University Press, 1969

Clark G. W., Markert T. H., Li F. K., 1975, ApJL, 199, L93

Colbert E. J. M., Mushotzky R. F., 1999, ApJ, 519, 89

Colbert E. J. M., Ptak A. F., 2002, ApJS, 143, 25

Colella P., Woodward P. R., 1984, J. Comp. Phys., 54, 174

Cowling T. G., 1941, MNRAS, 101, 367

Cox J. P., 1980, Theory of Stellar Pulsation. Princeton University Press, Princeton

Crowley R. J., Thorne K. S., 1977, ApJ, 215, 624

Davies M. B., Ritter H., King A., 2002, MNRAS, 335, 369

Dziembowski W., 1982, Acta Astronomica, 32, 147

Dziembowski W. A., 1971, Acta Astronomica, 21, 289

Edwards R. T., Bailes M., 2001, ApJL, 547, L37

Eggleton P. P., 1983, ApJ, 268, 368

Elson R., Hut P., Inagaki S., 1987, ARA&A, 25, 565

Fabian A. C., Pringle J. E., Rees M. J., 1975, MNRAS, 172, 15P

Fryer C. L., Woosley S. E., Herant M., Davies M. B., 1999, ApJ, 520, 650

Fryxell B., Olson K., Ricker P., Timmes F. X., Zingale M., Lamb D. Q., MacNeice P., Rosner R., Truran J. W., Tufo H., 2000, ApJS, 131, 273

Ghez A. M., Becklin E., Duchjne G., Hornstein S., Morris M., Salim S., Tanner A., 2003, Astronomische Nachrichten Supplement, 324, 527

Ghez A. M., Salim S., Hornstein S. D., Tanner A., Lu J. R., Morris M., Becklin E. E., Duchêne G., 2005, ApJ, 620, 744

Gingold R. A., Monaghan J. J., 1980, MNRAS, 191, 897

Goldstein H., 1980, Classical mechanics. Addison-Wesley, Reading, Massachusetts

Goodman J., Hut P., 1989, Nature, 339, 40

Hachisu I., 1986, ApJS, 62, 461

Hansen C. J., Kawaler S. D., 1994, Stellar interiors : physical principles, structure, and evolution. New York : Springer-Verlag, 1994. 1st ed.

Hawley J. F., Wilson J. R., Smarr L. L., 1984, ApJ, 277, 296

Heggie D. C., 1975, MNRAS, 173, 729

Hills J. G., 1975a, AJ, 80, 1075

Hills J. G., 1975b, AJ, 80, 809

Hills J. G., 1983, ApJ, 267, 322

Ho W. C. G., Lai D., 1999, MNRAS, 308, 153

Hopman C., Portegies Zwart S. F., Alexander T., 2004, ApJL, 604, L101

Hughes S. A., 2002, MNRAS, 331, 805

Hut P., 1983a, ApJL, 272, L29

Hut P., 1983b, AJ, 88, 1549

Hut P., McMillan S., Goodman J., Mateo M., Phinney E. S., Pryor C., Richer H. B., Verbunt F., Weinberg M., 1992, PASP, 104, 981

Iben I. J., Livio M., 1993, PASP, 105, 1373

Iben I. J., Tutukov A. V., Yungelson L. R., 1997, ApJ, 475, 291

Ivanov P. B., Papaloizou J. C. B., 2004, MNRAS, 347, 437

Iyer B. R., Will C. M., 1995, Phys. Rev. D, 52, 6882

Körding E., Falcke H., Markoff S., 2002, A&A, 382, L13

Kalogera V., Kim C., Lorimer D. R., Ihm M., Belczynski K., 2004, in ASP Conference Series Vol. CS-328: Binary Radio Pulsars The Galactic Formation Rate of Eccentric Neutron Star-White Dwarf Binaries. pp 261–+

Kaspi V. M., Lyne A. G., Manchester R. N., Crawford F., Camilo F., Bell J. F., D'Amico N., Stairs I. H., McKay N. P. F., Morris D. J., Possenti A., 2000, ApJ, 543, 321

Kim C., Kalogera V., Lorimer D. R., White T., 2004, ApJ, 616, 1109

King A. R., Davies M. B., Ward M. J., Fabbiano G., Elvis M., 2001, ApJL, 552, L109

Kippenhahn R., Weigert A., 1990, Stellar Structure and Evolution. Springer-Verlag, Berlin

Kochanek C. S., 1992a, ApJ, 398, 234

Kochanek C. S., 1992b, ApJ, 385, 604

Kokkotas K. D., Schäfer G., 1995, MNRAS, 275, 301

Kormendy J., Richstone D., 1995, ARA&A, 33, 581

Kovacs S. J., Thorne K. S., 1977, ApJ, 217, 252

Kumar P., Ao C. O., Quataert E. J., 1995, ApJ, 449, 294

Kumar P., Goldreich P., 1989, ApJ, 342, 558

Kumar P., Goodman J., 1996, ApJ, 466, 946

Lai D., 1994, MNRAS, 270, 611

Lai D., 1997, ApJ, 490, 847

Lai D., Rasio F. A., Shapiro S. L., 1993a, ApJS, 88, 205

Lai D., Rasio F. A., Shapiro S. L., 1993b, ApJL, 406, L63

Lai D., Rasio F. A., Shapiro S. L., 1994, ApJ, 420, 811

Landau L. D., Lifshitz E. M., 1969, Mechanics. Pergamon Press, Oxford

Landau L. D., Lifshitz E. M., 1975, The Classical Theory of Fields. Pergamon Press, Oxford

Lee H. M., Ostriker J. P., 1986, ApJ, 310, 176

Lichtenberg A. J., Lieberman M. A., 1992, Regular and Chaotic Dynamics. Springer-Verlag, Berlin

Liu Q. Z., van Paradijs J., van den Heuvel E. P. J., 2000, A&A Supp., 147, 25

Luminet J.-P., Carter B., 1986, ApJS, 61, 219

Maccarone T. J., 2004, MNRAS, 351, 1049

Manchester R. N., Lyne A. G., Robinson C., Bailes M., D'Amico N., 1991, Nature, 352, 219

Mardling R. A., 1995a, ApJ, 450, 722

Mardling R. A., 1995b, ApJ, 450, 732

Marsh T. R., 1995, MNRAS, 275, L1

Marsh T. R., Dhillon V. S., Duck S. R., 1995, MNRAS, 275, 828

Mayor M., Queloz D., 1995, Nature, 378, 355

McMillan S. L. W., McDermott P. N., Taam R. E., 1987, ApJ, 318, 261

Miller J. M., Fabbiano G., Miller M. C., Fabian A. C., 2003, ApJL, 585, L37

Miller J. M., Zezas A., Fabbiano G., Schweizer F., 2004, ApJ, 609, 728

Misner C. W., Thorne K. S., Wheeler J. A., 1973, Gravitation. W.H. Freeman and Co., San Francisco

Mizuno T., Kubota A., Makishima K., 2001, ApJ, 554, 1282

Monelli M., Corsi C. E., Castellani V., Ferraro I., Iannicola G., Prada Moroni P. G., Bono G., Buonanno R., Calamida A., Freyhammer L. M., Pulone L., Stetson P. B., 2005, ApJL, 621, L117

Motl P. M., Tohline J. E., Frank J., 2002, ApJS, 138, 121

Muller E., Steinmetz M., 1995, Comp. Phys. Comm., 89, 45

Murray C. D., Dermott S. F., 1999, Solar system dynamics. Cambridge Univ. Press, Cambridge

Nelemans G., Yungelson L. R., Portegies Zwart S. F., 2001, A&A, 375, 890

Nelson C. H., Green R. F., Bower G., Gebhardt K., Weistrop D., 2004, ApJ, 615, 652

Onken C. A., Ferrarese L., Merritt D., Peterson B. M., Pogge R. W., Vestergaard M., Wandel A., 2004, ApJ, 615, 645

Orosz J. A., 2003, in IAU Symposium Inventory of black hole binaries. pp 365–+

Osaki Y., Hansen C. J., 1973, ApJ, 185, 277

Ostriker J. P., Mark J. W.-K., 1968, ApJ, 151, 1075

Paczyński B., 1976, in IAU Symp. 73: Structure and Evolution of Close Binary Systems Common Envelope Binaries. pp 75–+

Papaloizou J., Pringle J. E., 1980, MNRAS, 193, 603

Papaloizou J., Pringle J. E., 1981a, MNRAS, 195, 743

Papaloizou J., Pringle J. E., 1981b, MNRAS, 196, 371

Peters P. C., 1964, Physical Review, 136, 1224

Peters P. C., Mathews J., 1963, Physical Review, 131, 435

Phinney E. S., Kulkarni S. R., 1994, ARAA, 32, 591

Polfliet R., Smeyers P., 1990, A&A, 237, 110

Portegies Zwart S. F., Baumgardt H., Hut P., Makino J., McMillan S. L. W., 2004, Nature, 428, 724

Portegies Zwart S. F., Dewi J., Maccarone T., 2004, MNRAS, 355, 413

Portegies Zwart S. F., McMillan S. L. W., 2002, ApJ, 576, 899

Portegies Zwart S. F., Yungelson L. R., 1999, MNRAS, 309, 26

Press W. H., Teukolsky S. A., 1977, ApJ, 213, 183

Press W. H., Teukolsky S. A., Vetterling W. T., Flannery B. P., 1992, Numerical recipes in C. The art of scientific computing. Cambridge: University Press, —c1992, 2nd ed.

Prix R., 2004, Phys. Rev. D, 69, 043001

Quataert E. J., Kumar P., Ao C. O., 1996, ApJ, 463, 284

Ramsay G., Hakala P., Cropper M., 2002, MNRAS, 332, L7

Ray A., Kembhavi A. K., Antia H. M., 1987, A&A, 184, 164

Reisenegger A., Goldreich P., 1994, ApJ, 426, 688

Rocca A., 1982, A&A, 111, 252

Rocca A., 1987, A&A, 175, 81

Rose W. K., 1998, Advanced Stellar Astrophysics. Cambridge: New York

Ruymaekers E., Smeyers P., 1994, A&AS, 104, 401

Saffer R. A., Liebert J., Olszewski E. W., 1988, ApJ, 334, 947

Saffer R. A., Livio M., Yungelson L. R., 1998, ApJ, 502, 394

Salmon R., 1988, Ann. Rev. Fluid Mech., 20, 225

Savonije G. J., Papaloizou J. C. B., 1983, MNRAS, 203, 581

Savonije G. J., Papaloizou J. C. B., 1984, MNRAS, 207, 685

Schödel R., Ott T., Genzel R., Eckart A., Mouawad N., Alexander T., 2003, ApJ, 596, 1015

Schäfer G., 1990, Astronomische Nachrichten, 311, 213

Sigurdsson S., Phinney E. S., 1993, ApJ, 415, 631

Sigurdsson S., Phinney E. S., 1995, ApJS, 99, 609

Sigurdsson S., Rees M. J., 1997, MNRAS, 284, 318

Smeyers P., Willems B., Van Hoolst T., 1998, A&A, 335, 622

Sod G. A., 1978, J. Comp. Phys., 27, 1

Stone J. M., Norman M. L., 1992, ApJS, 80, 753

Strickland D. K., Colbert E. J. M., Heckman T. M., Weaver K. A., Dahlem M., Stevens I. R., 2001, ApJ, 560, 707

Tauris T. M., Sennels T., 2000, A&A, 355, 236

Terquem C., Papaloizou J. C. B., Nelson R. P., Lin D. N. C., 1998, ApJ, 502, 788

Thorne K. S., Kovacs S. J., 1975, ApJ, 200, 245

Timmes F. X., Woosley S. E., Weaver T. A., 1996, ApJ, 457, 834

Turner M., Will C. M., 1978, ApJ, 220, 1107

Tutukov A. V., Yungelson L. R., 1993, Astronomy Reports, 37, 411

van den Heuvel E. P. J., 1992, Technical report, Endpoints of stellar evolution: The incidence of stellar mass black holes in the galaxy

van den Heuvel E. P. J., 1994, A&A, 291, L39

Van Hoolst T., 1994, A&A, 286, 879

van Kerkwijk M. H., Kulkarni S. R., 1999, ApJL, 516, L25

van Leer B., 1977a, J. Comp. Phys., 23, 263

van Leer B., 1977b, J. Comp. Phys., 23, 276

van Leer B., 1979, J. Comp. Phys., 32, 101

Willems B., van Hoolst T., Smeyers P., 2003, A&A, 397, 973

Witte M. G., Savonije G. J., 1999, A&A, 350, 129

Witte M. G., Savonije G. J., 2001, A&A, 366, 840

Wu Y., Goldreich P., 2001, ApJ, 546, 469

Zahn J.-P., 1970, A&A, 4, 452

Zahn J.-P., 1975, A&A, 41, 329

Zahn J.-P., 1977, A&A, 57, 383